Electrification & Renewable Energy Integration: A Case Study of Methanol Production



Chao Chen

A thesis submitted for the degree of

Doctor of Philosophy

Hilary Term 2021

Department of Engineering Science
University of Oxford

"At the age of thirty my deeds are nothing but dust, under the Moon and clouds my journey has taken me over eight thousand miles."

The River All Red Yue Fei (AD 1133)

Abstract

The electrification of the chemical industry is of paramount importance in meeting reduction targets in greenhouse gas emissions. However, it is tenable only if the electricity is generated from renewable sources. This project aims to investigate electrification schemes using methanol production processes as a case study, and to explore strategies for how to power such an electrified process with renewable energy. Taking a methanol production basis of 400,000 tonnes per annum, the energy and material flows are obtained from process simulations while renewable energy systems dedicated to the production are optimised through a modelling approach. In this work, direct (via heat pumps) and indirect electrification strategies (via sourcing alternative feedstocks) are compared, with results showing that the indirect electrification scheme has a more significant impact on the process energy structure. Based on the fully electrified methanol process, renewable power systems with an optional dispatchable power backup are modelled to fulfil the energy requirement aiming at the economic optimality. A two-regime behaviour of renewable penetration against dispatchable energy price has been found, which increases dramatically at the onset and slowly approaches 100 % when the dispatchable energy price is above a critical point. The optimal operation of the renewable energy systems results in voluntary curtailment of renewable power, of which the cost analysis shows modest economic potential for its further utilisation. The benefits of a flexible process are shown to be significant, which can reduce the levelised methanol cost by up to 35 %. Two geographical locations with distinct meteorological data are selected to investigate the impact of renewable source characteristics on the performance of methanol production and its renewable energy system. In particular, the diurnal and seasonal fluctuations of renewable sources and their impact on energy storage need are compared. The lessons of this project not only provide numerical results in terms of energy needs and production costs but also implications to policymaking, both of which will facilitate the energy transition from the current fossil fuels-based chemical industry to greener production.

Acknowledgements

I would like to thank my co-supervisor A/Prof. Aidong Yang for his help in developing modelling techniques and offering optimisation tutorials. Without his assistance, the project of flexible production (Chapter 6 of this thesis) would not be of the quality that it has.

I also would like to thank my primary supervisor Prof. Rene Banares-Alcantara for initiating the project, and in particular, for his suggestion of treating heat pump implementation as a means of electrification. To those who do not understand the reason why it is a big deal, please refer to Rene's comments, and I quote: *"the ideas about electrification of chemical industry, use of intermittent renewables, investigation of mix renewables input, use of meteorological data, focus on methanol production, selection of geographical sites, operation flexibility, consideration of process dynamics—to name the most important—were not conceived by Chao and were discussed in many meetings before Chao set out to perform the corresponding simulations and to generate results, some (if not most) of the research gaps were identified in those meetings."* Rene is not only a supervisor to me, but also a mentor, a policy guy, a true philosopher, a legend (and a mascot) of the Department, and a stickler for the rules, although his rules are sometimes as variable as renewable energies. Also, I am tremendously grateful for Rene's help in proofreading, which is far better than a ¥99.8 service I would get from taobao.com, although the latter takes far less time.

My publication list is a concise summary of my Ph.D life; the rapid change of corresponding authors provides additional (and profound) implications. I often feel that my research is something like *"too much blah blah but very little science"*. I guess I will inure myself very soon to my mediocre work and mundane life. Recently, I took the role as a post-doctoral researcher in "the other place", and I have to say that I miss Rene a lot—I wish I had Rene as my post-doc supervisor since he would allow me the freedom to explore and his noncommittal attitude would help to make my life easier. But it's ok; I'm as tough as a two-dollar steak. Well, there's no need in maintaining the charade—Rene, you're a .

A big thank you to my friends and co-workers from the Systems Engineering Group; in particular, Shangyi Zhao, Wenchan Qi, Ziming Yang, Till Weidner, Lei Xing, Christian Peters, Linnet Zohrabian, Farrukh Siddiqui, Ping Shen, Qian Xu, Hong Zeng, Sihao Di, Bo Zhang, Nadja Yang and Ao Fu are acknowledged. Special thanks to Till for collaborating with me in *Dota 2*, and to Ziming for *Overcooked*. I also would like to thank co-workers outside the group, such as Yangsiyu Lu and Guoping Hu, for their inspiration, discussions and fruitful collaborations.

No funding means no fun! I am extremely thankful to the China Scholarship Council and Jesus College (Oxford) for co-funding my studentship. I am grateful to the sponsors as I would not be able to complete my studies at the University of Oxford without their financial support. Although my scholarship was funded 50/50 by the both, my little maths tells me that the University's contribution is sort of like "left-pocket in, right-pocket out", and it is less "outs" and more "ins". Anyway, I am still very grateful for the University's generosity—in terms of making less profit. *"It is just good business."* I also would like to acknowledge the University for granting the grace period to the University Continuation Charge, which really helped to take the pressure off.

Finally, I would like to thank my parents, Jianxing Chen and Ling Gao, for their unrequited support along the way. My family and the good people from Zhangjiagang mean a lot to me—they are like a backup dispatchable power source easing my mind of variability.

Chao Chen

8th February 2021, Oxford





Publications

1. **C. Chen***. Using dispatchable energy price to influence renewable penetration in chemical production. *Journal of Cleaner Production*, 307:127274, 2021.

2. **C. Chen***, Z. Yang, and G. Hu. Signalling the cost of intermittency: What is the value of curtailed renewable power? *Journal of Cleaner Production*, 302:126998, 2021.

3. **C. Chen**, A. Yang, and R. Banares-Alcantara*. Renewable methanol production: Understanding the interplay between storage sizing, renewable mix and dispatchable energy price. *Advances in Applied Energy*, 2:100021, 2021.

4. **C. Chen**, Y. Lu, and Lei Xing*. Levelling renewable power output using hydrogen-based storage systems: A techno-economic analysis. *Journal of Energy Storage*, 37:102413, 2021.

5. **C. Chen** and A. Yang*. Power-to-methanol: The role of process flexibility in the integration of variable renewable energy into chemical production. *Energy Conversion and Management*, 228:113673, 2021.

6. **C. Chen**, Y. Lu, and R. Banares-Alcantara*. Direct and indirect electrification of chemical industry using methanol production as a case study. *Applied Energy*, 243(1):71-90, 2019.

7. G. Hu, **C. Chen**, H. T. Lu, Y. Wu, C. Liu, L. Tao, Y. Men, G. He, and G. Li*. A review of technical advances, barriers and solutions in the Power to Hydrogen (P2H) roadmap. *Engineering*, 6(12):1364-1380, 2020.

Nomenclature

Abbreviations

AEA	Aspen Energy Analyser
APEA	Aspen Process Economic Analyser
BTX	benzene/toluene/xylene
CapEx	capital expenditure
CEPCI	chemical engineering plant cost index
CF	capacity factor
COP	coefficient of performance
COP_{eff}	effective coefficient of performance
CR	combined reforming
DR	dry reforming
DSM	demand-side management
ESS	energy storage system
GCC	grand composite curve
GHG	greenhouse gas
HEX	heat exchanger
HHV	high heating value
HP	heat pump
HP	high pressure
IPA	isopropyl alcohol
IRR	internal rate of return
LCOMeOH	levelised cost of methanol
LEC	levelised energy cost
LHHW	Langmuir-Hinshelwood-Hougen-Watson
LP	low pressure
LREC	levelised renewable energy cost
MEA	monoethanolamine
MeOH	methanol
MP	medium pressure

MVR	mechanical vapour recompression
M&S	Marshall and Swift cost index
NG	natural gas
NLP	nonlinear programming
NPV	net present value
OpEx	operational expenditure
PCC	post-combustion capture
PV	photovoltaic
RES	renewable energy source
RTE	round-trip efficiency
RWGS	reverse water-gas-shift
SOFC	solid oxide fuel cell
SR	steam reforming
TFCC	total fixed capital cost
TR	tri-reforming
VHP	very high pressure
VRE	variable renewable energy
WGS	water-gas-shift

Parameters

a^k	constant utility coefficient for subsystem k
A	rearranged pre-exponential constant
b	constant material coefficient
B	rearranged activation energy term
c_j	unit price of utility j ($[1]/kg or $/kWh)
$C_{\mathrm{ELY}}^{\mathrm{ESS}}$	annualised cost of the electrolysers for ESS ($)
C_j	annualised cost of utility j ($)
C^k	annualised cost of subsystem k ($)
$C_{\mathrm{ELY}}^{\mathrm{SYN}}$	annualised cost of the electrolysers for MeOH synthesis ($)
C_t	cash flow of year t ($)

[1]$ denotes US dollar

$e_{\max}^{\mathrm{ELY}}$	maximum specific energy requirement for electrolyser ($\mathrm{kWh/kg_{H_2}}$)
$e_{\min}^{\mathrm{ELY}}$	minimum specific energy requirement for electrolyser ($\mathrm{kWh/kg_{H_2}}$)
$e^{\mathrm{ELY}}(t)$	specific energy requirement for electrolyser ($\mathrm{kWh/kg_{H_2}}$)
E_{a}	activation energy for reactions (J/mol or MJ/mol)
E_{cw}	total cooling duty (kWh)
E_{D}	energy from dispatchable source (MWh)
E_{G}	energy directly from renewable power generation (MWh)
E_{out}	curtailed renewable energy normalised by total load (MWh)
E_{ST}	energy from hydrogen storage system (kWh)
f	molar fraction (mol%)
f^{CR}	capital recovery factor
$f_{\mathrm{L}}^{\mathrm{ESS}}$	fraction of load met by energy from ESS
f_i	fraction of i source in renewable power generation
f_{m}	material correction factor for pressure vessel
f_{p}	pressure correction factor for pressure vessel
$f_{\mathrm{L}}^{\mathrm{RE}}$	renewable penetration in a load
$f_{\mathrm{ELY}}^{\mathrm{SYN}}$	fraction of load that goes to H_2 feedstock synthesis via electrolysis
F	process stream flowrate (kg/h)
FCp	aggregated heat capacity (kJ/K)
H	height (m)
k	kinetic constant
K	pre-exponential factor in reaction kinetics
L^{cap}	minimum storage capacity for a fully renewable operation (MWh)
L^{dv}	storage capacity as a decision variable (MWh)
$L_{\max}^{k}$	maximum storage capacity of subsystem k (kg or kWh)
$L^{k}(t)$	storage holdup level of subsystem k (kg or kWh)
$L(t)$	H_2 storage profile in time series (MWh)
M	M module, $M = (\mathrm{H_2} - \mathrm{CO_2})/(\mathrm{CO} + \mathrm{CO_2})$
M_{MeOH}	total mass of produced MeOH in a year (tonne)
M_{W}	molecular weight (kg/kmol)
n	life of a unit (years)

N	total hours in an operational year, i.e. 8,760 hours
P	pressure (bar)
$P_{\mathrm{D}}(t)$	time series of dispatchable power requirement (MW)
$P_{\mathrm{ch}}^{\mathrm{ESS}}(t)$	power charged to energy storage system (MW)
$P_{\mathrm{dis}}^{\mathrm{ESS}}(t)$	power discharged from energy storage system (MW)
$P_{\mathrm{ELY}}^{\mathrm{ESS}}$	rated power of the electrolysers for ESS (MW)
$P_{\mathrm{max}}^{\mathrm{ELY}}$	maximum rated power of the electrolysers for ESS (MW)
P_i	partial pressure of species i (Pa)
$P_{\mathrm{in}}(t)$	supply of electrical power at system inlet (kW)
$P_i(t)$	generated renewable power from source i (kW)
P_{L}	constant load requirement (MW)
$\overline{P_{\mathrm{L}}}$	average load of a period of interest (MW)
$P_{\mathrm{L}}(t)$	variable load as a function of time (kW)
$P_{\mathrm{out}}(t)$	curtailed electrical power at system outlet (kW)
$\overline{P_{\mathrm{S}}}$	year-average generation of solar power (MW)
$P_{\mathrm{S}}(t)$	base solar power in time series (MW)
$\overline{P_{\mathrm{W}}}$	year-average generation of wind power (MW)
$P_{\mathrm{W}}(t)$	base wind power in time series (MW)
$P_\delta(t)$	hourly power mismatch normalised by load (MW)
$P_\delta^{\mathrm{re}}(t)$	revised hourly power mismatch normalised by load (MW)
$\dot{Q}$	rate of heat or enthalpy change (kW)
r	discount rate, taken as 8 %
r_{MeOH}	rate of MeOH synthesis (mol/($\mathrm{kg_{cat}}$ s))
r_{RWGS}	rate of RWGS reaction (mol/($\mathrm{kg_{cat}}$ s))
R	ideal gas constant (J/(mol K))
t	time (h)
T	temperature (℃ or K)
U	velocity (m/s)
$\dot{W}$	mechanical work (kW)
x_j^k	consumption of utility j in subsystem k (kW)
z	open ground roughness level (m)

Greek Symbols

β	plant size factor
γ	renewable power provision factor
γ_{min}	minimum γ for a fully renewable operation
η_{c}	carbon efficiency
η_{ch}	conversion efficiency in charging mode
η_{dis}	conversion efficiency in discharging mode
η_{e}	energy efficiency
η_{refg}	efficiency of refrigeration cycle
$\dot{\xi}_0$	hourly baseline extent of hydrogenation reaction (kmol/h)
$\dot{\xi}(t)$	hourly extent of reaction (kmol/h)
ρ	density of a fluid (kg/m^3)
σ	standard deviation
ϕ_{min}	lower bound of operation envelope
$\phi(t)$	fraction of the maximum operation load in time series

Indices

cw	cooling water
CC	carbon capture
D	dispatchable power source
DT	methanol purification via distillation
el	electricity
ELY	electrolyser
GEN	generation of renewable power
i	type of renewable source (S, W)
j	type of utility (el, cw, pw)
k	process subsystem (CC, DT, ELY, STc, STh, STm, STq, SYN)
L	load
max	maximum value
min	minimum value
pw	process water

S	solar source
STc	carbon dioxide storage
STh	hydrogen storage
STm	raw methanol storage
STq	intermediate heat storage
SYN	methanol synthesis loop
W	wind source

Contents

Page

Abstract **v**

Acknowledgements **vii**

Publications **ix**

Nomenclature **xi**

List of Figures **xxi**

List of Tables **xxv**

Chapter 1 Introduction **1**

1.1 Objectives 4

1.2 Thesis Structure. 5

Chapter 2 Literature Review **7**

2.1 Industrial Energy Use and Carbon Emissions 8

2.2 Industrial Electrification 11

2.2.1 Technology 11

2.2.2 Strategy 14

2.3 "Green" Chemical Production 17

2.3.1 Hydrogen 18

2.3.2 Ammonia 21

2.3.3 Methanol 24

2.3.4 Chemicals in energy storage 28

2.4 Renewable Energy Systems 30

2.4.1 Levelling power output 31

2.4.2 Balancing power supply and demand 33

2.5 Challenges and Perspectives 36

Chapter 3 Electrification Schemes for Methanol Production 39
3.1 Introduction . . . 40
3.2 Methods . . . 42
3.2.1 Water electrolysis unit . . . 43
3.2.2 Carbon capture simulation . . . 44
3.2.3 Methanol production simulation . . . 46
3.2.4 Electrification . . . 52
3.2.5 Environmental assessment . . . 54
3.2.6 Financial assessment . . . 55
3.2.7 Summary of assumptions . . . 56
3.3 Results and Discussion . . . 57
3.3.1 Material and energy balance . . . 57
3.3.2 Energy integration and heat pump implementation . . . 59
3.3.3 Environmental assessment . . . 65
3.3.4 Financial assessment . . . 67
3.3.5 Sensitivity analysis . . . 70
3.3.6 Outlook . . . 73
3.4 Conclusions . . . 74

Chapter 4 Optimising Renewable Energy Supply 77
4.1 Introduction . . . 78
4.2 Methods . . . 81
4.2.1 Concept overview . . . 81
4.2.2 Renewable power generation . . . 83
4.2.3 Renewable energy storage . . . 84
4.2.4 Economic optimisation . . . 89
4.2.5 Renewable energy data . . . 91
4.2.6 Summary of assumptions . . . 93
4.3 Results . . . 94
4.3.1 Production without energy storage . . . 94
4.3.2 Production without dispatchable energy source . . . 96
4.3.3 Production powered by VRE and dispatchable energy . . . 101
4.3.4 Economic analysis . . . 103
4.3.5 Sensitivity analysis . . . 107

4.4 Discussion . . . 109
4.4.1 Limitations . . . 109
4.4.2 Significance of the optimum. . . . 110
4.4.3 Methods generalisation . . . 111
4.4.4 Implications to policymaking . . . 112
4.4.5 Outlook . . . 112
4.5 Conclusions . . . 113

Chapter 5 Quantifying the Value of Curtailed Renewable Power 115
5.1 Introduction . . . 116
5.2 Methods . . . 118
5.2.1 Concept overview . . . 118
5.2.2 Mathematical modelling . . . 119
5.3 Results and Discussion . . . 125
5.3.1 Energy analysis . . . 125
5.3.2 Cost analysis . . . 128
5.4 Conclusions . . . 131

Chapter 6 Introducing Process Flexibility to Methanol Production 133
6.1 Introduction . . . 134
6.2 Methods . . . 137
6.2.1 Concept overview . . . 137
6.2.2 Process description and modelling . . . 140
6.2.3 Flow and storage model . . . 142
6.2.4 Renewable energy model . . . 146
6.2.5 Economic model . . . 148
6.2.6 Optimisation strategy . . . 151
6.2.7 Summary of assumptions . . . 152
6.3 Results . . . 153
6.3.1 Base case scenario . . . 153
6.3.2 Impact of dispatchable energy price and process flexibility . . . 158
6.3.3 Costs of enforced renewable penetration targets . . . 160
6.3.4 Cost comparison and impact of technology prices . . . 163
6.4 Discussion . . . 165
6.5 Conclusions . . . 168

Chapter 7 Concluding Remarks **171**

Appendices **175**

A **175**

B **181**

C **195**

References **209**

List of Figures

Page

Figure 2.1. Energy composition of the four industry sectors in the EU28 in 2015. 9

Figure 2.2. Commodity matrix showing production quantity and energy intensity of key chemicals in the EU28. 10

Figure 2.3. Energy consumption and carbon footprint of high-volume commodity chemicals. 10

Figure 2.4. Schematic illustration of a closed-cycle heat pump system. . . . 13

Figure 2.5. Examples of implementation of MVR systems in a distillation column. 14

Figure 2.6. Energy input, production levels and carbon dioxide emissions for basic materials. 16

Figure 2.7. Current and envisioned coupling of the chemical and energy industries. 17

Figure 2.8. General process flowsheet for ammonia production using hydrogen from water electrolysis. 22

Figure 2.9. The production of methanol based on renewable energy taking supply and demand balancing into account. 26

Figure 2.10. General considerations undertook in renewable energy system. 31

Figure 2.11. Storage and balancing needs as a function of renewable mix and excess generation. 34

Figure 3.1. Process flow diagram of the carbon capture unit based on MEA absorption. 45

Figure 3.2. Process flow diagram of the reference MeOH production plant. 48

Figure 3.3. Process flow diagram of the non-conventional MeOH production plant simulated in Aspen Plus. 54

Figure 3.4. Block representation of the scenarios and the analysis boundaries. 58

Figure 3.5. Cascade diagrams and their corresponding Grand Composite Curves for different scenarios. 61

Figure 3.6. Energy structure and consumption of different scenarios. 64
Figure 3.7. Influence of renewable penetration on CO_2 abatement. 67
Figure 3.8. NPV values of each scenario with varying electricity prices. . . 69
Figure 3.9. Sensitivity analysis of all scenarios. 72

Figure 4.1. Overview of the general concept for the fully electrified MeOH production powered by renewable energy and its energy storage system. . . . 82
Figure 4.2. Normalised year-round availability of wind and solar power for Kramer Junction, US and Norderney, Germany. 93
Figure 4.3. Top: Requirement of dispatchable energy E_{D} as a function of γ and the share of wind power f_{W} at the demand side. Bottom: Time series of power mismatch in best scenarios when $\gamma = 1.5$. 95
Figure 4.4. L^{cap} as a function of f_{W} and γ for MeOH production without a dispatchable source. 97
Figure 4.5. Time series of $L(t)$ in terms of H_2 mass with optimised L^{cap} at selected γ for a 600 MW MeOH production process. 100
Figure 4.6. Dispatchable energy requirement E_{D} as a function of L^{dv} varied in a small range. 102
Figure 4.7. The impact of dispatchable energy price on LEC and renewable penetration. 104
Figure 4.8. Energy structure of the load at the most economical scenarios with and without dispatchable power. 107
Figure 4.9. Sensitivity analysis: (A) Kramer Junction and (B) Norderney. . 108

Figure 5.1. Overview of the general concept for the cascade design of a sequence of MeOH production plants. 119
Figure 5.2. Schematic illustration of the operation policy for the fully electrified MeOH production. 122
Figure 5.3. Time series of curtailed power for the cascade plants. 127
Figure 5.4. Time series of load composition for the cascade plants. 128
Figure 5.5. Cost breakdown for (A) LEC and (B) LCOMeOH. 129

Figure 6.1. Flowsheet of the electrified methanol production and its subsystems. 139
Figure 6.2. Contribution of the cost elements to LCOMeOH in the most economical case and the 100 % renewable operation case for (A) Norderney and (B) Kramer Junction. 156
Figure 6.3. Optimal LCOMeOH and its corresponding renewable penetration over a range of dispatchable energy price. 159
Figure 6.4. Cost of production at targeted renewable penetration. 161

Figure A.1. Flowrate of all species in the produced syngas with respect to reactor temperature. 175

Figure A.2. Profiles of H_2/CO, M module and CH_4 conversion with respect to reactor temperature.. 176

Figure A.3. Molar composition of species in the MeOH reactor. 176

Figure A.4. Fraction distribution of MeOH and water in both liquid (x) and vapour phase (y) at each corresponding distillation stage. 177

Figure B.1. Energy composition for the fully electrified MeOH production. 181

Figure B.2. Time series of unconstrained storage profiles at different fractions of wind energy. 182

Figure B.3. Time series of unconstrained storage profiles at different γ for $f_W = 0.6$. 182

Figure B.4. Representative storage profiles for Kramer Junction for a period of 4 years with varied γ. 183

Figure B.5. Storage profiles with decreasing efficiencies. 184

Figure B.6. Flow chart of how to determine $L(t)$. 186

Figure B.7. Scheduling of power for the fully electrified MeOH production with a load of 1 MW. 187

Figure B.8. Power curve for V90 3.0 MW turbine.. 190

Figure B.9. Total dispatchable energy requirement E_D for both locations at varied wind fractions in power generation. 191

Figure B.10. Standard deviation of year-round energy mismatch as a function of wind fraction in energy generation. 191

Figure B.11. Dispatchable energy requirement E_D as a function of L^{dv} for Norderney at $f_W = 99\,\%$ and $f_W = 1\,\%$. 192

Figure B.12. A sample of load met by E_D, E_G and E_{ST} plotted in the most economical scenario for a period of 1 week. 193

Figure C.1. Process flow diagram of the carbon capture subsystem (for Chapter 6) simulated in Aspen Plus. 195

Figure C.2. Process flow diagram of the CO_2 hydrogenation subsystem (for Chapter 6) simulated in Aspen Plus. 197

Figure C.3. (A) Schematic diagram of a traditional distillation column. (B) Process flow diagram of the distillation subsystem (for Chapter 6) modified with a design of mechanical vapour recompression. 198

Figure C.4. Requirement of mechanical work, cooling duty and minimum target pressure with respect to the flowrate of the working fluid.. 199

Figure C.5. Schematic illustration of a simplified operation policy on material and heat flow.. 201

Figure C.6. Analysis of the renewable penetration behaviour from a mechanistic viewpoint. 206

Figure C.7. Fraction of the curtailed renewable power P_{out} plotted against $f_{\mathrm{L}}^{\mathrm{RE}}$. 207

Figure C.8. Example of reactor operation for selected ramp limits. 207

Figure C.9. Fraction of the load met by E_{ST} plotted against $f_{\mathrm{L}}^{\mathrm{RE}}$. 208

Figure C.10. Average load of the methanol production process ($\overline{P_{\mathrm{L}}}$) plotted against (A) c_{D} and (B) $f_{\mathrm{L}}^{\mathrm{RE}}$ for the optimal operations. 208

Figure C.11. Levelised energy cost (LEC) and levelised renewable energy cost (LREC) plotted against $f_{\mathrm{L}}^{\mathrm{RE}}$ for the optimal operations in (A) Norderney and (B) Kramer Junction. 208

List of Tables

Page

Table 2.1. Ratio of electricity and heat utilisation in the four industries in the EU28 in 2015. 8

Table 3.1. Composition of the flue gas in the carbon capture unit. 46

Table 3.2. Reaction kinetic constants and parameters for the MeOH synthesis kinetic model. 51

Table 3.3. Utility savings and performance indicators for different scenarios. 62

Table 3.4. Summary of key environmental indicators for each scenario.. . . 66

Table 3.5. Main equipment cost estimation for each plant in Chapter 3. . . 68

Table 3.6. Parameters for 0 % variance in the sensitivity test. 70

Table 4.1. L^{cap} and empty hours of the storage system in Kramer Junction and Norderney. 100

Table 4.2. LEC optimised by excess power generation, renewable mix and storage capacity for production powered by both VRE and dispatchable energy. 104

Table 4.3. LEC optimised by excess power generation, renewable mix and storage capacity for production powered by VRE and its ESS only. 105

Table 4.4. CO_2 emissions for different operation scenarios in Chapter 4. . . 107

Table 5.1. Key energy indicators for the cascade plants.. 126

Table 6.1. Optimal performance of the base case scenario, where c_{D} is fixed at 100 \$/MWh and ϕ_{min} at 10 % for the flexible production. 155

Table 6.2. Optimal LCOMeOH for 100 % renewable operations based on conservative and progressive technology costs. 164

Table A.1. Summary of the utility use in the reference MeOH plant before heat integration. 177

Table A.2. Summary of the utility use in the CO_2 hydrogenation plant before heat integration.. 178

Table A.3. Summary of the utility use in the carbon capture process with regard to the reference plant.. 178

Table A.4. Summary of the utility use in the carbon capture process with regard to the CO_2 hydrogenation plant 178

Table A.5. CO_2 emission for different utilities.. 179

Table A.6. Price for utilities and their corresponding supply temperature. . 179

Table A.7. Raw material and product price. 179

Table A.8. Total fixed capital cost estimation for each plant. 180

Table B.1. Total fixed captial cost estimation for the MeOH plant.. 188

Table B.2. Raw material and process utility price for the analysis in Chapter 4. 188

Table B.3. Fixed annualised cost of electrolysers for MeOH synthesis ($C_{\mathrm{ELY}}^{\mathrm{SYN}}$), cooling water ($C_{\mathrm{cw}}$) and process water ($C_{\mathrm{pw}}$). 188

Table B.4. Renewable technology costs for the analysis in Chapter 4. . . . 189

Table B.5. Parameters for 0 % variance in the sensitivity test for Chapter 4. 189

Table B.6. Standard deviation (σ) of year-round wind and solar power in Kramer Junction and Norderney. 190

Table C.1. Key stream conditions for the carbon capture process (Figure C.1).. 196

Table C.2. Key stream conditions for the CO_2 hydrogenation process (Figure C.2). 197

Table C.3. Physical meaning of the key streams in Figure C.3. 198

Table C.4. Stream conditions for the distillation process (Figure C.3B). . . 199

Table C.5. Utilities and cost for the main equipments shown in Figure 6.1. 200

Table C.6. Key decision variables and their descriptions. 201

Table C.7. Summary of constant parameters. 202

Table C.8. Correction factors for pressure vessels. 203

Table C.9. Total fixed capital cost estimation for the methanol plant including the subsystems of CC, DT and SYN (with MCP1 listed separately) at the baseline size.. 204

Table C.10. Technology costs used for the base case scenario. 205

Table C.11. Conservative technology costs. 205

Table C.12. Progressive technology costs. 205

Table C.13. Size of individual units for the 100 % renewable operations in the two locations. 206

Table C.14. Key variables for Norderney at selected ramp limits.. 207

献给家人和故乡

Chapter 1

Introduction



The environmental impact of chemical production has drawn significant attention, and reduction in greenhouse gas (GHG) emissions has been called for to mitigate climate change. The European Commission (2011) published a roadmap for transforming into a low-carbon economy in 2050, with an objective to cut GHG emissions by at least 80 % relative to 1990. If a 2 ℃ scenario is assumed, the reduction of GHG emissions in all sectors is required to continue down to zero not later than 2060–2080 (Ahman et al., 2017). In the US, a national goal was established in 2009 to reduce GHG emissions approximately 17 % below 2005 levels by 2020 (Dennis et al., 2016). Many states have also imposed a cap on GHG emissions as their individual goals. To meet these targets, deep decarbonisation of energy-intensive industries, in particular the chemical industries, will be necessary. While one strategy towards decarbonisation would involve converting otherwise emitted GHG, such as carbon dioxide, into valuable commodity chemicals, a second route could involve avoiding the generation of GHG altogether. For instance, this may be achieved by synthesising hydrogen exclusively from water electrolysis instead of from natural gas reforming (Schiffer and Manthiram, 2017). The generalised strategy is to transform species with low free energy, such as water, nitrogen and carbon dioxide, to commodity chemicals that are higher up on the free energy landscape, such as ammonia, methanol and

their derivatives. A key to achieving this is to meet the energy requirement using "green" electrons in lieu of carbon-based fuels (Barton, 2020).

Currently, the chemical industry is mostly powered by the combustion of fossil fuels, which is responsible for a significant portion of anthropogenic GHG emissions. In the EU28 context, the chemical and petrochemical industry accounts for 30.7 % of the total energy consumption in the industrial sector in 2015, and among all sources of industrial consumption, only 0.6 % is directly from renewable heating (Eurostat, 2017b). To achieve the transition to renewables and meet decarbonisation targets, the necessity of electrification has been agreed and understood by many energy experts (Energy Transitions Commission, 2018), but it may appear counterintuitive to conventional wisdom: electricity generation and transmission involve substantial energy losses, and thus using electricity to provide heat in the chemical industry is less efficient than on-site combustion from an energy conservation point of view (Roberts, 2017). However, the potential of electrification mainly lies in a future scenario where there is a pathway leading to zero-carbon electricity. Specifically, policy goals are shifting from focusing on energy conservation towards achieving environmental targets such as the reduction in GHG emissions. Dennis et al. (2016) coined the term "emiciency", short for "emissions efficiency", to emphasise the importance of environmentally beneficial electrification. In fact, more than two decades ago, the importance of electrification was noted as an economical way to reduce the reliance of energy systems on carbon (Kafandaris, 1994).

The use of renewable energy sources (RESs) plays a pivotal role in electrification and yet poses a significant challenge: the intermittency and variability of RESs impact the stability of the grid and require improved planning and coordination to accommodate fluctuations in availability. To this end, there are solutions underway, particularly in electricity market rules, design and operations (Dupuy, 2018). While renewable electrification promotes decarbonisation of the chemical industry, electrified chemical processes also help to address the challenges in RES utilisation: transducing electrical energy into chemical bonds is essentially a method for storing electrical energy in the form of high heating value chemicals, which helps overcome the variability of renewable sources (Lewis and Nocera, 2006). Besides the

technology aspects, policy formation also poses additional difficulties. For instance, the consideration of energy security, often a top priority (Rudd, 2015), may impede the penetration of RESs in electricity generation (due to the variability of RESs). In addition, many public policies stress energy efficiency, which may be an inadequate metric to evaluate the energy structure as it misses the environmental benefits of electrification. Therefore, a targeted and farsighted policy will be required in the process of chemical industry electrification. Although there are many problems in electrification to be addressed, a broad consensus about the pathways towards clean electricity exists. The same may not yet be said of fossil fuel combustion, even with highly efficient technologies. Biofuels, as an alternative to fossil fuels, may lead to reduced carbon emissions (this has been questioned by Searchinger et al. (2008) when land-use change is taken into account), but they have proven less favourable in economic potential and scalability (Logan and Rabaey, 2012). For this and other reasons, the consensus is growing that electrification with renewable energy is required to meet GHG reduction goals.

One strategy to explore the impact of industrial electrification is to analyse the industry as a whole through a what-if thought experiment (Lechtenböhmer et al., 2016). However, this method misses the opportunities from process systems engineering, as the interplay between operating units can be used as a tool for optimisation (Soroush and Chmielewski, 2013). This detailed analysis at a process level becomes particularly important when renewable energy systems are taken into account in the context of electrification. Therefore, this project has focused on methanol production processes as a case study. Methanol is an important and valuable commodity—not only the raw material for essential chemical products such as formaldehyde, acetic acid and dimethyl ether but also an energy vector for direct fuel applications (Perez-Fortes et al., 2016). For more than a decade, researchers have been advocating to replace petroleum-based fuels with methanol and its derivatives, which is referred to as "methanol economy" (Olah, 2003). As opposed to its counterpart of "hydrogen economy", which has difficulties in distribution and storage, a large deployment of methanol applications have unique advantages: in contrast to hydrogen, methanol is a convenient fuel that provides an efficient means

to store energy (Olah, 2005). At present, although methanol is produced nearly exclusively from fossil fuels reforming, it can also be obtained by the reduction of carbon dioxide with "green" hydrogen (i.e. generated from renewable sources). This alternative synthesis pathway opens up the possibility of the chemical recycling of carbon dioxide, which has profound implications to decarbonisation in energy sectors (Yang and Jackson, 2012). The concept of green production has been demonstrated extensively in previous work focusing on hydrogen (Shaner et al., 2016) and ammonia (Morgan, 2013), whereas the same concept for methanol is rarely explored. Owing to the above reasons, it is urgent to investigate methanol production processes combining electrification and renewable energy systems.

1.1 Objectives

In view of the challenges in renewable energy utilisation and chemical process electrification, the main objective of this work is to develop electrification schemes for chemical production processes and evaluate the performance of an electrified methanol production process powered by RES at the economic optimality. The consideration of both aspects is of particular importance in the context of industry decarbonisation, given that process electrification and the penetration of renewable power in chemical production promote one another. The interplay between the components of chemical processes offers a unique opportunity to address the challenge of variable renewable energy (VRE) integration. Therefore, this work also aims to provide insights into the synergistic effects by bridging systems engineering. The objectives are listed as follows:

(1) Developing electrification schemes for chemical processes. To achieve this, a methanol production process is investigated as a case study to implement electrification schemes. The aim of this case study is to evaluate the performance and impact of different schemes based on economic and environmental assessments.

(2) Providing solutions to the integration of VRE with chemical production. To this end, the investigation continues with the same methanol production case study to evaluate different methods aiming at the economic optimality.

(3) Providing new ways of thinking about VRE integration and management. This is achieved by optimising the energy dispatch and process design using multi-system synergies, which bridges systems engineering thinking strategies.

(4) Understanding the interplay between operating units and subsystems. Modelling and optimisation of energy, storage and production subsystems would reveal the behaviour of a particular unit and how it responds to an input change. The understanding of this interplay would facilitate decision making from an engineering perspective.

(5) Quantifying the cost of intermittency. Although there is a consensus that the intermittency of renewable sources incurs additional costs, the evaluation of such costs is still missing. Understanding that the additional costs may vary depending on many factors, this work aims to signal the cost of intermittency using methanol production as a basis.

(6) Identifying implications to policymaking. The analysis not only aims to compare outcomes in different scenarios but also targets a holistic view of the potential of electrification scheme and RES utilisation from both engineering and policymaking perspectives. Based on the numerical results and correlations between the key variables, this work can provide profound insights.

1.2 Thesis Structure

This thesis contains four chapters of original work, which each presents detailed methods and results around a specific research topic. The research work complements a series of knowledge gaps in the field of chemical industry electrification and RES utilisation, which is presented in a hierarchical order. While Chapter

1 provides background and motivations for this work, the rest of this thesis is organised as follows:

Chapter 2 evaluates the relevant literature focusing on the electrification techniques and strategies, as well as the "Power-to-X" concept of converting renewable energy to green chemicals. The literature is reviewed critically to identify the research gaps and provide a rationale for this work.

In Chapter 3, electrification schemes for the chemical industry are explored, taking the production of methanol as a case study. The production process is simulated to provide a basis for energy, economic and environmental assessment. The energy structure analysis paves a pathway for the subsequent work in Chapters 4–6.

In Chapter 4, an optimisation problem regarding electrified methanol production powered by VRE is presented, with a focus on the role of the storage unit in optimising power scheduling. The optimal scheduling is designed, with storage sizing, renewable mix and dispatchable energy price as decision variables.

Chapter 5 quantifies the economic value of curtailed renewable power and investigates the cost of intermittency. To eliminate demand-side influences, the evaluation is performed using a constant load methanol production process as a basis, which is powered by a dedicated renewable energy system.

Chapter 6 continues with the same electrified methanol production process by incorporating process flexibility into the optimisation. This work aims to complement Chapter 4 by taking multi-system interplay into consideration. The model and the optimisation problem are reformulated to accommodate the new concept.

Chapter 7 concludes the work presented in this thesis, highlighting the significance and main contributions that have been made. Limitations of this project are also discussed along with an outlook for future directions.

Chapter 2

Literature Review



HIS chapter reviews the literature to date relevant to the development of chemical industry electrification, "green" chemicals produced from renewables and renewable energy systems. The energy structure of the current industry is first reviewed to identify the room for electrification, which is followed by a review of electrification methods and technologies. The production of key chemicals with new thinking strategies and the applications of renewable power systems are also covered in this chapter with a focus on how the strategies address the difficulties in renewable energy management. The purpose of this chapter is to critically identify the knowledge gaps and provide rationales for the research. The challenges and perspectives of the utilisation of renewable energy are also highlighted.

2.1 Industrial Energy Use and Carbon Emissions

The industry sector of the EU28 consumed 274,737 ktoe of energy in 2015, accounting for approximately 25 % of total energy consumption (Eurostat, 2017b). Figure 2.1 shows the energy consumption in four major industries in the EU28 in 2015, including (1) iron and steel, (2) chemical and petrochemical, (3) non-metallic minerals and (4) paper, pulp and printing industry. The ratios of electricity to thermal heating consumption for the respective industries are tabulated in Table 2.1. Apparently, electricity utilisation makes up an important part of the current energy structure but there is room for further electrification. Among the key industries, the chemical and petrochemical industry represents the largest energy consumer and is of particular importance. After decades of endeavour, energy efficiency has been improved significantly. However, the chemical industry is still largely powered by the combustion of fossil fuels, with oil and gas dominating its energy structure. Note that electrification may not be limited to the substitution of process heating with electrical power. For instance, fossil fuel-based syngas (an intermediate product for many chemical processes) may be alternatively generated via electrolysis with electricity from renewables. This represents a different strategy in electrification, whose its large-scale deployment would significantly change the energy structure of the current industry. Nevertheless, both electrified heating and materials play an important role in mitigating environmental challenges.

Table 2.1. Ratio of electricity and heat utilisation in the four industries in the EU28 in 2015. Data obtained from Eurostat (2017b).

Form of energy	Iron and steel	Chemical and petrochemical	Non-metallic minerals	Paper, pulp and printing
Total electricity	8,844	15,521	5,777	10,071
Total heat	40,909	36,296	28,067	23,313
Total energy	49,753	51,817	33,845	33,385
Electricity ratio (%)	17.8	30.0	17.1	30.2

To focus on the chemical and petrochemical industry, it is important to identify the energy intensity of individual chemicals. Figure 2.2 shows the commodity matrix of selected key chemicals on the basis of their production quantity and energy intensity. Note that various sources are considered to estimate the production

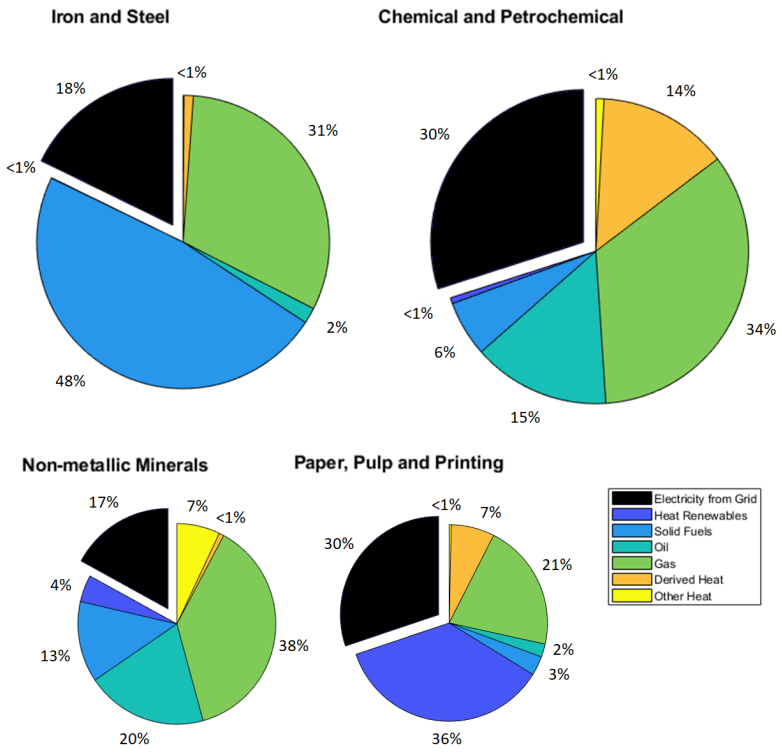


Figure 2.1. Energy composition of the four industry sectors in EU28 in 2015. Electricity consumptions are highlighted in black and offset from the pie chart. All other components represent heat as a primary energy form. The overall size of the pie charts represents the total amount of energy consumption. The energy balance is estimated according to Eurostat's methodology. Data obtained from Eurostat (2017b).

quantity in the EU28 and an average value has been used if the sources are inconsistent. The commodity matrix illustrates the significance of a chemical since the product of energy intensity and production quantity reflects the total energy utilisation. The energy contribution from feedstocks is excluded in order to focus on the utilities consumed in production processes. However, as mentioned earlier there are profound implications when feedstocks are taken into consideration.

As commented by Schiffer and Manthiram (2017), energy consumption or intensity itself is not necessarily a problem, it is however a relatively clear indicator of greenhouse gas (GHG) emissions. This is evidently illustrated in Figure 2.3 where the top five commodity chemicals with both the largest production volume and energy consumption are also higher up on the GHG emissions list. Although there are many chemicals higher up on the list, some of them, such as ethylene, propylene and aromatics, are the products of complex organic molecules, which are irreplaceable without substantial innovation in the current industry. On the

other hand, chemicals like methanol and ammonia, which can be produced from hydrogenation, are of particular importance as the fossil fuel-based feedstock can be substituted with electricity-based hydrogen. Apparently, hydrogen is likely to be the central pillar in the power-to-chemical roadmap (Hu et al., 2020).

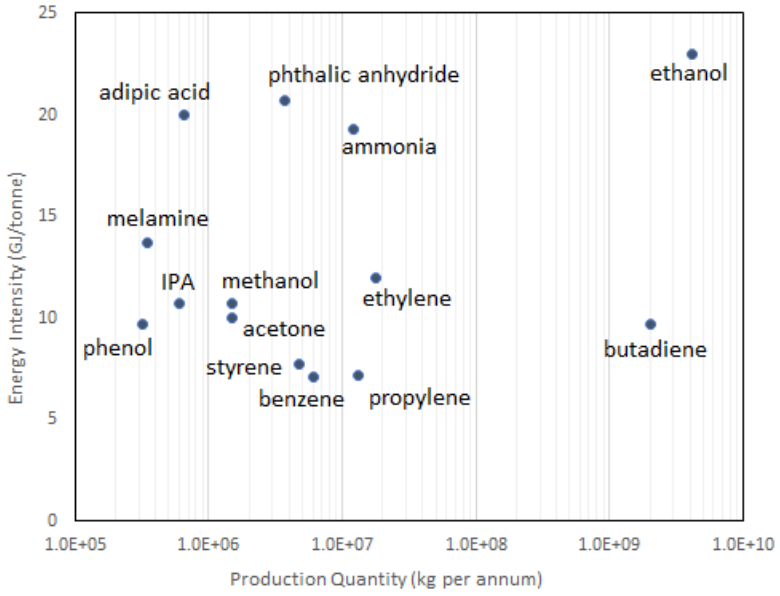


Figure 2.2. Commodity matrix showing production quantity and energy intensity of key chemicals in the EU28. Energy intensity is estimated based on best practical technology but not limited within the EU28. Feedstock energy terms are neglected. IPA stands for isopropyl alcohol. Data obtained from Eurostat (2016); Renewable Fuels Association (2017); Saygin et al. (2009); Weddle (2013); Worrell et al. (2000).

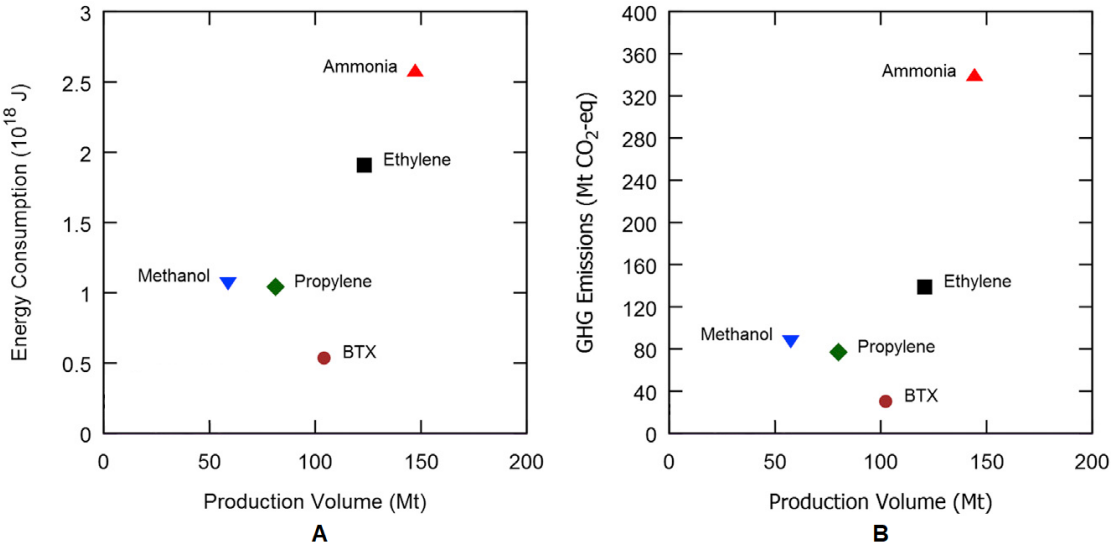


Figure 2.3. Energy consumption (A) and carbon footprint (B) of high-volume commodity chemicals. BTX stands for benzene/toluene/xylene. Picture reprinted from Schiffer and Manthiram (2017).

2.2 Industrial Electrification

2.2.1 Technology

As an important form of energy, electricity can meet not only household basic needs but also industry-related activities: heating in chemical synthesis processes, compression of process fluids, electrowinning in metal manufacturing—to name just a few examples. Industrial processes often involve materials modification, fluids compression, and the transformation of materials from one form to another. The electrical phenomena involving such transportation and transformation can be categorised into three types, namely electromotive, electrothermal, and electrolytic phenomena (Gellings and Blatt, 2009):

Electromotive phenomena. A prominent example of this is the electric motor, which is driven by the electromotive force generated when current flows in a conductor in a magnetic field. Electric motors have been used in almost all end-use sectors to drive devices such as compressors, mixers, pumps and other assorted equipment. In the implementation of a heat pump, electricity is primarily dissipated in the enthalpy of a working fluid through compression work, illustrating an application of such phenomena.

Electrothermal phenomena. The most significant advantage of using an electrothermal mechanism in process heating is that it generates heat within the unit. In direct contrast, conventional heating powered by fossil fuels generates heat and transfers it to the surface of process materials through radiation and convection, and the interior of materials can be subsequently heated up via conduction. Therefore, heating through electrothermal mechanisms is more effective and efficient in comparison to fossil-fuelled processes.

Electrolytic phenomena. These are the electromotive forces exerted at the molecular level which induce chemical changes in a conductive electrolyte. Examples of electrolytic systems are electrowinning for smelting primary metals, electroplating for metal coating and, very importantly, electrolysis of water to produce hydrogen.

Based on these electrical phenomena, cross-cutting technologies can be applied to fulfil the process requirement. Examples are electric ovens, resistor heaters, plasma torches, etc. The common ground of the techniques mentioned above is that they all provide heat by converting electric current. In the chemical industry, heating is mostly provided by steam generated from gas-fired central boilers. Nevertheless, the electric techniques have many advantages over thermal heating: (1) they have the ability to focus and deposit energy exactly where needed, thereby eliminating heating or cooling of entire parts; (2) electricity end use is controllable to a more precise degree. It can be adjusted to vary process conditions instantaneously, unlike thermal heating which requires long warm-up periods and has inertia, which often leads to it being left on continuously (Gellings and Blatt, 2009).

Although direct electric heating possesses certain advantages compared with fossil fuel-based heating, its overall energy efficiency is not much improved. On the other hand, highly energy-efficient technologies such as heat pumps can be implemented in a chemical process as a means of electrification, saving both hot and cold utilities at the expense of additional electric compression work. The efficiency of a heat pump is indicated by the coefficient of performance (COP), which is defined by

$$\mathrm{COP}_{heating}^{Carnot} = \frac{T^{\mathrm{H}}}{T^{\mathrm{H}} - T^{\mathrm{L}}} \tag{2.1}$$

for heating purpose in a Carnot cycle, wherein T^{H} and T^{L} denote the hot and cold temperature of the working fluid, respectively. The value of COP always exceeds 1.0 because the energy is moved from a lower temperature source to a higher temperature source.

There are two main types of heat pump system, namely closed- and open-cycle vapour recompression systems. Figure 2.4 illustrates the closed-cycle heat pump system, which consists of (1) a heat source (cold stream) providing the heat input to the heat pump, and (2) a heat sink (hot stream) receiving the heat discharged from the heat pump. In contrast to the closed-cycle vapour compression system, which utilises a recirculated working fluid, open-cycle vapour recompression uses

a process stream as the working fluid to exchange heat with sources and sinks. Due to this feature, an open-cycle heat pump is often implemented in distillation columns (Gao et al., 2013; Wang et al., 2012; Yang et al., 2010), whereas the closed-cycle system is used for general energy integration (Bagajewicz and Barbaro, 2003; Yang et al., 2013).

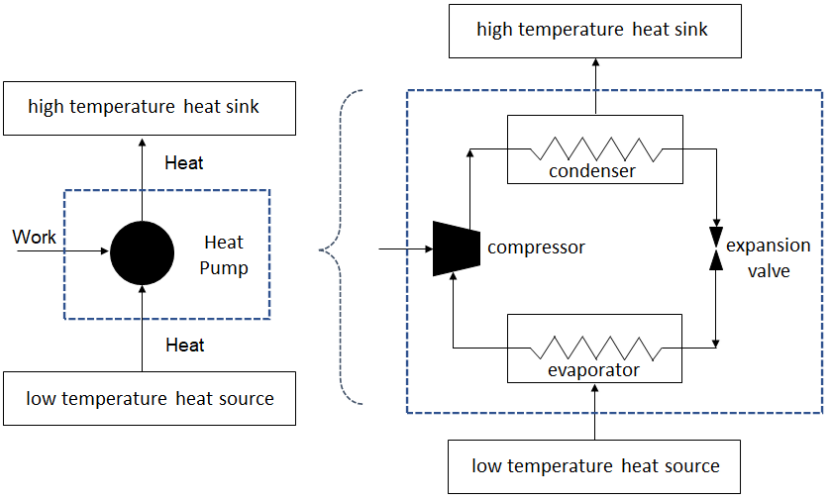


Figure 2.4. Schematic illustration of a closed-cycle heat pump system.

Heat pump implementation for distillation is of particular importance. A conventional distillation column consists of a top rectifying section with a condenser and a bottom stripping section with a reboiler. To achieve separation through vapour-liquid equilibrium, heat is added in the reboiler at the bottom and removed in the condenser at the top of the column. Typically, the heat grade of the stream around the condenser is too low to be utilised for heat integration. Consequently, distillation processes consume a significant amount of energy, accounting for approximately 3 % of global energy consumption (Engelien and Skogestad, 2004). Distillation processes demonstrate great potential to promote sustainability when a heat pump is implemented. Shenvi et al. (2011) demonstrated the application of an open-cycle heat pump via mechanical vapour recompression (MVR) for distillation columns, as shown in Figure 2.5. The implementation of the MVR system elevated the temperature of the heat source, thus facilitating heat exchange in a process. Although such implementation typically reduces both heating and cooling duties that outweighs the additional power for compression, its merits and cost-benefit analysis should be evaluated by taking capital and operating costs into account. As

a rule of thumb, the temperature lift in the process stream through MVR should be restrained to avoid extensive use of compression.

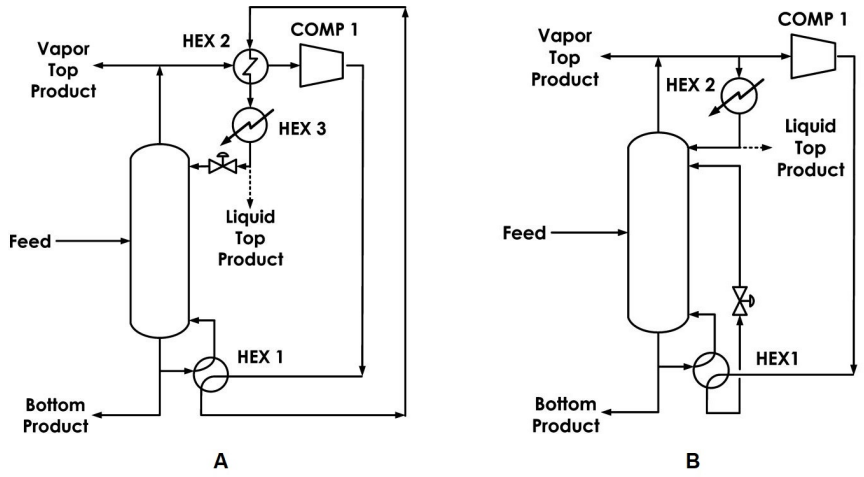


Figure 2.5. Examples of implementation of MVR systems in a distillation column: (A) increasing enthalpy; (B) increasing flowrate. COMP strands for compressor; HEX stands for heat exchanger. Pictures reprinted from Shenvi et al. (2011).

Another type of heat pump worth mentioning is the absorption refrigeration cycle, which is primarily driven by external thermal energy. Unlike the MVR heat pump, absorption refrigeration cycles use two fluids, namely a working fluid and an absorbent. While the compressor in MVR is used to circulate the working fluid, absorption refrigeration cycles use the absorbent to provide a pressure difference, through dissolution and stripping of the working fluid (EL-Halwagi, 2012). Traditionally, the study of heat pump implementation is outside the context of process electrification; rather, its consideration is mainly for the purpose of process integration. Given the fact that heat pump implementation eliminates process heating at a cost of electric power, it can be considered a technology for electrification.

2.2.2 Strategy

Depending on the objective, the electrification of chemical processes can be considered in a hierarchical manner. At the first level, process heating can be substituted with electrical heating. This strategy minimises the modification to the current

processes and benefits from a facile implementation. At the second level, fossil fuel-based feedstock or intermediate product can be substituted with electricity-based materials. The two strategies can generate variant electrification schemes, which are referred to as "Power-to-X" by Van Kranenburg et al. (2016). Depending on the final use of the produced chemicals, the electrified chemical process can also be viewed as a method for storing electrical energy. For instance, Nayak-Luke and Bañares-Alcántara (2018) reported a long-term energy storage method using ammonia as an energy carrier, in which context the produced ammonia is not only a commodity but also a vector transducing electrical energy into chemical bonds. This thinking strategy marks a new perspective of electrification, which helps to overcome the intermittency of sources such as solar and wind (Lewis and Nocera, 2006), given the fact that industrial electrification crucially relies on renewable sources.

The analysis of chemical process electrification often combines a number of strategies. As an example, Bühler et al. (2019) investigated the electrification of industrial sites, taking milk powder production as a case study. In their work, the authors proposed different electrification strategies based on the integration of heat pumps and electric heaters and compared their performance using energy, exergy, economic and environmental indicators, with results showing that the central heat pump system is the most energy-efficient strategy. While electrification analysis at a process level is important, the impact of deep electrification on the energy demand of the whole industry sector is also of significance. Lechtenböhmer et al. (2016) reported that the electrification of basic materials production in the EU would result in electricity demand of 1,713 TWh, about 1,200 TWh of which would be for producing hydrogen and hydrocarbons. Figure 2.6 shows the energy structure as well as carbon emissions before and after electrification for the production of steel, cement, glass, lime, petrochemicals, chlorine and ammonia. Clearly, the impact of electrified feedstock on energy demand significantly outweighs that of electrified heating. Another implication can be drawn from the energy allocations is that hydrogen plays a pivotal role in the context of electrification and decarbonisation, which has also been pointed out by many researchers (Lux and Pfluger, 2020).

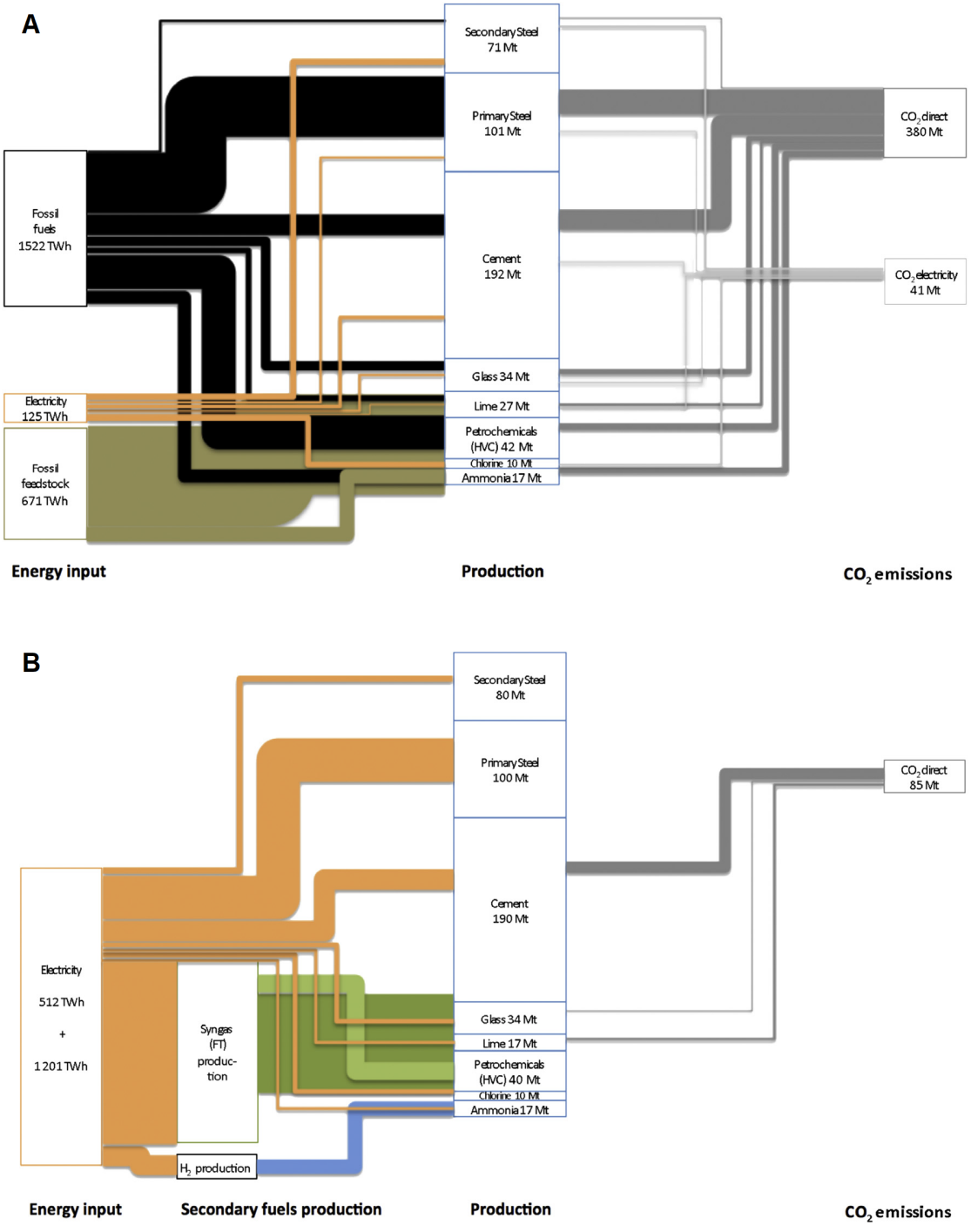


Figure 2.6. Energy input, production levels and carbon dioxide emissions for basic materials. (A) EU27 in 2010; (B) EU27 in 2050 with complete electrification of production processes. Picture reprinted from Lechtenböhmer et al. (2016).

2.3 "Green" Chemical Production

From the above discussion, it is clear that the electrification of materials, i.e. converting species at the bottom of the free energy landscape to commodity or intermediate products higher up on the free energy landscape, has a more profound impact on the energy sector. This marks a new paradigm of electrified chemical production, as depicted in Figure 2.7, meaning a requirement of innovation in process flowsheeting and production technologies. Consequently, new production processes and technologies have burgeoned in literature leading to the concept of "green" chemical production.

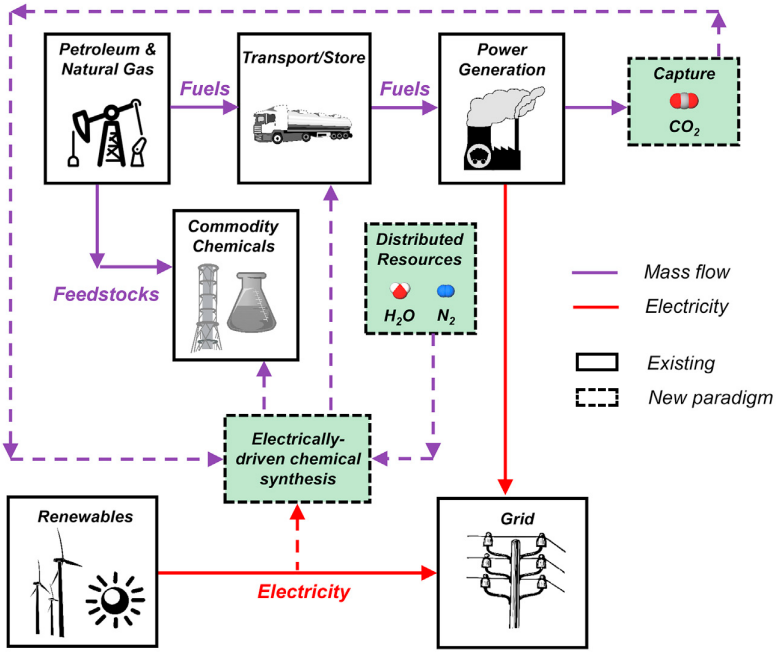


Figure 2.7. Current and envisioned coupling of the chemical and energy industries. Picture reprinted from Schiffer and Manthiram (2017).

Similar to the investigation on heat pumps, the work on "green" chemical production usually does not stress electrification. Instead, research typically emphasises the renewable sources that power the production. Since renewable energy usually takes the form of electricity, "green" chemicals can be viewed as an important element on the electrification roadmap. Depending on the final use of the produced chemicals, they may have a different role in the value chain of

renewable energy utilisation. This section focuses on a few selected key chemicals with a focus on their production, which are discussed as follows.

2.3.1 Hydrogen

Currently, global hydrogen production significantly relies on fossil fuels through processes such as natural gas reforming, oil cracking and coal gasification. Only a small fraction of hydrogen production is from electrical energy via electrolysis, often as a by-product of chlorine production. Regarding "green" hydrogen, the standard commercial technology is water electrolysis with electricity generated from renewables, which is arguably the only way to produce large quantities of green hydrogen. Other technologies such as photoelectrochemical water splitting, thermochemical reactions and biomass-to-hydrogen processes are still in the development stage (Turner et al., 2008).

An electrolyser is a device to split water using an electric current without moving parts (Holladay et al., 2009), making it one of the simplest synthesis processes. There are three main types of electrolyser available for hydrogen production, namely alkaline electrolyser, proton exchange membrane (PEM) and solid oxide electrolysis cells (SOEC) (Grigoriev et al., 2006; Pettersson et al., 2006). Although PEM and SOEC have higher energy efficiency, the alkaline electrolyser is the most well-developed technology with the lowest capital cost. In fact, when renewable energy is taken into account, energy efficiency becomes less important (from the decarbonisation viewpoint) in comparison with other technological difficulties such as device configuration and requirement of construction materials. Regarding the economics, Saba et al. (2018) reported a detailed cost analysis by comparing cost studies from the past 30 years. According to their forecast, the investment cost in 2030 would narrow towards 787–906 and 397–955 €/kW (output power based on the higher heating value) for alkaline and PEM electrolysers, respectively.

The energy efficiency of a typical commercial electrolyser ranges from 56–73 % or 70.1–53.4 $\mathrm{kWh/kg_{H_2}}$ (Ivy, 2004), while the theoretical minimum energy requirement

is 39.4 kWh/kg_{H_2} (Wang, 2006). In Contrast to thermal power generators, the specific energy requirement of water electrolysis is inversely proportional to its load fraction; in other words, the energy efficiency increases for lower loads (Leroy et al., 1980). As for the dynamic behaviour, Kopp et al. (2017) reported a ramp speed above 200 kW/s in the range of 0–4 MW. This fast response to load variation and the inverse relationship between load fraction and energy efficiency hold great promise for the variable power integration that characterises renewable sources. For example, the US National Renewable Energy Laboratory (2004) investigated the synergies from the coproduction of electricity and hydrogen to overcome the variability of wind power.

Other non-conventional pathways to produce hydrogen include thermolysis, photoelectrolysis and biomass-to-hydrogen. Thermolysis is a method to decompose water at high temperatures (Steinfeld, 2005). The challenge mainly lies in material stability at high temperatures and overall thermal efficiency (Funk, 2001). Regarding photoelectrolysis, its configuration is similar to photovoltaic (PV) technology, which is constructed based on semiconductor materials. Instead of generating an electric current, water is decomposed in a photoelectrolytic process (Karuturi et al., 2018). This technology is less well-developed and the current studies primarily focus on the materials used for photoelectrodes, which are pivotal in determining the performance of photoelectrolysis systems (Akikusa and Khan, 2002; Licht, 2003; Mor et al., 2006). Biomass-to-hydrogen pathways include several process options such as thermochemical (gasification/pyrolysis) and biological routes (fermentation). Each technology has its own limitations but the major barriers for biomass utilisation are the seasonal availability of feedstock and the high costs of handling (Demirbas, 2004).

Owing to the limitations of the non-conventional pathways, most of the existing literature about "green" hydrogen production focuses on water electrolysis with renewable electricity. In the seminal work of Levene et al. (2007), it is reported that the cost of renewable hydrogen ranges from 4.09–5.40 $/kg based on a production rate of 1,000 kg/day with electricity price being the dominant factor. To allow a competitive renewable hydrogen price (i.e. close to 2 $/kg), electricity prices would

have to be less than 0.01 $/kWh (Levene et al., 2007). Shaner et al. (2016) provided more insights into renewable hydrogen production using solar energy. From their base case techno-economic model, the levelised costs of 6.1 and 12.1 $/kg were reported for the hydrogen produced from solar PV (coupled with PEM electrolysers) with and without grid connection, respectively. It is interesting to see that the authors reported system efficiency being the greatest contributor to cost reductions, contradicting what Dennis et al. (2016) has been advocating from the environmental perspective. A possible explanation may be the omitted correlation between energy efficiency and technology capital cost, without which the sensitivity test would generate biased results.

When variable renewable sources are incorporated, grid supplemented systems have clear advantages for electrolytic hydrogen production due to the added flexibility. As a counterpart of this strategy, electrolytic hydrogen may be produced from excess grid electricity. Although this route does not power the hydrogen production with renewables directly, the excess electricity from the grid is usually a result of variable renewable power generation, which would be curtailed otherwise. Thus, the hydrogen produced from the excess electricity is also considered to be "green". An example of such a strategy was demonstrated by Simonis and Newborough (2017) as a case study of Germany, in which hydrogen admixtures were produced and injected into the gas grid. Both direct and indirect renewable-enabled hydrogen production rely on the flexibility of electrolysers, which are able to operate at varying loads with fast responses. Several studies have explored the opportunity of using this feature to reduce hydrogen production costs, such as the work of Mansilla et al. (2011) in the French context, Jørgensen and Ropenus (2008) in the Danish context and Naterer et al. (2008) in the Canadian context.

Although most of the above literature points out that it is currently infeasible to provide sufficient cost reductions to allow "green" hydrogen to compete with the hydrogen produced from fossil energy (barring a few studies using extraordinary renewable sources), it is believed that hydrogen is placed at the centre in the context of industrial electrification and "green" chemicals since it is an important vector for many other chemicals (Hu et al., 2020). Therefore, cost reductions and technological

advances for "green" hydrogen production, no matter what pathways, are of special interest from socio-economic, environmental and engineering perspectives.

2.3.2 Ammonia

As the world second most-produced industrial chemical (Cheema and Krewer, 2018), ammonia and its clean production have drawn significant attention. Currently, ammonia production relies heavily on natural gas feedstock, accounting for approximately 1.6 % of the global fossil fuel consumption (Appl, 2006). On the other hand, the classical production method—the Haber-Bosch process—itself has the capability of clean production provided that the hydrogen feedstock is synthesised from renewable energy sources. Clearly, the production of "green" hydrogen is a key precursor to "green" ammonia (Brown, 2019). Yet, ammonia production from renewables has its own challenges and opportunities. For instance, for the application of energy storage in the form of high heating value chemicals, ammonia has clear advantages over hydrogen, such as facile transportation and lower storage cost. Nevertheless, ammonia production requires careful planning and unit sizing when variable renewable power is integrated, as the synthesis process is much more complex than hydrogen production.

Since water electrolysis powered by renewables is arguably the most promising pathway for "green" hydrogen synthesis, the vast majority of the existing literature on "green" ammonia production also includes electrolysis in the analysis. Figure 2.8 schematically illustrates three main analysis envelopes presented hierarchically with respect to robustness for "green" ammonia production. The simplest boundary (Figure 2.8A) excludes the interaction between energy sources and production processes, i.e. the power supply, no matter renewable or not, is fully dependable. This type of analysis envelope is similar to a "thought-experiment" of energy analysis (Lechtenböhmer et al., 2016), which provides quick and yet sufficient information to the general public and policymakers. A recent example was demonstrated by Fúnez Guerra et al. (2020), in which the authors reported a techno-economic model of "green" ammonia production focusing on the sensitivity analyses of key

variables, such as ammonia sales price, electricity cost and facility size. However, this work lacks considerations at a process level, which is of interest from a systems engineering viewpoint.

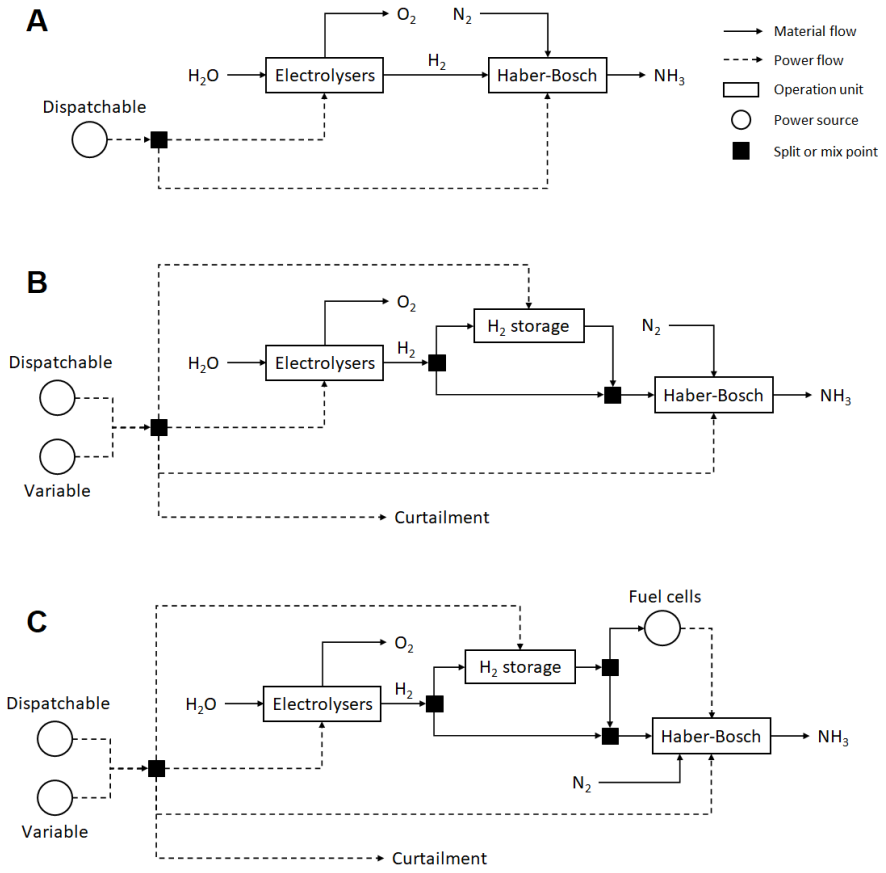


Figure 2.8. General process flowsheet for ammonia production using hydrogen from water electrolysis. (A) Simple process with a fully dependable power source. (B) Process including variable power sources and using hydrogen storage to accommodate the variability. (C) Process using hydrogen storage with fuel cells to accommodate the variability.

The major challenge of renewable chemical production is the variability of renewable sources. Thus, a simple analysis envelope using renewable but fully dependable power supplies is inadequate. To this end, Allman and Daoutidis (2018) proposed a model of wind-powered ammonia production that includes hydrogen storage to address the variability of the renewable source. In other words, excess hydrogen can be produced and stored during power surplus and then consumed during power deficit. The purpose of the hydrogen storage is to balance the mismatch between power supply and demand, which can be used in conjunction with a backup dispatchable power source (see Figure 2.8B). The additional means

of power balancing allow a competition between hydrogen storage and dispatchable power, which is of special interest for both economic and environmental assessments. The sustainability of the ammonia production system can be further improved by using hydrogen fuel cells (see Figure 2.8C). Nayak-Luke et al. (2018) referred to this strategy as material "cannibalisation", which enables the system to convert hydrogen—a high heating value, intermediate product—to power in order to sustain a minimum production rate during power deficit. This method, of course, entails a lower overall energy efficiency; however, it is essential for islanded systems located in remote areas where process sustainability and resilience become the top priority. In addition to islanded operations, the inclusion of hydrogen full cells may also be beneficial for the grid-connected system: the dispatchable power from the grid (usually very expensive), excess hydrogen production (storage is costly) and fuel cells (low energy efficiency) have their own limitations; thus, an additional option to address the variability of renewables is always a plus provided that careful planning and sizing are considered.

From the studies of renewable hydrogen production, it is obvious that flexible electrolysers are highly beneficial when variable renewable sources are integrated. This also holds true for ammonia production even though the ammonia synthesis itself is much less flexible. An example of such a study was demonstrated by Armijo and Philibert (2020), wherein the flexible production of both hydrogen and ammonia from variable solar and wind energy located in Chile and Argentina was investigated. The 0results suggest that the synthesis flexibility can reduce the hydrogen storage requirement, thereby reducing the production cost. Apart from the synthesis flexibility, the authors also stressed the importance of complementary renewable sources for a reduced overall variability in the power supply. Note that the stored hydrogen serves for multiple purposes: (1) a feedstock for ammonia synthesis; (2) an energy carrier (storage) for excess renewable power; and (3) an intermediate product to address the flexibility mismatch between electrolysis and ammonia synthesis. The last functionality of hydrogen is rarely mentioned by researchers, probably due to the fact that concurrent flexibility of different operation units at every time interval would never exist.

As discussed above, an analysis at a process level is of particular significance. Moreover, considerations at a unit level are also of interest. Beerbühl et al. (2015) presented a more sophisticated model of combined scheduling and capacity planning taking the variable electrolyser efficiency into account, whereas a vast majority of other studies assumed a constant efficiency. This detailed analysis is particularly beneficial because electrolyser efficiency is reversely proportional to its load, thus motivating a flexible operation with excess capacity. While this consideration provides a more accurate result, it also poses additional difficulties in modelling and optimisation.

Although it is widely believed that hydrogen feedstock from water electrolysis is the most promising source for "green" ammonia production, previous work rarely explores the gap between different pathways. Frattini et al. (2016) reported an energy evaluation of different renewable pathways including hydrogen from biomass gasification, anaerobic digestion and water electrolysis. Although the authors concluded that all three pathways have similar specific energy consumption, the work lacks an economic analysis. Moreover, if the electric equivalence ratios method were applied, the energy consumption of the electrolysis-based ammonia would be higher. Regarding the economics of the three pathways, Tunå et al. (2014) reported biomass-based ammonia being the cheapest, whereas electrolysis and biogas-based ammonia are much more expensive. However, it should be noted that this particular example assumed to use grid-based electricity to power ammonia production, which is not a cost-minimised case study. It is also noteworthy that the other feedstock for ammonia synthesis—nitrogen—is usually out of research interest because it can be easily obtained from the atmosphere with low energy consumption. Thus, very few little work focuses on nitrogen synthesis pathways in the context of "green" ammonia production.

2.3.3 Methanol

Traditionally, methanol is produced by the Fischer-Tropsch process, where syngas (a mixture of hydrogen and carbon monoxide) reacts in a catalytic reactor. Similar

to the current status of ammonia production, industrial methanol production is mostly fossil fuel-based, i.e. syngas is produced from either natural gas reforming or coal gasification. The global methanol installed capacity is significant. It has been growing steadily since 2009, reaching 60.6 million tonnes in 2013 (Methanol Market Services Asia, 2013), and is expected to triple by 2050 (Philibert, 2017), with China accounting for 50 % of the worldwide capacity and consumption (IHS Markit, 2017). Although electrolytic hydrogen is regarded as the easiest pathway for transducing renewable power into chemical bonds, there remains a motivation to further convert hydrogen to more convenient fuels, due to its costly storage and transportation. While ammonia offers a carbon-free route to store hydrogen, methanol is another option involving the chemical recycling of carbon—both pathways are important. Storing hydrogen in methanol has been advocated by Olah (2003) for almost two decades. Nielsen et al. (2013) also demonstrated an example of hydrogen retrieval from methanol for mobile device applications, showing a promising future for such a concept. Owing to the above reasons, the investigation of methanol production from renewables is imperative.

The most promising pathway of "green" methanol production is through carbon dioxide (CO_2) hydrogenation, with hydrogen obtained from renewables and CO_2 captured from flue gases. As an example, Van-Dal and Bouallou (2013) designed a methanol production plant through CO_2 hydrogenation and analysed the performance from energy-use and environmental perspectives. The CO_2 balance of the process shows an abatement of 1.6 kg/kg_{MeOH} provided that hydrogen is produced by water electrolysis using carbon-free electricity. Whilst this work focused on the carbon balance, Perez-Fortes et al. (2016) assessed the economic potential of the same methanol production process, reporting a break-even price of 723.6 €/tonne (or 881 $/tonne). Matzen et al. (2015) further explored the methanol production cost using a range of hydrogen price. Gonzalez-Garay et al. (2019) provided more insights into the cost breakdown using hydrogen and CO_2 from various sources, reporting a range of projected production cost from 743 to 2,045 $/tonne for 2030.

All the studies above have a limitation in common: a price was assigned to the hydrogen from different sources but its generation and how it would affect the

methanol production were not discussed, thus lacking a holistic view of "green" methanol production. Some studies specified the hydrogen production routes and took the cost of renewable power generation into account; however, the variability of renewable power supply was not addressed, with examples being the work of Kim et al. (2011) and Alsayegh et al. (2019) using solar power and Bos et al. (2020) using wind power. Hank et al. (2018) complemented the knowledge gap by using a highly novel concept of dynamic systems, which enables the methanol production process to react effectively to the variable power input. The significance of this work lies in the analysis boundary taking the variability of renewable power into account, of which the challenge is addressed using hydrogen storage and dynamic synthesis (see Figure 2.9). However, the work approached the problem using a scenario-based method along with specified parameters without sound justifications. For instance, the size of electrolysers was fixed at 12 MW and hydrogen storage size was investigated at selected values. Given that there has been much interest in the mechanistic insights of how unit sizes impact the overall production process, optimised power scheduling and capacity planning using a modelling approach is highly desirable. Furthermore, the competing role of hydrogen storage and heat integration as well as the management of plant-wide heat integration in the context of variable synthesis are interesting questions yet to be answered.

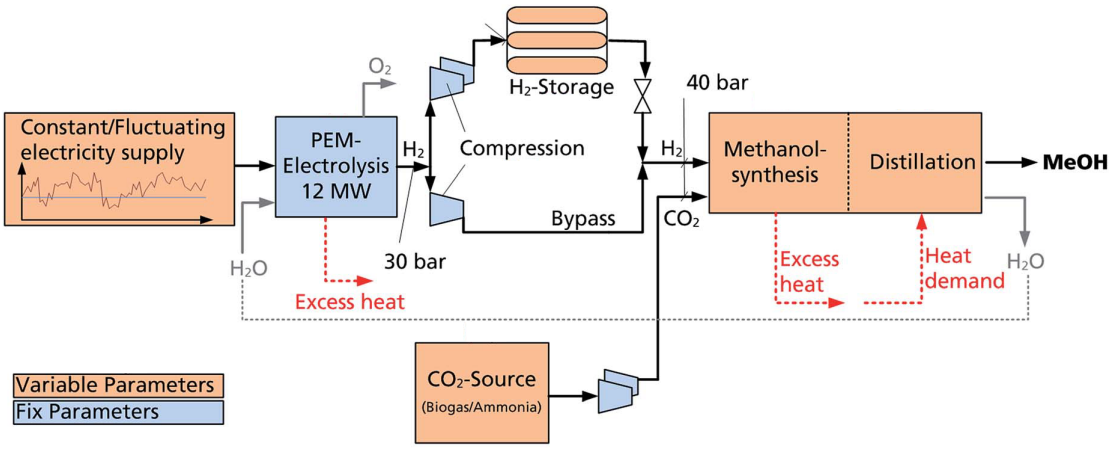


Figure 2.9. The production of methanol based on renewable energy taking supply and demand balancing into account. Picture reprinted from Hank et al. (2018).

From the financial assessment, it is clear that "green" methanol is economically unfavourable based on the current market prices. However, Perez-Fortes et al.

(2016) has shown a positive net present value in their work when the hydrogen price decreases by 2.5 times or the CO_2 value increases to 222 €/tonne (or 270 $/tonne). This implies a necessity for policy implementations in order to achieve the energy transition and meet environmental targets. In addition, Philibert (2017) also argued in his report that methanol production through water electrolysis would be close to being able to compete with the natural gas reforming process, providing excellent renewable sources are incorporated. Thus, it is envisioned that a global analysis taking the renewable source quality into account would be of special interest. This analysis has recently been reported by Nayak-Luke and Bañares-Alcántara (2020) for "green" ammonia, and yet to be reported for methanol production.

It should be noted that a substantial number of extant studies focus on improving traditional methanol production and achieving partially "green" production. Examples are analyses of the syngas process using high CO_2 content natural gas (Cañete et al., 2018, 2014). The economic potential of such a concept is usually better than that of methanol from electrolytic hydrogen. The partially "green" production is made possible because of the chemical recycling of CO_2—the consumption of itself can enable "green" production without taking syngas or hydrogen into account. In contrast to the nitrogen feedstock for ammonia synthesis, which is of little research interest, many initiatives are underway to focus on CO_2 capture and storage (Mores et al., 2012). Currently, post-combustion capture (PCC) for CO_2 is considered to be the most promising technique due to its advantages in facile process integration and modification (Freguia and Rochelle, 2003). Since the PCC technique captures CO_2 from large stationary facilities involving fossil fuel combustion (e.g. power plants), it may face diminishing flue gas sources in a future scenario of highly renewable industry. Direct air carbon capture may offer a solution in this regard, although it has been deemed impractical (by some researchers) due to its unrealistic energy and materials requirement (Chatterjee and Huang, 2020).

Apart from CO_2 hydrogenation, electrochemical reduction of CO_2 is also a feasible route for "green" methanol production. Examples are provided by Yamamoto et al. (2002), who investigated the production of syngas from CO_2 using an electrode-based electrolytic cell, and Ampelli et al. (2011), who reported a novel CO_2-to-fuel

approach based on a photo-electrochemical process, combining the utilisation of CO_2 and renewable energy sources. However, there are too many issues that have to be addressed, including cathode materials (Velu and Suzuki, 2003), cell/electrode configurations (Gattrell et al., 2006) and an improved understanding of reaction mechanisms (Ganesh, 2014; Peterson et al., 2010).

2.3.4 Chemicals in energy storage

The traditional energy storage technologies, such as batteries, pumped hydro and compressed air have been reviewed previously (Beaudin et al., 2010; Koohi-Fayegh and Rosen, 2020). Here, renewable energy storage combining chemical processes is highlighted, which is often referred to as "Power-to-Chemicals". Naturally, this concept largely overlaps the "green" chemical production with differences in the final use, i.e. used for energy purpose or sold as a commodity. An example of the overlap can be illustrated by the value chain of hydrogen in renewable energy systems: while grid supplemented system helps to accommodate the variability of renewable sources used in hydrogen production, electrolytic hydrogen also improves the sustainability of an electricity network integrated with variable renewable sources (Hwangbo et al., 2019).

Samsatli and Samsatli (2019) reported the use of renewable hydrogen in heating sectors in the UK and explored its role in inter-seasonal storage. The results suggest an optimal pathway to heat using 20 % hydrogen and 80 % electricity. Another example of using hydrogen as an intermediate energy carrier in a large-scale energy system has been demonstrated by Gutiérrez-Martín and Guerrero-Hernández (2012). In this case study focusing on the Spanish power system, hydrogen is produced via electrolysis during power surplus and reintroduced into the grid during power deficit, thereby balancing the grid loads. This method can reduce GHG emissions by minimising the excess provision of grid electricity, i.e. the overall energy efficiency is higher. Although using electrolytic hydrogen benefits from the flexible synthesis process, hydrogen storage requires significant compression work and expensive materials for the containers. In addition, its potential leakage also poses additional

safety issues. Thus, there is a motivation to convert hydrogen to liquids to meet the long-term and large-scale storage needs.

Both ammonia and methanol are promising alternative energy carriers in the context of renewable energy storage. However, much of the current literature has emphasised ammonia rather than methanol, probably due to the more complex synthesis processes for the latter. Regarding ammonia, Giddey et al. (2017) estimated the round-trip efficiency (RTE) of different routes for ammonia utilisation in the endpoint use. For residential applications, the best scenario gives an RTE of 50 %, and 21 % for the automotive sector. Wang et al. (2017) also analysed the power-to-ammonia-to-power concept based on a 100 MW system under time-invariant operation, with an RTE as high as 72 % and a levelised energy cost of 0.35 $/KWh, or RTE at 64 % with 0.24 $/kWh. However, neither of the studies had taken renewable variability into account.

Recently, Palys and Daoutidis (2020) complemented many research gaps by analysing the economics of both hydrogen and ammonia storage for islanded renewable energy supply systems in multiple American cities. The work concluded that the systems that use a combination of both chemicals outperform those that use only one storage option, and ammonia is generally more economical than hydrogen as a single vector for energy storage. Depending on the location, the overall levelised energy cost for a fully renewable system using both hydrogen and ammonia storage ranges from 0.17 to 0.28 $/kWh, which is comparable to today's energy cost.

In the aspect of renewable power management, considerations are often nested. For instance, storing energy in the form of chemicals is a method to mitigate the variability of renewable sources, but the power-to-chemical process itself requires in-process energy storage. The difference is that the excess power means differently in various scenarios: in the power-to-chemical concept, the excess power refers to a location with ample renewable sources but few end-users. Regarding the in-process energy storage, the excess power refers to the otherwise curtailed power that cannot be consumed downstream. These nested and strongly related considerations

incorporating renewable sources stimulate an expansion of the analysis envelope to cover renewable energy systems. In addition, the cost of renewable power generation contributes significantly to the production of "green" chemicals (Kim et al., 2012), meaning that it is inadequate to consider the production processes alone.

2.4 Renewable Energy Systems

Currently, most research in the literature focusing on renewable energy systems mainly aims to address the variability of renewable sources. Reduced variability in power output means fewer low or high power times, thus improving the reliability and reducing the levelised energy cost. As shown in Figure 2.10, there are two main targets for the energy systems involving variable renewable sources, namely (1) balancing the power mismatch between supply and demand and (2) achieving a levelled or controlled power output. Although the techniques to achieve these targets largely overlap, their role in variable power management is different.

In typical contemporary electricity networks, dispatchable generation such as nuclear and fossil fuel-based power plants account for a significant portion of the baseload. Thus, the electricity network is able to respond to the variable end-use sectors. However, in a future scenario of a highly renewable electricity network, the increasing share of variable sources would result in a more significant mismatch between power supply and demand, thus requiring additional mitigation techniques (see Figure 2.10A). Although the mechanism of these techniques varies, they all aim to balance power supply with demand. Another important area of study is the design of distributed renewable energy systems for a standalone application, such as chemical production (see Figure 2.10B). The management of distributed renewable energy systems aims to provide a controlled (or levelled if the end-use load is a constant) power output to meet a load requirement. Note that the technique of using backup dispatchable power sources for levelling power output resembles a hybrid electricity network. The difference between the role of management

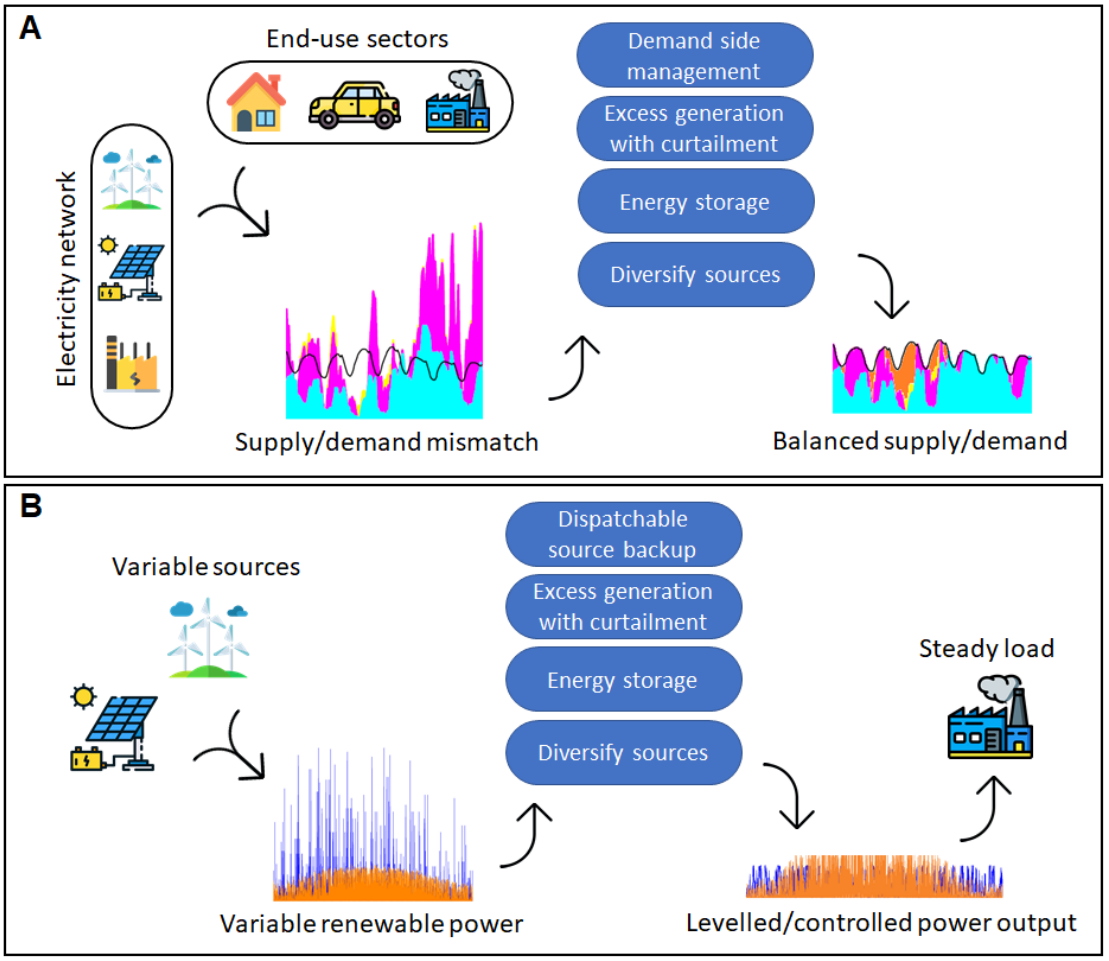


Figure 2.10. General considerations undertook in renewable energy system. (A) Balancing supply and demand for a highly renewable power network; (B) levelling renewable power generation for dedicated end-users.

techniques depends on the end-use application, the priority of aims and the specific challenges that need to be addressed. The following sections review the literature focusing on renewable energy systems from the viewpoint of the role of management techniques in addressing renewable source variability. Note that it is common to use a combination of techniques to manage the variability of renewable energy systems since synergistic effects may exist.

2.4.1 Levelling power output

Since each renewable source at a specific location has a unique intermittent pattern, aggregating renewable supply curves of different sources is an effective way to reduce the overall variability. Archer and Jacobson (2007) investigated the benefits

of interconnecting wind farms based on 19 sites located in the midwestern US. The authors reported reduced overall intermittency due to the reduced correlation of wind speed among the sites, i.e. the probability that all sites experience the same wind regime at the same time would be very low. Naturally, more connected farms across a wide area would always reduce the intermittency, but this improvement grows sublinearly as the number of interconnected sites increases. Although there are studies demonstrating an improved power steadiness when the renewable sources are relatively close (Milligan and Factor, 2000), proximate renewable sources would have fewer benefits compared with generators interconnected over longer separation distances (Kempton et al., 2010). This is attributed to local forcing conditions, which often lead to similar weather at the same time for two adjacent locations. While it is clear that diversifying the locations of renewable energy farms is beneficial, different combinations of geographically distributed renewable sources may bring diverse benefits (Milligan and Factor, 2000). A systematic analysis of how best to select locations has not yet been performed and may be of interest for future studies.

Similar to using geographically distributed renewable sources, diversifying the sources can also achieve the same target (i.e. levelling power output). If the selected sources have complementary supply curves, the economics is much better. For example, the aggregated wind power across Europe is much stronger in winter than in summer. The opposite is true for solar power generation. As a result, a mix of these sources is able to counterbalance the individual variability (Heide et al., 2010). Moreover, energy storage is another important method to mitigate the variability of power output. These methods may be used together to enhance the overall performance. As an example, Ekren and Ekren (2008, 2010) reported a series of studies focusing on dedicated renewable energy systems for a standalone application, in which the renewable power output from wind and solar sources is levelled using battery storage. A novelty of their analysis is the comparison with the same standalone application but powered by the grid. When the transmission cost is taken into account, the results show improved economics of dedicated renewable power systems for operation in remote areas (Ekren et al., 2009).

The importance of dispatchable power backup was highlighted by a pioneering work of Celik (2003), before which the reliability and sizing of variable renewable energy systems were commonly analysed based on the worst period scenarios, leading to overly costly designs. The source of dispatchable power is usually the grid and on-site diesel generators, which provide backup power during low renewable power times. Although dispatchable power sources can be fed from renewables, they have their individual limitations, e.g. end-use applications located in remote areas are unable to access the grid.

In the context of renewable energy utilisation, voluntary curtailment caused by excess generation is inevitable (Jacobsen and Schröder, 2012). Both social and economic optimality often lead to the excess provision of renewable energy, thereby overcoming the variability of renewable sources. The analysis of dedicated renewable energy systems rarely focuses on renewable power over provision. In contrast, excess generation and the resulting curtailed power are often investigated in the context of a larger electricity network with a focus on balancing the power supply and demand. Although excess power generation reduces the balancing needs, it also enhances the mismatch. Therefore, this method (i.e. generating excess renewable power) is usually a result of the optimal design when all other mitigation techniques have already been considered. The roles of excess generation along with other mitigation techniques in electricity networks are discussed in the following section.

2.4.2 Balancing power supply and demand

Renewable systems designed with an excess generation capacity can improve the reliability of power supply by reducing balancing needs. The overall economics depends on the trade-off of the saving from reduced storage costs and the additional capital investment for an excess capacity. Using a simplified European power system based on wind and solar generation only, Heide et al. (2011) quantitatively analysed how storage and balancing needs change with respect to excess renewable power generation and the renewable source mix, as demonstrated in Figure 2.11. Although

excess generation capacity can reduce both storage and balancing needs, further increase has diminishing effects on both factors. Despite the diminishing importance of excess generation, energy systems with a high level of renewable penetration often require a minimum excess generation capacity, below which the end-use sectors may encounter insufficient power supply due to the energy losses from storage (see Figure 2.11B, wherein the empty space indicates insufficient power supply).

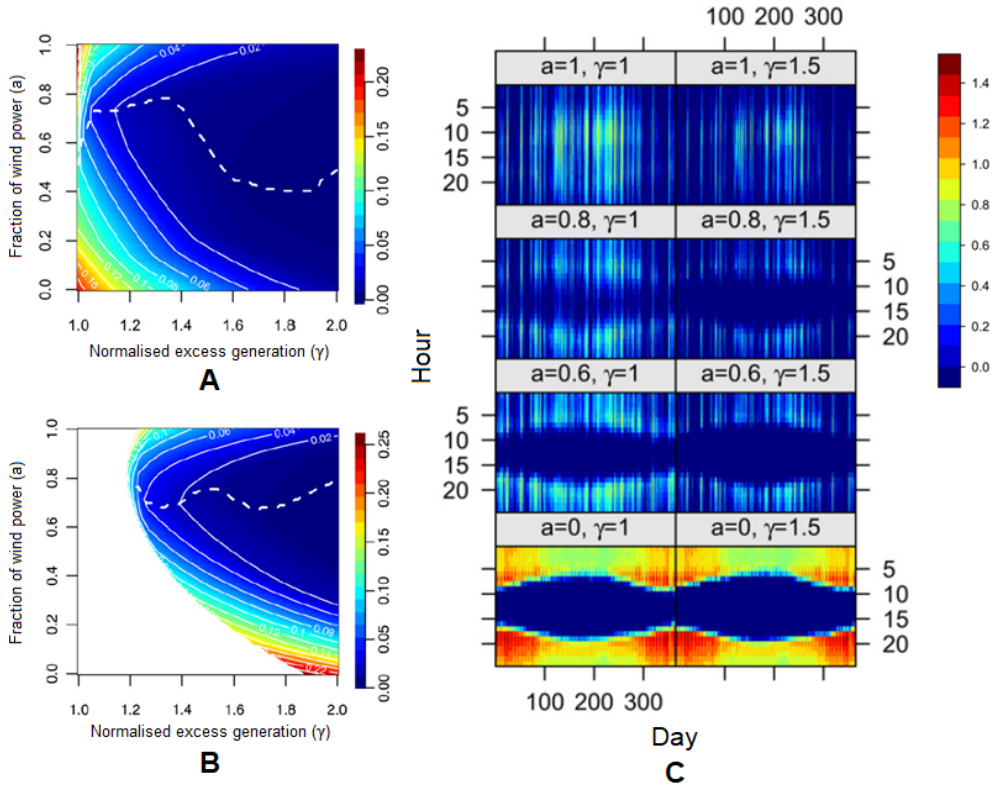


Figure 2.11. Storage and balancing needs as a function of renewable mix and excess generation. (A) Storage capacity without any energy loss; (B) storage capacity with a round-trip efficiency of 36 %; (C) fluctuation pattern of balancing power over all hours (y-axis) and days (x-axis) within on arbitrary year. The white dashed lines in A and B indicate the minimum values. Picture reprinted from Heide et al. (2011).

Rasmussen et al. (2012) analysed the same system from a different viewpoint: what is the correlation between storage and balancing needs? The authors explored the question by minimising the balancing needs for one given storage size, thereby reporting a hard upper limit on their synergy. Significantly, a small storage size equivalent to 6 hours of average consumption is able to reduce the balancing needs by 60–90 % (depending on the overall energy provision) due to the elimination of the largest impact of the intraday mismatch. These mechanistic insights have profound

implications, which motivate policymakers to stratify the storage needs; for instance, efficient but expensive storage technologies, such as batteries, shall be implemented for intraday balancing, whereas economical but less efficient technologies, such as storage in the form of chemicals, shall be used for seasonal balancing. Nevertheless, all of the above studies did not consider the economics of renewable energy systems.

Budischak et al. (2013) modelled and incorporated multiple renewable sources and storage methods into a large grid system covering one-fifth of the US electric grid. The authors indicated that excess renewable power generation is a competing factor to the storage capacity. The results have shown that the electric system can be powered 90–99.9 % of hours entirely on renewable electricity at costs comparable to today's, ranging from 90–250 $/MWh. Moreover, a profound finding indicates that the minimum levelised energy cost and excess renewable generation increase exponentially with respect to the increase in renewable penetration. For instance, it is found that a system providing 30 % renewable penetration requires average excess power of 1.2 GW, 90 % requires 31.7 GW and 99.9 % requires 56.9 GW. However, the analysis was performed using the selected levels of renewable penetration, thus lacking a holistic view of the correlation between the factors.

For large-scale systems, geographically interconnected renewable sources may have additional benefits other than levelling power output. As demonstrated by Sinden (2007) in a case study of the UK wind resources, the aggregated wind power in the UK has shown a supply curve concurrent to the electricity demand pattern. The concurrent supply and demand curves can be achieved alternatively through demand-side management (DSM), which reduces the balancing needs. The techniques, benefits and challenges of DSM have been discussed in depth by Strbac (2008). Another example of using various renewable sources at multiple geographically dispersed sites has been demonstrated by Hart and Jacobson (2011), in which a model of a high penetration variable renewable energy system integrated with the grid was analysed. A portfolio analysis based on a California operating area showed that the system is capable of providing 99.8 % of generation with renewables. The authors also stressed the importance of demand response in balancing power mismatch.

Note that when an electricity network approaches 100 % renewable, its analysis becomes similar to that of distributed renewable energy systems dedicated to standalone applications. The boundary dividing the analysis may be indicated by the composition of baseload power in a network: the analysis would focus on balancing the supply and demand mismatch if the baseload power is dominated by dispatchable generation. On the other hand, distributed renewable energy systems use dispatchable power only as a backup. Large-scale power systems often require constant baseload generators to provide electricity in a stable and reliable manner. As a result, these generators are usually powered by coal, natural gas and nuclear fuels. Renewable power alone is unable to fulfil these requirements. Nevertheless, Denholm et al. (2005) analysed wind power systems combined with energy storage in the midwestern US as a viable alternative to provide electricity supply that is equivalent to conventional baseload generators. Based on the same location, Archer and Jacobson (2007) provided a numerical recommendation that 33–47 % of yearly averaged wind power from interconnected farms can be used as reliable, baseload electric power. Although the environmental and energy efficiency assessments of such a system have shown a significant improvement, the economic feasibility was not reported.

2.5 Challenges and Perspectives

From the above analysis, it is clear that the current barrier in electrification and renewable energy utilisation is the variability that characterises the renewable sources, which leads to management difficulties as well as high levelised energy costs. Although there are various measurements implemented to tackle the variability, very few methods are available to quantify the characteristics of renewables in the current literature. One method to quantify the variability of renewables is the use of standard deviation (Holttinen et al., 2008), which by-and-large indicates how variable the sources are over a period of time. It is however unable to characterise the type of variation, i.e. intraday or seasonal. Without a sound quantification of renewable source characteristics, researchers often need to perform a case-specific

analysis to draw implications for policymaking, thus lacking generalisability to other locations or type of systems.

Regarding renewable energy systems, a significant challenge lies in the balance of the trilemma: renewable penetration, reliability and economics—an improvement of one factor is often at a cost of the other two. For instance, energy systems with highly renewable power are desirable from the environmental perspective, but are likely to be overly costly (at current technology costs) and less reliable (due to variable sources). While reliability can be improved by using backup dispatchable sources, such improvements incur significant costs due to the increasing number of start-ups for a highly renewable power network (Schill et al., 2017). The marginal environmental gain and its impact on economics have been touched on (Budischak et al., 2013), but far less than what policymakers would expect to know. Similarly, the reliability of variable renewable systems is often evaluated based on the loss-of-hour analysis, but its subsequent impact and quantification of reliability requirement are rarely reported. For these reasons, studies leading to robust and sound evaluation metrics are imperative to both policymakers and corporate decision-makers. This involves the quantification of externalities and social benefits, which are however highly variable in different contexts.

At the technology level, the specifications, and in particular, the economic parameters require further attention. The accuracy and preciseness of techno-economic models of renewable energy systems greatly rely on these data, which vary significantly from different sources. While technological advances and policy shift influence the performance and cost of a particular technology, locations, scales and manufacturing volume also have to be taken into account. As a related issue, the dynamics of markets may be another factor that has never been considered; for instance, the fast transition towards a renewable industry may lead to very low demand of fossil fuels, its implication on the prices is of special importance to the work focusing the economic incentives. Thus, it can be foreseen that a holistic analysis from both social and techno-economic perspective is required in future work.

Chapter 3

Electrification Schemes for Methanol Production



HIS chapter aims to explore the electrification of chemical industry taking the production of methanol as a case study. A reference process, with a basis of 400,000 tonnes per annum, is first simulated in Aspen Plus to produce methanol via traditional natural gas reforming. As an indirect electrification strategy, a non-conventional carbon dioxide hydrogenation methanol plant is then designed to substitute fossil fuel feedstock. Standalone heat pumps are implemented as a direct electrification method in both processes at various extents generating different scenarios. It has been found that direct electrification has a small impact on energy consumption in all scenarios. In the reference process, direct electrification can only substitute 7.1 MW of heating, accounting for 7.8 % of the total heating. In contrast, the energy structure of the indirectly electrified process is completely changed from the reference process: (1) very high-temperature heating is eliminated; (2) electricity consumption is increased from 14.2 to 604.1 MW due to feedstock (hydrogen) synthesis. Renewable energy penetration and electricity price are taken into consideration when financial and environmental assessments are performed. At approximately 88 % of renewable penetration, carbon neutrality is achieved in the indirectly electrified process. The net present value of the indirectly electrified process breaks even at an electricity

price of 25 $/MWh and exceeds its counterpart reference process at 3 to 5 $/MWh. This analysis will enable the integration and management of renewable energy for methanol production and will facilitate future studies in the electrification of chemical production.

3.1 Introduction

There are many types of electrification that can be implemented in the current chemical industry. Van Kranenburg et al. (2016) proposed a Power-to-X scheme in their white paper to categorise electrification into four types. However, this work simplifies the categorisation to direct and indirect electrification: direct use of electricity in a chemical process to provide heating and mechanical work or indirect use to synthesise alternative feedstock with higher energy content. This is justified by the fact that fossil fuel dependency is determined by its energy and/or feedstock requirements (Nayak-Luke et al., 2018); however, it is impossible to completely substitute fossil-based feedstock with electricity. Many chemicals, such as ethylene, propylene, and aromatics, are produced from crude oil or other complex organic molecules. Without substantial innovation, the fossil-based feedstock will continue to play a vital role in chemical production. On the other hand, hydrogen (H_2) from electrolysis has demonstrated a great promise for the energy transition. In conjunction with carbon dioxide (CO_2) capture and air separation technologies, energy vectors such as methanol (MeOH) can be synthesised, paving the way to a zero-carbon industry in the future.

In addition to chemical production through hydrogenation, routes such as direct electro- (Peng et al., 2018) and photo-catalytic (Zhao et al., 2009) reactions to synthesise chemicals also represent highly electrified processes. However, they are excluded from this work due to scalability and economic feasibility. Regarding direct electrification for process heating, the simple replacement of heating using electricity is inefficient; thus, this work focuses on the implementation of heat pumps to facilitate process heat integration. The implementation of heat pumps

requires minimum modification to current industrial processes, as opposed to the indirect electrification scheme. Therefore, to explore the potential of electricity in chemical production, an analysis of direct and indirect electrification schemes is proposed.

The idea of direct hydrogenation is not new and has been largely demonstrated in MeOH synthesis. For instance, Van-Dal and Bouallou (2013) proposed a conceptual design to produce MeOH from CO_2 hydrogenation. In light of this work, Perez-Fortes et al. (2016) evaluated the performance of such a plant based on environmental and economic metrics. Bukhtiyarova et al. (2017) and Deng and Adams (2018) also investigated the production of MeOH from high CO_2 content sources. In a more recent work, Alsayegh et al. (2019) reported CO_2 hydrogenation to produce MeOH with an innovative process layout. This idea also holds great potential for a large variety of chemicals (Arakawa, 1998) and appears the most promising synthetic application (Aresta and Dibenedetto, 2007). All of these studies focus on carbon capture and utilisation and specific catalytic reactions but lack a holistic view of chemical process electrification and its implications, i.e. alternative electrification options are not considered and the energy structure of an electrified process remains unexplored. This gap prevents or at best inhibits the introduction of renewable energy sources (RESs) in MeOH production (or any other chemical processes) as the current designs are not scoped for electrification. Harnisch et al. (2015) reported the electrification of bioelectrochemical systems and analysed its economic potential; however, this work is hardly applicable to the wide chemical industry.

In a recent study, Nayak-Luke and Bañares-Alcántara (2018) quantified the requirement of RES storage for a fully electrified process and utilised this method to demonstrate the design of "green" ammonia production powered by RESs. Such a concept for MeOH production is still missing at present. However, to consider the utilisation of RES the electricity and/or energy consumption at a process level is required. The importance of electrification and fuel switching has been demonstrated in end-use sectors (Ebrahimi et al., 2018) but very few studies have focused on the impact of electrification from a chemical process

perspective. As commented by Lechtenböhmer et al. (2016), the future scenario of a fully electrified system is an area with several knowledge gaps where the potential for the electrification of the chemical industry requires more knowledge regarding technology and system options. Therefore, it is imperative to explore the electrification schemes at a process level to identify their opportunities as well as potential barriers.

The aims of this work are to provide technological options and strategies for chemical process electrification and analyse process performance based on environmental and economic metrics. Concretely, this work investigates MeOH production as a case study to evaluate the impact of electrification on process design by proposing alternative technological scenarios generated from different electrification schemes. Understanding of the energy structure of the electrified process is also key because such an analysis is a first step before introducing RESs in chemical production, as the optimisation of energy scheduling and unit sizing requires an insight of the fully (or almost fully) electrified process. This work will build a foundation for the use of RES as well as provide insights for policymaking in terms of future electricity demand.

3.2 Methods

This work aims to probe the potential of the electrification of chemical production processes and investigates the MeOH production process as a case study. To this end, a conventional MeOH synthesis route through natural gas reforming has been proposed as a reference process. The electrification is considered at two levels: (1) direct electrification by heat pump implementation, and (2) indirect electrification using an alternative feedstock or intermediate that can be produced from electrolysis. In particular, MeOH synthesis through CO_2 hydrogenation is simulated as an indirectly electrified process. The direct electrification does not alter the process design but it changes the energy structure of the process, i.e. substituting thermal energy with electricity. In contrast, the use of alternative

feedstocks may substantially change the flowsheet of the design. Therefore, to make a sound comparison it is of particular importance to define the boundary of the assessment. In this work, both the energy consumption of the production processes and the utilities associated with feedstock production are considered. However, the price of electricity is considered as an exogenous factor and details about electricity generation from renewable sources are outside the scope of this chapter. Detailed assumptions are listed at the end of this section (see Section 3.2.7).

The MeOH production processes are simulated with the commercial software Aspen Plus at a basis of 400,000 tonnes per annum with a product purity of 99.8 wt%. The carbon capture from flue gas is modelled as a chemical absorption process using a monoethanolamine (MEA) solution. Water electrolysis is not simulated but it is considered in the performance analysis since its energy consumption is readily available from the published literature. The viability of electrification is assessed based on economic and environmental analyses.

3.2.1 Water electrolysis unit

The production of hydrogen is typically achieved through alkaline electrolysis that splits water into oxygen (O_2) and hydrogen (Mansilla et al., 2011). This process essentially stores electrical energy as chemical energy in the form of hydrogen (Holladay et al., 2009), and thus it is of significance in the electrification of chemical processes. The specific energy consumption of commercial electrolysers ranges from 70.1 to 53.4 kWh/kg_{H_2} at 1 atm and 25 °C (Turner et al., 2008).

Since the water electrolysis process produces hydrogen and oxygen simultaneously, it would be correct to allocate the energy consumption to both products. To make a sound comparison between electrification schemes, a cryogenic air separation process, which is the traditional method to produce commercial oxygen, was simulated. The simulation resulted in electricity consumption of approximately 1 kWh/kg_{O_2}, which is much lower than for the aforementioned water electrolysis process (70.1 to 53.4 kWh/kg_{H_2}). Therefore, it is a fair approximation to allocate

all the energy consumed in electrolysis to the hydrogen product. In this work, an energy consumption of 4.5 $kWh/Nm^3_{H_2}$ is assumed in a water electrolysis process (Zeng and Zhang, 2010). This is equivalent to 55.7 kWh/kg_{H_2} at the feed conditions of the simulated process.

3.2.2 Carbon capture simulation

The feedstock CO_2 used in natural gas dry reforming and CO_2 hydrogenation is captured from the flue gases of a pulverised coal power plant with an overall recovery of 80 %. The simulation flowsheet adopted in this work was originally proposed by Aspen Technology, Inc. (2012) in an example of the rate-based monoethanolamine absorption process; thus, the physical property models in Aspen Plus are also inherited from the original design (the key physical property prediction model for vapour-liquid equilibrium is ENRTL-RK, i.e. an electrolyte NRTL activity coefficient model for the liquid phase and the Redlich-Kwong equation of state model for the vapour). Nevertheless, modifications are made in the absorber that models the WASH unit as a two-stage packed column (see Figure 3.1). Li et al. (2016) also simulated a CO_2 capture process based on the same example with improvements in temperature adjustments mapping their experimental results. In this work, the temperature adjustments that account for heat losses are neglected for the sake of simplicity.

Figure 3.1 shows the carbon capture process through MEA absorption and regeneration. After desulfurisation (a pretreatment not shown in this work), the flue gas is fed to the bottom of the absorber, whereas the lean CO_2 MEA solvent is fed to the top of the column. The scrubbed gas is then introduced at the top of a washing column in order to minimise the waste of MEA. Both columns are modelled with a RADFRAC unit using a rate-based model. RADFRAC is a model that performs rigorous calculations involving stage-by-stage vapour-liquid equilibrium coupled with chemical reactions, which can be used in both rating and design mode (Taqvi et al., 2017). Regarding the internals, both columns are designed as packed columns with 20 and 2 stages, respectively. The rich solvent from the bottom

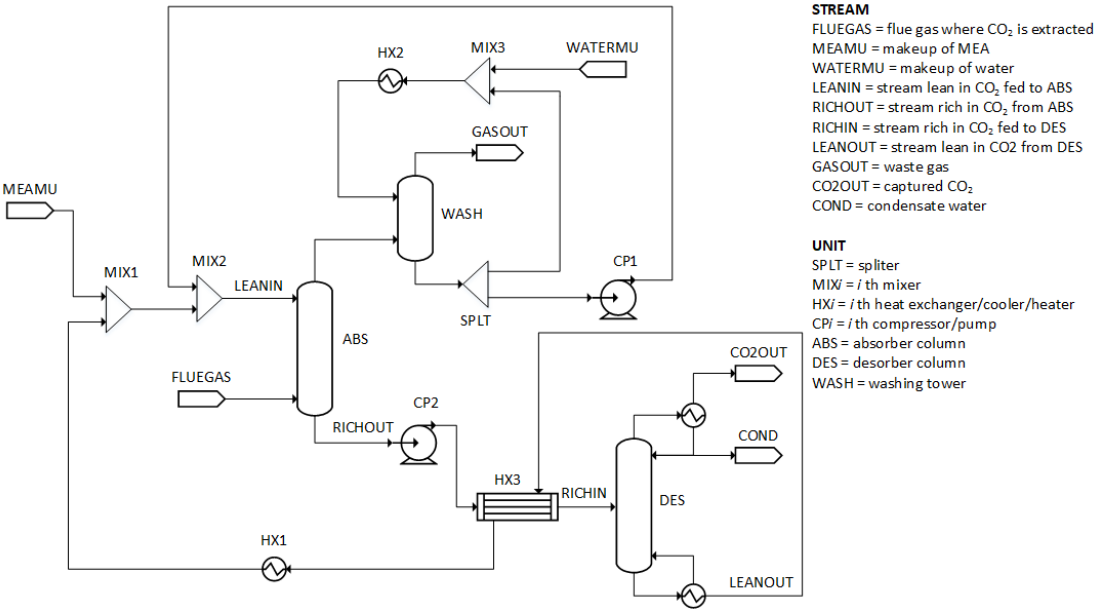


Figure 3.1. Process flow diagram of the carbon capture unit based on MEA absorption.

of the absorber is fed to the desorber to recover CO_2 and MEA. The desorber is also modelled with RADFRAC as a reactive distillation column. A partial condenser is employed to dehydrate CO_2 at a fixed temperature of 18.0 °C with a reflux ratio of 0.58. Since the operating temperature is below the temperature of cooling water, refrigeration is required to chill the condenser. The reboiler of the desorber is designed to have a boilup ratio of 0.06 operating at 119.3 °C. After regeneration, the lean solution is mixed with a small fraction of the water stream from the washing section and then reinjected into the absorber. The carbon capture unit has embedded a heat exchanger to recover heat from the MEA regeneration. This exchanger is included in the plant-wide heat integration to minimise energy utilities.

The captured CO_2 from the unit has a purity of 99.4 wt% with impurities such as water and nitrogen. For simplicity, the impurities are neglected when the stream is fed to the downstream MeOH production process. Due to the specification of the condenser operation, the captured CO_2 is chilled at a temperature (18 °C) lower than ambient; however, the heating duty to bring CO_2 to ambient temperature is neglected since the value is insignificant. At the condenser, it is assumed that the vapour product is cooled to 40 °C by cooling water, and chilled further to 18 °C by

refrigeration. The mechanical power ($\dot{W}$) required to run the refrigeration cycle is calculated by

$$\dot{W} = \dot{Q}\Big(\frac{T^{\mathrm{H}}}{T^{\mathrm{L}}} - 1\Big)\frac{1}{\eta_{\mathrm{refg}}} \tag{3.1}$$

where $\dot{Q}$ is the rate of heat extracted or the enthalpy change per unit time of the process stream from 40 to 18 °C, T^{H} is the temperature (308.15 K) at which heat is rejected to a heat sink, T^{L} is the temperature (281.15 K) at which heat is extracted from a heat source and η_{refg} is the efficiency of the refrigeration process, assumed to be 50 %.

The flue gas is assumed to be free of charge and pre-treated before carbon capture, and its composition is shown in Table 3.1. For simplicity, the carbon capture process is only simulated on the same scale as the example in Aspen Technology, Inc. (2012), which is adopted in this work; thus, the energy utilities are linearly scaled up in the plant-wide integration.

Table 3.1. Composition of the flue gas in the carbon capture unit. Data obtained from Aspen Technology, Inc. (2012).

Component	wt%
N_2	74.3
O_2	10.1
CO_2	8.5
H_2O	7.1

3.2.3 Methanol production simulation

In the reference process, MeOH is produced with syngas from natural gas reforming. The overall process is illustrated in Figure 3.2. The production process is composed of three main sections: (1) natural gas reforming, (2) MeOH synthesis and (3) MeOH distillation process. To simplify the chemistry of the reforming process, natural gas is assumed to be pure methane (CH_4); in the simulation, the trace amounts of nitrogen, hydrogen sulfide, heavy alkanes (C2 and above) and other gases are neglected. In the first section of the flowsheet, methane is compressed and fed to the reformer to produce syngas, which is a mixture with varying proportions

of hydrogen and carbon monoxide (CO). Traditionally, syngas is produced from the steam reforming (SR) of natural gas through a catalytic process to obtain a high H_2/CO ratio. An alternative process to produce syngas is through CO_2 reforming (also known as dry reforming or DR, as opposed to SR) of natural gas. Although this method has many disadvantages, including a low H_2/CO ratio in the produced syngas and coke formation due to a large C/O ratio, it has drawn focus over the last decade due to its potential to use CO_2 as a feedstock. In addition, reports have indicated that there are many natural gas fields having high CO_2 content (up to 30 %) all over the world, such as natural gas reservoirs in Indonesia's Natuna (Suhartanto et al., 2001), Malaysia in general (Tan et al., 2012) and Colorado Plateau (White et al., 2003). Developments in catalytic systems such as Rh supported on Al_2O_3 (Kohn et al., 2010), Mo_2C on ZrO_2 (Ross, 2005) and Ni-Ce on Al_2O_3 (Ocsachoque et al., 2011) have also facilitated the application of the DR process. However, in the base case scenario of this work, the CO_2 input to the reforming processes is from a carbon capture process rather than from natural gas. Another motivation to feed CO_2 in the reformer is because the downstream MeOH synthesis loop generates a surplus of low-grade heat (relative to the natural gas reforming process) which can be integrated with the CO_2 capture process.

Despite the promising future of DR, this work focuses on a more conservative process to reform natural gas since the aim of this work is to assess the electrification based on current industrial technologies. Consequently, this work formulates the natural gas reforming process based on the work of Olah et al. (2013) and Cañete et al. (2017), which proposed a combined reforming (CR) process consisting of DR (Reaction 3.2) and SR (Reaction 3.3). The water-gas-shift (WGS) reaction also occurs (Reaction 3.4) in the reformer. It is noteworthy that the Boudouard reaction and the methane decomposition reaction have been neglected due to the fact that minimal formation of coke has been found in the thermodynamic analysis (Cañete et al., 2014).

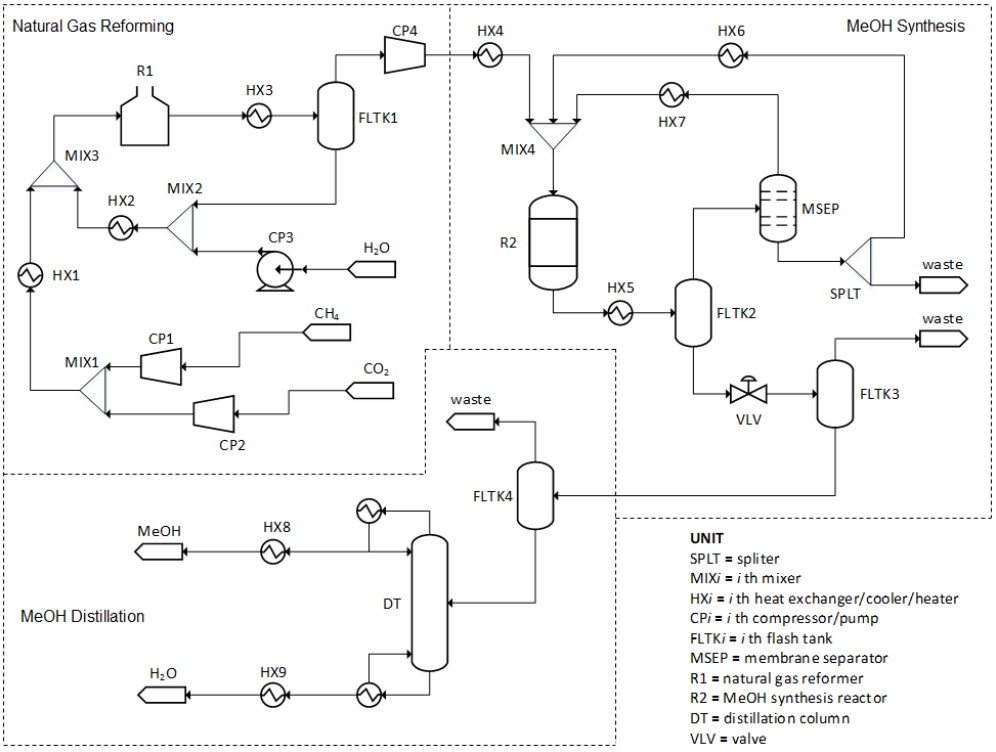


Figure 3.2. Process flow diagram of the reference MeOH production plant.

$$CH_4 + CO_2 \longleftrightarrow 2CO + 2H_2 \tag{3.2}$$

$$CH_4 + H_2O \longleftrightarrow CO + 3H_2 \tag{3.3}$$

$$CO + H_2O \longleftrightarrow CO_2 + H_2 \tag{3.4}$$

As shown in the process flowsheet, water is fed to the reformer (R1 in Figure 3.2) to enable the SR and WGS reactions. From a thermodynamic analysis, it has been found that the yield of carbon dramatically decreases with respect to the increase of H_2O/CH_4 ratio and it reaches zero when H_2O/CH_4 ratio is 0.7 or above (Cañete et al., 2014). Furthermore, the ratio of H_2/CO is directly proportional to the H_2O/CH_4 ratio due to the facilitated WGS reaction. The major drawback of a high H_2O/CH_4 ratio is the low conversion of CO_2, which implies a requirement for CO_2 removal in downstream processes. Moreover, a high water content also incurs additional energy consumption, hence the increase in operating cost. As a compromise, the H_2O/CH_4 ratio is set to be approximately 2.0 in order to maximise

the H_2/CO ratio in the product while the conversion of CO_2 is adequate enough to avoid its removal downstream.

The gaseous product and unreacted water are separated in a flash tank. The syngas product is fed to the MeOH synthesis loop, whereas water is recycled back to the reformer. The reformer is modelled with a REQUIL reactor operating at 950 °C and 20 bar. Reaction temperature is determined through a sensitivity test in order to obtain the optimal H_2/CO ratio and M module (defined as $M = (H_2 - CO_2)/(CO + CO_2)$) whilst keeping high methane conversion. Details of product flowrate and design parameters at different reformer temperatures can be found in Figures A.1 and A.2 in Appendix A. For simplicity, perfect separation of gas and liquid is assumed in the syngas flash tank (Van-Dal and Bouallou, 2013), and thus it is modelled with a SEP separator (FLTK1 in Figure 3.2) in Aspen Plus. Nevertheless, the subsequent vapour-liquid separations are modelled with a rigorous flash drum.

The second section of the production flowsheet addresses the synthesis of MeOH from syngas through hydrogenation. Although there is a lack of consensus around the involved reactions, this work uses a simplified set of reactions including the hydrogenation of CO (Reaction 3.5) and CO_2 (Reaction 3.6), and the reverse water-gas-shift (RWGS) reaction (Reaction 3.7) that co-occurs with the MeOH conversion. Other reactions that produce by-products are neglected, which is in accordance with other reports (Perez-Fortes et al., 2016; Van-Dal and Bouallou, 2013). This results in a stoichiometric H/C ratio of 2.5. As a rule of thumb, the CO_2/CO ratio is limited to 0.5 to prevent the formation of water and catalyst deactivation (Lee et al., 1989). MeOH synthesis typically requires a high H_2/CO ratio of up to 3.5 in the feed syngas; as a comparison, this ratio is approximately 1.0 for dimethyl ether production and 2.0 for gas-to-liquid processes (Ross, 2005).

$$CO + 2H_2 \longleftrightarrow CH_3OH \tag{3.5}$$

$$CO_2 + 3H_2 \longleftrightarrow CH_3OH + H_2O \tag{3.6}$$

$$CO_2 + H_2 \longleftrightarrow CO + H_2O \tag{3.7}$$

In industry, the MeOH synthesis loop is often composed of a series of adiabatic reactors with inter-stage cooling. The economic removal of the heat generated in the MeOH synthesis is a separate study and a major challenge in the design for MeOH production (Manenti et al., 2013). Therefore, to simplify the process, the MeOH reactor is modelled as a single RPLUG reactor (R2 in Figure 3.2) in Aspen Plus operating at a constant temperature and pressure of 255 ℃ and 71 bar. The kinetic model implemented in this work is based on that of a commercial $Cu/ZnO/Al_2O_3$ catalyst proposed by Vanden Bussche and Froment (1996) with adjusted parameters (Mignard and Pritchard, 2008). The rate equations for Reactions 3.6 and 3.7 are rearranged to suit the requirements of the LHHW (Langmuir-Hinshelwood-Hougen-Watson) kinetic model in Aspen Plus (Van-Dal and Bouallou, 2013), as shown in Eqs. 3.8 and 3.9:

$$r_{\mathrm{MeOH}} = \frac{k_1 P_{\mathrm{CO_2}} P_{\mathrm{H_2}} - k_6 P_{\mathrm{H_2O}} P_{\mathrm{MeOH}} P_{\mathrm{H_2}}^{-2}}{(1 + k_2 P_{\mathrm{H_2O}} P_{\mathrm{H_2}}^{-1} + k_3 P_{\mathrm{H_2}}^{0.5} + k_4 P_{\mathrm{H_2O}})^3} \quad [\frac{\mathrm{mol}}{\mathrm{kg_{cat}s}}] \tag{3.8}$$

$$r_{\mathrm{RWGS}} = \frac{k_5 P_{\mathrm{CO_2}} - k_7 P_{\mathrm{H_2O}} P_{\mathrm{CO}} P_{\mathrm{H_2}}^{-1}}{1 + k_2 P_{\mathrm{H_2O}} P_{\mathrm{H_2}}^{-1} + k_3 P_{\mathrm{H_2}}^{0.5} + k_4 P_{\mathrm{H_2O}}} \quad [\frac{\mathrm{mol}}{\mathrm{kg_{cat}s}}] \tag{3.9}$$

where r_{MeOH} and r_{RWGS} denote the reaction rate of MeOH synthesis and RWGS, respectively, and P_i denotes the partial pressure of i species. The kinetic constants are derived from the Arrhenius law, as shown in Eq. 3.10:

$$k_i = K_i e^{-\frac{E_{\mathrm{a}i}}{RT}} \tag{3.10}$$

where R denotes the ideal gas constant and T denotes temperature measured in Kelvin. The pre-exponential constants (K_i) and activation energy terms ($E_{\mathrm{a}i}$) are

rearranged in Eqs. 3.11–3.13:

$$\ln k_i = A_i + \frac{B_i}{T} \tag{3.11}$$

$$A_i = \ln K_i \tag{3.12}$$

$$B_i = -\frac{E_{ai}}{R} \tag{3.13}$$

Values for these parameters are summarised in Table 3.2. It is worthwhile to note that the thermodynamic equilibrium constants of Reactions 3.6 and 3.7 are rearranged and incorporated into the kinetic constants k_6 and k_7, respectively; thus, they are not shown explicitly. The NRTL-RK physical properties method is employed (due to its capability to model non-ideal behaviour) to calculate the thermodynamic properties in MeOH synthesis (Carlson, 1996). The product composition at the corresponding reactor volume is illustrated in Figure A.3 in Appendix A.

Table 3.2. Reaction kinetic constants and parameters for the MeOH synthesis kinetic model. Data obtained and rearranged from Vanden Bussche and Froment (1996).

Reaction Constant	E_{ai} (J/mol)	A_i	B_i (K)
k_1	$-40,000$	-29.870	4,811.16
k_2	–	8.147	0
k_3	$-17,197$	-6.452	2,068.44
k_4	$-124,119$	-23.440	14,928.92
k_5	98,084	4.804	$-11,797.45$
k_6	18,705	17.550	$-2,249.80$
k_7	58,393	0.131	$-7,023.50$

Because of the equilibrium limitations, the synthesis of MeOH through hydrogenation requires a large excess of hydrogen. The unreacted gas is first separated from the liquid product and then undergoes a polymeric membrane separator to enrich hydrogen. This operating unit is also modelled with a SEP unit (MSEP1 in Figure 3.2) in Aspen Plus, wherein the data are provided by previous studies (original data are obtained from Phair and Badwal (2006) and demonstrated by Cañete et al. (2017)). The enrichment of hydrogen can also be achieved through different reforming techniques, such as a combination of DR and partial oxidation (Amin and Yaw, 2007), or tri-reforming of DR, SR and partial oxidation (Song

and Pan, 2004). However, partial oxidation often requires air separation units which may significantly increase the total capital cost of a plant. A fraction of the unreacted gas is purged to eliminate the accumulation of inert components. This effluent is flared producing CO_2 and water, but the heat it generates is not integrated due to technical and economic barriers (Abdulrahman et al., 2015).

The products from the RPLUG reactor (R2 in Figure 3.2) flow through a series of flash tanks to separate the gaseous and liquid fractions. The first flash tank (FLTK2 in Figure 3.2) separates most of the gaseous product at high pressures but at low temperatures in order to minimise recompression work. The second flash tank (FLTK3 in Figure 3.2) is operated at reduced pressure for better vapour-liquid separation. Although the liquid product from the second flash tank only contains trace amounts of light components, a third flash tank modelled with a SEP unit (FLTK4 in Figure 3.2) is employed assuming perfect vapour-liquid separation, giving a liquid product composed of water and MeOH only. The low to trace amounts of light components in the liquid product have an insignificant impact on the energy requirements of the distillation column; however, sharp separation is assumed for clarity. The distillation column is modelled with a RADFRAC unit, giving a MeOH product at the top with a purity of 99.8 wt%. In the reference MeOH plant, the distillation column is optimised with a reflux ratio of 0.95 and 17 equilibrium stages in total. The raw product is fed at stage 10 of the column. Detailed fraction distribution at each corresponding stage is shown in Figure A.4 in Appendix A.

3.2.4 Electrification

The purpose of electrification is to substitute fossil fuel-based heating and feedstock with electricity. The proposal for the electrification of MeOH production is presented in two ways. First, the reference process is electrified directly by implementing heat pumps to reduce its heating requirement at an additional cost of mechanical work. Other direct electrification techniques based on electrothermal phenomena can be readily implemented in most chemical processes. However, heat pumps

are considered as a better option because they simultaneously reduce heating and cooling duties by upgrading the heat sources through mechanical compression, thus facilitating energy transshipment to the heat sinks. The efficiency of heat pumps depends crucially on the temperature difference between heat source and sink. A graphical method based on the Grand Composite Curve (GCC) analysis is employed to determine the savings of hot and cold utilities as well as the required power for additional mechanical work.

The production of MeOH can also be electrified in an indirect way when alternative feedstocks are taken into account within electrification. Concretely, hydrogen from water electrolysis is considered for the MeOH synthesis via CO_2 hydrogenation. This alternative path essentially substitutes the thermodynamic energy of natural gas by the electricity that is consumed in hydrogen production. The process flowsheet, adjusted to suit the change of feedstock, is shown in Figure 3.3. The same reaction model is employed in the simulation of the MeOH synthesis via CO_2 hydrogenation. The change of feedstock from syngas (CO and H_2) to CO_2 and H_2 (Streams 1 and 3 in Figure 3.3) inherits the same kinetics; however, the exothermic reaction heat is less due to the lower energy content of the feed. In addition, the concentration of MeOH at the reactor outlet is much lower than that of a conventional plant based on natural gas reforming, resulting in higher energy intensity at the downstream distillation. Indeed, the number of stages in the distillation column (DT1 in Figure 3.3) is optimised to be 27 (larger than for the reference process) due to the lower MeOH concentration in the crude product (Stream 26 in Figure 3.3).

After plant-wide integration, the CO_2 hydrogenation plant can also be electrified directly by implementing a heat pump, leading to a combined direct and indirect electrification case. The impacts of both strategies are evaluated through sensitivity tests. All the scenarios are analysed in the following sections based on environmental and economic assessments.

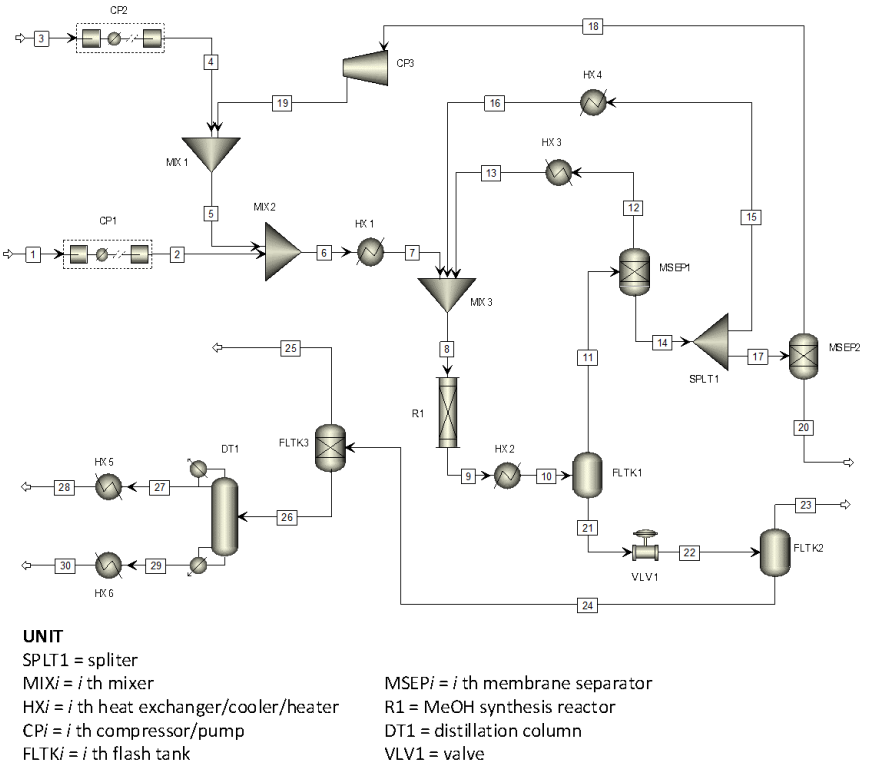


Figure 3.3. Process flow diagram of the non-conventional MeOH production plant simulated in Aspen Plus.

3.2.5 Environmental assessment

The environmental metrics take into account the process and indirect CO_2 emissions caused by energy utilisation (i.e. CO_2 generated due to heating or electricity consumption). The CO_2 emissions with respect to different energy sources are tabulated in Table A.5 in Appendix A; it is assumed that the marginal CO_2 emission from RESs is zero. The net CO_2 balance is calculated by

$$ {}_{net}\mathrm{CO_2} = {}_{consumed}\mathrm{CO_2} - \left({}_{outlet}\mathrm{CO_2} + {}_{indirect}\mathrm{CO_2}\right) \tag{3.14} $$

where ${}_{net}\mathrm{CO_2}$ is the net abatement of CO_2 measured in kg, ${}_{consumed}\mathrm{CO_2}$ is the mass of feedstock CO_2 that has been consumed in the process, ${}_{outlet}\mathrm{CO_2}$ represents the mass of emitted CO_2 from the process and ${}_{indirect}\mathrm{CO_2}$ is the emission resulting from energy consumption. Note that the unreacted components and waste MeOH in the purge stream are combusted to CO_2 and water before purging to the environment, and thus they are included in the ${}_{outlet}\mathrm{CO_2}$ term. The energy (η_e) and carbon

efficiency (η_c) are also selected as environmental indicators and calculated by

$$\eta_e = \frac{\mathrm{HHV_{MeOH}}}{\mathrm{HHV_{NG}} + Utilities} \times 100\,\% \tag{3.15}$$

$$\eta_c = \frac{Carbon\ in\ methanol}{Carbon\ in\ feedstock} \times 100\,\% \tag{3.16}$$

where $\mathrm{HHV_{MeOH}}$ and $\mathrm{HHV_{NG}}$ indicate the high heating values of the MeOH product and natural gas feedstock, respectively. Note that in the assessment the *Utilities* term excludes cooling duties.

3.2.6 Financial assessment

The financial performance of individual scenarios is evaluated based on two economic indicators, namely net present value (NPV) and internal rate of return (IRR). The NPV is calculated by

$$\mathrm{NPV} = \sum_{t=1}^{20} \frac{C_t}{(1+r)^t} \tag{3.17}$$

where C_t is the cash flow of year t and r is the discount rate. The hurdle rate (the minimum expected return rate of a project) is assumed to be 8 % in the analysis. The value of IRR indicates the discount rate r at which the NPV is zero. The annual C_t is determined by the difference between product revenue and operational expenditures (OpEx). The depreciation of the capital investment is also taken into account in the OpEx by assuming a linear depreciation over a course of 20 years with a salvage value of 5 % total fixed capital cost (TFCC) after decommissioning. The value of TFCC is estimated by ratio factors based on the equipment cost of the main units as per the work of Zhang et al. (2016, 2017). The calculation is shown in Eq. 3.18:

$$\mathrm{TFCC} = Main\ unit\ cost \times \left(1 + \sum Ratio\ factor\right) \tag{3.18}$$

Most equipment costs are directly reported after the simulation with Aspen Process Economic Analyser (APEA) based on the chemical engineering plant cost index (CEPCI) of 2018, whereas catalytic reactors (reformer and MeOH reactors) are estimated via the six-tenths factor rule based on literature values (Zhang et al., 2015) and then updated to 2018 using the annual CEPCI. Since the CO_2 capture processes associated with each MeOH plant are not simulated up to scale (for simplicity, see assumptions in Section 3.2.7), their equipment costs are also determined via the six-tenths factor rule.

The calculation of OpEx considers utility and raw material costs, which are listed in Tables A.6 and A.7, respectively (see Appendix A). The cost factors used to estimate utility costs in Table A.6 are obtained from Aspen Energy Analyser (AEA). Taking electricity price as a basis, which is taken as 63.0 \$/MWh (Zhang et al., 2017), the remaining utility costs are determined according to the cost factors. The product price is also summarised in Table A.7 in Appendix A.

3.2.7 Summary of assumptions

The following assumptions have been used in this work: (1) the operation time of the processes is 8,000 hours per annum. (2) All the CO_2 feedstock is obtained via carbon capture from a flue gas source with conditions specified in Table 3.1. Although carbon capture from the MeOH production effluent consumes less energy (due to a higher CO_2 concentration), its additional capital cost may outweigh the saving from energy consumption. Since CO_2 capture is an auxiliary process, economic optimisation of the carbon capture unit is out of the scope of this work. (3) Energy from the process flare is excluded from heat integration. (4) Multiple heat pump implementation is not considered because its complexity (and its additional cost) significantly outweighs the potential benefits. (5) The compressors modelled in process simulation are assumed to be isentropic with an efficiency of 75 %. (6) All mechanical work for both process and heat pump compression is powered by electricity only. (7) The TFCC calculation only considers the main equipment cost (excluding heat pumps and other auxiliary units). (8) The price of electricity in the

financial analysis is considered as an exogenous factor. However, it is assumed to be 20 $/MWh in the base scenario of sensitivity tests. (9) Both environmental and financial assessments do not consider infrastructure construction and its potential impact.

3.3 Results and Discussion

Several scenarios are considered in the analysis and then reported with their energy profiles. In the base case scenario (S1), a reference MeOH plant based on conventional natural gas reforming is analysed and its utility consumption after energy integration is reported. This scenario represents most existing MeOH plants and its utility consumption is representative of current energy requirements. Scenario 2 (S2) reports utilities after direct electrification by implementing a heat pump, which aims to explore the potential of electrification for the conventional MeOH plants using the best available technology. The integrated CO_2 hydrogenation plant (Scenario S3) is regarded as an indirectly electrified process as its hydrogen feedstock is obtained through electrolysis. This scenario represents a different strategy in the electrification of chemical processes but it requires a re-design of the flowsheet. Scenarios S4–S6 consider combined direct and indirect electrification based on a CO_2 hydrogenation plant at an incremental level (increased energy transshipment). An overview of the analysis, integration boundaries and the resulting scenarios is illustrated in Figure 3.4.

3.3.1 Material and energy balance

The conceptual designs simulate a medium-size MeOH production facility producing approximately 400,000 tonnes per annum at an industry-grade purity of 99.8 wt%. In the base case scenario, the process consumes approximately 170,000 tonnes of natural gas and 200,000 tonnes of captured CO_2 per annum. The process also consumes approximately 160,000 tonnes of water per year. The purge and effluent streams are flared, thus producing CO_2 and water. For this reason, the heat from

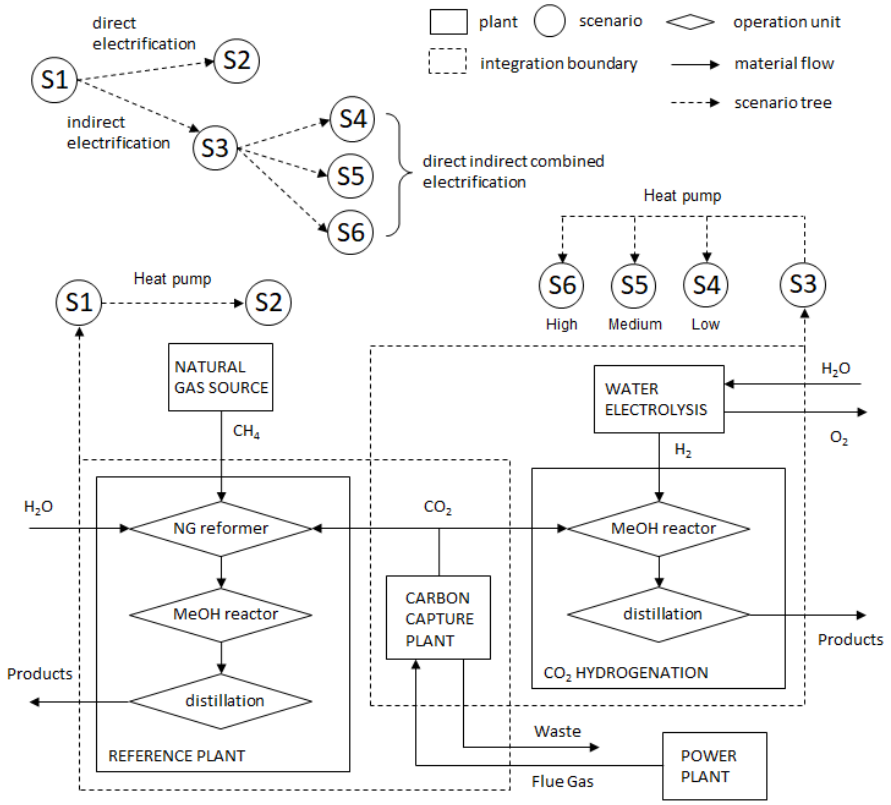


Figure 3.4. Block representation of the scenarios and the analysis boundaries.

these exothermic reactions (combustion) is not recovered. The overall purge rate is approximately 2 % of the total production, which is consistent with conceptual designs from other sources (Perez-Fortes et al., 2016; Van-Dal and Bouallou, 2013). It is possible to further reduce the amount of valuable product in the purge by adjusting flash tank conditions, thus increasing the capital cost of the recycling units. However, the optimisation of capital cost and product waste is beyond the scope of this work, and thus a typical operating condition is assumed.

In the reference process, the reformer (R1 in Figure 3.2) is the major energy consumer powered by fossil fuel combustion at high temperatures. The process is in heat surplus; however, the major heat generator (R2 in Figure 3.2) and its outlet stream can only provide low-grade heating; external heating is therefore required to meet the outstanding high-grade heating. After plant-wide integration, this process becomes Scenario S1 in the analysis. The electrified reference process after heat pump implementation has the same material balance but fewer hot and cold utilities (Scenario S2). The detailed energy utilities with respect to the individual

units in the reference process are shown in Table A.1 in Appendix A.

To produce the same amount of MeOH, the indirectly electrified process via CO_2 hydrogenation consumes approximately 78,000 tonnes of hydrogen and 650,000 tonnes of captured CO_2 as feedstock per annum. The CO_2 feedstock is more than three times that required in the reference MeOH plant but no fossil fuel feedstock is needed. The total energy consumption of the CO_2 hydrogenation plant is much higher when water electrolysis is taken into account. The loss of MeOH product due to the flashing process accounts for approximately 2 % of the total production rate, which is consistent with the reference plant. The energy utilities of individual units in the CO_2 hydrogenation plant are summarised in Table A.2 in Appendix A. The integrated CO_2 hydrogenation plant is used for the sensitivity analysis as Scenario S3 while Scenarios S4–S6 represent the same plant but implemented with a heat pump at incremental levels.

The carbon capture process is designed to provide CO_2 feed to both the reference MeOH plant and the CO_2 hydrogenation plant. The energy utilities of individual units, summarised in Tables A.3 and A.4 in Appendix A, are scaled up in accordance with the requirement of the respective process they feed. Note that the cooling utility of the desorber (DES in Figure 3.1) is composed of two parts: (1) cooling water is used to cool the process stream to 40 ℃, and (2) refrigeration is used to further cool it down to 18 ℃. A makeup stream of MEA of 25.1 and 82.1 kg/h for the respective plant is used to compensate for the material lost to the ambient.

3.3.2 Energy integration and heat pump implementation

The integration of energy utilities is analysed using the AEA software. The heat cascade flow and GCC diagrams for each of the MeOH plants are plotted. Following a graphical analysis of the GCC diagrams, heat pumps are implemented resulting in reduced theoretical hot and cold utilities at a cost of additional mechanical work. Such implementation provides an efficient way of increasing heat quality and thus facilitates the design of a heat exchanger network. However, the challenge often lies

in the proper placement of the heat pumps. In the seminal work of Townsend and Linnhoff (1983a,b), it is concluded that the heat pumps should be implemented across the pinch in order to reduce energy utility requirements.

Figure 3.5 illustrates the GCCs and their corresponding cascade diagrams for selected scenarios (GCCs for Scenarios S4 and S5 are omitted). Scenarios S1 and S3 represent the reference and the CO_2 hydrogenation plant, respectively, and based on the resulting GCCs, direct electrification (S1 to S2, S3 to S4–S6) can be implemented. The original GCCs before heat pump implementation (blue curves in Figure 3.5A and B) indicate the theoretical minimum heating ($\dot{Q}_{\mathrm{h}}$) and cooling ($\dot{Q}_{\mathrm{c}}$) utilities, and their values are shown in the cascade diagrams of Figure 3.5. The shape of the respective GCCs is determined by the individual operating unit and its energy consumption characteristics. For instance, the top section of the GCC for S1 in Figure 3.5A extends to a large enthalpy value at a constant temperature due to the reformer operating at 950 °C, which is too high a temperature to be integrated. Since all scenarios contain heating or cooling requirements at a virtually constant temperature, there are sections on the GCC that show nearly zero gradients, indicating infinite aggregated heat capacity (FCp) of a process stream. To circumvent this computational difficulty, a temperature change of 0.1 °C is assumed for heating or cooling when the temperature is constant. This characteristic of the process streams also results in large overlapping areas of the original and revised GCC (after heat pump implementation). For clarity, the revised GCC of Scenarios S4 and S5 are not shown.

As an example of the graphical analysis, the implementation of a heat pump in S3 (resulting in S6) is shown in Figure 3.5B. Concretely, an amount of heat per unit time ($\dot{Q}_2$) is extracted from interval 15 at a temperature of T_2 and transferred to interval 9 at T_1. Note that $\dot{Q}_2$ is marginally smaller than the enthalpy rate at the extraction temperature of T_2 ($\dot{Q}_{T2}$). This is because when $\dot{Q}_2$ is larger than $\dot{Q}_{T2}$, it results in a new pinch below T_2 and thus violates the cross-pinch rule. When $\dot{Q}_2$ is equal to $\dot{Q}_{T2}$, it results in a double pinch GCC at T_2 and at the original pinch temperature. The heating utility saving, $\Delta\dot{Q}_{\mathrm{H}}$, is equivalent to $\dot{Q}_1$ while the cooling utility saving $\Delta\dot{Q}_{\mathrm{C}}$ is given by $\dot{Q}_2$. Therefore, the revised GCC is shifted

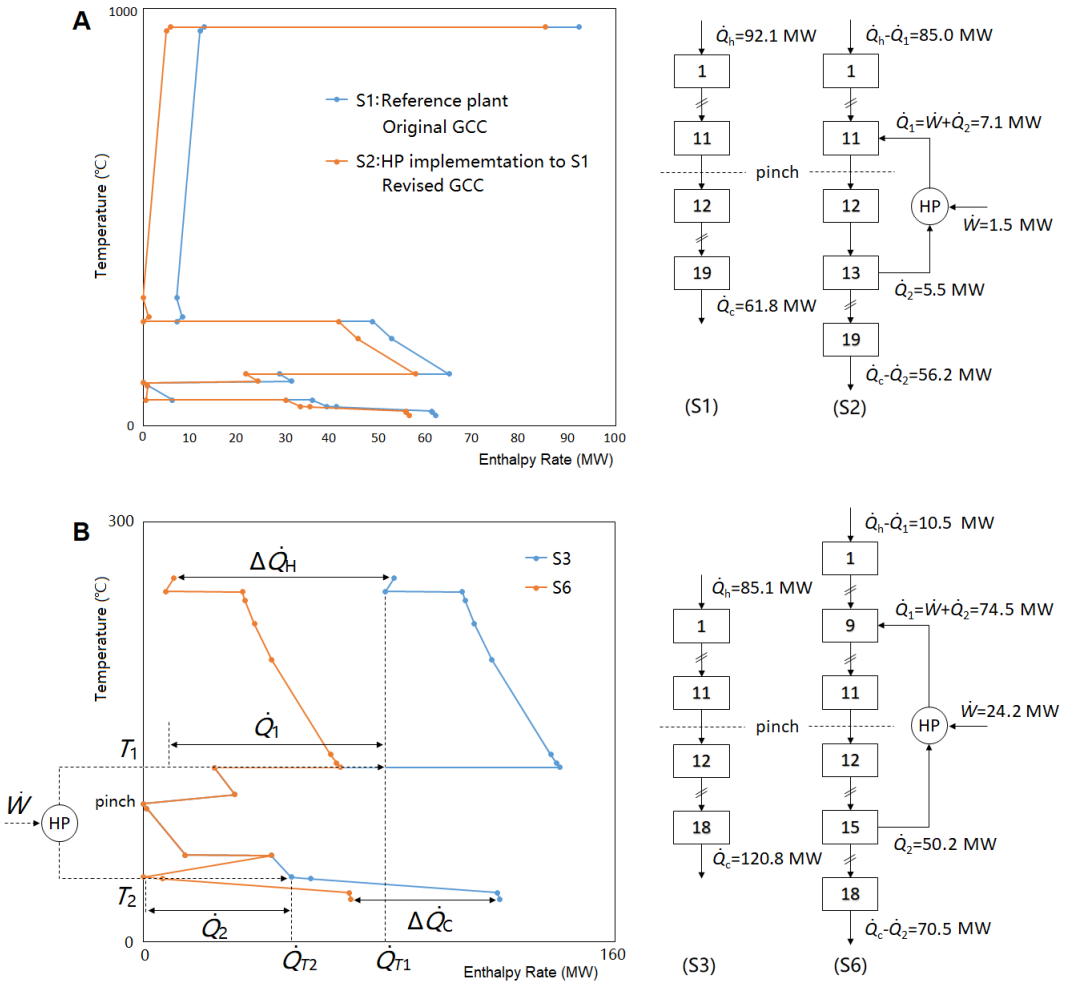


Figure 3.5. Cascade diagrams and their corresponding Grand Composite Curves for (A) reference MeOH plant (S1) and its derived scenario (S2); (B) CO_2 hydrogenation MeOH plant (S3) and its derived scenario (S6). HP stands for heat pump.

to the left horizontally by $\Delta\dot{Q}_{\mathrm{H}}$ above the pinch and by $\Delta\dot{Q}_{\mathrm{C}}$ below the pinch. In the intervals between T_1 and T_2 (exclusive), the GCC is unchanged, and thus the revised GCC superimposes the original sections. The coefficient of performance (COP) of heat pumps is determined by

$$\mathrm{COP} = \frac{\dot{Q}_1}{\dot{W}} = \frac{T^{\mathrm{H}}}{T^{\mathrm{H}} - T^{\mathrm{L}}} \tag{3.19}$$

where T^{H} and T^{L} are the hot and cold temperatures (in Kelvin) of the working fluid, respectively. Note that the temperature axis of the GCC diagrams is plotted using the average value of the hot and cold sides. When above the pinch, the working fluid acts as a hot stream and its temperature T^{H} coincides with the registered temperature on the hot side, i.e. $T^{\mathrm{H}} = T_1 + 0.5\Delta T_{\mathrm{min}}$, where ΔT_{min}

is the temperature driving force, assumed to be 10 K for both heat integration and heat pump operation. On the other hand, T^{L} coincides with the registered temperature on the cold side since heat is extracted from the cold side to the working fluid; hence $T^{\mathrm{L}} = (T_2 - 0.5\Delta T_{\min}) - \Delta T_{\min}$, where $T_2 - 0.5\Delta T_{\min}$ denotes the registered temperature on the cold side. Since the mechanical work ($\dot{W}$) equals to the difference between $\dot{Q}_1$ and $\dot{Q}_2$, the COP equation can be rearranged into

$$\dot{Q}_2 = \frac{\dot{Q}_1(\mathrm{COP} - 1)}{\mathrm{COP}} \tag{3.20}$$

Therefore, either $\dot{Q}_1$ or $\dot{Q}_2$ is required to determine the other. The guideline is to choose the largest $\dot{Q}_1$ or $\dot{Q}_2$ while complying with the cross-pinch rule, i.e. satisfying the constraints that $\dot{Q}_1 \leqslant \dot{Q}_{T1}$ and $\dot{Q}_2 \leqslant \dot{Q}_{T2}$, simultaneously. As demonstrated in Figure 3.5B, $\dot{Q}_{T2}$ is the limiting factor determining the maximum effective heat transshipment, whereas $\dot{Q}_{T1}$ is the limiting factor in Figure 3.5A (not shown). The detailed utility savings and performance indicators of different scenarios are summarised in Table 3.3. Note that in the calculation an effective COP ($\mathrm{COP}_{\mathrm{eff}}$) is employed assuming 75 % of Rankine cycle efficiency.

Table 3.3. Utility savings and performance indicators for different scenarios. Utility savings of S2 is derived taking S1 as a benchmark; utility savings of S4–S6 are derived taking S3 as a benchmark. HP stands for heat pump.

	Scenario description	Utility saving		HP	T^{L}	T^{H}	$\mathrm{COP}_{\mathrm{eff}}$
		Hot	Cold				
		MW	MW	MW	K	K	
S1	Base case scenario of the reference plant	–	–	–	–	–	–
S2	Direct electrification by HP implementation	7.12	5.57	1.70	320	382	4.61
S3	Indirect electrification using H_2 as feedstock	–	–	–	–	–	–
S4	Combined electrification at low level	18.55	14.28	4.27	320	387	4.34
S5	Combined electrification at medium level	59.81	43.43	16.38	320	403	3.65
S6	Combined electrification at high level	74.54	50.27	24.27	304	403	3.07

Although a heat pump can theoretically be placed at a wide range of temperatures, in most practical cases its temperature lift is limited to ensure a satisfactory COP (Feng and Berntsson, 1997). The exact location of temperature interval for heat pump implementation is typically optimised through linear or nonlinear programming (NLP) based on an objective function of utility cost (Bagajewicz and Barbaro, 2003; Colmenares and Seider, 1987), which is out of the scope of this work. Besides, the consideration of RES complicates the objective function of a traditional

NLP. In the demonstrated examples, the placement of the heat pump is decided using a heuristic method. For instance, in Figure 3.5A the delivery temperature (T_1) is determined to be 109 ℃ because any hot utility saving greater than $\dot{Q}_1$ requires a much higher temperature lift (>300 ℃). As for the cold side, since $\dot{Q}_1$ is the limiting factor to satisfy the constraint, the optimal $\dot{Q}_2$ and its corresponding temperature can be estimated accordingly. Regarding S3 and its derived scenarios, heat pumps are placed at an incremental level yet within reasonable temperature intervals (i.e. satisfactory COP). Another simplification for the work is that only a single heat pump is considered for energy transshipment, and constraints are introduced to comply with the cross-pinch rule. However, in the case of multiple heat pumps implementation, these constraints are not necessarily true for an effective heat transfer. As first introduced by Rodera and Bagajewicz (1999), heat transfer above or below the pinch by one heat pump may act as "assisting" heat that can facilitate heat transfer when another heat pump is implemented.

The electricity demands for heat pump work and other operation units are consolidated and illustrated in Figure 3.6 along with other utility consumptions for the two MeOH plants and their derived scenarios. The heating utility is further stratified into low pressure (LP), medium pressure (MP), high pressure (HP), very high pressure (VHP) steam and fired heat (note HP steam consumption is zero in all scenarios).

As depicted in Figure 3.6, Scenarios S1 and S2 have very similar energy structures because the direct electrification for the base case scenario (S1) can only substitute 7.8 % of its total heating at additional electricity consumption of 1.6 MW; both values are insignificant. The barrier preventing direct electrification is the large amount of high-grade heating (fired heat, accounting for 91.5 % of the total heating in S1) required in natural gas reforming, which is difficult to substitute with electricity. Regarding the indirect electrification of S1 (S1 vs. S3), a significant increase in electricity demand (from 14.2 MW in S1 to 579.8 MW in S3) can be observed, which is attributed to the hydrogen production in the CO_2 hydrogenation plant (accounting for 94.0 % of the total electricity consumption in S3). Another noticeable difference between S1 and S3 is the heating requirement: although the

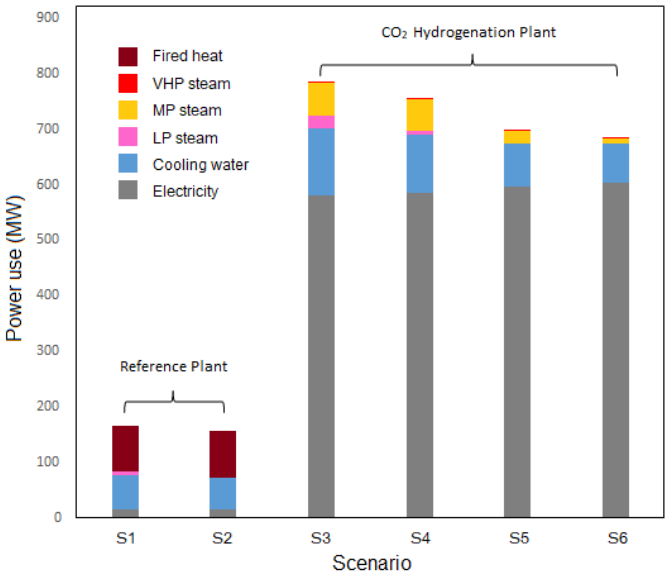


Figure 3.6. Energy structure and consumption of different scenarios. (S1) Base case scenario of the reference MeOH plant; (S2) direct electrification of S1 by heat pump implementation; (S3) indirect electrification of S1 using hydrogen produced from electrolysis; (S4) combined direct and indirect electrification with low heat pump power; (S5) combined direct and indirect electrification with medium heat pump power; (S6) combined direct and indirect electrification with high heat pump power.

reduction is insignificant (reduced from 92.1 MW in S1 to 85.1 MW in S3), the fired heat requirement is completely eliminated in S3, leaving only low-grade heating demand. This change in heating utilities provides additional opportunities when combined indirect and direct electrification is considered. Significantly, Scenarios S4–S6 gradually reduce the use of heating from 66.6 MW in S4 to 25.3 MW in S5 and eventually to 10.6 MW in S6. The reduction in heating (i.e. a trend in achieving an almost fully electrified process) is of special interest as it facilitates the implementation and management of RES in chemical production. Although the direct electrification (S1 vs. S2) is insignificant, it has the advantage of a straightforward implementation. On the contrary, the indirect electrification strategy requires a new flowsheet design and is thus not applicable to existing chemical plants.

The energy content of fossil fuels is not a product of human effort, and thus it has no cost except extraction, refining and transport costs. In direct contrast, hydrogen production has a significant cost (aside from its transport and distribution costs) since a large amount of electricity is required to compensate for the low energy

content of the feedstock, i.e. water fed to the electrolysis plant has minimum energy content, as opposed to natural gas fed to the conventional MeOH plant. Therefore, from the energy balance the CO_2 hydrogenation plants (Scenarios S3–S6) consume significantly more total energy in comparison with the reference plants (Scenarios S1 and S2); however, the economic potential of the CO_2 hydrogenation plant is not necessarily inferior to its counterpart, since their feedstock is of different value. The economic value of water and flue gas, which are the major feeds to the CO_2 hydrogenation plant, are much lower than that of natural gas. Another important factor that has to be taken into consideration is the source of electricity generation. If the electricity used to substitute natural gas is generated from fossil fuels, the overall process may not be energy efficient. However, electricity can be produced from RESs and may thus have a lower price (close to zero if RESs are in surplus) than fossil fuels. Most importantly, its implication on the environment is crucial.

3.3.3 Environmental assessment

The CO_2 balance, energy consumption and efficiency indicators for different scenarios are tabulated in Table 3.4. From the process CO_2 balance, both the reference and the CO_2 hydrogenation plant (and their derived scenarios) consume more CO_2 as a feedstock than the directly emitted CO_2 in their flue gas. However, it may not necessarily result in an overall CO_2 abatement when CO_2 emissions from indirect sources are taken into consideration, as indicated by Eq. 3.14. Regarding the efficiency indicators, although the CO_2 hydrogenation plants (Scenarios S3–S6) demonstrate slightly better carbon efficiency, the energy efficiency is much lower than their counterpart reference plants. This is mainly ascribed to the limit in water electrolysis, which may become a barrier to energy transformation in the future. However, when RESs are introduced, the energy efficiency of a particular process may not be as important. As commented by Dennis et al. (2016), the term "emiciency" (a coined word for emissions efficiency) may become more important in the future. It is also noteworthy that direct electrification via a heat pump implementation improves the energy efficiency in all scenarios, and is particularly

effective in the CO_2 hydrogenation plants. This is attributed to the change in heating utilities (fired heat is eliminated) that facilitates such an implementation.

Table 3.4. Summary of key environmental indicators for each scenario.

	S1	S2	S3	S4	S5	S6
Balance (kg/kg_{MeOH})						
$_{consumed}CO_2$	0.50	0.50	1.64	1.64	1.64	1.64
$_{outlet}CO_2$	0.30	0.30	0.25	0.25	0.25	0.25
Utility (MW)						
Heating	92.1	85.0	85.1	66.6	25.3	10.6
Electricity	14.2	15.7	579.8	584.1	596.2	604.1
Efficiency (%)						
η_e	73.2	74.1	47.6	48.7	50.9	51.5
η_c	82.0	82.0	83.6	83.6	83.6	83.6

Since the CO_2 emissions from the electricity generated via coal are much higher than from direct heating via natural gas, the use of RES in electrification becomes pivotal in achieving the environmental targets. As illustrated in Figure 3.7, CO_2 abatement of the CO_2 hydrogenation plant (and its derived scenarios, S3–S6, with combined direct and indirect electrification) is highly sensitive to renewable penetration, surpassing the conventional processes (Scenarios S1 and S2) at a renewable penetration of approximately 85 % and achieving CO_2 emission neutrality at 88 %. Note that the negative numbers mean a net CO_2 emission instead of abatement. At 100 % renewable penetration, the CO_2 hydrogenation plant with a heat pump implemented at the highest level (Scenario S6) can achieve a CO_2 abatement of up to 1.35 kg/kg_{MeOH}, demonstrating a great potential in meeting environmental targets as well as CO_2 utilisation.

It is also noteworthy that in the analysis renewable sources are not considered for thermal heating because (1) Scenarios S1 and S2 require heating at an extremely high temperature which is difficult to be met by renewable sources; and (2) thermal heating utility is far less than the electricity consumption in Scenarios S3–S6. Consequently, the sensitivity to the change of renewable penetration is directly (and only) correlated to the total electricity consumption in each scenario. For instance, Scenarios S1 and S2 are fairly insensitive to renewable penetration due to the low electricity content in their utilities. The direct electrification by heat

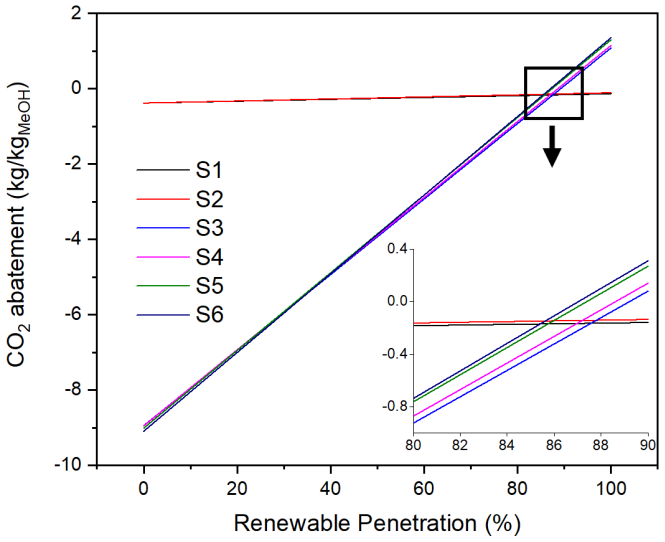


Figure 3.7. Influence of renewable penetration on CO_2 abatement for different scenarios. The inset shows the enlarged section in the range of 80–90 % of renewable penetration.

pump implementation in CO_2 hydrogenation plants reduces the CO_2 abatement when renewable penetration is low; however, an opposite trend is shown when the penetration is high (shown in the inset of Figure 3.7). This is attributed to the fact that CO_2 abatement from hot utility savings outweighs the additional CO_2 contribution from the mechanical work of the heat pump when the renewable penetration is high.

3.3.4 Financial assessment

Before assessing the economic feasibility of each scenario, the equipment costs of the main units with respect to the reference plant and the CO_2 hydrogenation plant are estimated, as shown in Table 3.5. Most of the values are directly reported from simulation results except the catalytic reactors (reformer and MeOH reactor). The cost of the reactors is scaled via the six-tenths factor rule based on literature values (Zhang et al., 2015). As demonstrated in Table 3.5, a noticeable difference in the respective plant is from the equipment cost of compressors, which is attributed to the change of feedstock in the CO_2 hydrogenation plant. The values of TFCC are estimated by ratio factors and detailed items are summarised in Table A.8 in Appendix A. Note that the TFCC of the heat pump is ignored since its value is too small in comparison with the plant cost. However, the additional electricity

consumption due to the heat pump implementation is considered in the OpEx. The electrolysers are costed separately from TFCC because it is a non-conventional process unit, meaning that it is not suitable to use the ratio factors for traditional chemical processes. Here, the CapEx of electrolysers is assumed to be 350 $/kW based on the cost for central production facilities (Matzen et al., 2015).

Table 3.5. Main equipment cost estimation for each plant. Note that the electrolysers cost for the CO_2 hydrogenation plant is not included in TFCC.

No.	Unit	Reference plant (M$)	CO_2 hydrogenation plant (M$)	Source
1	Reformer	13.91	–	Zhang et al. (2015)
2	MeOH reactor	15.93	14.96	Zhang et al. (2015)
3	Syngas flash tank	0.03	–	APEA
4	Distillation column	0.66	0.83	APEA
5	MeOH flash tanks	0.21	0.29	APEA
6	Compressors	7.62	47.41	APEA
7	Coolers	0.35	0.56	APEA
8	Heaters	0.10	0.24	APEA
9	Absorber	15.89	32.35	APEA
10	Desorber	5.95	12.12	APEA
11	Electrolysers	–	191.00	Matzen et al. (2015)

Figure 3.8 shows the NPV of all scenarios by varying the price of electricity. The current market price of electricity varies significantly from country to country. The EU average household electricity price is approximately 230 €/MWh (262 $/MWh) (Eurostat, 2017a) while the electricity price in the US ranges from 103 to 128 $/MWh, depending on end-use sectors (US Energy Information Administration, 2020). In the context of electrification, the electricity for industry use is usually cheaper than household use. For instance, Varone and Ferrari (2015) adopted an electricity price of 50 €/MWh (or 57 $/MWh) in their analysis for the German *Energiewende*. Nevertheless, the current electricity price is not economically justified for industry electrification. On the other hand, it is possible to find RESs with a price lower than 20 $/MWh (Evans et al., 2009). In the case of surplus renewable energy, the generated electricity often has a very low price or is even close to free of charge. In the current market, the CO_2 hydrogenation plant and its derived scenarios (S3–S6) all have a negative NPV, whereas the reference plant and its derived scenarios (S1–S2) have an NPV above 900 M$. However, electricity from RES may have a lower price, thus facilitating the profitability of

the electrified scenarios. It is estimated that the CO_2 hydrogenation plants would achieve a positive NPV when the electricity price is below 25 \$/MWh, and their economic potential exceeds the reference MeOH plants when the electricity price is in the range of 3–5 \$/MWh, depending on the extent of direct electrification (see the inset in Figure 3.8). The NPV of CO_2 hydrogenation plants is also compared with a similar design (and size) process proposed by Perez-Fortes et al. (2016). In the current market, the NPV of CO_2 hydrogenation plants from our simulation is around −1,400 M\$, whereas Perez-Fortes et al. (2016) reported −1,200 M\$ in the base case scenario. The difference may be attributed to the alternative methods in CapEx and TFCC estimation.

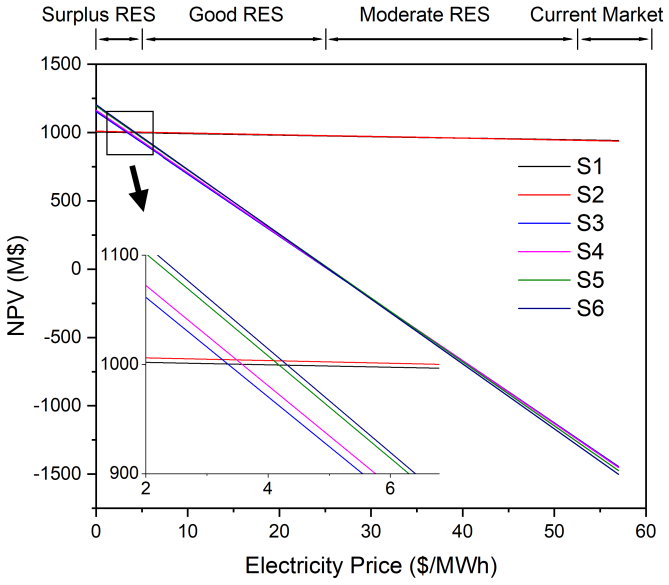


Figure 3.8. NPV values of each scenario with varying electricity prices. The inset shows the enlarged section ranging from 2–6 \$/MWh.

In analogy to the CO_2 emissions, the influence of heat pump implementation on NPV switches at a specific electricity price. For instance, heat pump reduces the NPV when the electricity price is higher than 30 \$/MWh for the CO_2 hydrogenation plants, but its implementation improves the NPV when the price is below 20 \$/MWh. From the thermodynamic principle of a heat pump, the economic performance can be derived and is governed by

$$\mathrm{COP}_{\mathrm{min}} = \frac{Electricity\ price + Cooling\ price}{Heating\ price + Cooling\ price} \tag{3.21}$$

where COP_{min} is the minimum coefficient of performance that would result in an economical implementation of a heat pump. In the current energy market the COP_{min} is calculated to be 6.68, which is higher than the COP of the heat pumps implemented in all scenarios (see Table 3.3). When RESs are used (implying a lower electricity price), it eases the constraint on COP_{min}, thus improving the economic feasibility of direct electrification.

It is also worthwhile to note that the influence of a heat pump is marginal when compared to the indirect electrification schemes (i.e. S1 and S3). However, the significance of heat pumps lies in their facile implementation. In contrast, indirect electrification requires new flowsheeting to accommodate the change of feedstock, which is inapplicable to most existing plants.

3.3.5 Sensitivity analysis

The uncertainties in selected key variables (e.g. electricity price, MeOH price, TFCC, natural gas price and CO_2 price) are investigated through sensitivity analyses. Since the influence of indirect electrification significantly outweighs the direct electrification in the economic evaluation, the sensitivity analyses of S1 and S2 behave similarly (and the same can be said for S3 and its derived Scenarios S4–S6). In contrast, S1 and S3 (the latter representing indirect electrification) behave differently. The parameters for 0 % variation (base case in the sensitivity test) are tabulated in Table 3.6.

Table 3.6. Parameters for 0 % variance in the sensitivity test.

	Reference plant	CO_2 hydrogenation plant	Unit
Electricity	20	20	$/MWh
MeOH price	456	456	$/tonne
TFCC	306	548	M$
Natural gas price	208	–	$/tonne
OpEx (excluding natural gas)	6.7	98.5	M$/year
CO_2 price	45	45	$/tonne

As illustrated in Figure 3.9, the IRR values for all scenarios are highly dependent on MeOH price. When MeOH price is increased from 456 to 684 $/tonne, the IRR

values of Scenarios S1 and S3 increase to 75.4 and 36.1 %, respectively. Scenario S3 (and its derived Scenarios S4–S6) is more sensitive to the change of CO_2 price and electricity price than S1 and S2. This is attributed to the large quantity of CO_2 feedstock and electricity consumed in the CO_2 hydrogenation plants. The price of CO_2 means that the process receives revenue for using captured CO_2 and a baseline price of 45 \$/tonne is assumed in the analysis. The IRR value of the reference plants (S1 and S2) is least dependent on the change of natural gas price. Regarding the CO_2 hydrogenation plants (S3–S6), their IRR is independent of natural gas since no fossil fuels are used in the process.

The influence of TFCC is also significant for all scenarios, highlighting the importance of economies of scale (since TFCC per unit mass of product reduces when the scale of production increases). The simulated processes have an annual production rate of 400,000 tonnes, which is a medium-size plant in the context of modern MeOH production. Thus, there is room to improve economic performance when a larger scale is considered.

It is important to point out that the reference plant (S1) and its derived scenario (S2) have shown a satisfactory IRR in all circumstances within the range considered. The same cannot be said of the CO_2 hydrogenation plants (S3–S6, note the hurdle rate is set to be 8 %). Clearly, the economic potential of the conventional MeOH process is unimpeachable compared with the indirectly electrified process. Nevertheless, the significance of electrification lies mainly in the environmental impact. Moreover, in the case of surplus RES, the electrified process has shown better economic performance. The use of surplus RES to power MeOH production is of special interest because it is not only economically viable but also provides a solution to store renewable energy in the form of MeOH. This idea can be extended to the electrified production of any other high heating value chemicals, and thus it opens up new ways of thinking about renewable energy storage and management.

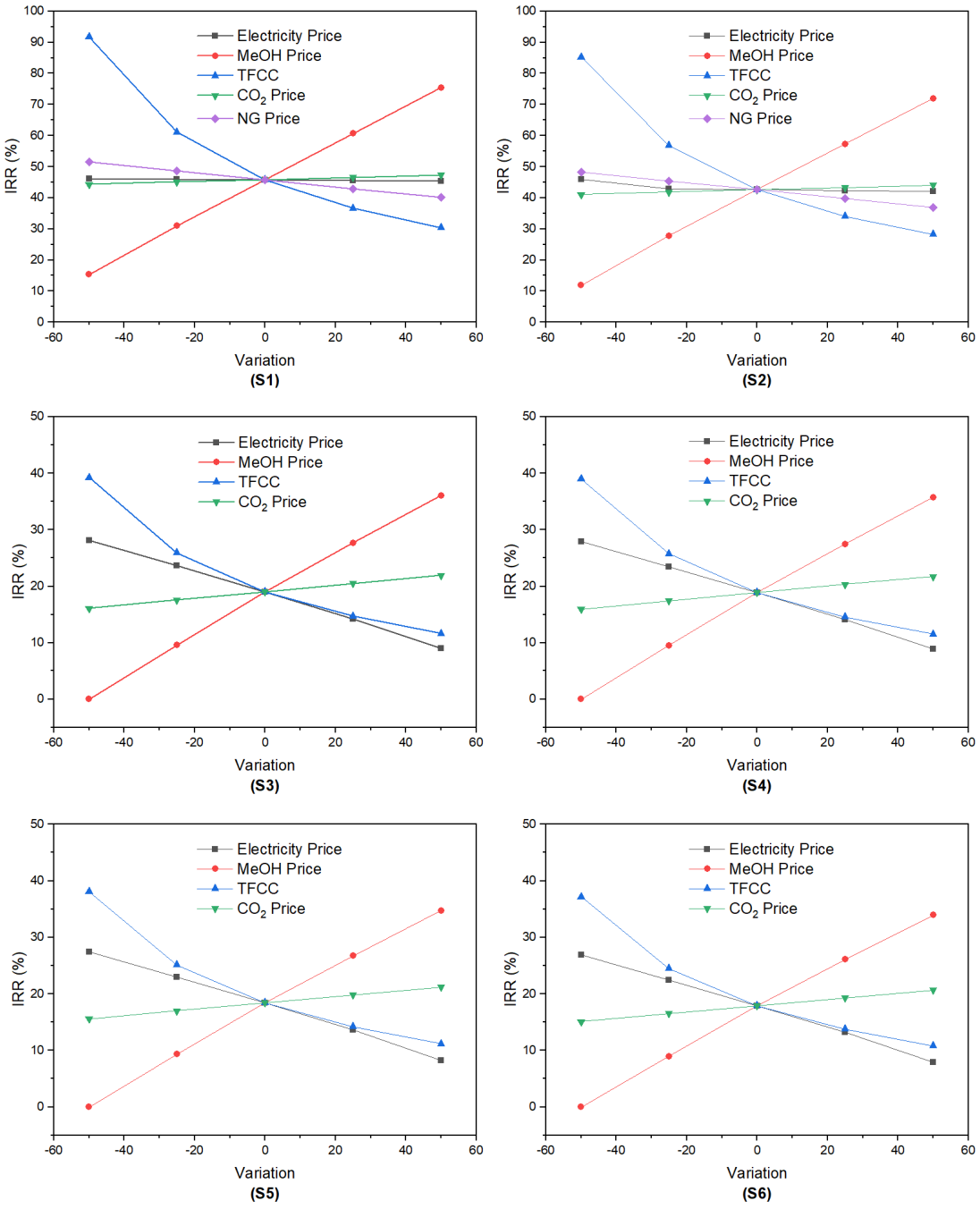


Figure 3.9. Sensitivity analysis of all scenarios. NG stands for natural gas.

3.3.6 Outlook

This work is the first step towards renewable energy utilisation in the chemical industry, which relies on the electrification of chemical processes. As a next step, and based on the energy analysis of this work, RESs will be introduced to power the fully electrified MeOH production process. In previous studies, Beerbühl et al. (2015) reported a novel optimisation method to integrate RES with electricity-based ammonia production. Nayak-Luke et al. (2018) also investigated the impact of RES intermittency on plant sizing and economic performance. However, most previous studies of RES integration have focused on ammonia, and the same concept for MeOH production is rare. This concept for MeOH is of particular significance not only because of its energy and market value but also because of its process characteristics: the distillation of raw MeOH product, which is an important energy consumer in the process, provides an additional handle for RES management. Intermittency would be accounted for by storing raw MeOH as an intermediate product to match RES variability. As a comparison, ammonia production can mainly accommodate RES intermittency through the excess generation and/or hydrogen-based energy storage system (ESS), resulting in over-sized electrolysers, hence the increase in process CapEx (Nayak-Luke et al., 2018). The separation of the catalytic reaction (to produce raw MeOH) and distillation process (to produce refined MeOH) enhances the process flexibility to better suit the variability of RES. To this end, new design variables will be considered to address the combined scheduling (renewable and dispatchable energy) and sizing (electrolyser, catalytic reactor and distillation column) of electricity-based MeOH production.

Other than producing MeOH as a commodity, ESS can be designed with MeOH as an energy vector. Originally, Bañares-Alcántara et al. (2015) proposed a conceptual design of an ammonia-based ESS for an islanded system, and Wang et al. (2017) analysed the time-invariant performance of such a concept. With the developments in direct methanol fuel cell technology (Baronia et al., 2019a,b), the same concept can be applied to MeOH-based ESS with advantages in long-term storage and facile transportation. Although the complexity in MeOH production poses a

modelling difficulty, it offers additional design variables for optimisation. It is envisioned that the design of MeOH-based ESS, which benefits from its unique process characteristics, may become a future solution to the utilisation of surplus renewable energy.

3.4 Conclusions

The analysis in this work considers both direct and indirect electrification schemes in MeOH production. Indirect electrification using alternative feedstock has demonstrated remarkable potential in both environmental and economic assessments. However, due to the feedstock change to low energy content materials (water and flue gas), the total energy consumption of a CO_2 hydrogenation plant (which is considered as an indirectly electrified plant) is inevitably and substantially larger than the traditional process. The low energy efficiency (mainly because of the water electrolysis units) of the CO_2 hydrogenation plant also contributes to the large energy demand. In addition, the economic performance of electrification crucially relies on renewable penetration, as the cost of electricity generated from fossil fuels outweighs that of their use for heating per unit energy. In other words, it is viable to substitute the energy content in fossil fuels with electricity only if inexpensive RESs are used. The almost fully electrified process (S6) reaches a break-even point and improves on a conventional plant (S1) at an electricity price of 25 and 4 \$/MWh, respectively. Regarding the environmental impact, the best scenario of combined direct and indirect electrification can reach a CO_2 abatement of up to 1.35 kg/kg_{MeOH} at 100 % renewable penetration.

Direct electrification through heat pump implementation is insignificant when compared with indirect electrification. Its impact is limited by the heat that can be delivered by a heat pump. As an example, the largest case of direct electrification (S3 to S6) can only convert 74.5 MW of heating (accounting for 87.5 % of total heating in S3) at an additional cost of 24.3 MW of electricity (accounting for 4.0 % of total electricity in S6). In contrast, indirect electrification (S1 to S3) increases

the electricity consumption from 14.2 MW in S1 to 604.1 MW in S3, with 90.3 % of the electricity (545.7 MW) consumed in feedstock (hydrogen) synthesis. The key implications for policymakers are clear: (1) modification of current industrial processes may have an insignificant impact on energy transition, and thus new process designs should be explored instead. (2) Energy policies should plan for a significant increase in power demand. From the analysis, the fully electrified MeOH production consumes 6–7 times more energy than the traditional fossil-based process. (3) Renewable power deployment has to be accelerated in the near future and in tandem with the progress in electrification, ensuring that increased electricity demand will be met by zero-carbon resources.

Chapter 4

Optimising Renewable Energy Supply to Power a Fully Electrified Methanol Process

ELECTRIFICATION of the chemical industry is tenable only if electricity is generated from renewable energy. The variable and intermittent nature of renewable sources poses additional difficulties when incorporated into the energy system. Aiming to power a fully electrified methanol plant, this chapter investigates the interplay between systems and the optimal operation of a renewable power system with backup dispatchable power located in Kramer Junction (USA) and in Norderney (Germany), which have excellent solar and wind source, respectively. When the storage size is optimised by renewable mix and excess generation, it has been found that the introduction of renewable energy storage significantly reduces the dispatchable energy requirement at the outset, but its influence levels off when the storage size is larger than 18 times the hourly load. The two-regime nature of the relation between storage size and dispatchable energy requirement becomes more apparent if the variability of the renewables is dominated by diurnal fluctuation, as opposed to seasonal fluctuation. The minimum levelised energy cost, which is optimised in terms of renewable power generation, renewable mix, and storage size, is found to be 202 and 111 $/MWh

for Kramer Junction and Norderney, respectively, based on a dispatchable energy price of 230 $/MWh. This leads to a levelised cost of methanol to be 2,692 and 1,561 $/tonne with a respective renewable penetration of 65 and 93 % in the production. The correlation between renewable penetration and dispatchable energy price in the most economical scenario also exhibits a two-regime behaviour: the renewable penetration increases dramatically at the beginning and then slowly approaches 100 % when the dispatchable energy price is above a critical point. For a fully renewable operation, the optimised levelised energy cost is found to increase to 370 and 130 $/MWh for Kramer Junction and Norderney, respectively.

4.1 Introduction

Chemical production is generally energy intensive and is responsible for a significant portion of greenhouse gas emissions. To reduce the reliance on fossil fuels, the electrification of the chemical industry is considered a promising method as there exists a growing consensus of pathways towards clean electricity (Kafandaris, 1994), i.e. generating electricity from renewable energy sources. However, one of the most significant barriers in variable renewable energy (VRE) integration is its intermittent nature, which causes a fluctuating power output in electricity generation.

There are a number of technologies and strategies to level power output from VRE, such as geographical expansion (Archer and Jacobson, 2007; Kempton et al., 2010), diversifying resources (Hart and Jacobson, 2011; Markvart et al., 2006), storage of surplus VRE (Denholm et al., 2005) and dispatchable energy backup. Instead of levelling power output, generation curtailment is another option to improve the stability of power output from VRE through generating excess electricity. The opportunities for demand-side management (DSM) are discussed in depth by Strbac (2008), which is also an important way of balancing generation and demand. However, there is little room for DSM in the traditional chemical industry since most existing chemical processes require a steady-state operation (and thus

a constant load). The implementation of renewable energy storage is of special importance to large scale industrial electrification. However, inter-seasonal storage for electricity is challenging at present. On the other hand, energy carriers in the form of chemicals, such as hydrogen (H_2) and its derivatives, can be produced using surplus renewable power, offering an effective approach to overcome the energy mismatch between VRE supply and demand (Samsatli and Samsatli, 2019).

Although there are several studies focusing on the electrification of the chemical industry (Bühler et al., 2019; Schiffer and Manthiram, 2017), renewable power systems for chemical processes have been rarely explored and most of the work has been focused on the production of ammonia (Beerbühl et al., 2015; Nayak-Luke et al., 2018). In the past, systems with high renewable penetration were often investigated within large scales of operation. For instance, Heide et al. (2011) studied a simplified European power system based on wind and solar power generation. They reported the impact of excess generation on balancing needs and the importance of renewable mix, especially when the wind and solar sources exhibit opposite seasonal behaviours (Heide et al., 2010). In a similar study, Rasmussen et al. (2012) investigated the synergies of storage and balancing in a highly renewable pan-European power system. However, these studies lack the economic analysis, which is important as the optimal renewable mix and storage size may change when economic feasibility is taken into consideration. Budischak et al. (2013) investigated the cost-minimised combinations of renewable sources and electrochemical storage powering one-fifth of the US electric grid. They reported that the electric system can be powered by 90 % renewable energy at costs comparable to today's provided that 2030 estimated technology costs are used. As an example of a small-scale application, Ekren et al. (2009) investigated a standalone system powered by a solar and wind hybrid system with battery storage, reporting the required solar and wind power size and battery capacity optimised by economic potential. The above studies have a challenge in common: both demand and power generation vary during the day and during the year. To use renewables to power a chemical process with a constant load, demand variation is circumvented, which however also means that there is little room for DSM. On the other hand, a

chemical may be used as both an energy carrier and a feed to a chemical process; therefore synergies may exist between energy storage and chemical production. These characteristics of powering a chemical process with renewables are yet to be studied. Among all chemical processes, methanol (MeOH) production through carbon dioxide (CO_2) hydrogenation has attracted broad attention in light of the importance of CO_2 valorisation (Kondratenko et al., 2013) and the potential of MeOH as a vector to synthetic hydrocarbons (Yarulina et al., 2018). Recently, Gonzalez-Garay et al. (2019) has presented an insightful work by assessing the sustainability of the CO_2-based MeOH processes through multi-scale analysis from plant to planet. Although the wide scope of the assessments prevails over purely economic arguments, the (renewable) power systems for hydrogen production is missing. In fact, most of the research focusing on CO_2 hydrogenation uses a benchmark price to represent the power systems for hydrogen production (Nguyen and Zondervan, 2019; Perez-Fortes et al., 2016). Similarly, studies focusing on renewable hydrogen production often lack a subsequent consideration for hydrogen conversion (Shaner et al., 2016). The analysis of a single system fails to convey a holistic picture of the role of renewable energy in the chemical industry. Therefore, it is pressing to explore a multi-system model with its interplay, which potentially offers new functional handles for systems optimisation.

Herein, the utilisation of VRE to power a fully electrified MeOH process is reported as a case study. This work aims to investigate the dual functionality of hydrogen (as an energy vector and a material buffer) in the renewable power system and its impact on the required storage capacity. This work also demonstrates the economic potential of the power system and the MeOH plant, which are optimised by the renewable mix, excess power generation, and storage capacity. The feasibility of renewable energy implementation in chemical production is evaluated taking locations (quality of renewable sources) and markets (dispatchable energy price and renewable energy costs) into account. The analysis is performed using renewable sources from two locations, namely Kramer Junction (USA) and Norderney (Germany), which have excellent solar and wind sources respectively. To investigate the synergies between systems by conjugating renewable power

generation with chemical processes is of particular significance, especially when the concepts of electrification and CO_2 valorisation are combined. This work can provide insights into a chemical industry powered by renewable energy and offer a basis for quantifying the feasibility of implementing a renewable power system for chemical processes in a specific location.

4.2 Methods

4.2.1 Concept overview

The electrified MeOH process is adapted from Chapter 3, consisting of a MeOH synthesis loop, a carbon capture process to source CO_2 from a flue gas stream, and electrolysers for hydrogen feedstock production. Note that the MeOH is synthesised via CO_2 hydrogenation to fully substitute the fossil fuel-based energy and feedstock. From the energy analysis, the electricity consumption for the fully electrified and integrated MeOH process is reported to be 12.4 kWh/kg_{MeOH} with 89 % consumed in hydrogen feed production. The detailed energy composition is illustrated in Figure B.1 in Appendix B. The MeOH production is designed with a constant load of 600 MW, corresponding to approximately 400,000 tonnes of MeOH per annum.

To power the chemical production using VRE, an energy storage system (ESS) is vital in order to minimise both the curtailment of generated renewable power and the reliance on dispatchable sources. The ESS is composed of alkaline electrolysers (operated at 1 atm), storage tanks of compressed hydrogen (stored at 170 atm) and solid oxide fuel cells (SOFC). A SOFC has been chosen due to its relatively low cost and high efficiency. Note that, although the choice of technology does not affect the formulation of the modeling approach, it is specified since the economic analysis requires the specific and corresponding cost parameters. This work focuses on a H_2-based ESS because of its interaction with the chemical process: the stored hydrogen can be fed to the MeOH synthesis directly (avoiding the fuel cells), thus increasing the overall conversion efficiency.

The analysis considers two operation scenarios, i.e. operation with and without dispatchable power backup. The former eases the constraint of storage capacity since all the remaining power mismatch (after being balanced by the ESS) would be covered by the dispatchable power. However, the inclusion of a dispatchable source increases the degrees of freedom of the scheduling, and thus an appropriate approach is required to cope with the system's design. The latter scenario is of special interest because it features a fully renewable energy operation (all power is from the VRE and its ESS) and it is often a requirement for an operation in islanded or remote areas where dispatchable sources are not available. The general concept of an electrified MeOH production powered by VRE and its ESS is shown in Figure 4.1. The dispatchable power backup is optional and it would only power the MeOH production, contrasting to the renewable power that would feed both the MeOH production and the ESS.

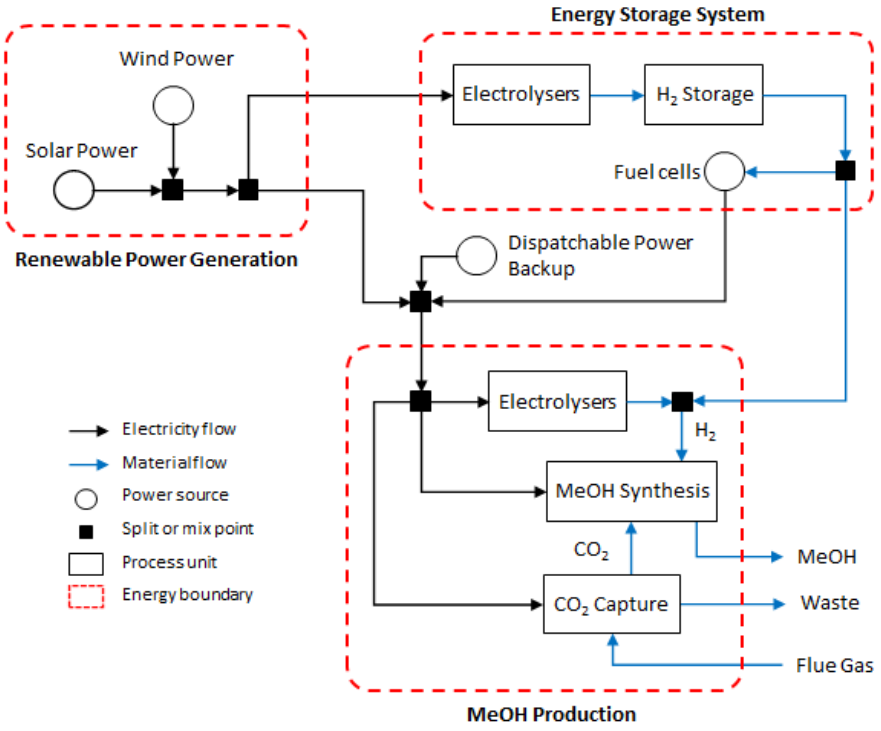


Figure 4.1. Overview of the general concept for the fully electrified MeOH production powered by renewable energy and its energy storage system.

4.2.2 Renewable power generation

The renewable power generation consists of wind and solar power, for which the renewable mix is of special interest. To approach the problem, two base power profiles for wind ($P_{\mathrm{W}}(t)$) and solar ($P_{\mathrm{S}}(t)$) are defined and scaled such that the cumulative power generation throughout the period of analysis is equal to the total load, as shown in Eqs. 4.1 and 4.2:

$$\sum_{t=1}^{N} P_{\mathrm{W}}(t) = P_{\mathrm{L}} N \tag{4.1}$$

$$\sum_{t=1}^{N} P_{\mathrm{S}}(t) = P_{\mathrm{L}} N \tag{4.2}$$

where P_{L} is the hourly load of the MeOH process and N is the total time of analysis taken as 8,760 hours, which is equivalent to 1-year operation. Note that P_{L} is assumed as a time-invariant constant (600 MW) due to the steady-state operation.

Due to the intermittency of VRE, it is inevitable to generate excess renewable power in order to reliably meet the load requirement, especially when a dispatchable source is not available or too costly. Here, the over-provision factor, γ, is introduced to quantify the extent of surplus generation. Note that γ is independent of the variability of power source, and it only indicates the average generation relative to the load without taking the ESS into account. For example, $\gamma = 1.5$ indicates that the year-averaged combined wind and solar power generation is 1.5 times the load requirement. The time series of power mismatch between the generation and the load (excluding the ESS), termed as $P_{\delta}(t)$, is directly related to γ and is calculated by

$$P_{\delta}(t) = \gamma\left(f_{\mathrm{W}} \frac{P_{\mathrm{W}}(t)}{P_{\mathrm{L}}} + f_{\mathrm{S}} \frac{P_{\mathrm{S}}(t)}{P_{\mathrm{L}}}\right) - 1 \tag{4.3}$$

where f_{W} and f_{S} respectively indicate the average fraction of wind and solar power in the renewable power generation. Note that $P_{\delta}(t)$ is normalised by the constant load P_{L}. The power mismatch calculation for the cases with an ESS is introduced in Section 4.2.3.

A larger γ will increase the likelihood of a power surplus in the time series. Here, γ is considered as an exogenous parameter, which is usually determined by factors such as the land availability to construct the renewable energy harvesting plant and the technological or economic limitations in such a construction. Although larger excess generation would always increase the reliability of power output, it also increases the cost of electricity generation. In the analysis of minimum storage capacity for a fully renewable operation (i.e. no dispatchable source is required), a range of γ from 1.0 to 2.0 is analysed because the power generation would not be sufficient to fulfil the load requirement when $\gamma < 1$ even if the ESS is 100 % efficient and any value above $\gamma = 2$ would mean an excessively over-sized (and hence overly costly) system. For the case of dispatchable source backup, the operation could be feasible when $\gamma < 1$ as all the remaining power deficit is met by the dispatchable source. In the economic assessment, γ is determined by optimisation, and a minimum value ($\gamma_{\min}$) exists in the case of an islanded system in order to permit a fully renewable operation.

4.2.3 Renewable energy storage

4.2.3.1 The case without dispatchable power. The storage profile of the ESS is of particular importance because it dictates the overall energy composition of the chemical process. Depending on the operation scenarios, the storage profile can be determined using different approaches. In the scenario of a fully renewable operation (all power is from VRE and its ESS), the time series of storage holdup, $L(t)$, can be calculated directly from $P_\delta(t)$: when the power mismatch is positive, the surplus VRE is stored in the ESS; when a power deficit occurs, energy is withdrawn from the ESS. However, the simple summation of positive and negative power mismatches does not represent the true storage profile as the storage capacity is constrained. As an illustration, the unconstrained $L(t)$ profiles are plotted in Figures B.2 and B.3 in Appendix B. The time series of constrained storage profile

is calculated by

$$L(t) = \begin{cases} L(t-1) + \eta_{\mathrm{ch}} P_\delta(t) & P_\delta(t) \geqslant 0 \\ L(t-1) + \frac{1}{\eta_{\mathrm{dis}}} P_\delta(t) & P_\delta(t) < 0 \\ 0 & L(t-1) + \eta_{\mathrm{ch}} P_\delta(t) \geqslant 0 \end{cases} \tag{4.4}$$

where η_{ch} and η_{dis} denote the conversion efficiency in charging (when $P_\delta(t) > 0$) and discharging (when $P_\delta(t) < 0$) mode, respectively. The cap value of the storage is defined as $L(t) = 0$ (a choice made for mathematical convenience), which means that at such a status the storage is full and the surplus VRE has to be curtailed. Consequently, the absolute value of $L(t)$ indicates the remaining storage capacity for charging. This approach enables the $L(t)$ profile to search for the minimum storage capacity (L^{cap}) that permits a fully renewable operation. Note that L^{cap} is specific at a given γ, f_{W} and location provided that $\gamma \geqslant \gamma_{\mathrm{min}}$. This is because any value smaller than L^{cap} would not permit the fully renewable operation and any value larger than L^{cap} requires extra storage capacity that would not be utilised.

The charging and discharging terms in Eq. 4.4 represent the change of energy in the storage over one unit time (i.e. 1 hour). For conciseness, the time interval of 1 hour is not shown in Eq. 4.4. It is important to point out that Eq. 4.4 considers all power deficit to be met by the ESS because a fully renewable operation is assumed. The energy flow around the storage at a particular time t is defined by $L(t+1) - L(t)$, where a positive value indicates charging and a negative value indicates discharging. Since L^{cap} is normalised by the hourly energy consumption, its value also represents the number of production hours that can be powered solely by the ESS.

When the storage system is to be connected to a chemical production process, its conversion efficiency needs to be revised to take the chemical process characteristics into account. Traditionally, the efficiency is assumed to be 0.6 in both charging and discharging of a H_2-based ESS with a technical nature similar to the one considered in this study (Heide et al., 2011), which coincides with the round-trip efficiency of 30–40 % reported by Beaudin et al. (2010). The overall efficiency

takes into account the energy losses from water electrolysis, hydrogen compression and energy output from the fuel cells. In this work, the energy consumption of electrolysers, which has already accounted for the energy losses, is taken as $4.5\,\mathrm{kWh/Nm^3_{H_2}}$ (Zeng and Zhang, 2010). This is equivalent to $55.7\,\mathrm{kWh/kg_{H_2}}$ at the electrolyser outlet conditions, and thus the conversion efficiency is found to be 70.7 % based on the theoretical energy requirement of $39.4\,\mathrm{kWh/kg_{H_2}}$ (Wang, 2006). Therefore, η_{ch} is set to 0.9 (only addressing the energy losses in the compression process) so that the round-trip efficiency is comparable to the literature value. More justifications regarding the charging efficiency are provided in Section 4.2.6. In the discharging mode, the stored hydrogen can be used as either feedstock ($\eta_{\mathrm{dis}} = 1$) or for electricity generation through fuel cells ($\eta_{\mathrm{dis}} = 0.6$). The discharge efficiency is set to 0.6 when the stored hydrogen is fed to the fuel cells. Note that this is a conceptual discharge efficiency resulting in a round-trip efficiency of 36 %, which complies with the literature value (Beaudin et al., 2010).

Since the two destinations of the stored hydrogen are of different efficiency, it would be more efficient to prioritise the use of the stored hydrogen as feedstock for the MeOH synthesis than its use for electricity generation. Since the synthesis of hydrogen feedstock accounts for 89 % of the total load, the requirement of hydrogen feedstock (in terms of power equivalent) is 0.89 normalised by the load (i.e. if the total load is 1 MW, the power required for hydrogen feedstock synthesis would be 0.89 MW). Therefore, in discharging mode the stored hydrogen will first feed the MeOH synthesis as feedstock when $-0.89 \leqslant P_\delta(t) < 0$; if the deficit is larger ($-1 \leqslant P_\delta(t) < -0.89$), the stored hydrogen will feed both the MeOH synthesis (as feedstock, $\eta_{\mathrm{dis}} = 1$) and the fuel cells (to generate electricity, $\eta_{\mathrm{dis}} = 0.6$). Consequently, Eq. 4.4 is modified to

$$L(t) = \begin{cases} L(t-1) + \eta_{\mathrm{ch}} P_\delta(t) & P_\delta(t) \geqslant 0 \\ L(t-1) + P_\delta(t) & -f_{\mathrm{ELY}}^{\mathrm{SYN}} \leqslant P_\delta(t) < 0 \\ L(t-1) - f_{\mathrm{ELY}}^{\mathrm{SYN}} + \frac{1}{\eta_{\mathrm{dis}}}\left[P_\delta(t) + f_{\mathrm{ELY}}^{\mathrm{SYN}}\right] & P_\delta(t) < f_{\mathrm{ELY}}^{\mathrm{SYN}} \\ 0 & L(t-1) + \eta_{\mathrm{ch}} P_\delta(t) \geq 0 \end{cases} \tag{4.5}$$

where $f_{\mathrm{ELY}}^{\mathrm{SYN}}$ represents the fraction of load that goes to the hydrogen feedstock synthesis through electrolysis (which is 0.89 in the MeOH production considered in this work). This parameter is of special meaning as it implies how efficient the H_2-based ESS would be for a chemical process that requires hydrogen as feedstock.

4.2.3.2 The case with dispatchable power. Although the inclusion of a dispatchable source reduces the management difficulties, this flexibility poses an additional complexity in modelling due to the extra degree of freedom. In Eqs. 4.4 and 4.5, the time series of storage profile and its corresponding L^{cap} target a fully renewable operation. In the scenario of a partial renewable operation (due to the use of dispatchable energy), storage size is not required at L^{cap}. Consequently, dispatchable power will be required at time intervals when the VRE and ESS combined output is insufficient. To determine the time series of $L(t)$ in a scenario with dispatchable source backup, the power mismatch needs to be revised by considering the storage capacity as a decision variable (L^{dv}). Note that the revised power mismatch, $P_{\delta}^{\mathrm{re}}(t)$, indicates the mismatch between the renewable power system and the load taking the ESS into account, whereas $P_{\delta}(t)$ is the power mismatch between the renewable power generation (excluding the ESS) and the load. The algorithm for the calculation is shown in Algorithm 1 in Appendix B. Also note that $L(t)$ and $P_{\delta}^{\mathrm{re}}(t)$ are related in that $L(t)$ determines $P_{\delta}^{\mathrm{re}}(t)$ and $P_{\delta}^{\mathrm{re}}(t)$ in turn determines $L(t+1)$.

In the analysis, the operation starts and ends with full storage, i.e. $L(t=1) = L(t=8760) = L^{\mathrm{dv}}$. The range of L^{dv} is varied from 0 to L^{cap} since L^{cap} is the storage size indicating a fully renewable operation, and thus any value higher than L^{cap} will not reduce the dispatchable energy requirement. Note that the full storage is defined as a positive number, contrasting to 0 in the fully renewable operation. This is because in the fully renewable operation L^{cap} is calculated from the storage profile, whereas L^{dv} in the partial renewable operation is a decision variable that determines the storage profile. Nevertheless, both definitions are equivalent since the energy flow from the ESS at time t, defined by $L(t+1) - L(t)$, being the same.

The energy structure of the load can be derived from the same algorithm as

the cumulative dispatchable energy is obtained from the profile of $P_{\delta}^{\mathrm{re}}(t)$, and the energy from the ESS is obtained from $L(t)$. The time series of dispatchable power requirement, $P_{\mathrm{D}}(t)$, is calculated by

$$P_{\mathrm{D}}(t) = \begin{cases} |P_{\delta}^{\mathrm{re}}(t)| & P_{\delta}^{\mathrm{re}}(t) < 0 \\ 0 & P_{\delta}^{\mathrm{re}}(t) \geqslant 0 \end{cases} \tag{4.6}$$

The normalised dispatchable energy requirement, E_{D}, is essentially the integration of dispatchable power over the period of analysis divided by the total number of hours. Since the original VRE data is available on an hourly scale, E_{D} can be approximated by

$$E_{\mathrm{D}} = \frac{1}{N} \sum_{t=1}^{N} \left[P_{\mathrm{D}}(t) \times 1 \right] \tag{4.7}$$

Note that E_{D} is normalised by the total energy load in a year, which is $8760 \times P_{\mathrm{L}}$ (i.e. 5,256 GWh). Due to the normalisation, the numerical value of E_{D} also represents the fraction of load that has been met by dispatchable energy, and $1 - E_{\mathrm{D}}$ indicates the renewable penetration ($f_{\mathrm{L}}^{\mathrm{RE}}$), i.e. the fraction of load met by renewable energy.

The power scheduling is essentially determined from $L(t)$ profiles as all other time series are dependent on $L(t)$. The production is powered by the energy sources that are prioritised as follows: (1) power from renewable generation; (2) hydrogen from the ESS as feedstock (which is power equivalent); (3) power from the ESS via SOFC and (4) power from a dispatchable source (if it is available). This implies that the dispatchable energy cost is higher than that of the renewable power system (including the power generation and the ESS). The cases of lower dispatchable energy prices are discussed in the section on economic analysis. The power scheduling for both fully and partially renewable operations is visualised in Figure B.7 in Appendix B.

4.2.3.3 Define start time and status. It is important to note that the $L(t)$ profile depends on both the initial state of storage and the start time of operation in a year. For convenience, a complete cycle of storage operation is defined as

full-to-null-to-full (in contrast to null-to-full-to-null). As an illustration, examples of $L(t)$ profiles are plotted with varied γ at fixed f_{W} over a 4-year period (Figure B.4 in Appendix B). The $L(t)$ profile continues to the next year by repeating the same meteorological data, thus generating perfect cycles of charging and discharging profiles. If true meteorological data of consecutive years were used, the charging/discharging cycle would vary accordingly (and so the value of L^{cap}). There is more discussion in Section 4.4.1 regarding the use of historical VRE data and its limitations. Nevertheless, the purpose of the plot (Figure B.4) is (1) to demonstrate that the start time of operation has to be considered, and (2) to identify the characteristic period of operation, which is equivalent to 1 year. Consequently, the analysis is performed at the beginning of the characteristic period instead of at the beginning of a calendar year.

4.2.4 Economic optimisation

The economic potential of the concept is evaluated by the levelised cost of MeOH (LCOMeOH, calculated in \$/tonne), which is defined by

$$\mathrm{LCOMeOH} = \frac{1}{M_{\mathrm{MeOH}}}\Big[\frac{\mathrm{TFCC}\cdot r(1+r)^n}{(1+r)^n-1} + P_{\mathrm{L}}N\cdot\mathrm{LEC} + C_{\mathrm{ELY}}^{\mathrm{SYN}} + \sum_j C_j\Big] \quad (4.8)$$

where TFCC stands for the total fixed capital cost of the MeOH plant (including CO_2 capture and MeOH synthesis), LEC stands for the levelised energy cost (\$/MWh) of the energy delivered from the renewable power system (including power from the generation and the ESS) to the MeOH production, $C_{\mathrm{ELY}}^{\mathrm{SYN}}$ is the annualised cost of the electrolysers for the MeOH synthesis loop, C_j is the annual cost of utility j (including process water and cooling water), M_{MeOH} is the total mass of MeOH produced in a year, r represents the discount rate (taken as 8 %) and n is the life of the plant (assumed to be 30 years). The material cost of flue gas (source of CO_2) is assumed to be free. Note that all parameters in Eq. 4.8 are fixed except LEC since the production is operated on a steady-state basis. Therefore,

minimising LCOMeOH is equivalent to minimising LEC, which is calculated by

$$\begin{aligned}\mathrm{LEC} = \frac{1}{P_\mathrm{L} N}\Big[&\sum_{i=\mathrm{W,S}} \Big[\gamma f_i P_\mathrm{L} \frac{1}{\mathrm{CF}_i} \frac{r(1+r)^n}{(1+r)^n - 1} \mathrm{CapEx}_i^{\mathrm{GEN}}\Big] \\ &+ \sum_{i=\mathrm{W,S}} \Big[\gamma f_i P_\mathrm{L} \frac{1}{\mathrm{CF}_i} \mathrm{OpEx}_i^{\mathrm{GEN}}\Big] + C_{\mathrm{ELY}}^{\mathrm{ESS}} \\ &+ \frac{\eta_{\mathrm{ch}} L^{\mathrm{dv}} P_\mathrm{L}}{e^{\mathrm{ELY}}} \frac{r(1+r)^n}{(1+r)^n - 1} \mathrm{CapEx}^{\mathrm{ST}} + c_\mathrm{D} E_\mathrm{D} P_\mathrm{L} N\Big]\end{aligned} \tag{4.9}$$

where CF_i stands for the capacity factor of renewable source i, $\mathrm{CapEx}_i^{\mathrm{GEN}}$ is the capital expenditure of renewable source i per unit power generation capacity, $\mathrm{CapEx}^{\mathrm{ST}}$ is the storage capital expenditure per unit hydrogen capacity (in tonne), $\mathrm{OpEx}_i^{\mathrm{GEN}}$ is the operational expenditure of renewable source i per unit power generation capacity, c_D is the unit price of dispatchable power and e^{ELY} is the specific energy consumption of water electrolysis, which is taken as $55.7\,\mathrm{kWh/kg_{H_2}}$. Unlike the constant annualised electrolyser cost for the synthesis loop ($C_{\mathrm{ELY}}^{\mathrm{SYN}}$), the annualised electrolyser cost for the ESS ($C_{\mathrm{ELY}}^{\mathrm{ESS}}$) is a variable subject to the optimiser, as shown in Eq. 4.10:

$$C_{\mathrm{ELY}}^{\mathrm{ESS}} = \frac{r(1+r)^n}{(1+r)^n - 1} \mathrm{CapEx}^{\mathrm{ELY}} P_{\mathrm{ELY}}^{\mathrm{ESS}} \tag{4.10}$$

where $\mathrm{CapEx}^{\mathrm{ELY}}$ is the electrolyser capital expenditure and $P_{\mathrm{ELY}}^{\mathrm{ESS}}$ denotes the rated power of the electrolysers for the ESS.

For the partially renewable operation, the model aims to minimise LEC with an objective function defined by

$$\begin{aligned} \text{min.} \quad & \mathrm{LEC} = f(\gamma, f_\mathrm{W}, L^{\mathrm{dv}}) \\ \text{s.t.} \quad & 0 \leqslant \gamma \\ & 0 \leqslant f_\mathrm{W} \leqslant 1 \\ & 0 \leqslant L^{\mathrm{dv}} \leqslant L^{\mathrm{cap}} \\ & \text{Energy balances outlined in Figure B.6} \end{aligned} \tag{4.11}$$

Note that the constraint of γ is loose because all power deficit can be met by dispatchable source if the combined power of the generation and the ESS is

insufficient. For the fully renewable operation, LEC can be minimised subject to the condition that the production is sustainable without any dispatchable source. This leads to

$$\begin{aligned} \text{min.} \quad & \text{LEC} = f(\gamma, f_{\text{W}}) \\ \text{s.t.} \quad & \gamma_{\text{min}} \leqslant \gamma \\ & 0 \leqslant f_{\text{W}} \leqslant 1 \\ & \text{Energy balances outlined in Figure B.6} \end{aligned} \tag{4.12}$$

The condition of $\gamma_{\text{min}} \leqslant \gamma$ is equivalent to $P_{\delta}^{\text{re}}(t) \geqslant 0$ for all t, which implicitly determines γ_{min}. Note that for a fully renewable operation L^{dv} is equal to L^{cap} in Eq. 4.9, which is calculated at a given γ (provided that $\gamma_{\text{min}} \leqslant \gamma$) and a given f_{W} (i.e. L^{cap} is a function of γ and f_{W}, $\gamma_{\text{min}} \leqslant \gamma$ is a constraint and γ_{min} is a function of location and f_{W}). The optimisation problems are solved using the *FMINCON* solver in Matlab, which employs a nonlinear programming (NLP) method.

The TFCC of the MeOH plant is adopted from Chapter 3, which is scaled via the six-tenths factor rule based on the work of Zhang et al. (2017) and updated to 2018 using the annual chemical engineering plant cost index (CEPCI). Detailed TFCC, raw material costs, utility price and renewable power system costs are available in Tables B.1–B.4 in Appendix B.

4.2.5 Renewable energy data

To incorporate renewable energy in chemical production it is often vital to select a suitable location with sufficient VRE availability and necessary infrastructure. Here, meteorological data for wind and solar sources from two locations (Kramer Junction and Norderney) are used as an example to perform the numerical studies of VRE integration, as well as explore the impact of their characteristics on the storage and balancing synergies.

The solar and wind data are obtained from Meteonorm, a meteorological database that provides hourly data for different locations. The global horizontal radiation

(measured in kWh/m^2) is used as available solar power with a 15 % efficiency. The wind velocity provided in Meteonorm (measured at a height of 10 m) is first converted to a hub height of 80 m, which is calculated by Eq. B.1 in Appendix B. The hub height velocity then inputs to the power profile of a specific turbine to generate wind power. The turbine that has been selected in this study is a Vestas V90 model with a power profile shown in Figure B.8 in Appendix B. The cut-in and cut-out speeds are set as 4 and 25 m/s, respectively (Vestas Wind Systems, 2004).

Since the model of the wind turbines (3.0 MW) is given, the yearly mean power generation per turbine can be calculated according to the wind speed at each location. This gives the CF of wind power to be 4.3 % for Kramer Junction and 29.4 % for Norderney, respectively. Regarding the solar power, the CF for Kramer Junction is assumed to be 25.0 % (this is the CF of solar PV farms used in the work of Matzen et al. (2015)), whereas the CF for Norderney is calculated to be 12.1 % based on its relative strength to Kramer Junction. As discussed previously, neither a standalone wind nor a solar energy system can provide a continuous supply of energy. Therefore, a combination of complementary energy sources is considered in this work for the purpose of levelling renewable power output, although the wind source in Kramer Junction and the solar source in Norderney are unfavourable.

Figure 4.2 depicts the time series of wind and solar power profiles for Kramer Junction (top panel) and Norderney (bottom panel). Note that the data are normalised to the respective yearly mean value, and thus they only reflect the variability of the sources but give no information about their strength or availability. Clearly, the two places feature different VRE characteristics, especially in wind energy. The wind power in Kramer Junction varies significantly throughout the year, and it often peaks to as high as 20 times its yearly mean value. In direct contrast, the wind power profile in Norderney has shown remarkable smoothness with the highest variation less than 4 times its mean. The standard deviation (σ) is used to measure the variability of the renewable sources (tabulated in Table B.6 in Appendix B) and finds that the wind power in Norderney is the least variable source. Its consistent power availability is a motivator that drives the wind farm

installation in the region. Regarding the solar power, both locations show moderate variations on the demonstrated time scale. However, it has significant fluctuation on the diurnal time scale, which may impede its integration into chemical production or any other power demand that requires a steady input. In addition, solar power has a clear seasonal pattern: abundant in the summer and lean in the winter. Since the investigated chemical production has a constant load, the operation would also have a seasonal pattern of power mismatch if solar power dominates the renewable mix.

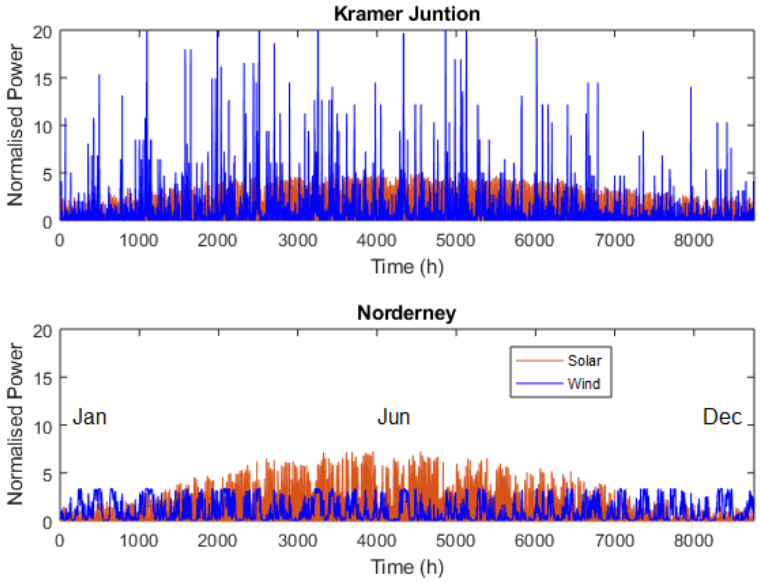


Figure 4.2. Normalised year-round availability of wind and solar power of a selected year. (Top) Data obtained from a weather station near Kramer Junction, US; (Bottom) data obtained from Norderney, Germany. Each series is shown in 1-hour resolution and normalised to the respective yearly mean value.

4.2.6 Summary of assumptions

This section lists the key assumptions in the analysis as well as the justifications: (1) the operation starts at the beginning of the characteristic period of 8,760 hours, which is equivalent to 1 year. (2) The downtime of MeOH production is ignored. (3) The dispatchable source is assumed from the grid with a CO_2 emission calculated according to the generation methods, which is location dependent. (4) The electrolysers can ramp instantaneously from 0 to 100 % with a constant efficiency, which translates to a constant specific energy consumption of 55.7 kWh/kg_{H_2} at

the outlet conditions. (5) A separate set of electrolysers can be considered in the ESS because (i) the operation of the electrolysers in the ESS and the MeOH production has concurrent peaks, (ii) the costing is assumed to be linear with respect to size, and (iii) the efficiency of the electrolysers is assumed to be constant and independent of load. (6) Hydrogen for the ESS is stored in steel tanks at a pressure of 2,500 psi (approximately 172 bar), and the standby losses of hydrogen in the ESS are ignored. (7) The ESS is not limited by power input or output because additional electrolysers (for charging) and fuel cells (for discharging) can always be implemented to meet the requirement. (8) The charging mode efficiency of the ESS is assumed to be 60 %, which takes the electrolyser efficiency (70.7 %) and the compression efficiency (approximately 90 %, i.e. the loss due to compression accounts for 10 % of the total feed energy) into account. The compression efficiency is justified by Aspen Plus simulations, showing that when hydrogen is fed to the MeOH synthesis (at 71 bar) and goes through the ESS, the energy loss due to the ESS (hydrogen compressed to 172 bar and then decompressed to 71 bar) accounts for approximately 10 % of the total feed energy.

4.3 Results

4.3.1 Production without energy storage

This section investigates the optimal renewable mix and the dispatchable power requirement when the ESS is excluded from the renewable power system. Without an ESS, levelling the power output becomes the key as all surplus power would have to be curtailed. Also, a large amount of dispatchable energy is required because power deficit is more likely to occur, or alternatively, large excess generation is required to reduce the likelihood of deficit.

The E_{D} calculated for Kramer Junction and Norderney are shown in Figure 4.3A and B, respectively. Since γ is a measurement of excess generation, the requirement of E_{D} decreases with increasing γ. Both locations have shown lower E_{D} at

intermediate f_{W}; however, their minimum valley pathways vary slightly, which is attributed to the characteristics of their wind/solar availability. It is also interesting to see that the worst scenarios (highest E_{D}) for Kramer Junction and Norderney lie in opposite f_{W}. This is ascribed to the different variability of VRE in the two locations, i.e. wind energy is more variable in Kramer Junction, whereas solar energy is more variable in Norderney (see Table B.6 in Appendix B).

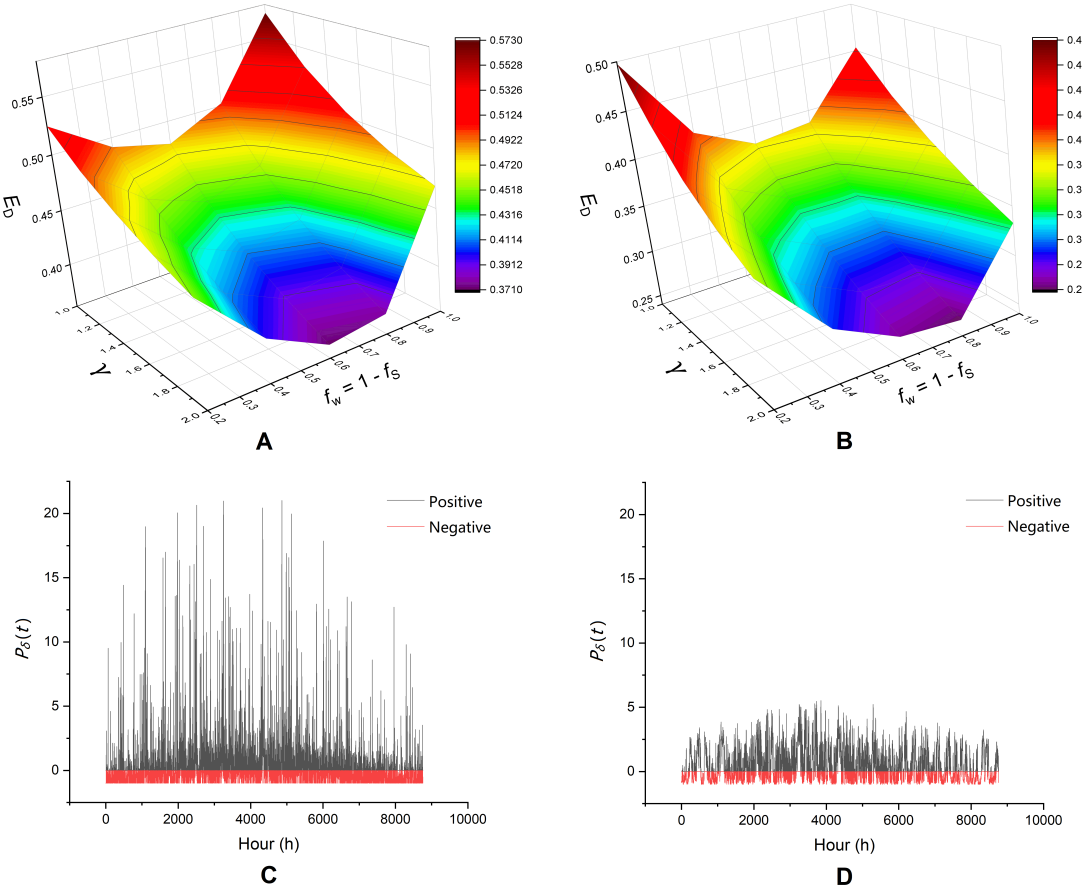


Figure 4.3. Top: Requirement of dispatchable energy E_{D} as a function of γ and the share of wind power f_{W} at the demand side for (A) Kramer Junction and (B) Norderney. Bottom: Time series of power mismatch in best scenarios when $\gamma = 1.5$, (C) Kramer Junction with the best scenario at $f_{\mathrm{W}} = 0.65$; (D) Norderney with the best scenario at $f_{\mathrm{W}} = 0.70$. Positive values indicate power surplus that has been curtailed and negative values indicate power deficit. The unit of $P_{\delta}(t)$ and γ is given in load requirement (MW) at the demand side, whereas E_{D} is normalised by the total annual energy requirement (MWh).

The intersecting profiles of Figure 4.3A and B at $\gamma = 1.5$ are analysed and plotted with finer granularity in Figure B.9 in Appendix B. It has been found that the best scenarios (lowest E_{D}) at $\gamma = 1.5$ for Kramer Junction and Norderney are at $f_{\mathrm{W}} = 0.65$ and $f_{\mathrm{W}} = 0.70$, and their corresponding minimum E_{D} are 0.41 and

0.30, respectively. Since E_D is normalised by the annual energy requirement at the demand side, this means that the energy for chemical production from the dispatchable source constitutes 41.1 % in Kramer Junction or 30.2 % in Norderney. This is a significant dispatchable energy requirement even though the average renewable power generation is 1.5 times the load requirement.

The representative energy mismatch profiles for both locations with $\gamma = 1.5$ at their optimal VRE mix are shown in Figure 4.3C and D. The mismatch profile is strongly correlated to the availability profiles illustrated in Figure 4.2. Since the average generation of both locations is the same and equals to 1.5 times the load requirement ($\gamma = 1.5$), more positive mismatch comes with more negative mismatch so that the total amount of energy is a constant, i.e. Figure 4.3C has denser negative mismatch as well as more positive mismatch compared to Figure 4.3D. This variability is undesired and results in additional management difficulties. As an example, Kramer Junction has shown much larger dispatchable requirement than Norderney due to its significant variance. The positive mismatch also represents the amount of energy that can potentially be stored. Notice that Figure 4.3C and D are plotted on the same scale to reflect the relative variability of the VRE sources at the two locations.

4.3.2 Production without dispatchable energy source

To power a chemical process with only renewable power can be challenging but it is of significance for production located in an islanded or remote area. This section intends to report the minimum storage capacity (L^{cap}) that permits the fully renewable operation and how its corresponding optimal renewable mix varies with increasing renewable power generation.

The dependence of L^{cap} on f_W and γ is demonstrated for MeOH production located in Kramer Junction and Norderney in Figure 4.4A and B, respectively. The optimal f_W (the f_W resulting in the minimum L^{cap}) at the corresponding γ forms a minimum valley along the contour lines, which is indicated by the dashed

line with white markers. In Kramer Junction, the optimal f_W varies significantly from 71 % at $\gamma = 1.09$ to 30 % at $\gamma = 1.45$. In contrast, the minimum valley of f_W in Norderney varies in a narrow range of 82–96 %. This may be attributed to the convexity of the contour lines in Norderney: variation in f_W significantly influences the value of L^{cap} at a given γ. Thus, the optimal mix becomes more deterministic and lies in a narrow range. The shape of contour lines in Kramer Junction is rather flat, meaning that a wide range of f_W would result in a similar L^{cap} provided that γ is unchanged. In summary, L^{cap} is mainly determined by γ in Kramer Junction, whereas it is mainly determined by renewable mix in Norderney.

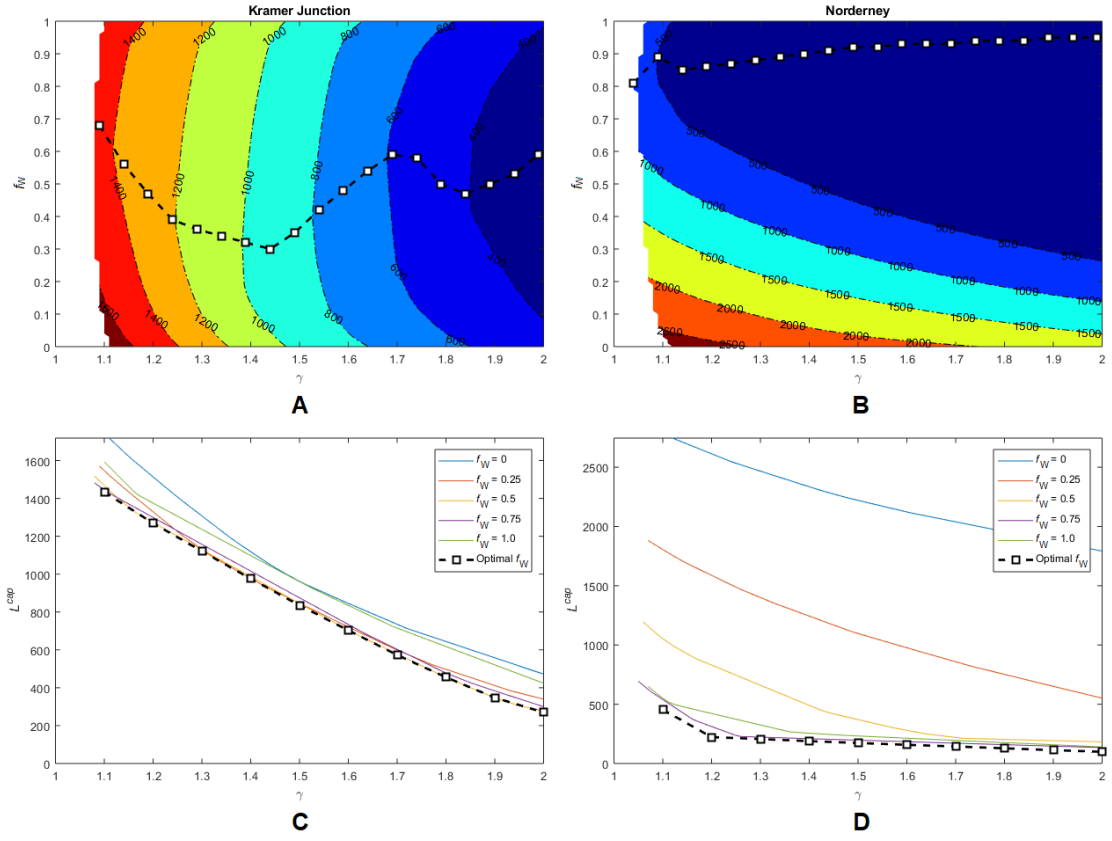


Figure 4.4. L^{cap} as a function of f_W and γ for MeOH production without a dispatchable source. Top panel: contour plots of L^{cap} for production located in (A) Kramer Junction and (B) Norderney. Bottom panel: L^{cap} cuts through selected f_W for (C) Kramer Junction and (D) Norderney.

The sensitivity of L^{cap} to f_W is also shown in Figure 4.4C and D where L^{cap} cuts through selected f_W are plotted. The optimal (minimum) L^{cap} is indicated by the dashed line with white markers and the value of the corresponding f_W is shown in the respective contour plots. In Kramer Junction, all ranges of f_W result

in a L^{cap} that is close to the optimal L^{cap} (at a given γ). On the contrary, the lines of L^{cap} cuts in Norderney vary dramatically when a different renewable mix is used. Nevertheless, both locations have shown a L^{cap} cut at a particular f_{W} that is close to the optimal L^{cap} cut at all γ. The value of such a f_{W} is approximately 50 % in Kramer Junction and 75 % in Norderney. These plots demonstrate that although the optimal f_{W} is specific to each L^{cap} and may vary significantly when γ is varied, there may exist a single value of f_{W} that would result in a L^{cap} close to the optimum in the whole range of γ. This particular f_{W} is of importance when a power system needs to tackle a variable load (variation from the demand side). In this case study, although the load of chemical production is a constant, such flexibility is desired to tackle the variation from the generation side since the calculation of L^{cap} is based on past data. For instance, the wind and solar harvesting plants designed with an optimal f_{W} for a given γ in a historical year may encounter a different γ in real-time operation due to the inconsistency in yearly renewable energy availability.

From Figure 4.4C it is also observed that L^{cap} decreases significantly and almost linearly with the increase of γ in Kramer Junction. In contrast, L^{cap} in Norderney (Figure 4.4D) varies in a narrow range from approximately 500 to 100 when γ is increased from 1.1 to 2.0. In particular, when $\gamma > 1.2$ the value of L^{cap} is almost independent of γ. This is attributed to the consistent availability of VRE in Norderney: the maximum power mismatch is only around 5 times the load in the entire year, contrasting with 20 times the load in Kramer Junction (c.f. Figure 4.3C and D). This characteristic of the VRE sources greatly eases the management and reduces the cost of running a renewable energy system.

Notice that in Figure 4.4A and B there is empty space when γ lies between 1.0 to approximately 1.1. This is because the generation is not sufficient to power the chemical production solely with VRE and its storage (i.e. $\gamma < \gamma_{\text{min}}$). If the energy conversion and storage scheduling were perfect, the generation may be able to meet the load at $\gamma = 1.0$. In this analysis, the operation is tenable only when γ is above 1.1. This is remarkably small excess generation compared to the results from Budischak et al. (2013), in which they have reported a system that generates

180 % (equivalent to $\gamma = 1.8$) of the electrical energy needed by the load when 90 % of hours are covered by VRE or 290 % ($\gamma = 2.9$) of need when 99.9 % of hours are covered by VRE. At an extreme renewable mix (very large or very small f_{W}), it is more likely to have insufficient generation (larger γ_{min} required), which indicates the importance of introducing complementary renewable sources in the fully renewable operation.

Benefited by the chemical process (taking stored hydrogen as a feedstock instead of feeding to fuel cells), the storage system is highly energy-efficient and is able to provide sufficient power even at small γ. However, the $L(t)$ profile (and its corresponding L^{cap}) depends on both energy efficiency and γ. Operations at small γ may incur a significant increase in L^{cap}, thus increasing the cost of an ESS. To demonstrate the impact of γ on $L(t)$ and L^{cap}, profiles at selected γ are plotted for Kramer Junction (Figure 4.5A) and Norderney (Figure 4.5B) over its characteristic period of operation, starting from full storage and ending in a fully charged status. For clarity, the $L(t)$ profiles are converted from the energy term normalised by the load to its equivalent hydrogen mass in tonne on the basis of a 600 MW MeOH plant. A unique difference of the profiles between the two locations is the dependence of L^{cap} on γ. As suggested in Figure 4.4C and D, L^{cap} in Kramer Junction is linearly dependent on γ while L^{cap} in Norderney is relatively insensitive to γ when $\gamma > 1.2$. Thus, the $L(t)$ profiles for Norderney at $\gamma = 1.55$ and 2.00 almost superimpose onto each other (Figure 4.5B). Another noticeable fact is that L^{cap} for Norderney is smaller than that for Kramer Junction in the whole range of γ, indicating much easier management of the power system.

The value of L^{cap} and the fraction of empty hours at different γ for both locations are summarised in Table 4.1. It is found that the number of empty hours increases with increasing γ for both locations. This is expected as the system is less likely to encounter a power deficit when the generation is greatly in excess. By analysing the profile of $L(t)$, the empty hours are found concentrated in a certain period of operation for both locations when γ is small, implying a strong seasonal pattern. However, at higher γ the $L(t)$ profiles for Norderney are not seasonally dependent as the empty hours spread throughout the period of operation. On the other hand,

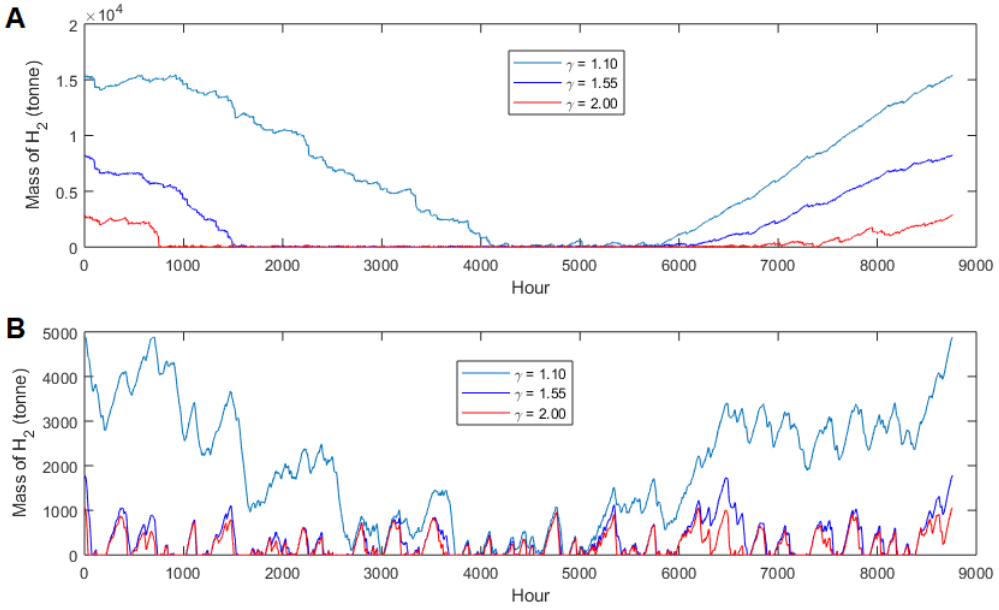


Figure 4.5. Time series of $L(t)$ in terms of H_2 mass with optimised L^{cap} at selected γ for a 600 MW MeOH production process located in (A) Kramer Junction and (B) Norderney. Note that the y-axis scale is different in the two plots.

Table 4.1. L^{cap} and empty hours of the storage system in Kramer Junction and Norderney.

	Kramer Junction			Norderney		
γ	1.10	1.55	2.00	1.10	1.55	2.00
L^{cap} (tonne of H_2)	15,438	8,279	2,909	4,889	1,788	1,063
empty hours (%)	1.0	15.8	24.2	2.9	21.9	31.8

Kramer Junction has demonstrated reduced seasonal dependency at a higher γ. The implication that may be drawn from the analysis is that a large quantity of seasonal storage is essential for operation in Kramer Junction, whereas a small but more efficient short-term storage may be used in Norderney to reduce the cost. The underlying reason may be the fact that the wind power dominates in Norderney (optimal f_{W} ranges from 88 to 95 %), which is not seasonally dependent, whereas solar and wind power play an equal role in Kramer Junction (optimal f_{W} ranges from 43 to 65 %), wherein solar power has a strong seasonal pattern. It is noteworthy that the $L(t)$ profile for Norderney at $\gamma = 1.1$ is affected by both the seasonal and short-term (e.g. weekly scale, contrasting to diurnal scale) variation as the optimal mix is determined to be $f_{\text{W}} = 88\,\%$, wherein solar power has an increased share in the generation.

4.3.3 Production powered by a mix of VRE and dispatchable energy

To meet a load solely by renewable power poses a stringent constraint on the system design. In the aforementioned example, Budischak et al. (2013) have reported an 80 % increase in the renewable power generation to increase the hours of grid operation covered by all renewables from 90 to 99.9 % in the cost-minimised case. In this work, to power the chemical plant solely by renewables requires either large excess generation or significant VRE storage capacity. The immediate question is how much we are willing to pay for a fully renewable system. To answer the question, it is important to explore the marginal benefit if a small fraction of the load can be met by dispatchable energy. This can be approached by demonstrating the dispatchable energy requirement with different storage size ranging from 0 to L^{cap}. Note that the storage size at 0 and L^{cap} are two special cases, which respectively represent an operation without storage and an operation without dispatchable energy (i.e. fully renewable).

The correlation between dispatchable energy requirement and storage size is illustrated in Figure 4.6. From the insets of Figure 4.6 it can be seen that both locations demonstrate a highly concave E_{D} with respect to the increase of L^{dv}, leading to two regimes of different behaviour. At the outset, a small introduction of storage dramatically reduces E_{D}, whereas the reduction levels off at subsequent increases of the storage capacity. The threshold L^{dv} lies in the range of 16–18. Since L^{dv} is normalised by the hourly energy requirement, its value also indicates the number of production hours that can be solely powered by the storage starting from full to null. For simplicity, Figure 4.6 is plotted with constant f_{W} (50 % for Kramer Junction and 75 % for Norderney) for all γ. This is because at the selected f_{W} the result is very close to the optimum (c.f. Figure 4.4C and D).

The two regimes of different behaviour in Figure 4.6 may be ascribed to the diurnal pattern of the solar power as it is only abundant around the midday (6 hours) and it is more likely to encounter an energy deficit in the rest of the day (18 hours). Therefore, a small introduction of storage becomes vital to the intraday

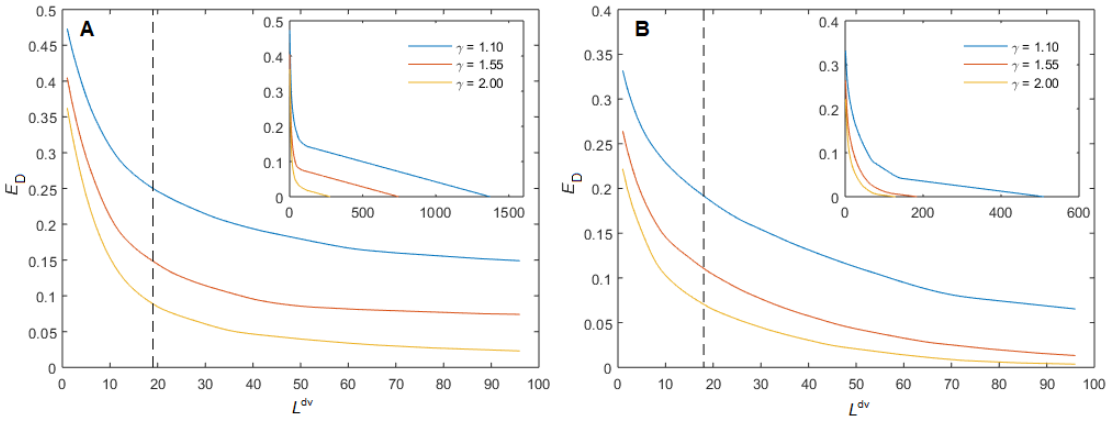


Figure 4.6. Dispatchable energy requirement E_D as a function of L^{dv} varied in a small range. The insets show full range of L^{dv} up to L^{cap}. E_D is normalised by total annual energy requirement ($8760 \times P_L$) while L^{dv} is normalised by hourly energy requirement. (A) for Kramer Junction (f_W is fixed at 50 % for all γ) and (B) for Norderney (f_W is fixed at 75 % for all γ). The dashed lines indicate the threshold L^{dv}.

operation, which stores positive $P_\delta(t)$ during the daytime and balances negative $P_\delta(t)$ during the night. As a comparison, the relation between storage capacity and dispatchable energy requirement is plotted at $f_W = 0.01$ and $f_W = 0.99$ in Figure B.11 in Appendix B. Clearly, the concavity of the plot is reduced at the high wind fraction. In contrast, a sharp change is observed at a high solar fraction, indicating the significant impact of intraday storage on the operation when solar power dominates the generation.

Since the marginal benefit (reduced E_D) decreases dramatically when L^{dv} is above 18, it may not be economically attractive to achieve a higher renewable penetration. Significantly, at $L^{dv} = 18$, the renewable penetration is already as high as 84.7 % in Kramer Junction and 88.9 % in Norderney at the intermediate excess generation (i.e. $\gamma = 1.55$). To further increase the renewable penetration up to 99 %, it would require a L^{dv} to increase by 36.6 times ($L^{dv} = 659$) for Kramer Junction and 6.1 times ($L^{dv} = 110$) for Norderney, respectively. This large amount of storage is required because the synoptic and seasonal pattern span a large time scale with significant variability, particularly in the case of Kramer Junction.

4.3.4 Economic analysis

The economic potential of the MeOH production is mainly determined by the LEC that is optimised by γ, f_{W} and L^{dv} (or L^{cap} if the objective function aims at a fully renewable operation). To take renewable harvesting plants into economic consideration is challenging not only because of the influence of policy on the price of electricity generated from VRE but also due to the fast development of renewable technologies. Here, benchmark prices of inland wind farm, photovoltaic (PV) farm and H_2-based ESS are used to report the true economic potential by excluding the subsidies and renewable incentives.

In the scenario of a partial renewable operation, a benchmark price of dispatchable energy is assumed to be 230 \$/MWh (this is the EU average electricity price in 2017 according to Eurostat (2017a)). Table 4.2 summarises the optimal LEC (see Eq. 4.9, in which the results are obtained from the *FMINCON* NLP solver) and its corresponding γ, f_{W} and L^{dv}. The LEC for Kramer Junction is found to be 202 \$/MWh, which is close to the dispatchable energy price. This is because the CapEx of solar power is too high and the wind power is not satisfactory (CF is 4.3 %), and in turn, it results in an expensive power system with small renewable generation of only solar power. The optimal renewable power generation is merely 68 % of the load requirement ($\gamma = 0.68$), giving a low renewable penetration level of 65 % (calculated from the time series of $P_{\delta}^{\mathrm{re}}(t)$). On the other hand, the renewable source in Norderney has demonstrated a promising economic potential, leading to a low LEC (111 \$/MWh) and considerable renewable power generation (though it consists of only wind power generation due to the low CF and high CapEx of the solar power). The corresponding renewable penetration is calculated to be 93 %, indicating a highly renewable operation. As a result, the required storage capacity (at the optimum) is found to be 159 (normalised by the hourly load), which is 11 times higher than the one in Kramer Junction (due to higher renewable power generation in Norderney). The corresponding LCOMeOH for Kramer Junction and Norderney at the optimum is found to be 2,692 and 1,561 \$/tonne, respectively.

Table 4.2. LEC optimised by excess power generation, renewable mix and storage capacity for production powered by both VRE and dispatchable energy.

	LEC ($/MWh)	γ	f_W	L^{dv}
Kramer Junction	202.4	0.68	0	14
Norderney	111.3	1.06	1	159

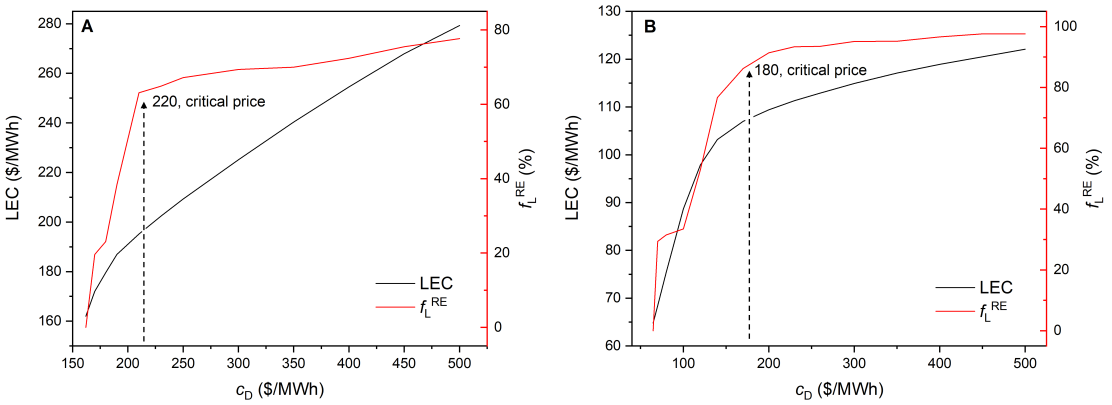


Figure 4.7. The impact of dispatchable energy price on LEC and renewable penetration. (A) is plotted for Kramer Junction and (B) is for Norderney.

The dispatchable power is usually (but not necessarily) the electricity from the grid, and its price varies significantly by region. The optimised LEC (and its corresponding γ, f_W and L^{dv}) is highly dependent on the dispatchable power: when the dispatchable power is expensive, the implementation of renewable power is largely justified economically; when the dispatchable power is cheap, the chemical production may simply run on dispatchable power without any renewable energy. Therefore, it is of importance to report the correlation between dispatchable energy price and renewable penetration at its optimal LEC. Figure 4.7A and B reveal the trend of optimal LEC and its corresponding renewable penetration at a range of dispatchable energy price for Kramer Junction and Norderney, respectively. There exists a threshold dispatchable energy price below which no renewable energy would be implemented (due to higher costs). This threshold price is 162 and 65 $/MWh for Kramer Junction and Norderney, respectively. More importantly, the resulting renewable penetration for both locations has a two-regime behaviour: when dispatchable energy is below the critical price, the renewable penetration (in the most economical scenario) increases dramatically with the increase of dispatchable energy price. Above the critical price, the renewable penetration levels off. In general, the increase of dispatchable energy price would encourage the

implementation of renewable energy. However, when it is increased higher than the critical price, the marginal benefit is decreased. Notice that the renewable penetration does not increase smoothly because the optimum is determined by both the renewable power generation and the storage capacity. Therefore, it can only be determined empirically as a function of the synergy between renewable source quality, storage costs and dispatchable energy price.

In the case of an islanded operation where dispatchable power is not available, the chemical production has to rely solely on VRE and its ESS. The optimised LEC without dispatchable power for both locations are tabulated in Table 4.3. In the optimum, excess generation is required at a higher level in Kramer Junction than in Norderney, as opposed to the results in Table 4.2. This is attributed to the less desirable renewable source in Kramer Junction, which requires excess generation to fulfil the load. Consequently, the required storage capacity also increases accordingly. Although the optimal LEC is increased for both locations for the fully renewable operation, the cost in Norderney only increases to 1.2 times the original value. In contrast, the cost in Kramer Junction increases to 1.8 times. It is also interesting to see that the optimised LEC for Kramer Junction is obtained when a complementary renewable source is introduced ($f_{\mathrm{W}} = 0.01$). This is because the storage unit becomes vital for Kramer Junction (i.e. storage is required at a large size as L^{cap}= 940) when dispatchable power is not available. If the objective function focuses on the storage sizing, the renewable mix would be more important (see Figure 4.4).

Table 4.3. LEC optimised by excess power generation, renewable mix and storage capacity for production powered by VRE and its ESS only.

	LEC (\$/MWh)	γ	f_{W}	L^{cap}
Kramer Junction	369.7	1.41	0.01	940
Norderney	130.2	1.35	1.00	260

The LCOMeOH for Kramer Junction and Norderney with 100 % renewable energy is increased to 4,768 and 1,796 \$/tonne, respectively. In a recent study, Bos et al. (2020) reported an analysis of wind-powered MeOH production with a cost of 800 €/tonne (or 938 \$/tonne). However, the authors did not consider the

variability of the renewable source when integrated into MeOH production, which could be a major cost driver. Gonzalez-Garay et al. (2019) also reported a range of production cost for wind- (approximately 1,400–1,800 \$/tonne) and solar-powered (2,300–2,400 \$/tonne) MeOH. Tountas et al. (2019) reviewed the solar-assisted MeOH production thoroughly and analysed the economic performance however using a simplified method. In their report, the minimum selling price for the solar-powered MeOH through PV-electrochemical is 5,800 \$/tonne. All of the above work circumvented the challenge of renewable source variability by using either a fixed energy cost (Bos et al., 2020), fixed hydrogen price (Gonzalez-Garay et al., 2019) or fixed production cost (Tountas et al., 2019). This current work filled the gap by taking the renewable characteristics into account, in which the variability and intermittency are addressed by the ESS and the production process itself.

The energy structure of the load in the most economical and fully renewable scenarios for both locations is plotted in Figure 4.8. In the fully renewable operation, the dispatchable energy (E_{D}) for both locations is eliminated by an increased share of the energy from the storage unit (E_{ST}). Note that for Kramer Junction the share of the energy from direct renewable generation (E_{G}) only increases by a small fraction (from 39 to 44 %) even though γ is doubled. This implies that the renewable source in Kramer Junction is too variable to be integrated into the chemical process. A sample of energy flow, which is composed of E_{D}, E_{ST} and E_{G}, is plotted over a period of 1 week for both locations in Figure B.12 in Appendix B.

Although the fully renewable operation is much more costly than the most economical operation (i.e. with dispatchable power backup), its significance lies in industrial decarbonisation. For the MeOH production in this work, the fully renewable energy operation would result in a CO_2 avoidance (due to consumption of CO_2 in MeOH synthesis) of 1.35 $\mathrm{kg/kg_{MeOH}}$ (obtained from carbon balance), whereas the most economical operation would have a CO_2 avoidance of 0.71 $\mathrm{kg/kg_{MeOH}}$ for Norderney (CO_2 emission from dispatchable energy is assumed to be 0.49 kg/kWh based on the German power generation industry (Moro and Lonza, 2018)), and would result in a CO_2 emission of 1.57 $\mathrm{kg/kg_{MeOH}}$ for Kramer Junction (CO_2 emission from dispatchable energy is calculated to be 0.69 kg/kWh based on the data

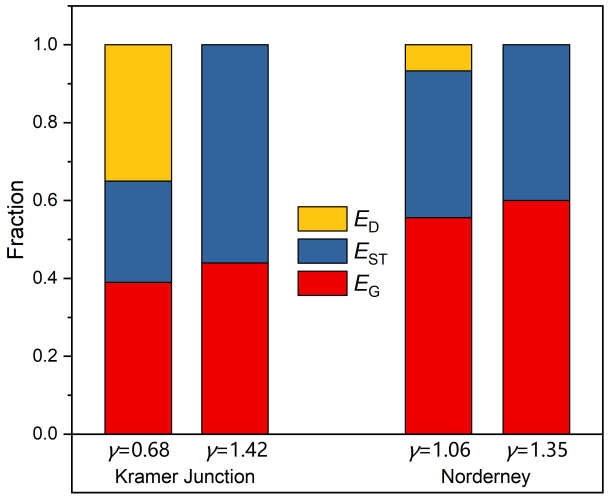


Figure 4.8. Energy structure of the load at the most economical scenarios with (left of the group) and without dispatchable power (right of the group). E_D denotes the energy from dispatchable power, E_{ST} denotes the renewable energy that goes through the ESS, E_G denotes the energy directly from the renewable power generation.

Table 4.4. CO_2 emissions for different operation scenarios. Negative value indicates CO_2 avoidance. The CO_2 emission from traditional MeOH process is obtained from Kajaste-Rudnitskaja et al. (2018).

Scenario	Location	CO_2 from E_D (kg/kWh)	CO_2 emissions (kg/kg_{MeOH})
Traditional	–	–	2.97
Fully renewable	–	–	−1.35
Most economical	Kramer Junction	0.69	1.57
	Norderney	0.49	−0.71

from the US Energy Information Administration (2019)). The CO_2 emissions for all operation scenarios are tabulated in Table 4.4 and compared with a traditional MeOH production process using coal as feedstock. Clearly, the electrified MeOH production significantly reduces the CO_2 emissions even in a partially renewable operation. Although such a concept is not currently economically justified, with advances in renewable technologies and enforced environmental policies, its economic performance will enhance particularly in regions with abundant renewable sources.

4.3.5 Sensitivity analysis

Due to the fast development in renewable technologies as well as policy incentives, cost reduction in renewable implementation may continue to be foreseen in the near

future. Consequently, an economic analysis based on current costs is not adequate. The uncertainties in selected key cost variables are thus investigated through a sensitivity analysis. Note that the sensitivity test focuses on the cases with ESS and dispatchable energy backup because they are more likely to be implemented, contrasting to the fully renewable operation that is less economically feasible. The parameters for 0 % variation, i.e. the base case in the sensitivity test, are tabulated in Table B.5 in Appendix B. Here, LCOMeOH is reported in the sensitivity analysis because the CapEx of the electrolysers in the MeOH plant is also considered.

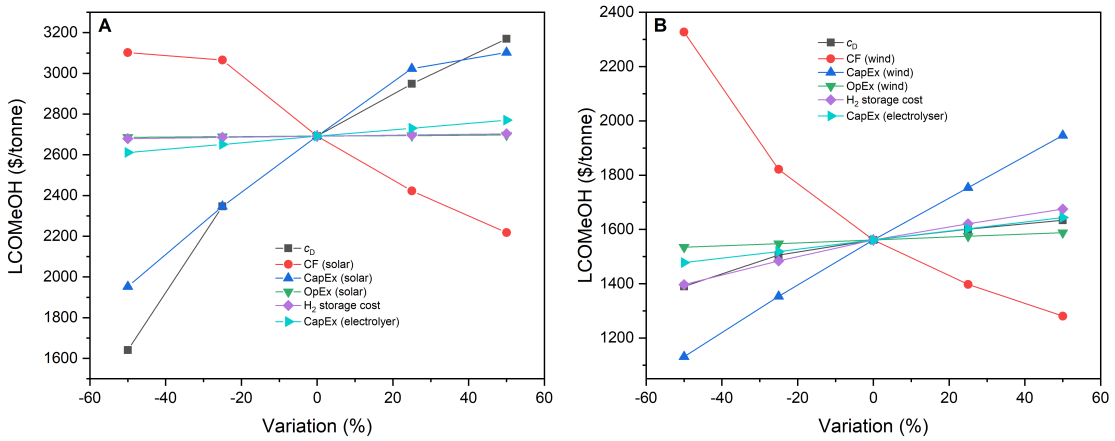


Figure 4.9. Sensitivity analysis: (A) Kramer Junction and (B) Norderney.

As illustrated in Figure 4.9, the LCOMeOH for the two different locations behaves differently with respect to the change of the selected variables. However, both locations are highly sensitive to CF, which is an indicator of the quality of the renewable source. Moreover, the OpEx of renewable power has a negligible impact on the LCOMeOH in both locations. A unique difference between the two locations is the influence of dispatchable energy price: the LCOMeOH in Kramer Junction is highly dependent on the dispatchable energy price, whereas its impact is insignificant in Norderney. This is attributed to the high renewable penetration in Norderney, which reduces its reliance on dispatchable power. Another difference is their sensitivity to the cost of hydrogen storage. Since the storage capacity in Norderney (in the optimal case) is about 9.5 times larger than that in Kramer Junction, the cost of hydrogen storage has a relatively significant impact on the LCOMeOH in Norderney. Note that only solar power is considered for Kramer Junction and only wind power for Norderney as the most economical scenario results

in no complementary renewable source. Also, note that there are some nonlinear behaviours observed in the sensitivity test. This is attributed to the interplay between variables. For instance, when CF is varied, the renewable penetration at the optimum will also vary accordingly, leading to new optimal storage capacity and LCOMeOH.

4.4 Discussion

4.4.1 Limitations

A significant limitation in the analysis is the use of historical meteorological data, which limits its use for future implementation. For instance, an optimised ESS for a chemical plant for a particular year may not be sustainable if the year of actual implementation has less abundant renewable energy, or alternatively, it may be over-designed (thus not optimised) if the renewable energy is more abundant than usual. A popular method to generalise the analysis based on non-deterministic variables is to adopt a random-input simulation using probability distributions (Ekren and Ekren, 2010). However, the theoretical distribution is often based on historical data, and thus its improvement should be questioned. It would be more helpful to use predicted meteorological data so that the designed renewable power system would be more reliable in a future scenario. Nevertheless, the seasonal behaviour of the VRE in a particular location by-and-large remains the same. Although the time series of energy flow may be different at a specific point, both diurnal and seasonal variations are relatively predictable. Therefore, analysis based on historical data is able to provide an indicative result. Most importantly, the results of sensitivity analysis and the correlation between renewable quality and storage capacity can provide important insights for policymaking.

Another related limitation is the use of the meteorological data obtained from a specific location. The two case study locations, i.e. Kramer Junction and Norderney, are selected because they are traditionally good spots for solar and wind energy

harvesting, respectively. For instance, Luz International developed a series of solar electricity generating systems at Kramer Junction in the 1980s to 1990s Boyle (2004), and Norderney is known for its large offshore wind farm installation. The calculated CF value for wind power in Norderney (29.4 %) also justifies the choice of the location since a typical CF of renewable power generators ranges from 20 to 40 % Esposito (2017). However, the study focusing on a specific location lacks generalisation. Currently, it is challenging to provide a generalised framework using a typical location as a case study. On the other hand, the gap can be complemented by performing a global analysis. Such an analysis has recently been performed by Nayak-Luke and Bañares-Alcántara (2020) for renewable ammonia production, a similar analysis should also be performed for renewable MeOH in the global context.

4.4.2 Significance of the optimum

The analysis considers two different objectives, i.e. (1) identify the minimum storage capacity for a fully renewable operation, which is a function of f_{W} and γ; and (2) minimisation of LEC for both scenarios of fully and partially renewable operation. Many researchers believe that hybrid renewable power systems are usually more reliable and less costly than single-source systems (Budischak et al., 2013; Celik, 2003). However, in this economic assessment, the best scenario results in a single renewable source for the case study locations. Complementary renewable sources would become vital in certain scenarios, such as (1) relatively equal CF and similar cost for generating power from the complementary source, (2) motivated implementation of the renewable ESS, i.e. load requirement in islanded and remote areas or much cheaper storage than the generation. In summary, the renewable mix in the most economical scenario is often determined by the synergies of the renewable source quality, cost of technologies and operation priority (e.g. reliability, sustainability and economic feasibility) set by the users. Under the current energy market and the cost of renewable technologies, renewable quality dominates the economic potential. This explains why the most economical scenario is composed

of only solar energy for Kramer Junction and only wind for Norderney in the power generation.

It is also important to report the sensitivity of the optimum to the change of variables. For instance, in the optimisation of storage capacity, the optimal L^{cap} in Norderney is extremely sensitive to the change of f_{W} but not sensitive to the change of γ. The optimal L^{cap} in Kramer Junction has the opposite sensitivity to the same variables. This provides insights into how the optimum responds to the change of variables and allows certain flexibility in design if the optimum becomes insensitive.

In the optimisation of LEC for the fully renewable operation, a local optimum has been found, which is close to the global optimal LEC. This is because a minimum LEC can be achieved at either a small γ with a large L^{dv} or a large γ with a small L^{dv}. It is envisioned that the inclusion of additional decision variables will lead to a non-convex problem, which gives similar results at different combinations of the variable values. Although the results are similar, a different value of the decision variables implies a different operation scenario. For instance, a small γ coupled with a large L^{dv} and a large γ coupled with a small L^{dv} lead to a similar LEC but the latter has much higher renewable curtailment.

4.4.3 Methods generalisation

As mentioned earlier, using VRE to meet a constant load does not necessarily reduce the complexity in management. In the demonstrated analysis, the chemical process with a constant load is met by two renewable sources. The same method can be applied to variable loads with multiple renewable sources by modifying Eq. 4.3 to

$$P_{\delta}(t) = \gamma\Big(\sum f_i \frac{P_i(t)}{\overline{P_{\mathrm{L}}}}\Big) - \frac{P_{\mathrm{L}}(t)}{\overline{P_{\mathrm{L}}}} \tag{4.13}$$

where the subscript i denotes the different renewable sources, $P_{\mathrm{L}}(t)$ denotes variable loads as a function of time and $\overline{P_{\mathrm{L}}}$ is the average load of the period of interest. The

management difficulty can be predicted from the profiles of the renewable power and the load. It is desirable to have counterbalanced profiles to reduce the required ESS capacity. The implementation of time-invariant renewable sources, such as geothermal power, can provide a base power generation, reducing the overall power mismatch.

4.4.4 Implications to policymaking

The implications to policymakers are clear: (1) chemical production is not preferred in islanded areas where no dispatchable energy is available; (2) dispatchable energy price can be used as a tool to influence or predict renewable penetration from the economic perspective; (3) economic incentives or penalties such as carbon tax should be implemented to facilitate industrial decarbonisation since the current market does not favour a highly renewable operation; (4) renewable mix is more important when storage becomes vital, e.g. in the case of islanded operation when there is no dispatchable power or when renewable generation is relatively expensive. Under the current market conditions, the complementary renewable source is less important and investment should go to the harvesting of the energy source that is of the best quality.

4.4.5 Outlook

The significance of this work lies in the improvement of system efficiency owing to the interplay between the chemical processes and the ESS. For a fully renewable operation, the $\gamma_{\min}$ is as low as 1.10 (c.f. Figure 4.4, meaning that the average generation could be only 10 % larger than the load requirement provided that the ESS capacity is sufficient). Furthermore, the most economical scenario in Norderney has reported a renewable penetration level of 93 % while the average generation is only 1.06 times the load (c.f. Table 4.2), translating to an overall efficiency of 88 % for the renewable power system. If the same analysis were performed for

general energy purposes (i.e. the stored hydrogen is only used to generate power), the overall efficiency would be much lower.

As a next step, the process of MeOH plant can be further investigated as a functional handle for optimisation: in addition to using hydrogen as an intermediate energy carrier, raw MeOH product (before distillation process) can be produced as a material buffer using surplus VRE. Thus, the intermittency of VRE would be addressed by both hydrogen storage and the intermediate raw MeOH product. The modular operation of a chemical process with excess storage of intermediate products allows DSM for energy scheduling and simultaneously remains steady-state operation for the individual operation unit (except the MeOH synthesis reactor). The separation of the catalytic reaction (to produce raw MeOH) and distillation process (to produce refined MeOH) also provides additional flexibility to better suit the variable nature of renewable sources.

4.5 Conclusions

This work explores a fully electrified MeOH process powered by VRE. The meteorological data of two locations of either good solar (Kramer Junction) or wind (Norderney) source have been used to investigate the feasibility of renewable MeOH production and the impact of the renewable source variability on systems design. It has been found that the variability increases the difficulty in balancing energy mismatch and it often requires large excess generation of renewable power to level its output, resulting in large curtailment and high costs. This work also analyses two different objectives: (1) minimum storage capacity for a fully renewable operation optimised by excess generation and renewable mix, and (2) the LEC of energy from a renewable power system (including generation and storage) delivered to the MeOH plant, which is optimised by excess generation, renewable mix and storage capacity. It has been found that the renewable mix is important for minimising storage capacity because it allows a complementary renewable source to level their power output, thus reducing the variability in power mismatch. However, for

the two selected locations renewable mix has shown no or very little influence on optimising LEC as the costs are primarily determined by the quality of renewable sources. The optimum of both objective functions responds to the change of variables in different ways between the two locations due to the characteristics of their renewable sources.

The correlation between key variables is also explored in this work. In general, the increase in storage size reduces the requirement of dispatchable energy. However, this correlation exhibits a two-regime behaviour where its marginal benefit is significant at the outset but reduces when the storage is larger than 18 (meaning that the production can solely rely on it for 18 hours). This implies the importance of intraday balancing, especially when solar power dominates the generation. Similarly, in the economic analysis, the renewable penetration (in the most economical scenarios) increases dramatically at the beginning with the increase of dispatchable energy price but levels off when the price is above a critical point. From the economic perspective, both results question the desirability of achieving a fully renewable operation as the required storage capacity and the economic incentive will have to increase significantly. Nevertheless, powering the chemical industry with renewable sources is of significant importance from the viewpoint of industrial decarbonisation.

Chapter 5

Quantifying the Value of Curtailed Renewable Power



URTAILMENT of renewable power, which results from the intermittency of renewable sources, is inevitable from an economic perspective, especially for islanded systems. This chapter explores the economic value of curtailed renewable power using methanol production with a dedicated renewable power system as a basis. A cascade design of methanol plants is proposed where the first plant is powered by the generated renewable power, whereas the subsequent plants are powered using the curtailed energy from the previous plant. The sizes of subsequent plants and energy storage units are optimised using a modelling approach. When the first and the second plant are compared, it is found that the levelised energy cost of the second plant is significantly reduced by 34.9 %. However, the reduction in levelised cost of methanol is negligible since the optimal size of the second plant is only 2.8 % of the first plant, which in turn reduces its economic potential due to economies of scale. After the second plant, the subsequent plants at the economic optimality have shown a dramatic increase in the production cost, meaning that the utilisation of the renewable power curtailed twice or more is economically infeasible. The cost breakdown shows that the main hurdle in curtailed renewable power utilisation is

the electrolysers, which are designed with excess rated power in order to accommodate the enhanced variability of the curtailed power. The analysis concludes that the curtailed renewable power has promising economical potential; however, the portion of the curtailed power that can be used economically is insignificant.

5.1 Introduction

The use of variable renewable energy (VRE), such as wind and solar energy, poses significant difficulties in load management in the end-use sectors. Concretely, the variability and intermittency of renewable sources require advanced technologies and strategies to level their power output. This has been demonstrated by Kempton et al. (2010) using geographically interconnected sources and by Hart and Jacobson (2011) using complementary renewable sources. Instead of levelling power output, excess overall generation with sporadic curtailment is another option to improve the reliability of power output from VRE. In fact, the curtailment of renewable power generation has occurred since the start of the renewable energy industry. Unlike the traditional fossil fuel-based electric power in which curtailment is often induced by the operators due to transmission congestion or lack of transmission access (Bird et al., 2014), the power curtailment in renewable energy is mainly attributed to the variability and intermittency of renewable sources and its generation curtailment can be either voluntary or involuntary. This means a market-based protocol may dispatch more excess power generation than the load requirement and result in curtailment based on economics. Moreover, renewable power generation has no additional fuel costs (meaning zero or near-zero marginal cost), and thus the potential use of the curtailed renewable power may be of interest. This research question can be viewed together with quantifying the cost of intermittency. After all, the curtailment is a direct result of the variable and intermittent nature of renewable sources.

In the current literature, a large number of studies have focused on the quantification of curtailed renewable energy. As an example, Demiroren and Yilmaz (2010)

reported curtailment of 64.2 % of the total electricity generation in the most economical scenario for a standalone application with a hybrid power system consisting of a battery storage unit and renewable power generators. Regarding a flexible power generation with diesel generators, Khatib et al. (2011) reported curtailment of 2.3 % of the total power generation. Clearly, a dispatchable power source would make the generation system more resilient, thus reducing the curtailment of power generation. In direct contrast, the power curtailment is strongly correlated to the penetration of a variable source in the generation, as demonstrated by Shaahid et al. (2014) using photovoltaic (PV) solar power as an example. Jacobsen and Schröder (2012) commented that the loss from curtailing generation is generally seen as an unacceptable solution by the public. Indeed, there are studies focusing on the reduction or avoidance of renewable energy curtailment (Li et al., 2015). This may be valid for certain involuntary curtailment. However, most voluntary curtailment for islanded or standalone systems is a result of the socio-economic optimisation; thus, its avoidance may drive away from the optimality. Alternatively, utilisation of such curtailed renewable power may be a solution. However, the challenge in quantifying the economic value of curtailed renewable power still exists.

To analyse the utilisation of curtailed power, it is important to define the boundary of curtailment. National Renewable Energy Laboratory has defined renewable energy curtailment as a reduction in power output from what it could otherwise produce given available renewable resources (Bird et al., 2014). Ismail et al. (2015) used a concept of excess renewable energy in their analysis, which is similar to curtailed energy. In their work, the authors summarised three potential destinations for the excess renewable energy that is not directly consumed in a load: (1) reintroduction to the grid; (2) storage in a battery bank and (3) redirection to dump loads. Yanine and Sauma (2013) commented that the grid acts as an unlimited battery bank; thus, the curtailment of renewable energy would not exist for a grid-connected system. However, this consideration is over-simplified since it assumes a grid system composed of mainly dispatchable generators, whereas a future trend predicts that more variable sources would be involved in a grid system (Schill et al., 2017).

Herein, the curtailment is defined as the dumped energy resulting from the economic optimisation taking storage into account, i.e. it would not be economical to use even if storage is considered. This work does not intend to propose a solution to the utilisation of curtailed renewable power. Rather, the purpose of this analysis is to evaluate the cost of intermittency and quantify the economic value of such curtailed power. To this end, a load is carefully chosen as a basis for this study since the load profile directly affects the curtailment. For instance, if the load profile is concurrent to the variability of renewable sources, the curtailment would be minimal. To eliminate the demand-side influence, the analysis is performed using a dedicated renewable power system for a constant load methanol (MeOH) production process without any dispatchable power sources, so that a true economic value of the curtailed renewable power can be evaluated. A hydrogen-based energy storage system (H_2-based ESS) is included in the optimisation since it is essential in the integration of intermittent renewable energy (Hu et al., 2020). The aim of this work is to provide an insight into the economic potential of curtailed renewable power as well as demonstrate the impact of renewable source intermittency on overall energy costs.

5.2 Methods

5.2.1 Concept overview

A fully electrified MeOH production process with a constant load is analysed as a basis to investigate the value of curtailed renewable power. The capacity of renewable power generation and its auxiliary ESS is optimised aiming at an optimal economic potential of the MeOH production. The curtailed renewable power, which is the focus of this study, results from the power mismatch between the variable renewable power generation and the constant load requirement. The use of curtailed power is considered to be free; however, it may not be economically justified due to its intermittent pattern, which is even more variable than the original renewable energy profiles before the curtailment. Thus, the economic

value of the curtailed renewable power is quantitatively analysed using the same MeOH production process through a cascade design strategy. Note that due to the reducing strength of the curtailed power, the size of the MeOH process is supposed to decrease but with an increasing ESS due to the significant intermittency of the available power. This concept is schematically illustrated in Figure 5.1.

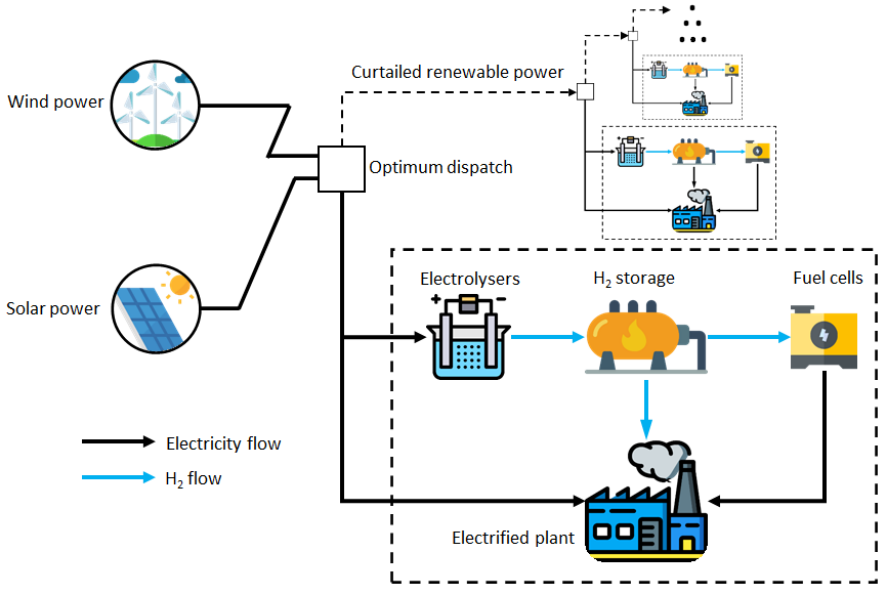


Figure 5.1. Overview of the general concept for the cascade design of a sequence of MeOH production plants.

5.2.2 Mathematical modelling

The modelling approach is adopted from Chapter 4 with modifications to suit the analysis. The data of renewable energy sources are obtained from Norderney, Germany as a case study. The original meteorological data and the power conversion methods are introduced in Chapter 4 and Appendix B, respectively. There are two renewable sources, namely wind and solar sources, considered in the analysis since a complementary renewable source may help to reduce the variability of generated renewable power (Heide et al., 2010). Nevertheless, the renewable mix in power generation is determined by the optimiser, which may or may not include the complementary renewable source. The capacity factor (CF) for wind and solar energy is 29.4 and 12.1 %, respectively. The detailed methods and assumptions for CF calculation are introduced in the Methods section of Chapter 4.

The renewable power generation model is formulated based on two baseline profiles for wind ($P_{\mathrm{W}}(t)$) and solar power ($P_{\mathrm{S}}(t)$), which are defined and scaled such that the cumulative power generation throughout the period of analysis is equal to the total load, as shown in Eqs. 5.1 and 5.2:

$$\sum_{t=1}^{N} P_{\mathrm{W}}(t) = P_{\mathrm{L}} N \tag{5.1}$$

$$\sum_{t=1}^{N} P_{\mathrm{S}}(t) = P_{\mathrm{L}} N \tag{5.2}$$

where P_{L} denotes the time-invariant hourly load of the MeOH production normalised to 1 MW and N is the total number of hours in one year operation, taken as 8,760 hours in this study. Since excess generation from renewables is inevitable due to their intermittent nature, an over-provision factor, γ, is adopted to quantify the excess generation. Therefore, the generated power from renewables is calculated by

$$P_{\mathrm{in}}(t) = \gamma \Big[f_{\mathrm{W}} P_{\mathrm{W}}(t) + (1 - f_{\mathrm{W}}) P_{\mathrm{S}}(t) \Big] \tag{5.3}$$

where P_{in} denotes the generated renewable power available to the production and f_{W} denotes the fraction of wind energy in renewable power generation. Since there are only two renewable sources considered in this study, $1 - f_{\mathrm{W}}$ denotes the fraction of solar energy (f_{S}) in renewable power generation. The definition of γ is the same for subsequent plants however with a different formulation since the subsequent plants are powered by the otherwise curtailed energy.

For modelling convenience, the storage is formulated using energy terms, though it is a H_2-based ESS. The conversion from hydrogen measured in mass to its equivalent energy takes the charging (η_{ch}) and discharging efficiency (η_{dis}) into account. The charging efficiency is assumed to be 90 %, which only accounts for the energy loss in the compression process for the ESS (see Section 4.2.6 of Chapter 4). The energy losses in the electrolysers are accounted for by the specific energy requirement. Note that the specific energy requirement of the electrolysers (e^{ELY}) is assumed to be a load-invariant constant with a value of

$4.5\,\mathrm{kWh/Nm^3_{H_2}}$ (Zeng and Zhang, 2010), which is in line with the work of Nayak-Luke et al. (2018). However, Beerbühl et al. (2015) used a variant energy efficiency inversely proportional to the load fraction of electrolysers. Although the use of a constant specific energy requirement significantly simplifies the model formulation, it generates a conservative economic potential since a lower bound of electrolysis efficiency is used regardless of its load fraction. Note that the stored hydrogen can be used as both an energy vector (feed to fuel cells to generate electrical power) and a material buffer (feed to MeOH production as feedstock), which entails a different discharge efficiency. The discharge efficiency is assumed to be 60 % (so that the round-trip efficiency is comparable with the literature value (Beaudin et al., 2010)) when the stored hydrogen is used an energy vector, whereas no energy loss occurs when used as a material buffer. This dual functionality of the stored hydrogen allows a highly efficient operation over the traditional H_2-based ESS due to the interactions with the process downstream, in which the overall efficiency is governed by the fraction of overall load that goes to hydrogen feedstock synthesis ($f_{\mathrm{ELY}}^{\mathrm{SYN}}$). The value of $f_{\mathrm{ELY}}^{\mathrm{SYN}}$ is taken as 89 % (c.f. Chapter 4).

The operation policy is optional in modelling; however, its implementation significantly reduces the total number of variables and equations since singular variables can be calculated as opposed to otherwise time domain variables. In this work, the power allocation has a clear operation boundary, which makes the pre-defined operation policy possible. The operation policy can be formulated by

$$L(t) = \begin{cases} L(t-1) + \eta_{\mathrm{ch}} P_\delta(t) & P_\delta(t) \geqslant 0 \\ L(t-1) + P_\delta(t) & -f_{\mathrm{ELY}}^{\mathrm{SYN}} \leqslant P_\delta(t) < 0 \\ L(t-1) - f_{\mathrm{ELY}}^{\mathrm{SYN}} + \frac{1}{\eta_{\mathrm{dis}}}\left[P_\delta(t) + f_{\mathrm{ELY}}^{\mathrm{SYN}}\right] & P_\delta(t) < f_{\mathrm{ELY}}^{\mathrm{SYN}} \\ 0 & L(t-1) + \eta_{\mathrm{ch}} P_\delta(t) \geqslant 0 \end{cases} \tag{5.4}$$

where $L(t)$ denotes the current storage holdup (at time t) of hydrogen measured in energy terms, and $P_\delta(t)$ denotes the power mismatch between generation and load (i.e. $P_\delta(t) = P_{\mathrm{in}}(t) - P_{\mathrm{L}}$). Note that in Eq. 5.4 the power terms are converted to energy by multiplying power by 1 h; however, this is not shown for conciseness.

This operation policy can also be illustrated graphically, as shown in Figure 5.2.

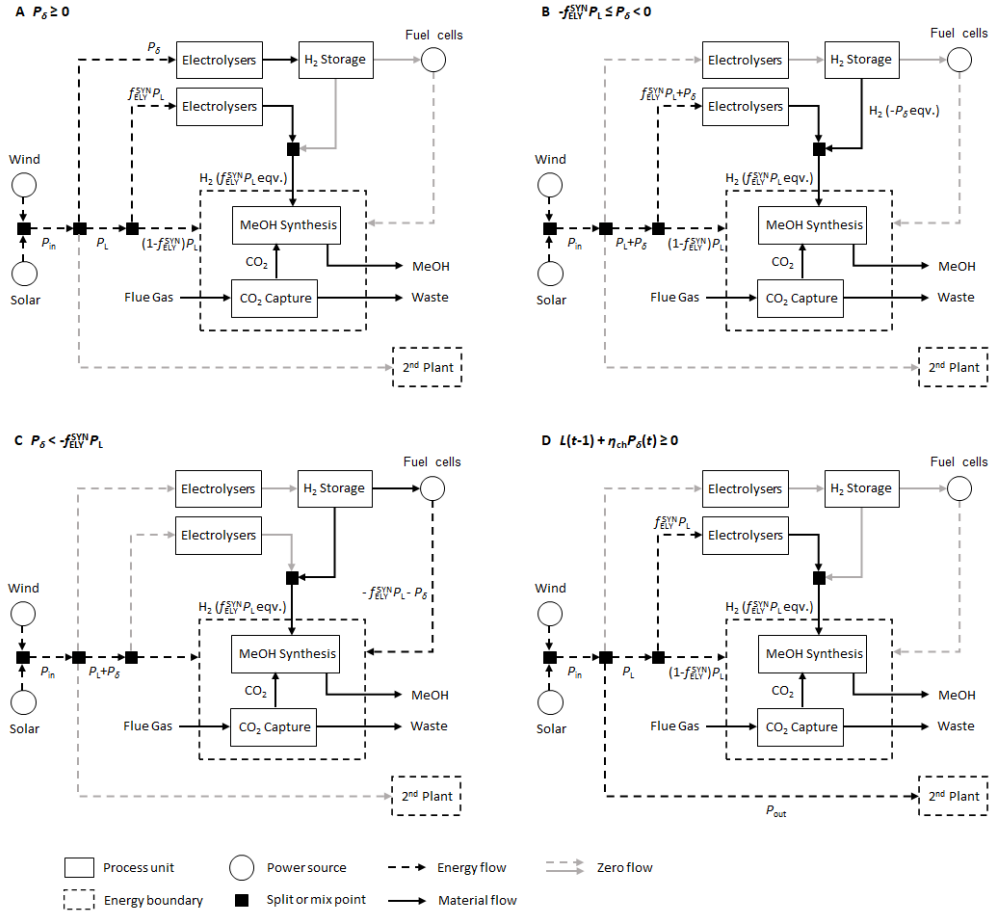


Figure 5.2. Schematic illustration of the operation policy for the fully electrified MeOH production: (A) charging mode; (B) discharging mode when power deficit is small, i.e. H_2 fuel cells are not in operation; (C) discharging mode when deficit is large, i.e. H_2 fuel cells are in operation; (D) VRE curtailment due to full storage. Grey arrows indicate zero flow.

The holdup of storage is key in the formulation as it dictates all energy flow to the MeOH production through a pre-defined operation policy. For mathematical convenience, the cap of the storage is set to zero, which is reflected by the last term in Eq. 5.4. This formulation is adopted because it guarantees a minimum storage capacity (L^{cap}) that permits a fully renewable operation. This variable also caps the benefits of a storage unit, i.e. any size larger than L^{cap} would not be beneficial because there would be no surplus renewable power to be stored. Eq. 5.4 also implicitly requires a corresponding minimum over-provision factor, below which a dispatchable power source would be required (meaning a fully renewable energy operation is infeasible). Note that the dispatchable power source

is excluded in the modelling and optimisation since it would play a dominant role in a hybrid renewable and dispatchable power system under the current market. Consequently, the intermittency of renewable power would be (partially) addressed by the dispatchable power and the model would not be able to fully quantify the cost of intermittency.

The curtailed renewable power, termed as P_{out}, is essentially the leftover power after meeting the production load requirement and charging the ESS. Therefore, it can be defined by

$$P_{\text{out}}(t) = \begin{cases} P_{\text{in}}(t) - P_{\text{ch}}^{\text{ESS}}(t) - P_{\text{L}} + P_{\text{dis}}^{\text{ESS}}(t) & P_{\text{in}}(t) - P_{\text{ch}}^{\text{ESS}}(t) - P_{\text{L}} + P_{\text{dis}}^{\text{ESS}}(t) \geqslant 0 \\ 0 & P_{\text{in}}(t) - P_{\text{ch}}^{\text{ESS}}(t) - P_{\text{L}} + P_{\text{dis}}^{\text{ESS}}(t) < 0 \end{cases} \tag{5.5}$$

where $P_{\text{ch}}^{\text{ESS}}(t)$ and $P_{\text{dis}}^{\text{ESS}}(t)$ denote the power charged and discharge from the ESS, respectively. Note that the two operation modes of ESS cannot take place at the same time. This restriction can be defined by

$$P_{\text{ch}}^{\text{ESS}}(t) = \begin{cases} L(t+1) - L(t) & L(t+1) - L(t) \geqslant 0 \\ 0 & L(t+1) - L(t) < 0 \end{cases} \tag{5.6}$$

$$P_{\text{dis}}^{\text{ESS}}(t) = \begin{cases} L(t) - L(t+1) & L(t) - L(t+1) \geqslant 0 \\ 0 & L(t+1) - L(t) < 0 \end{cases} \tag{5.7}$$

The curtailed renewable energy normalised by the total energy requirement (which is $P_{\text{L}}N$ or 8,760 MWh since P_{L} is normalised to 1 MW) is calculated by

$$E_{\text{out}} = \frac{1}{P_{\text{L}}N} \sum_{t=1}^{N} \left[P_{\text{out}}(t) \times 1 \right] \tag{5.8}$$

The optimisation aims at a minimum levelised energy cost (LEC) of the combined power from both generation and storage. Since the MeOH production has a constant load, the optimal LEC also leads to an optimal levelised cost of MeOH (LCOMeOH). Note that only the LEC of the first plant involves renewable generation cost,

whereas the subsequent plants do not have generation cost since they are powered by curtailed energy. The value of LEC for the first plant is calculated by

$$\begin{aligned}\mathrm{LEC} = \frac{1}{N}\Bigg\{ &\sum_{i=\mathrm{W,S}} \left[\gamma f_i \frac{1}{\mathrm{CF}_i} f^{\mathrm{CR}} \mathrm{CapEx}_i^{\mathrm{GEN}}\right] + \sum_{i=\mathrm{W,S}} \left[\gamma f_i \frac{1}{\mathrm{CF}_i} \mathrm{OpEx}_i^{\mathrm{GEN}}\right] \\ &+ f^{\mathrm{CR}} \mathrm{CapEx}^{\mathrm{ELY}} P_{\max}^{\mathrm{ELY}} + \frac{\eta_{\mathrm{ch}} L^{\mathrm{cap}}}{e^{\mathrm{ELY}}} f^{\mathrm{CR}} \mathrm{CapEx}^{\mathrm{ESS}} \Bigg\}\end{aligned} \tag{5.9}$$

where CapEx stands for capital expenditure, OpEx stands for operational expenditure and $P_{\max}^{\mathrm{ELY}}$ denotes the rated power of the electrolysers for the ESS. The superscripts of GEN and ELY denote generation system and electrolyser unit, respectively. The capital recovery factor, f^{CR}, is calculated by

$$f^{\mathrm{CR}} = \frac{r(1+r)^n}{(1+r)^n - 1} \tag{5.10}$$

where n denotes the life of a unit and r denotes the discount rate, taken as 8 % in this work. Note that Eq. 5.9 neglects the P_{L} term since it is normalised to 1 MW.

Although the optimal LEC coincides with the optimal LCOMeOH, the relative change (either increase or decrease) may be different when economies of scale are taken into consideration. Concretely, LCOMeOH estimation involves production facilities, which benefits from economies of scale. In contrast, linear cost functions are used for energy cost estimation. Therefore, LCOMeOH is also reported based on a production rate of 400,000 tonnes per annum for the first plant, which is equivalent to approximately 600 MW if it is fully electrified (c.f. Chapter 3). The subsequent plant size is determined by the optimiser based on the size of the first plant. The value of LCOMeOH is calculated by

$$\mathrm{LCOMeOH} = \frac{1}{M_{\mathrm{MeOH}}}\left[f^{\mathrm{CR}} \cdot \mathrm{TFCC} + P_{\mathrm{L}} N \cdot \mathrm{LEC} + C_{\mathrm{ELY}}^{\mathrm{SYN}} + C_{\mathrm{cw}} + C_{\mathrm{pw}}\right] \tag{5.11}$$

where M_{MeOH} denotes the production rate of a plant measured in tonne, $C_{\mathrm{ELY}}^{\mathrm{SYN}}$ denotes the annualised cost of electrolysers for MeOH synthesis, C_{cw} denotes the annualised cost of cooling water, C_{pw} denotes the annualised cost of process water and TFCC stands for the total fixed capital cost of a plant, which is subject to economies of scale via the six-tenths factor rule. Note that there are two separate

sets of electrolysers for MeOH synthesis and the ESS. Their costs are thus included in LCOMeOH and LEC, respectively. Although both sets of electrolysers have the same linear cost function, the size of electrolysers for the ESS is obtained from the optimiser while $C_{\mathrm{ELY}}^{\mathrm{SYN}}$ is directly proportional to the plant size. Technology costs, process utility costs, and a detailed breakdown of TFCC for the first plant are inherited from Chapter 4 (see Tables B.1–B.4 in Appendix B).

5.3 Results and Discussion

5.3.1 Energy analysis

The assessment follows a cascade design of plants where the curtailed power is fed to the subsequent plant as input power, i.e. the first plant is powered by the generated renewable energy, whereas the subsequent plants are powered by the curtailed renewable power from the previous plant. The optimisation setup for the first plant is slightly different in order to cope with the renewable generation system, in which the over-provision factor (γ) and renewable mix (f_{W}) is optimised aiming at a minimum LEC. In contrast, the subsequent plants are optimised by determining the size of the plant and the ESS to obtain a minimum LEC. The size of the subsequent plant is measured as a fraction of the first plant, termed as β. Therefore, the size of the first plant is taken as a basis, i.e. $\beta = 1$. The first part of the investigation is centred on assessing the energy structure of the load for each plant. The energy use indicators—including the over-provision factor (γ), plant size factor (β), curtailed energy normalised by the total annual load (E_{out}), size of the ESS (L^{cap}) and the fraction of load met by the energy from ESS ($f_{\mathrm{L}}^{\mathrm{ESS}}$)—are summarised in Table 5.1.

A noticeable trend in the subsequent plants is that their plant size reduces significantly, which is indicated by both γ and β. Consequently, the change of curtailed energy (between the second and third plant) is insignificant because only a small fraction of the input power has been used in the production. The time series

Table 5.1. Key energy indicators for the cascade plants. Note that E_{out} is normalised by the total energy requirement of the first plant, whereas L^{cap} is normalised by the hourly load of the first plant.

	γ	β	E_{out}	L^{cap}	$f_{\text{L}}^{\text{ESS}}$
First plant	1.35	1.00	0.3466	260.96	0.40
Second plant	12.42	2.79×10^{-2}	0.3187	6.17	0.60
Third plant	5.94×10^{2}	5.36×10^{-4}	0.3182	0.08	0.62

of the curtailed power is plotted in Figure 5.3 for the three plants, which details the relative strength over the period of analysis. Significantly, when Figure 5.3A and B are compared it shows that the optimiser only dispatches the less variable power to the load, whereas the power spikes of extreme values are not utilised. Note that the curtailed power from the previous plant becomes the input power for the subsequent plant. Since the less variable power has been used in the second plant, the third plant becomes significantly small with a β of merely 5.36×10^{-4}. This result corroborates that it is difficult to integrate highly variable power especially with spikes in their time series. If the subsequent plant is designed with a larger size than its optimum, it would have a larger load and thus forcing the system to dispatch more power from the variable sections in the time series at an additional cost of the storage system (due to the larger capacity) and electrolysers (due to the higher rated power). Since the third plant is sufficiently small, further extension of the same concept becomes insignificant, i.e. a negligible amount of curtailed power would be utilised in the subsequent plants, as shown in Figure 5.3C and D.

Although all power is from renewables, the pathways of the utilised power can be different, i.e. either directly from the input power or through the ESS. The energy structure of the load for the three plants is plotted in Figure 5.4, which illustrates the time series of the load met by energy from both pathways. Clearly, the storage plays an increasingly important role in the subsequent plants. However, the increase of $f_{\text{L}}^{\text{ESS}}$ for the third plant is inappreciable (see Table 5.1), which may be attributed to the significant reduction in the optimal plant size. Another noticeable trend in the load structure is that the use of a hybrid of energy sources at a particular time t becomes less likely in the subsequent plants, i.e. the load is more likely to be met by either all energy directly from the input or all energy

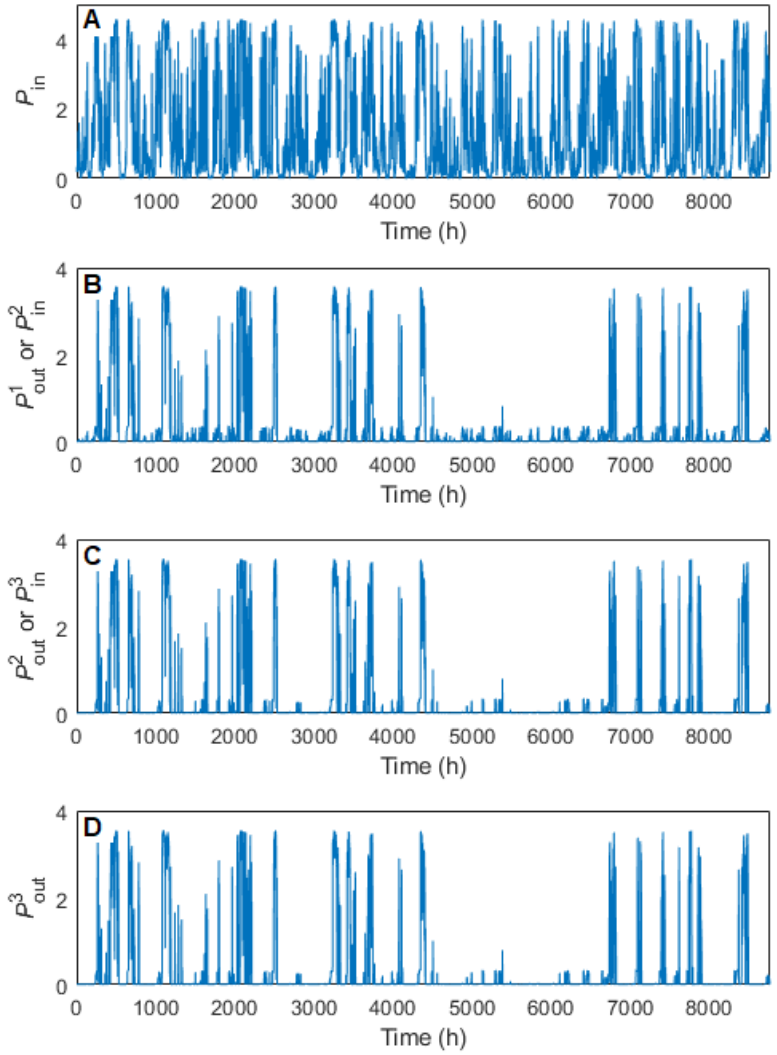


Figure 5.3. Time series of curtailed power for the cascade plants. The superscript index indicates the order of plants in sequence.

from the ESS. It is difficult to interpret the deterministic load structure from a mechanistic viewpoint. However, it is evident that the optimal dispatch chooses a benchmark input power element in the time series (this determines the optimal plant size) which minimises the empty gaps (i.e. intermittency) along the profile capped by the value of the benchmark power. Consequently, the plant size would be smaller and the load structure would be more deterministic if the input power becomes more variable.

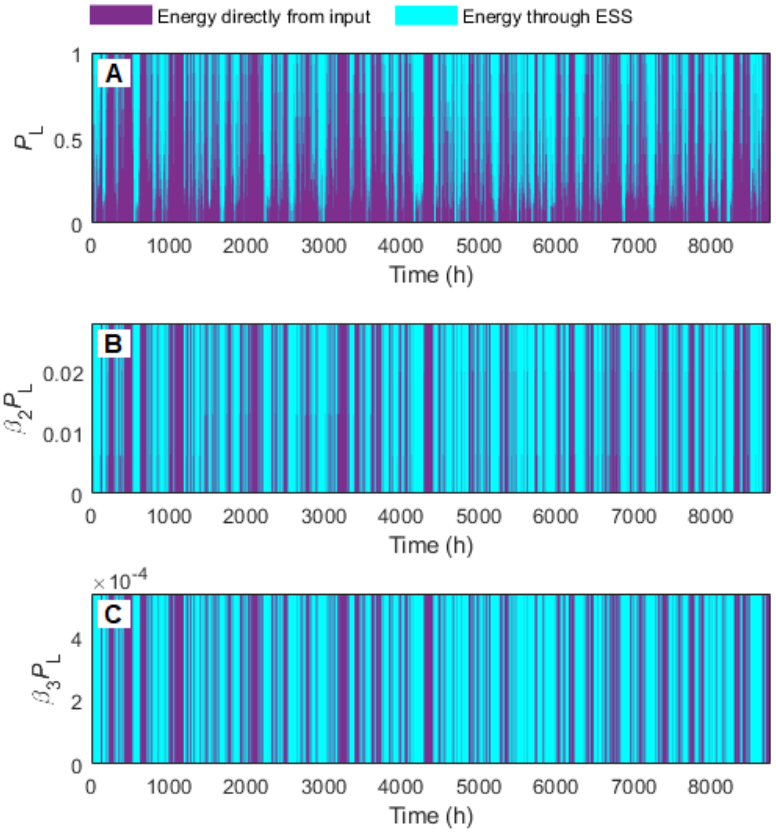


Figure 5.4. Time series of load composition for the cascade plants. The subscript index indicates the order of plants in sequence.

5.3.2 Cost analysis

The overall cost and the cost breakdown for each plant are of particular interest in this analysis. Figure 5.5 illustrates the LEC and LCOMeOH for each plant with a breakdown of the subsystems contributing to the overall cost. The LEC concerns the cost associated with the energy delivered to the production plant, and thus it includes the cost of renewable energy generation and storage. The fuel cells cost is neglected since its value is too small. This simplification is justified by the operation policy, in which the operation of fuel cells has the lowest priority due to its unfavourable energy efficiency.

The LCOMeOH concerns both energy and production costs. Note that the renewable energy generation is only applicable to the first plant as the subsequent plants are powered by the otherwise curtailed power, which is free of charge. The value of TFCC, which is a part of the production cost, takes the economies of

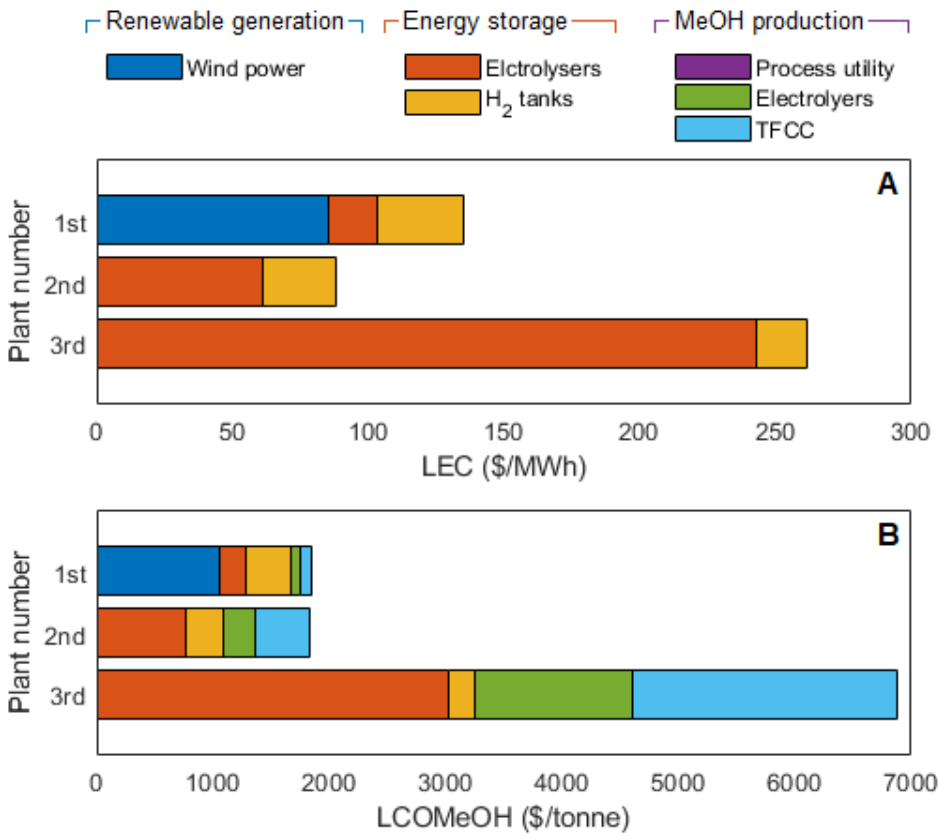


Figure 5.5. Cost breakdown for (A) LEC and (B) LCOMeOH. Note that the process utility cost is plotted but it is too small to show in the graph.

scale into account, whereas all other costs are linear with respect to the unit or subsystem size. This implies that LEC is independent of the production scale (this is why all energy analysis is performed based on a normalised load of 1 MW), whereas LCOMeOH depends on the production scale. In order to provide a basis, the first plant is assumed to have an annual production rate of 400,000 tonnes, which corresponds to a load of approximately 600 MW if it is fully electrified. It is interesting to see that the second plant has a lower LEC and LCOMeOH when compared with the first plant. However, while the LEC for the second plant is significantly reduced by 35 % (from 134.9 to 87.8 $/MWh), its LCOMeOH is reduced negligibly from 1,854.1 to 1,837.7 $/tonne. This is mainly attributed to the reduced economies of scale due to the smaller production size of the second plant. Concretely, the TFCC is increased from 111.6 $/tonne (accounting for 6 % of the LCOMeOH for the first plant) to 467.1 $/tonne (accounting for 25 % of the LCOMeOH for the second plant).

The cost of renewable energy generation is the largest component in both LEC and LCOMeOH for the first plant, accounting for 63 and 57 %, respectively. Although the subsequent plant does not comprise renewable energy generation, it requires electrolysers with higher rated power to accommodate the increased variability of the curtailed power. From the LEC cost breakdown, the cost of electrolysers for the second and third plant increases by 3.3 and 13.1 times, respectively, compared with that for the first plant. A significant finding from the analysis is that the change of LEC (and LCOMeOH) for the subsequent plants flips: while the overall economic performance of the second plant improves on the first plant, it dramatically decreases (both from the energy and production perspective) for the third plant. The reduction in economic feasibility is mainly attributed to the increased share of electrolyser cost, which outweighs the saving from using free curtailed power. Additionally, the reduction in optimal plant size also increases the TFCC of production facilities per unit MeOH produced, as can be seen from the increased share of TFCC in the LCOMeOH breakdown for the subsequent plants.

Although both wind and solar power are considered in the optimisation, the renewable energy generation only comprises wind power. This is attributed to the low availability of solar source in the selected location, which in turn increases the cost of solar power generation.

The analysis is performed based on an electrified MeOH plant with an annual production of 400,000 tonnes. This is a medium-size MeOH plant as the modern plants could be much larger and benefit from the enhanced economies of scale. Thus, if the subsequent plants are optimised based on a larger basis (i.e. larger first plant), LCOMeOH would improve. Nevertheless, the value of LEC is independent of the economies of scale as all cost functions of energy generation and storage are linear. More importantly, the cost breakdown provides insights into how the subsystems and units respond to the increased variability of the input power.

In the past, there are some researchers proposed the potential utilisation of curtailed power, such as Li et al. (2015) and Ismail et al. (2015). However, their "what if" thought experiment was performed on an ideal basis that does not address

how to quantify the economic value and how to overcome the increased variability of curtailed renewable power. This analysis not only provides an example of economic value quantification but also offers a new thinking strategy in the evaluation of curtailed renewable power.

5.4 Conclusions

The curtailment of renewable power has been overlooked in the past probably because of the facts that the curtailment is voluntary and necessary to ensure the reliability and economics of renewable power systems. However, with the increasing deployment of renewable power generators, the total quantity of the curtailed renewable power will become significant, which calls for new strategies to evaluate and reintroduce such power. This work addressed the gap in knowledge about curtailed power utilisation by analysing its economic value, using methanol production as a test bed. The dedicated renewable power with a constant end-use load provides an analysis boundary that excludes the impact of dispatchable supply/demand on the curtailed renewable power. Therefore, the economic value of curtailed renewable power is solely affected by its intermittency. The results suggest that although the curtailed power is much more variable than its original output from generation, using the curtailed power is economically justified since the saving from renewable generation outweighs the additional cost for addressing the enhanced variability. However, the portion of the curtailed power that can be used economically is insignificant, meaning that the overall economics may be compromised if the end-use load is sensitive to the economies of scale. The economic value of the secondary curtailed power (i.e. curtailed twice) has also been analysed, which shows firm economic infeasibility in its utilisation. The results conclude that although the use of strategies such as power levelling through storage methods would improve the economics of curtailed power utilisation, the improvement is insignificant when the size of the useable power is considered. Therefore, a dispatchable load or demand-side management is probably the future direction for curtailed power utilisation.

Chapter 6

Introducing Process Flexibility for the Integration of Variable Renewable Energy



HEMICAL process electrification and renewable energy integration facilitate one another along the pathway towards a greener industry. However, integrating intermittent and variable renewable power into large-scale chemical processes, which conventionally operate at a steady state with a constant load, could lead to prohibitive costs if intermittency is addressed solely by energy storage. This chapter considers the concept of a flexible chemical process that can operate with a variable load throughout the year while meeting a specified annual production target. Using methanol production via carbon dioxide hydrogenation as a case study and by means of process conceptual design and optimisation, this work investigates how the over-sizing of flexible process units and the introduction of intermediate storage in the chemical process offer the possibility to improve the overall performance of systems. The impact of the characteristics of renewable power is also explored by performing an analysis using meteorological data from two locations dominated respectively by wind and solar energy. This study shows clear potential benefits of process flexibility when the renewable energy supply is highly variable and is sought to achieve a high

level of penetration. For a 100 % renewable process, the introduction of flexibility reduces the levelised cost of methanol by approximately 21 and 34 % for the two case study locations, respectively. The cost attribution reveals further insights into the origin of the economic advantages through examining the comparative costs of chemical production, energy generation, intermediate product storage and renewable energy storage. The learning from this work suggests that incorporating process flexibility through a holistically optimised design of energy storage and chemical production has the potential to offer an economically viable route to large-scale green chemical production through renewables-enabled electrification.

6.1 Introduction

The previous chapters have discussed the importance of electrification with renewable energy. However, high penetration of variable renewable sources in power systems poses significant operational challenges. Unlike other energy uses where demand-side flexibility could be brought in to address the variability and intermittency of renewable energy (Li and Pye, 2018), conventional chemical processes typically operate continuously at a steady state, imposing a constant (and rigid) energy requirement. Such a rigid requirement, on the other hand, cannot be adequately met by the management of the generation side for mitigating renewable energy variability, such as diversifying renewable sources (Heide et al., 2011) and excess renewable energy provision (Heide et al., 2010). To date, the limitation in renewable chemical production is largely addressed by energy storage, particularly in the form of compressed hydrogen (H_2) to level renewable power output, which has been demonstrated in both "green" ammonia (Nayak-Luke et al., 2018) and methanol (MeOH) production (Bos et al., 2020). Although hydrogen plays a critical role in renewable energy storage, its technical barriers (Hu et al., 2020) are significant—expensive storage tanks, high-pressure storage and potential safety issues—making it less favourable for long-term storage and large-scale applications. In light of this, it is urgent to explore new concept and techniques specifically for chemical production powered by variable renewables.

To tackle the burden of energy storage for integrating renewables into the chemical industry, a separate line of thinking is on tapping into the flexibility in chemical processes, which has not been much emphasised in conventional steady-state production. A flexible chemical process allows the demand side to adjust according to the variable pattern of renewable energy, thus incorporating demand-side management to balance power generation and end-use load. In fact, the reason why a H_2-based energy storage system (ESS) has been widely used in balancing renewable power generation (Rasmussen et al., 2012) can be attributed to its flexible operation, i.e. water electrolysis can generally run at flexible loads to accommodate the variability of renewable sources. Unlike the electrolysers, chemical synthesis reactors and other complex chemical processes require careful management in order to accommodate the capacity of being flexible.

Several recent studies have recognised the importance of the operational flexibility of chemical reactors, with the anticipation of increasing integration with renewable resources (Cheema and Krewer, 2018). It should be pointed out that disparity exists in the level of flexibility rendered by different chemical process units. For example, a wide range of feasible load was reported of a fixed-bed methanation reactor with the lower and upper bounds of the superficial velocity being 10 times apart (Matthischke et al., 2018). In contrast, cryogenic distillation for air separation is considered to be much less flexible, with the feasible load being no lower than 60 % of its full capacity (Morgan, 2013). A chemical plant typically comprises multiple types of units for distinct tasks such as chemical conversion and separation; the difference in their flexibility makes it very challenging to vary the load of the chemical plant as a whole. Instead, these units may have to operate at different load levels within the limits they can individually accommodate. This would necessitate storage of intermediate products (exchanged between upstream and downstream processing) and energy (such as heat due to energy integration between process units) to align the operation of multiple units. Furthermore, the use of such storage would need to be optimally coordinated with the use of renewable energy storage, hence the need for optimal coordination between flexible energy generation and flexible chemical production. This complexity has not been

understood in existing power-to-chemical studies that consider some degree of process flexibility (Hank et al., 2018), typically with the involved chemical reactor. Despite the added complexity, this strategy may lead to the enhanced economic feasibility of renewables-powered chemical production, provided that the benefits of the flexibility-enabling storage introduced within the chemical plant outweighs its cost. Should such a "flexible" system be proven to be more advantageous than integrating variable renewable energy into chemical production that operates at a constant load mediated solely by (expensive) energy storage, it could become one of the new paradigms for chemical process design in the era of renewables.

Renewable MeOH as a commodity (Nguyen and Zondervan, 2019) or a vector to synthetic hydrocarbons (Yarulina et al., 2018) has received increasing attention in the recent literature, often with an emphasis on carbon dioxide (CO_2) valorisation (Gonzalez-Garay et al., 2019). In this work, a detailed model-based evaluation of power-to-MeOH production has been undertaken. MeOH has been chosen for a detailed case study not only because of its own importance as a platform chemical that can be further converted to a wide range of other chemicals and materials but also because it presents a good range of challenges in terms of exploiting process flexibility to cope with the variable supply of renewables: (1) it involves reaction and separation process sections which are both fairly complex; (2) its use of CO_2 as a feed and its production of crude MeOH as an intermediate product introduce the potential need for storage of both gaseous and liquid materials; (3) the process also offers an opportunity to investigate the implication of process flexibility on heat integration across multiple units which is commonly encountered in a sophisticated modern chemical plant. These features are representative of future renewables-powered production of chemicals and fuels.

This chapter considers a MeOH plant which acquires CO_2 by carbon capture from a point source and hydrogen from electrolysis, with a MeOH synthesis loop centred on a catalytic reactor and a distillation-based step for product purification. The plant investigated in this work is fully electrified, supplied by a wind and/or solar power generation facility which is optionally complemented by dispatchable power. In this system, the variability of renewable energy supply is tackled by a

combination of a H_2-based ESS and process flexibility enabled by the storage of process materials and energy (heat). A detailed optimisation model is constructed to establish the economically best design of the combination, in terms of the sizes of system components, power mix, and the arrangement of energy and material flows between different system units. The optimal design is contrasted with the non-flexible conventional production under different settings of the renewables' profile, the price of dispatchable power and the level of attainable process flexibility. In this analysis, both the cost for MeOH production and level of renewables penetration (as an environmental consideration) are assessed. As a new effort in the emerging area of combining process electrification with CO_2 utilisation, the intention of this work is to reveal the key mechanisms by which process flexibility can potentially improve the economic and environmental performance of chemical production powered by variable renewable sources.

6.2 Methods

6.2.1 Concept overview

The process flowsheet is centred on fully electrified MeOH production as described in Chapter 4, i.e. an annual production rate of approximately 400,000 tonnes is considered for two geographical locations, namely Norderney (Germany) and Kramer Junction (US). As shown in Figure 6.1, the system that converts power (from both variable renewables and the dispatchable backup) to MeOH consists of four production subsystems, namely electrolysis (ELY) for producing H_2, carbon capture (CC) for supplying CO_2, MeOH synthesis (SYN) for producing raw MeOH and distillation (DT) for product purification. The disparity in the operational flexibility between these subsystems is modelled by adopting a constant load for the carbon capture subsystem (which is supposed to process a flue gas stream from a constant external supply) and the distillation subsystem (with known limited flexibility), while the load of electrolysers and MeOH synthesis is flexible and each can vary within a broad range with an excess capacity (compared with that defined

by the stoichiometric requirement). When the renewable power is in surplus, excess hydrogen (via electrolysis) and/or raw MeOH (via synthetic reactor) can be produced and stored in respective storage subsystems (i.e. STh and STm) for subsequent consumption when the renewable power is in deficit. When the power deficit is too large, the stored hydrogen can additionally be fed to the fuel cells to sustain a minimum level of operation of the MeOH plant. The backup dispatchable power is a fail-safe measure to ensure sustainable production. In addition, the CO_2 storage subsystem (STc) is required to handle the load mismatch between carbon capture and MeOH synthesis. Also placed between these two subsystems is a heat storage subsystem (STq). This is to facilitate the heat integration between the exothermic CO_2 hydrogenation reactor (as a heat source) and the regeneration column for amine-based CO_2 capture (as a heat sink), which may operate at different load levels.

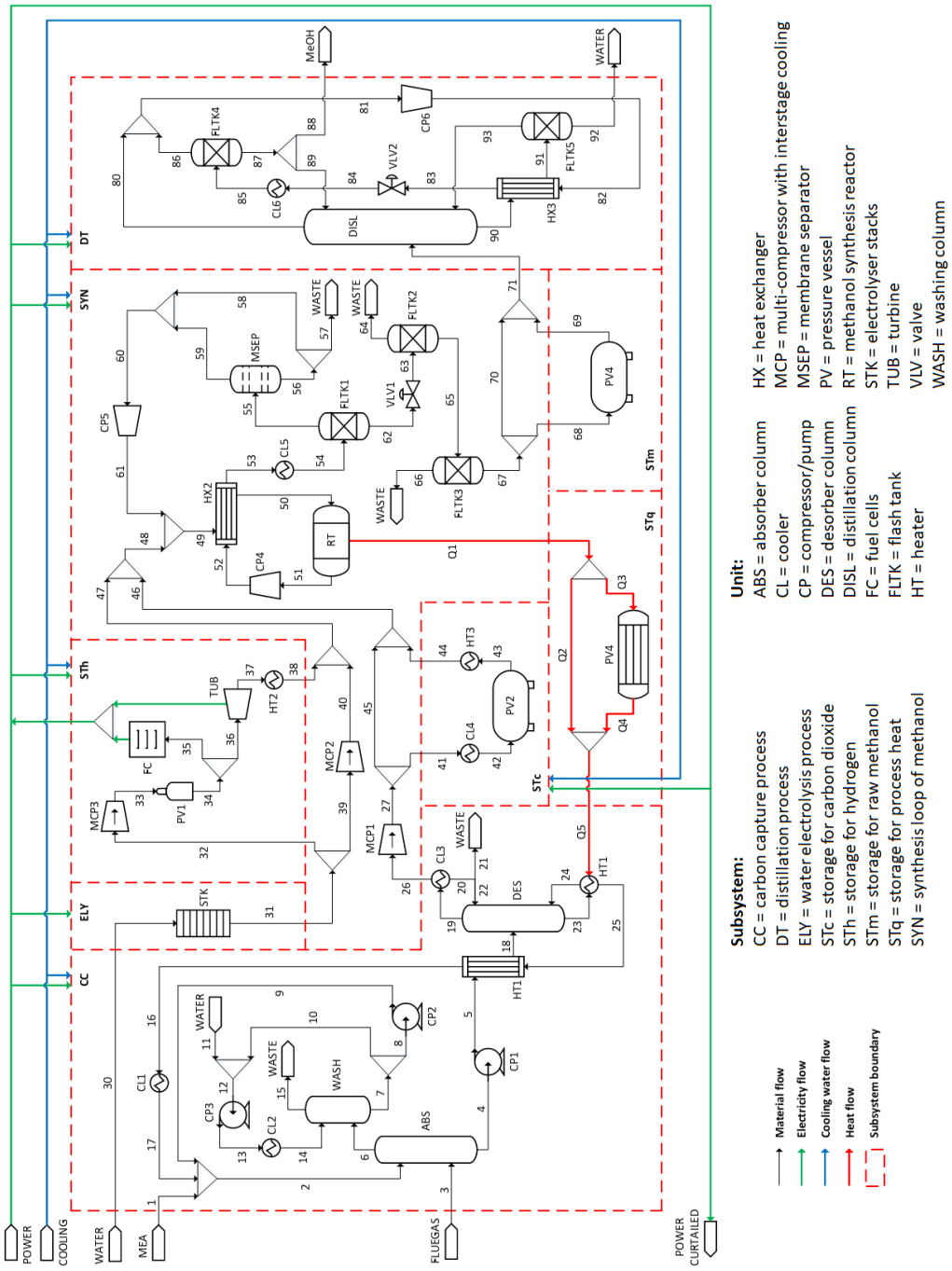


Figure 6.1. Flowsheet of the electrified methanol production and its subsystems.

6.2.2 Process description and modelling

The carbon capture and MeOH synthesis subsystems are adapted from Chapter 3, with slight modifications in the MeOH synthesis flowsheeting. Details of process design and stream information for the two subsystems are elaborated in Appendix C (see Figures C.1 and C.2, and Tables C.1 and C.2). However, substantial modifications have been made to the distillation process, storage subsystems and water electrolysis process, which are described in the following sections.

6.2.2.1 Methanol distillation process. The distillation column is modelled with a RADFRAC unit aiming to produce a 99.8 wt% MeOH product. The number of equilibrium stages is optimised to be 27, with a reflux ratio of 0.92 using design functions embedded in Aspen Plus. To maximise the heat integration within the subsystem, a design of a heat pump via mechanical vapour recompression (MVR) is proposed (Díez et al., 2009). The MVR system upgrades the second stage vapour (heat source) to facilitate the energy transshipment to the reboiler (heat sink), thus simultaneously reducing the heating (reboiler) and cooling (condenser) duties. With an optimised flowrate of the working fluid, the MVR system leads to 100 % reduction in heating (originally 33,423 kW) and 94.8 % reduction in cooling (originally −29,111 kW) at additional mechanical work of 5,828 kW. The process flowsheet of the MVR, key stream notations, process stream properties and results of optimisation are provided respectively in Figure C.3, Table C.3, Table C.4 and Figure C.4 in Appendix C.

6.2.2.2 Storage systems. The storage subsystems are auxiliary units to balance the time-mismatched energy and material flow resulting from the optimal scheduling. They are essential for a variable load and an intermittent power supply. The storage for materials comprises (1) a H_2-based system that includes compressors, fuel cells, a heater and a turbine (used to recover the energy from high pressure hydrogen) and (2) liquefied CO_2 and raw MeOH storage tanks. The H_2-based storage is a costly compressed gas system (172 bar) involving a complex network interplay and operation policy. In contrast, the CO_2 and raw MeOH storage systems are rather simple: they are stored in pressure vessels under moderate conditions with

straightforward connections with the rest of the system. While raw MeOH is stored at room conditions, CO_2 is stored at 71 bar (a required pressure for downstream processes) and 29.3 °C (dew point of CO_2 at the storage pressure). Note that the CO_2 and raw MeOH storage are conjugated due to material balance, i.e. for one unit of CO_2 stored, a fixed ratio (governed by the reaction stoichiometry) of raw MeOH will be withdrawn from its storage tank, and vice versa. The H_2-based storage is not conjugated because hydrogen is used as both an energy vector (to fuel cells) and a material buffer (to downstream processes).

The heuristic principle in the conceptual process design is to arrange heat integration primarily within each subsystem (e.g. the MVR-based design in distillation) and to minimise integration across different subsystems. This is to avoid (1) expensive cross-system heat storage and (2) reduced operability resulting from a complex heat integration network. However, there is a heat-sink/source pair across two subsystems that has shown viable economical integration from an initial assessment. This cross-system heat integration transships the heat generated from the exothermic reactions in SYN subsystem to the reboiler in CC subsystem.

6.2.2.3 Water electrolysis process. The water electrolysis process (ELY subsystem) is a simple subsystem and yet of a special interest. It is common to assume a constant energy efficiency for the electrolysers for the sake of simplicity (Nayak-Luke et al., 2018). However, its unique performance curve provides an opportunity for optimisation: its energy efficiency improves when operation load reduces, implying a lower total energy consumption rate when designed with an excess capacity. The energy efficiency of the electrolysers is represented by the specific energy consumption per unit mass of produced hydrogen (e^{ELY}), which is typically a nonlinear function with respect to load. For simplicity (Beerbühl et al., 2015), it is linearised and approximated by

$$e^{\mathrm{ELY}}(t) = e^{\mathrm{ELY}}_{\mathrm{max}} - \big[1 - \phi(t)\big]\big(e^{\mathrm{ELY}}_{\mathrm{max}} - e^{\mathrm{ELY}}_{\mathrm{min}}\big) \tag{6.1}$$

where ϕ denotes the load fraction, and $e^{\mathrm{ELY}}_{\mathrm{min}}$ and $e^{\mathrm{ELY}}_{\mathrm{max}}$ denote the minimum (when the load approaches 100 %) and maximum (when the load approaches 0) specific

energy requirement, respectively. The values of $e_{\min}^{\mathrm{ELY}}$ and $e_{\max}^{\mathrm{ELY}}$, along with other constant parameters, are tabulated in Table C.7 in Appendix C.

6.2.3 Flow and storage model

This part of the optimisation model concerns the energy and material flows between all subsystems and the corresponding storage units. It excludes pre-defined operation policy but provides the physical bounds to the optimiser. Since the analysis is based on a fully electrified chemical plant, the energy flow mainly comprises electricity and cooling water, with one exception in the SYN subsystem where excess heat from the catalytic reactor is fed to the reboiler in the CC subsystem. The overall energy balances for electricity and cooling duty are modelled respectively by

$$0 = P_{\mathrm{in}}(t) - \sum_{k} x_{\mathrm{el}}^{k} - P_{\mathrm{out}}(t) \tag{6.2}$$

$$0 = E_{\mathrm{cw}} - \sum_{k} \sum_{t=1}^{N} x_{\mathrm{cw}}^{k}(t) \tag{6.3}$$

where P_{in} denotes all power (including renewable and dispatchable power) provided to the whole system, P_{out} denotes the curtailed power, E_{cw} denotes the total cooling duty required by the whole system, x_j^k is the consumption of j utility in k subsystem and N is the total operational hours in a year, which is assumed to be 8,760 h. Both electricity and cooling duty are measured in kilowatt. The electricity and cooling water flows to the individual subsystems are quantified by Eqs. 6.4–6.9:

$$x_{\mathrm{el}}^{\mathrm{SYN}}(t) = a_1^{\mathrm{SYN}} + a_2^{\mathrm{SYN}} F_{39}(t) + a_3^{\mathrm{SYN}} \dot{\xi}(t) \tag{6.4}$$

$$x_{\mathrm{el}}^{\mathrm{STh}}(t) = a_1^{\mathrm{STh}} F_{32}(t) + a_2^{\mathrm{STh}} F_{36}(t) - a_3^{\mathrm{STh}} F_{35}(t) - a_4^{\mathrm{STh}} F_{36}(t) \tag{6.5}$$

$$x_{\mathrm{el}}^{\mathrm{STc}}(t) = a_1^{\mathrm{STc}} F_{44}(t) \tag{6.6}$$

$$x_{\mathrm{cw}}^{\mathrm{SYN}}(t) = a_4^{\mathrm{SYN}} + a_5^{\mathrm{SYN}} F_{39}(t) + a_6^{\mathrm{SYN}} \dot{\xi}(t) \tag{6.7}$$

$$x_{\mathrm{cw}}^{\mathrm{STh}}(t) = a_5^{\mathrm{STh}} F_{32}(t) \tag{6.8}$$

$$x_{\mathrm{cw}}^{\mathrm{STc}}(t) = a_2^{\mathrm{STc}} F_{41}(t) \tag{6.9}$$

where F denotes the flowrate of a process stream, $\dot{\xi}$ the hourly extent of reaction and a^k the constant process coefficient for subsystem k (obtained from Aspen Plus simulations).

The electricity consumption of the ELY subsystem ($x_{\mathrm{el}}^{\mathrm{ELY}}$) and the extent of reaction (i.e. the MeOH synthesis rate) of the SYN subsystem ($\dot{\xi}$) are of special interest because they are governed by the load fraction and the maximum capacity of the corresponding units. Therefore, the two variables are modelled explicitly using Eqs. 6.10 and 6.11 with additional decision variables:

$$x_{\mathrm{el}}^{\mathrm{ELY}}(t) = \phi(t) x_{\mathrm{el,max}}^{\mathrm{ELY}} \tag{6.10}$$

$$\dot{\xi}(t) = \phi(t) \dot{\xi}_{\mathrm{max}} \tag{6.11}$$

where $x_{\mathrm{el,max}}^{\mathrm{ELY}}$ denotes the maximum capacity of the electrolysers measured in rated power and $\dot{\xi}_{\mathrm{max}}$ denotes the maximum size of the catalytic reactor measured in terms of extent of reaction.

Since the DT subsystem is non-flexible and has no interactions with other subsystems except the feed stream, x_j^{DT} becomes a constant for both electricity and cooling duty. Although the CC subsystem is also non-flexible, its reboiler is partially powered by the heat from the SYN subsystem. Therefore, the electricity consumption of the CC subsystem is calculated by

$$x_{\mathrm{el}}^{\mathrm{CC}}(t) = x_{\mathrm{el,0}}^{\mathrm{CC}} - \dot{Q}_5(t) \tag{6.12}$$

where $x_{\mathrm{el,0}}^{\mathrm{CC}}$ denotes the constant electricity consumption when process heat is not integrated and $\dot{Q}_5$ denotes the process heat from SYN via heat storage subsystem (STq). This equation also implicitly takes a physical bound into account, i.e. the recovered heat ($\dot{Q}_5$) can never exceed the load requirement of the reboiler for all t. The heat generated from the catalytic reactor is calculated by

$$\dot{Q}_1(t) = b_{\mathrm{q}} \dot{\xi}(t) \tag{6.13}$$

where b_{q} is a constant parameter denoting the specific heat output. Similarly, this

equation also implicitly suggests that all heat from the catalytic reactor has to be integrated. This is justified by the cheaper heating from the STq subsystem in comparison with electrical heating.

The material flows include the feed water to the electrolysers (Eq. 6.14), the generated hydrogen from the electrolysers (Eq. 6.15), the hydrogen fed to the MeOH synthesis (Eq. 6.16), the CO_2 fed to the MeOH synthesis (Eq. 6.17), and the raw MeOH generated from the synthesis subsystem (Eq. 6.18). These are quantified respectively by

$$F_{30}(t) = \frac{M_{\mathrm{W}}(\mathrm{H_2O})}{M_{\mathrm{W}}(\mathrm{H_2})} F_{31}(t) \tag{6.14}$$

$$F_{31}(t) = \frac{x_{\mathrm{el}}^{\mathrm{ELY}}(t)}{e^{\mathrm{ELY}}(t)} \tag{6.15}$$

$$F_{47}(t) = b_{\mathrm{h}} \dot{\xi}(t) \tag{6.16}$$

$$F_{46}(t) = b_{\mathrm{c}} F_{47}(t) \tag{6.17}$$

$$F_{67}(t) = b_{\mathrm{m}} F_{47}(t) \tag{6.18}$$

where M_{W} denotes molecular weight and b denotes the constant parameters for species indicated by the subscripts.

There are four storage subsystems considered in this work, namely STh (for hydrogen), STm (for raw MeOH), STc (for CO_2) and STq (for process heat), with their holdup quantified by

$$L^{\mathrm{STh}}(t) = L^{\mathrm{STh}}(t-1) + F_{32}(t) - F_{34}(t) \tag{6.19}$$

$$L^{\mathrm{STc}}(t) = L^{\mathrm{STc}}(t-1) + F_{41}(t) - F_{44}(t) \tag{6.20}$$

$$L^{\mathrm{STm}}(t) = L^{\mathrm{STm}}(t-1) + F_{68}(t) - F_{69}(t) \tag{6.21}$$

$$L^{\mathrm{STq}}(t) = L^{\mathrm{STq}}(t-1) + \dot{Q}_3(t) - \dot{Q}_4(t) \tag{6.22}$$

where $L^k(t)$ denotes the storage level of subsystem k at time t, which is updated by the previous storage level at time $t-1$ and the current material or energy flow at time t. The material and energy balances around the storage units are calculated

by Eqs. 6.23–6.31:

$$0 = F_{31}(t) - F_{32}(t) - F_{39}(t) \tag{6.23}$$

$$0 = F_{34}(t) - F_{35}(t) - F_{36}(t) \tag{6.24}$$

$$0 = F_{36}(t) + F_{39}(t) - F_{47}(t) \tag{6.25}$$

$$0 = F_{67}(t) - F_{68}(t) - F_{70}(t) \tag{6.26}$$

$$0 = F_{69}(t) + F_{70}(t) - F_{71} \tag{6.27}$$

$$0 = F_{26} - F_{41}(t) - F_{45}(t) \tag{6.28}$$

$$0 = F_{44}(t) + F_{45}(t) - F_{46}(t) \tag{6.29}$$

$$0 = \dot{Q}_1(t) - \dot{Q}_2(t) - \dot{Q}_3(t) \tag{6.30}$$

$$0 = \dot{Q}_2(t) + \dot{Q}_4(t) - \dot{Q}_5(t) \tag{6.31}$$

where Eqs. 6.23–6.25 are for hydrogen storage, Eqs. 6.26 and 6.27 are for raw MeOH storage, Eqs. 6.28 and 6.29 are for CO_2 storage, Eqs. 6.30 and 6.31 are for heat storage, and F_{26} and F_{71} denote the constant flowrate of the generated CO_2 from the carbon capture subsystem and the feed of raw MeOH to the distillation subsystem, respectively.

The production is also subject to additional operational constraints. The year-round material and energy balances are bound to ensure a sustainable production, as shown in Eqs. 6.32–6.35 for hydrogen, CO_2, raw MeOH and process heat, respectively:

$$\sum_{t=1}^{N} F_{32}(t) = \sum_{t=1}^{N} F_{34}(t) \tag{6.32}$$

$$\sum_{t=1}^{N} F_{41}(t) = \sum_{t=1}^{N} F_{44}(t) \tag{6.33}$$

$$\sum_{t=1}^{N} F_{68}(t) = \sum_{t=1}^{N} F_{69}(t) \tag{6.34}$$

$$\sum_{t=1}^{N} \dot{Q}_3(t) = \sum_{t=1}^{N} \dot{Q}_4(t) \tag{6.35}$$

The storage units are bound by the physical requirement that the storage level should be below its maximum capacity ($L^k_{\max}$, which is one of the decision variables to be optimised) for all times t, as defined by

$$0 \leqslant L^k(t) \leqslant L^k_{\max} \tag{6.36}$$

Due to the flexible operation, the synthesis process is designed with a larger capacity than that for the baseline operation (i.e. without process flexibility). This constraint is modelled with

$$\dot{\xi}_0 \leqslant \dot{\xi}_{\max} \tag{6.37}$$

where $\dot{\xi}_0$ and $\dot{\xi}_{\max}$ denote the hourly extent of reaction at the baseline operation and the maximum extent of reaction designed for the flexible operation, respectively. The load fraction of a subsystem is constrained by its operability, which is modelled with

$$\phi(t) \geqslant \phi_{\min} \tag{6.38}$$

where $\phi_{\min}$ denotes the minimum load fraction, which governs the flexibility of a subsystem.

Some of the physical bounds are redundant because the material or energy balance has implicitly imposed the constraint. For example, Eq. 6.34 has already been bounded due to the constant flowrate of raw MeOH to the downstream DT subsystem. All redundancy has been removed prior to the solution of the optimisation model.

6.2.4 Renewable energy model

The case study locations in this work are same as the ones in Chapter 4, i.e. Norderney (Germany) and Kramer Junction (US), which are locations with world-class wind and solar power, respectively. Thus, the meteorological data and the

renewable power conversion methods are inherited from Chapter 4. The capacity factor (CF) of wind source is calculated based on the wind strength and the selected turbine mode, giving 29.4 and 4.3 % for Norderney and Kramer Junction, respectively. The CF of solar photovoltaics (PV) for Kramer Junction is adopted from the work of Matzen et al. Matzen et al. (2015), in which they assumed a value of 25.0 % for solar PV based on the estimated US average levelised energy cost (LEC) for renewable generation resources entering service in 2019. The CF of solar source in Norderney is calculated by comparing the solar profiles of the two locations, which gives a value of 12.1 %.

Since the total power supply (P_{in}), introduced earlier in Eq. 6.2, consists of both generated renewable power and dispatchable power, its value can be calculated by

$$P_{\text{in}}(t) = P_{\text{W}}(t) + P_{\text{S}}(t) + P_{\text{D}}(t) \tag{6.39}$$

where $P_{\text{W}}(t)$, $P_{\text{S}}(t)$ and $P_{\text{D}}(t)$ denote the hourly wind, solar and dispatchable power at time t, respectively. P_{D} is optional backup power, which may be a competing source to the renewable power depending on its price and policy implementation. Its impact on the overall and marginal performance of the system is of particular interest.

To quantify the renewable power generation, the model adopts the provision factor, γ, to indicate the ratio of generated renewable power to production load requirement. Their relationship is quantified by

$$\sum_{i} \sum_{t=1}^{N} P_i(t) = \gamma N \overline{P_{\text{L}}} \tag{6.40}$$

where $\overline{P_{\text{L}}}$ denotes the average hourly load of the production and the subscript i denotes the type of renewable source (i.e. either wind or solar). The renewable mix is indicated by the fraction of one source in the renewable power generation (f_i), as calculated by

$$f_i = \frac{\sum_{t=1}^{N} P_i(t)}{\gamma N \overline{P_{\text{L}}}} \tag{6.41}$$

The total dispatchable energy is essentially the summation of the hourly dispatchable energy use over the period of analysis, which is calculated by

$$E_{\mathrm{D}} = \sum_{t=1}^{N} P_{\mathrm{D}}(t) \tag{6.42}$$

where E_{D} denotes the total dispatchable energy requirement. The energy from the hydrogen storage subsystem (STh), termed as E_{ST}, is always part of renewable energy since the optimiser would not schedule the dispatchable power to the storage unit. Due to the operational restrictions, all E_{ST} is fed to the production load, contrasting to the energy from renewable generation which may be curtailed. Thus, the portion of load met by the energy from STh subsystem is calculated by

$$E_{\mathrm{ST}} = \sum_{t=1}^{N} \left[a_3^{\mathrm{STh}} F_{35}(t) + a_4^{\mathrm{STh}} F_{36}(t) \right] \tag{6.43}$$

where a_3^{STh} and a_4^{STh} denote the specific power output per unit mass of hydrogen for the fuel cells and turbine, respectively. Note that STh is the only storage subsystem that can output electrical power, whereas all other storage units are used as a material buffer. The renewable penetration in the load, termed as $f_{\mathrm{L}}^{\mathrm{RE}}$, can be calculated by

$$f_{\mathrm{L}}^{\mathrm{RE}} = 1 - \frac{E_{\mathrm{D}}}{N\overline{P_{\mathrm{L}}}} \tag{6.44}$$

6.2.5 Economic model

The cost functions are mainly divided into three groups: (1) renewable power generation, (2) production utilities, and (3) subsystems of the production plant. The subsystems can be further divided into groups of storage and production facilities. For convenience, all costs are annualised with a unit of \$/year. The annualised cost of renewable power generation is calculated by

$$\sum_i C_i^{\mathrm{GEN}} = \sum_i \left(\gamma f_i \overline{P_{\mathrm{L}}} \frac{1}{\mathrm{CF}_i} f^{\mathrm{CR}} \mathrm{CapEx}_i^{\mathrm{GEN}} \right) \tag{6.45}$$

where CapEx stands for capital expenditure. The capital recovery factor, f^{CR}, is defined by

$$f^{\mathrm{CR}} = \frac{r(1+r)^n}{(1+r)^n - 1} \tag{6.46}$$

where n denotes the life of a unit and r denotes the discount rate, taken as 8 % in this work.

The utilities consist of dispatchable energy, cooling duty and process water. The annual utility cost is calculated by

$$\sum_j C_j = c_{\mathrm{D}} E_{\mathrm{D}} + c_{\mathrm{cw}} E_{\mathrm{cw}} + c_{\mathrm{pw}} \Big[\sum_{t=1}^{N} F_{30}(t) - 0.98 N F_{92} \Big] \tag{6.47}$$

where the subscript j denotes the type of utilities, c_{D}, c_{cw} and c_{pw} denotes the unit price of dispatchable energy, cooling water and process water, respectively. It is assumed that the waste water stream (with a purity of 98 wt%) is recycled and purified before feeding to the electrolysers. The cost for water purification is neglected. Note that Streams 1 and 11 in Figure 6.1 respectively represent the makeup for monoethanolamine and water losses during the operation. Their costs are neglected since the economic impact is negligible. The subsystems of the production facilities require different cost functions due to their specific technical nature. The annualised cost of ELY and STh subsystem is determined from their maximum size, as shown in Eqs. 6.48 and 6.49:

$$C^{\mathrm{ELY}} = x_{\mathrm{el,max}}^{\mathrm{ELY}} f^{\mathrm{CR}} \mathrm{CapEx}^{\mathrm{ELY}} \tag{6.48}$$

$$\begin{aligned} C^{\mathrm{STh}} =& L_{\mathrm{max}}^{\mathrm{STh}} f^{\mathrm{CR}} \mathrm{CapEx}^{\mathrm{STh}} \\ &+ a_3^{\mathrm{STh}} F_{35,\mathrm{max}} f^{\mathrm{CR}} \mathrm{CapEx}^{\mathrm{FC}} \\ &+ a_4^{\mathrm{STh}} F_{36,\mathrm{max}} f^{\mathrm{CR}} \mathrm{CapEx}^{\mathrm{TUB}} \end{aligned} \tag{6.49}$$

where $F_{35,\mathrm{max}}$ and $F_{36,\mathrm{max}}$ denote the maximum flowrate of hydrogen charged to the fuel cells and the turbine, respectively. The cost data for solid oxide fuel cells (SOFC) are used due to the maturity of this technology. The CapEx of

STh subsystem includes steel tanks and compressors (as the reference provides an integrated cost (Steward, 2009)). The heater cost is neglected since it is negligible. Nevertheless, the electricity consumed by the heater is considered in the energy balance. The costs of subsystems of CC, SYN and DT are estimated by ratio factors based on the main equipment cost as per the work of Zhang et al. (2017). Since the subsystems of CC and DT are non-flexible, their annualised cost is independent of the size, as shown respectively in Eqs. 6.50 and 6.51:

$$C^{\mathrm{CC}} = f^{\mathrm{CR}}\mathrm{TFCC}^{\mathrm{CC}} \tag{6.50}$$

$$C^{\mathrm{DT}} = f^{\mathrm{CR}}\mathrm{TFCC}^{\mathrm{DT}} \tag{6.51}$$

where TFCC^{k} stands for the total fixed capital cost of k subsystem. Due to the flexible feature of SYN subsystem, its annualised cost is estimated via the six-tenths factor rule based on the size. Therefore, the annualised cost of SYN is calculated by

$$C^{\mathrm{SYN}} = \left[26.76 \times 10^{6} + \mathrm{TFCC}^{\mathrm{SYN}}\left(\frac{\dot{\xi}_{\max}}{\dot{\xi}_{0}}\right)^{0.6}\right] f^{\mathrm{CR}} \tag{6.52}$$

where $\mathrm{TFCC}^{\mathrm{SYN}}$ denotes the total fixed capital cost of SYN (barring MCP1 unit) at the baseline operation (its size is measured in terms of extent of reaction, i.e. $\dot{\xi}_0$). The constant coefficient in Eq. 6.52 represents the TFCC of MCP1 unit. The actual size of SYN taking flexibility into account is denoted by $\dot{\xi}_{\max}$, which is obtained from the optimiser. Note that $\mathrm{TFCC}^{\mathrm{SYN}}$ excludes the MCP1 unit because the latter is independent of the SYN size (due to the constant flowrate of F_{26}). The main equipment costs for the production subsystems are given in Table C.5 in Appendix C. The breakdown of all subsystems' TFCC at the baseline operation is given in Table C.9 in Appendix C.

The storage unit for liquefied CO_2 and raw MeOH is essentially a pressure vessel, whose cost can be estimated from empirical correlations using Douglas's method (Douglas, 1988). While the cost of a pressure vessel can benefit from the economies of scale, the capacity of a single vessel has to be constrained. From an initial estimate, it is found that the required storage size is in the range of thousands of

tonnes (the final result shows 52,000 and 54,000 tonnes for raw methanol and CO_2 storage, respectively), which is far above a single vessel's capacity. Therefore, the cost functions for STm and STc are modified to

$$C^{\mathrm{STc}} = 107.3 L_{\max}^{\mathrm{STc}} \tag{6.53}$$

$$C^{\mathrm{STm}} = 53.1 L_{\max}^{\mathrm{STm}} \tag{6.54}$$

where the constant prefactors represent the cost per unit mass based on a single vessel capacity of 200 tonnes. Full derivation from the empirical correlations to the linearised approximation is elaborated in Note 1 of Appendix C. The capital costs of the cooler and the heater in STc are ignored due to their insignificant magnitudes. Regarding the heat storage, a thermo-chemical ESS is used in this work due to its maturity in large-scale applications (Sarbu and Sebarchievici, 2018). The annualised cost for STq is calculated by

$$C^{\mathrm{STq}} = L_{\max}^{\mathrm{STq}} f^{\mathrm{CR}} \mathrm{CapEx}^{\mathrm{STq}} + \dot{Q}_{4,\max} \mathrm{OpEx}^{\mathrm{STq}} \tag{6.55}$$

where OpEx stands for operational expenditure and $\dot{Q}_{4,\max}$ denotes the maximum discharging rate of STq subsystem.

The raw materials and utility costs are adopted from Chapter 3. The cost parameters for renewable generation, electrolysers and storage technologies are tabulated in Table C.10 in Appendix C.

6.2.6 Optimisation strategy

The aim of the modelling is to minimise the levelised cost of methanol (LCOMeOH, measured in \$/tonne) by optimising the energy and material dispatch supported by the suitable sizing of all units operating flexibly. This leads to an objective function defined by

$$\mathrm{LCOMeOH} = \frac{1}{0.001 N F_{88}} \Big(\sum_i C_i^{\mathrm{GEN}} + \sum_j C_j + \sum_k C^k \Big) \tag{6.56}$$

where the notation i denotes the source of renewable energy, j denotes the type of utility and k denotes the subsystem. The annualised cost terms are introduced in Eqs. 6.45–6.55, respectively. The denominator, $0.001NF_{88}$, denotes the annual production of MeOH measured in tonnes. The optimisation problem is summarised as follows:

min.	Objective function	Eq. 6.56
s.t.	System models	Eqs. 6.2–6.31
	Operational constraints	Eqs. 6.32–6.38
	Specifications	Table C.7 in Appendix C

The key decision variables to be determined by the optimisation are listed in Table C.6 in Appendix C. All constant parameters in the physical and renewable energy model are summarised in Table C.7 in Appendix C. For a given set of parameters, the solution of the optimisation problem will indicate the corresponding optimal dispatch of the material and energy flows. A qualitative illustrative example is given by Figure C.5 in Appendix C.

To reduce the computational complexity, linearisation techniques have been applied, which include cost functions linear approximation (see Eqs. 6.53 and 6.54), bilinear variables replacement (for Eq. 6.15) and storage level reformulation to avoid discontinuities (for Eqs. 6.19–6.22). The modification results in a linear programming model, which is implemented in GAMS (General Algebraic Modelling System) and solved using the CPLEX solver.

6.2.7 Summary of assumptions

The following assumptions have been used in this work: (1) the analysis focuses on one-year operation with no downtime of MeOH production. (2) All process units are assumed to have a life of 30 years. (3) Makeup streams in carbon capture process are excluded in cost because the economic impact (around 0.2–0.4 %) is

negligible. (4) The energy from the purge stream is ignored since it is difficult to recover the heat from a process flare. (5) The compressors modelled in this work are assumed to be isentropic with an efficiency of 75 %. (6) All mechanical work and process heating (except the integrated heating) are powered by electricity only. (7) The electrolysers can ramp instantaneously from 0–100 %. (8) The storage units are not limited by charging or discharging rate. (9) The standby losses of energy and material in the storage units are neglected.

6.3 Results

The optimisation results are shown to be strongly affected by two factors, i.e. the dispatchable energy price and the degree of process flexibility, which are of special interest from both policymaking and engineering perspectives. Thus, a base case scenario is first evaluated with fixed values for these two parameters, which renders a detailed cost breakdown and yields insight into the impact of process flexibility on key design choices. Subsequently, the analysis scope extends to explore the impact of dispatchable energy price and process flexibility on the (minimised) MeOH production cost and the corresponding penetration level of renewables. A separate analysis focuses further on the environmental perspective, exploring how the intended penetration level of renewables would alter the economics with or without process flexibility. Recognising the uncertainties in the technology costs, this section also assesses the economics of a conservative and a progressive scenario for costing, to test the robustness of the observations made from the base case scenario.

6.3.1 Base case scenario

The base case scenario is defined by using fixed dispatchable energy price (c_{D}) and flexibility of the MeOH plant. The purchase of dispatchable electricity plays an important role in determining the overall economic performance; its price can be used as a tool to influence the renewable penetration in chemical production

(Chen, 2020) and can be highly volatile subject to both local policies and market conditions. For Germany, an electricity price of 57 \$/MWh (50 €/MWh) was quoted in a previous study (Varone and Ferrari, 2015) while a recent work provided more insights into electricity purchase by taking spot market price, taxation, fees, subsidies and apportionments into account, reporting a price range from 35 to 166 \$/MWh (Hank et al., 2018). Regarding the US, the average electricity price ranges from 103 to 128 \$/MWh depending on end-use sectors (US Energy Information Administration, 2020). For easy comparison, the base case scenario uses a benchmark price of 100 \$/MWh for the dispatchable energy in both locations. The evaluation based on the same dispatchable energy price means that the economics difference is solely attributed to the renewable sources of the respective location.

On process flexibility, the base case scenario considers no lower limit on the load fraction of electrolysers (Beerbühl et al., 2015) but applies a minimum load ($\phi_{\min}$) for the synthesis reactor. In principle, the load range of a catalytic reactor depends on the nature of the chemical reactions, catalysts and the reactor design, and is limited by key operational issues such as temperature management (Cheema and Krewer, 2018). Currently, there is no experimental or theoretical data publicly available regarding the load range of a MeOH synthesis reactor. Matthischke et al. (2018) has investigated the load range of an adiabatic reactor for CO_2 methanation using superficial velocity as a basis, which translates to a minimum load fraction of 9.8 %. Nayak-Luke et al. (2018) has used a minimum load fraction of 20 % for ammonia synthesis. In this chapter, the value of $\phi_{\min}$ is assumed to be 10 % for the base case scenario, further with a range of $\phi_{\min}$ investigated to elaborate the impact of flexibility on the overall performance of the system.

Table 6.1 summarises the key indicators for the most economical performance of the base case scenario in both locations. These operation indicators include the renewable energy provision (γ), renewable penetration ($f_{\mathrm{L}}^{\mathrm{RE}}$) and renewable mix measured in terms of wind fraction in power generation (f_{W}). Regarding Norderney, the flexible process offers a moderate reduction to the LCOMeOH compared with the non-flexible process, but it achieves a significantly greater level of renewable penetration (90 vs. 48 %). This implies a significantly improved environmental

performance at a lower cost (approximately 8 % reduction) when flexible production is implemented. The renewable mix indicates that only wind power is generated for the case of Norderney. As for Kramer Junction, the improvement caused by the flexible production is insignificant for both the production cost (933 vs. 946 \$/tonne) and the level of renewable penetration (81 vs. 73 %). This is because the mitigation of the variable input power, which is where the benefits of a flexible process would be derived, is in this case already tackled economically by the excess provision of renewable (solar) power. In conclusion, with relatively cheap renewable power, the benefits from a flexible process would be limited.

Table 6.1. Optimal performance of the base case scenario, where c_{D} is fixed at 100 \$/MWh and ϕ_{min} at 10 % for the flexible production.

Location	Flexibility	LCOMeOH \$/tonne	LEC \$/MWh	γ –	$f_{\mathrm{L}}^{\mathrm{RE}}$ %	f_{W} %
Norderney	Flexible	960.8	64.9	0.70	90.1	100
	Non-flexible	1,046.7	78.9	0.39	48.3	100
Kramer Junction	Flexible	932.6	62.7	0.66	81.3	0
	Non-flexible	946.0	66.1	0.61	73.0	0

Further inspection of the limited economic improvement by process flexibility shows that the benefit is restricted by the level of renewable penetration in the design that minimises the production cost. Figure 6.2A and B compare the current most economical case with an enforced fully renewable operation (i.e. $f_{\mathrm{L}}^{\mathrm{RE}} = 100\,\%$) for both locations, with a detailed display of the cost elements contributing to LCOMeOH. The potential benefits of flexible production are fully demonstrated when a 100 % renewable operation is imposed, wherein the cost-saving is mainly attributed to the cost reduction in the hydrogen storage (Norderney) and renewable power generation (Kramer Junction). The reliance on hydrogen storage is reduced because the variability of renewable sources is tackled by the alternative subsystems, i.e. CO_2 and raw MeOH storage, which are much cheaper than hydrogen storage. The substitution of energy storage using a material buffer is achieved by the flexible production at an additional cost of the (over-sized) synthesis units. Clearly, the overall saving from a flexible operation significantly outweighs the additional costs.

In addition to the saving from the hydrogen storage subsystem, a flexible operation also reduces the renewable generation cost in the fully renewable case

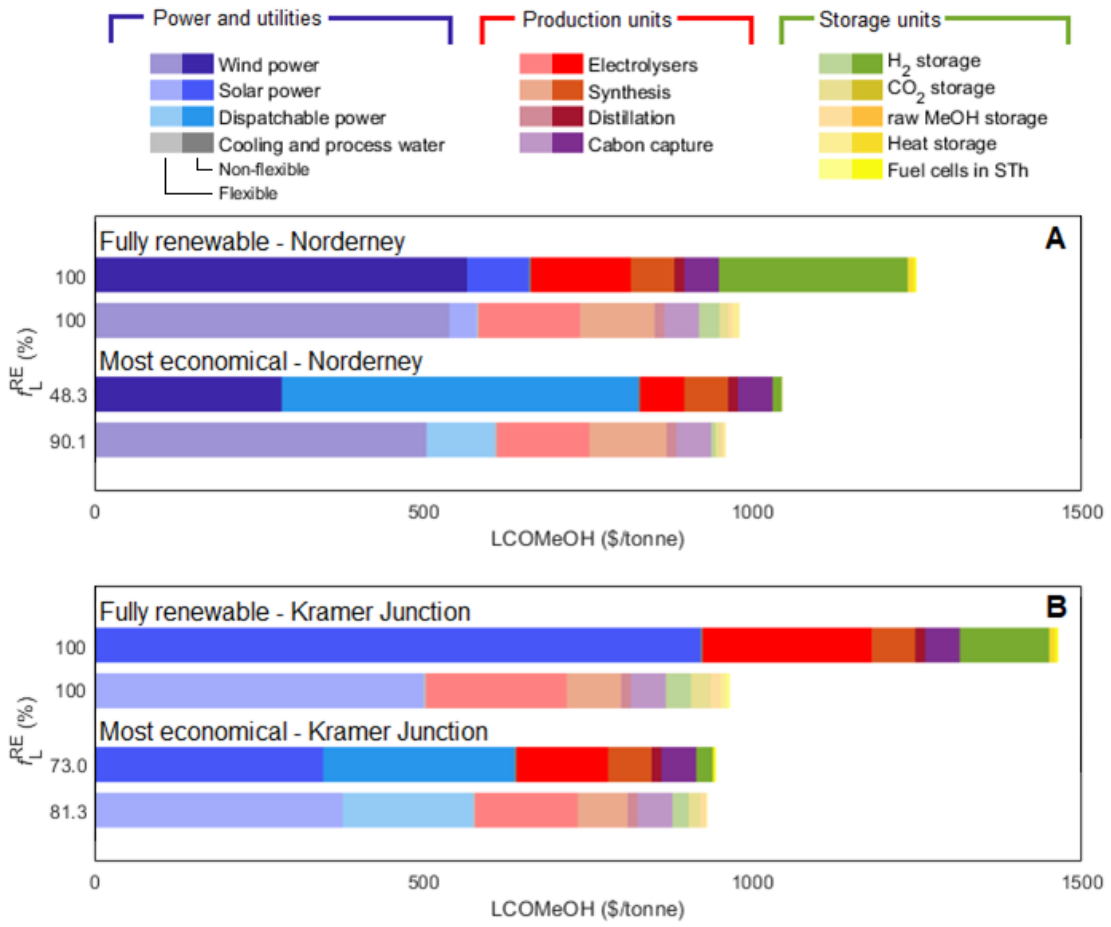


Figure 6.2. Contribution of the cost elements to LCOMeOH in the most economical case and the 100 % renewable operation case for (A) Norderney and (B) Kramer Junction. Note that the costs of H_2 storage includes tanks and compressors. Shaded areas indicate the flexible processes.

(Figure 6.2B, upper). If the renewable generation is relatively cheap, which is the case for Kramer Junction, the excess provision of renewable power may occur in lieu of renewable energy storage (i.e. the H_2-based ESS). The benefits of process flexibility in such a case would be mainly from the reduction of renewable over-provision. The optimisation result confirms that the process flexibility would lead to reduced curtailment, which represents improved utilisation of renewable energy (see Figure C.7 in Appendix C). Note however that the flexible operation for the most economical scenario in both locations (Figure 6.2A and B, lower) incurs a higher renewable generation cost despite the reduction of the overall cost. This corresponds to an increase in renewable energy intake, which is made more affordable (compared with the use of dispatchable energy) thanks to the process flexibility.

To further elucidate the impact of the variability of renewable energy on the potential benefits of process flexibility, the upper panels of Figure 6.2A and B compare the fully renewable operation scenarios for the two locations (see Table C.13 in Appendix C for the detailed cost elements and the associated sizes of individual units). The fully renewable operation (without flexibility) in Kramer Junction is much more expensive than that in Norderney (1,466 vs. 1,251 $/tonne), even though the solar (the major renewable source in Kramer Junction) technology is cheaper than wind (the major renewable source in Norderney). The LCOMeOH difference can be attributed to the characteristics of renewable sources. Between the two locations, the variability of the solar power source in Kramer Junction is significantly greater than that of the wind power source in Norderney (see Figure 4.2 in Chapter 4). One can see from the upper panels of Figure 6.2A and B that, without process flexibility, the LCOMeOH for Kramer Junction is approximately 17 % higher than its counterpart of Norderney, which is largely due to the excess solar energy generation needed to handle its high variability. By introducing process flexibility, the excess generation is greatly circumvented. Consequently, the LCOMeOH for Kramer Junction is significantly reduced, which becomes even cheaper than its counterpart of Norderney (967 vs. 982 $/tonne). In the case of Kramer Junction, process flexibility reduces its LCOMeOH by approximately 34 %; in comparison, the reduction is 22 % for Norderney. This indicates that the potential benefits of flexible production would be more significant if the renewable energy source is more variable.

Although the ramping of the synthetic reactor is not constrained in the base case scenario, analyses have been performed to verify the impact of ramping on system performance. Currently, there is no literature reporting the ramp limit of a MeOH reactor. However, Armijo and Philibert (2020) reported an hourly ramp limit of 20 % (based on the rated capacity) for ammonia reactors. In light of this, key variables are reported at selected ramp limits up to 20 % (for both ramp-up and -down) for operations in Norderney as an example, which are tabulated in Table C.14 in Appendix C. Significantly, at 20 % ramp limit the LCOMeOH is almost same as the unlimited case (982.4 vs. 982.2 $/tonne for Norderney). Further

inspection on the ramp limit shows that the reduction of LCOMeOH due to the relaxing of ramp limit results from the saving of hydrogen storage, which is in accordance with the benefits of flexibility. In fact, ramp constraint is an alternative measure of process flexibility. Examples of the MeOH reactor load at selected ramp limits are plotted in Figure C.8 in Appendix C.

6.3.2 Impact of dispatchable energy price and process flexibility

The above analysis focuses on the base case scenario, wherein a constant dispatchable energy price (reflects the current market) and fixed flexibility (reflects the technology limits) have been chosen. Given that the market and technology may change, it is of special interest to know how the dispatchable energy price and flexibility limits impact the overall economical potential. Thus, the trend of LCOMeOH and its corresponding renewable penetration ($f_{\mathrm{L}}^{\mathrm{RE}}$) are plotted in Figure 6.3 for a range of dispatchable energy price (c_{D}) at selected levels of process flexibility indicated by the minimum load of the MeOH reactor (ϕ_{min}). Regardless of the location, LCOMeOH and $f_{\mathrm{L}}^{\mathrm{RE}}$ share the same trend: both significantly increase with c_{D} initially, followed by a much reduced increase rate subsequently. The critical point that divides the two-regime behaviour is at a dispatchable energy price around 120 \$/MWh for both locations. Note that the non-flexible production means $\phi_{\mathrm{min}} = 1$, i.e. the MeOH synthesis subsystem is always at its full load.

From Figure 6.3A and C, it can be seen that the degree of reduction in LCOMeOH due to process flexibility is directly affected by the price of dispatchable energy; the economic benefit becomes more noticeable only after c_{D} is higher than a certain level, as it drives the increase in renewable penetration and hence the importance of process flexibility to handle the increased variable energy supply. Ultimately, the saving from introducing flexibility is capped by the LCOMeOH difference at a fully renewable operation (see Figure 6.2). In Figure 6.3C, the LCOMeOH reduction between $\phi_{\mathrm{min}} = 0.1$ and 0.4 is much smaller than the reduction between $\phi_{\mathrm{min}} = 0.4$ and 0.7 or that between 0.7 and 1 (i.e. the non-flexible case). This indicates that

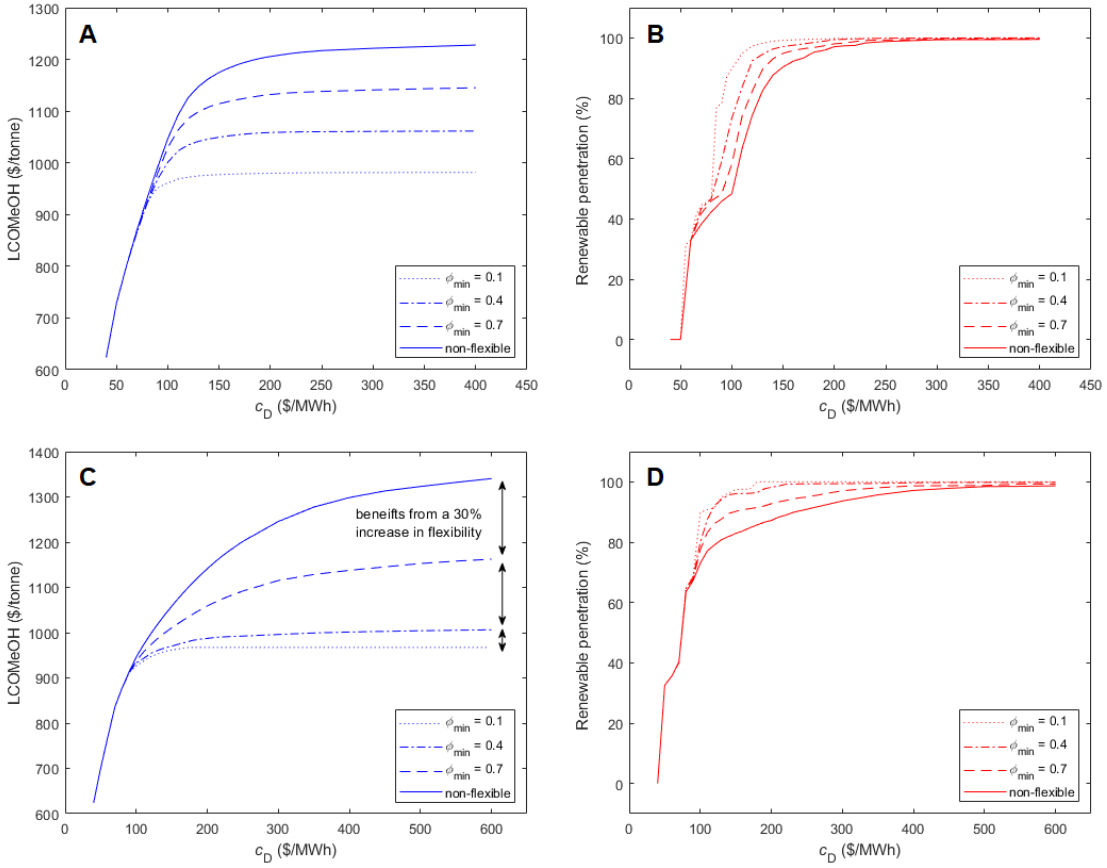


Figure 6.3. Optimal LCOMeOH and its corresponding renewable penetration at different process flexibility over a range of dispatchable energy price. (A) and (B) are plotted for Norderney; (C) and (D) for Kramer Junction.

the benefits of a flexible process may exist only within a limited range of flexibility, beyond which further gains could vanish.

The corresponding trends of $f_{\mathrm{L}}^{\mathrm{RE}}$ are shown in Figure 6.3B and D. In general, the flexible processes tend to facilitate the use of renewable power, hence the increase in renewable penetration at a given c_{D}. However, this environmental benefit gradually vanishes when the dispatchable energy price increases, as the renewable penetration at all levels of flexibility approaches 100 %. The exact shape of a $f_{\mathrm{L}}^{\mathrm{RE}}$ curve, on the other hand, is the result of the (economically) optimal selection and the combination of measures that can contribute to the handling of variable energy supply. These measures include the sizing of electrolysers and the synthesis reactor as well as the adoption and sizing of hydrogen and other in-process storage subsystems. A detailed analysis on the introduction of these measures along with the increase of c_{D} is provided in Figure C.6 in Appendix C.

6.3.3 Costs of enforced renewable penetration targets

Although the dispatchable energy price may be used as an economic tool to steer renewable penetration, its influence on achieving the desirable targets is limited by the two-regime behaviour of the $f_{\mathrm{L}}^{\mathrm{RE}}$ profiles (see Figure 6.3B and D), which makes it less effective after the critical point as $f_{\mathrm{L}}^{\mathrm{RE}}$ becomes insensitive to c_{D}. Even with dispatchable energy prices below the critical point, its increase would result in a dramatic rise in LCOMeOH accompanying the increase of $f_{\mathrm{L}}^{\mathrm{RE}}$. Thus, this section explores the economic implication of directly enforcing the environmental targets, i.e. the levels of renewable penetration, based on the LCOMeOH and the breakdown of the cost elements obtained from the optimisation model with an added equality constraint on $f_{\mathrm{L}}^{\mathrm{RE}}$.

Figure 6.4 shows the LCOMeOH at targeted $f_{\mathrm{L}}^{\mathrm{RE}}$ ranging from 90 to 100 %, a region with high renewable penetration where a flexible process is expected to be important (low renewable penetration reduces the impact of flexibility, as illustrated earlier in Figure 6.3). The two locations feature similar trends in the total cost variation but show different weights of individual cost elements, which is attributed to the difference in both renewable source characteristics and technology prices. The costs of renewable power generation account for more than half of the total LCOMeOH for both locations. Barring the renewable power costs, the cost elements for all cases are plotted in Figure 6.4a–d on the same scale. Clearly, the benefits of flexible production, which is achieved by producing excess raw MeOH using the surplus renewable power, are shown to arise primarily from the reduction in hydrogen storage cost (more significant for Norderney) and renewable generation cost (more significant for Kramer Junction) throughout the range of renewable penetration. The three competing factors—flexibility, H_2-based ESS and renewable power over-provision—form an interplay triangle (see the scheme in Figure 6.4, upper-left). Thus, the cost reduction of a particular element from introducing flexibility greatly depends on the existing trade-off between the other two competing factors. Note that the cost of CO_2 storage is conjugated with raw MeOH in accordance with material balance and the reaction stoichiometry.

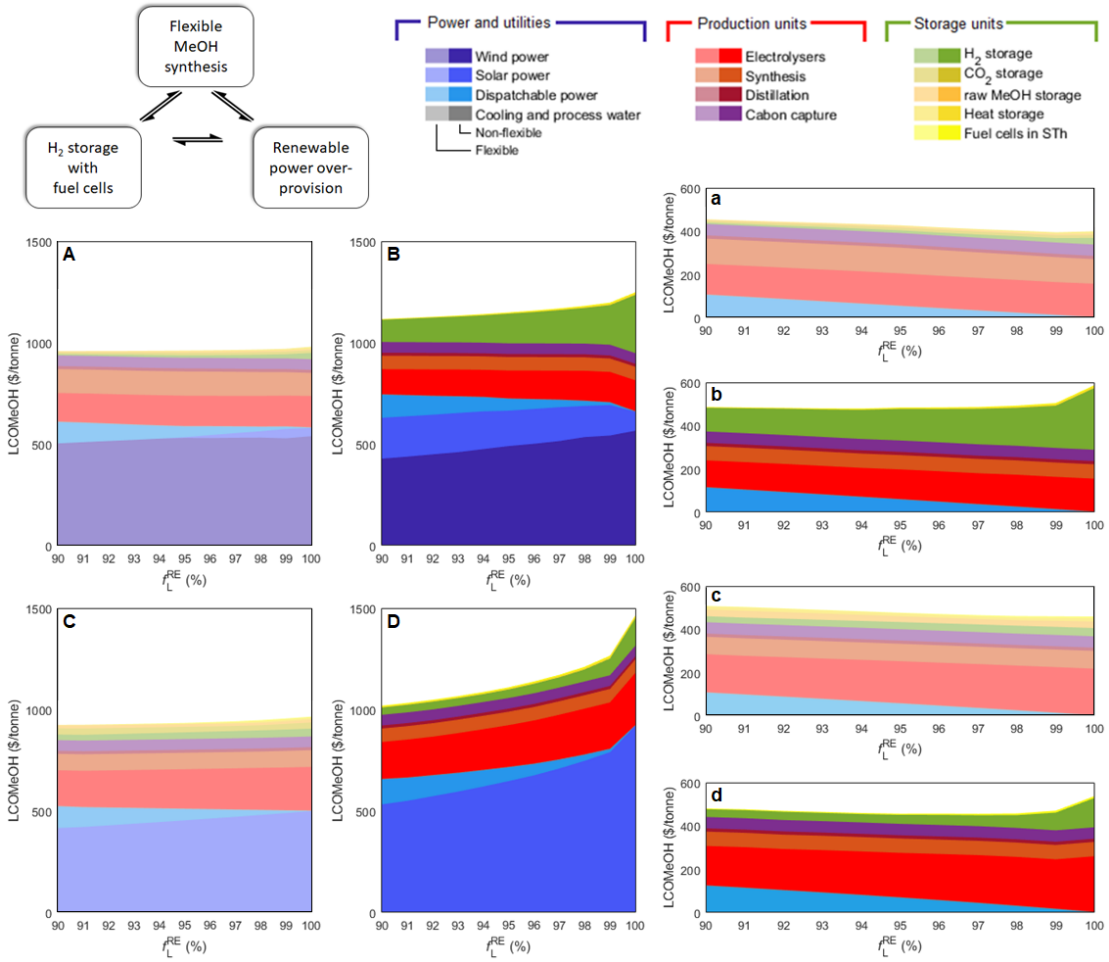


Figure 6.4. Cost of production at targeted renewable penetration. (A) Flexible process for Norderney; (B) non-flexible process for Norderney; (C) flexible process for Kramer Junction; (D) non-flexible process for Kramer Junction. Subsets (a)–(d) illustrate the enlarged cost elements by excluding renewable power costs, which respectively correspond to (A)–(D). The upper-left triangle schematic illustrates the interplay between three measures for mitigating the variable renewable power.

In Kramer Junction, the costs of hydrogen storage and fuel cells are insignificant (compared to Norderney), yet they play a more important role for this site. This is because more hydrogen is used as a fuel (as opposed to feedstock for MeOH synthesis) in this case, which is indicated by the fraction of load met by the energy from the hydrogen storage unit (see Figure C.9 in Appendix C). This is also attributed to the characteristics of the solar power in Kramer Junction, i.e. its diurnal variation leads to complete (renewable) power outage during the nights, thus requiring larger fuel cells to sustain a minimum production rate.

Another noteworthy feature in Figure 6.4 is the significant increase in the overall cost from $f_{\mathrm{L}}^{\mathrm{RE}} = 99$ to 100 % in the non-flexible processes, which is largely mitigated

in the flexible processes. This cost increase originates from two different sources for the two locations. In the case of Norderney, a significant increase in the cost originates from the hydrogen storage unit. Interestingly, the increase in hydrogen storage unit does not lead to an increased energy use from the fuel cells (see Figure C.9 in Appendix C). To further probe the mechanism of the cost increase, profiles of energy and materials dispatch are investigated. It can be seen that the average load of the whole production significantly reduces from 584 MW at $f_{\mathrm{L}}^{\mathrm{RE}} = 99\,\%$ to 536 MW at $f_{\mathrm{L}}^{\mathrm{RE}} = 100\,\%$ (see Figure C.10 in Appendix C), which is attributed to the increase of electrolyser efficiency. Due to the inverse correlation between electrolysers load and energy efficiency (see Eq. 6.1), a higher overall energy efficiency means a lower capacity factor. Significantly, the operation profiles of electrolysers show a full load hour equivalent of 3,283 at $f_{\mathrm{L}}^{\mathrm{RE}} = 99\,\%$ and 2,868 at $f_{\mathrm{L}}^{\mathrm{RE}} = 100\,\%$. Thus, the increase in hydrogen storage results from the change of the optimal power dispatch to electrolysers. Regarding Kramer Junction, the significant increase in overall cost from 99 to 100 % renewable operation is mainly attributed to the excess solar power generation, which is preferred due to the cheaper solar PV costs (thus facilitating the over-provision of solar power). As a result, the renewable power curtailment becomes significantly higher at $f_{\mathrm{L}}^{\mathrm{RE}} = 100\,\%$ (see Figure C.7 in Appendix C).

The above observation is consistent with the work of Budischak et al., who reported a significant increase in the storage units capacity when the load met by renewable energy is increased from 90 to 99.9 % (Budischak et al., 2013). This result may question the policymakers on the necessity of achieving a fully renewable energy supply, as a small fraction of dispatchable power would significantly reduce the storage requirement (and hence the reduction in overall cost). On the other hand, the results shown here suggest that introducing process flexibility can help to ease the tension between economics and environmental targets.

It is worth noting that for a non-flexible electrified chemical process, its optimised production cost is dictated by the optimised cost of energy, as the chemical process in such a case merely plays a role of a fixed demand and offers no room for optimisation. In power-to-MeOH, the design that leads to a minimum LEC would

also lead to a minimum LCOMeOH. In a system with process flexibility, however, the interplay between subsystems means that the value of LEC is unable to determine the optimality of the whole system. Concretely, the functionality of the units overlaps as the over-sized synthetic reactor improves the economics of energy utilisation, of which the additional cost is however outside the boundary of power generation (thus not reflected in LEC). Flexible production also entails a variable load, contrasting to the constant load for non-flexible production. The variable load and energy costs are plotted in Figures C.10 and C.11 in Appendix C, respectively.

Although previous reports have stressed the importance of complementary renewable mix in balancing demand and supply (e.g. the work of Fiaschi et al. (2012)), only Norderney has shown to have a fraction of the complementary source (i.e. solar source) in the optimal renewable power generation. Kramer Junction has shown no incorporation of the complementary source (i.e. wind source) in all operational scenarios. The sole renewable source in power generation for Kramer Junction can be ascribed to the low CF of the other source: the CF is 25.0 % for solar and 4.3 % for wind power in Kramer Junction (the value of CF is calculated based on the meteorological data and selected renewable technology, see Methods). In contrast, the CF is 29.4 % for wind and 12.1 % for solar power in Norderney. It is believed that if a location has multiple renewable sources of similar availability or variability (which results in a similar CF), a sophisticated renewable mix would be expected in its power generation.

6.3.4 Cost comparison and impact of technology prices

The range of the production cost is compared with previous studies. For example, Bos et al. (2020) reported a cost range of 750–800 €/tonne (or 887–946 $/tonne) for renewable MeOH produced from air captured CO_2, water and renewable electricity, which is comparable to the results of this work. Gonzalez-Garay et al. (2019) reported the production cost of renewable MeOH produced from a wide range of routes, including hydrogen from solar, wind, nuclear and biomass, and CO_2 from

coal, natural gas and air. Thus, a wide range of MeOH cost can be seen from their work, which is from 1,200 to 2,500 $/tonne.

Apart from the production routes, another issue commonly facing techno-economic analyses of renewable energy utilisation is uncertainty in the economic evaluation, as the renewable technology costs are fast changing. In particular, the total installed cost for solar energy has dropped dramatically over the last decade—faster than any previous prediction. As an example, Delucchi and Jacobson (2011) performed a detailed study in 2011 focusing on future renewable energy supply using a predicted CapEx for solar PV of 2,705 $/kW for 2030. In contrast, the International Renewable Energy Agency reported a global weighted average of 995 $/kW in 2019 (Gielen et al., 2020). Furthermore, technology costs vary significantly depending on the utility scale and manufacturing volume. Thus, in addition to the cost parameters adopted for the base case scenario, LCOMeOH has also been estimated based on conservative and progressive costs (tabulated respectively in Tables C.11 and C.12 in Appendix C). The results have shown an upper and lower bound of LCOMeOH for 100 % renewable operations, i.e. 1,496 and 787 $/tonne for Norderney and 1,852 and 777 $/tonne for Kramer Junction (see Table 6.2). Although the gap between the two bounds is large for both locations, the cost reduction from process flexibility is consistent and significant for all scenarios (i.e. conservative, progressive and base case scenario), ranging from 21 to 35 % in cost reduction.

Table 6.2. Optimal LCOMeOH for 100 % renewable operations based on conservative and progressive technology costs.

Location	Flexibility	LCOMeOH ($/tonne)	
		Conservative	Progressive
Norderney	Flexible	1,496.1	787.0
	Non-flexible	1,885.3	1,036.2
	Reduction due to flexibility (%)	20.6	24.0
Kramer Junction	Flexible	1,851.8	776.8
	Non-flexible	2,840.7	1,159.1
	Reduction due to flexibility (%)	34.8	32.8

6.4 Discussion

The results of this study show the clear potential of process flexibility in facilitating the integration of variable renewable energy (VRE) into a chemical process, by accommodating the variability of renewable sources with reduced reliance on expensive VRE over-provision and its subsequent storage. However, for a viable flexibility implementation there are two prerequisites derived from the interplay triangle shown in Figure 6.4: (1) the cost of the core flexible chemical process units, i.e. those that need to be over-sized to enable load adjustment, should not be a dominant element in the total production cost; and (2) the storage cost for intermediate products in the chemical process—incurred due to the need for handling flexibility disparity between process units—should be sufficiently lower than the energy storage system for VRE. Generally, the cap of the benefits from a flexible process can be calculated from the extent to which the above two prerequisites are met. In our case study, the cap is sufficiently large so that a flexible process would be economically justified for a wide range of operational scenarios. In particular, the MeOH synthesis process produces raw MeOH as an intermediate product, of which the storage cost is much cheaper than that of hydrogen for storing surplus VRE. This however may not be always true for other chemical processes and will depend on the nature of their process units and that of their intermediate products, although broadly speaking the storage costs of chemicals are likely to be lower than that of hydrogen given the particularly high cost of the latter with the currently available technology. Furthermore, it has been clearly shown in this work that the positive role of process flexibility becomes more significant with a large penetration of highly variable sources, which is an important factor to be considered when assessing its suitability in a particular local context.

While a flexible process allows space for optimising the energy and material dispatch potentially leading to a reduced overall cost, its implementation brings additional complications to energy integration—an energy-saving measure widely adopted in modern chemical processes. In the MeOH case study, this is reflected

by the need for introducing a heat storage subsystem between MeOH synthesis (heat source) and carbon capture (heat sink), to coordinate the heat recovery between the two subsystems which frequently operate at different load levels. In a chemical process that requires a more sophisticated heat exchanger network, heat storage mediated integration could become economically non-viable; the introduction of process flexibility would thus entail a significant opportunity cost of energy integration. In a sense, process flexibility is a competing factor to process integration; its implementation requires an analysis on a case-by-case basis. Nevertheless, if the range of cost reduction (20–35 %) brought by implementing process flexibility as demonstrated in this work can be attained, its potential gains would most likely exceed the opportunity cost of energy integration for many chemical processes. On the other hand, it is envisioned that the smart design of energy integration dedicated to flexible production may be a focus of future research. In this work, an MVR system has been implemented in the distillation process as an example of an energy integration strategy guided by two principles: (1) maximising the energy integration within a subsystem and (2) minimising the energy integration across different subsystems. Similar principles have previously been adopted in processes with sections subject to different production schedules (e.g. the work of Miah et al. (2014)) and may be further developed for flexible production to enable the integration of variable renewables.

The formulation of the optimisation simplifies the heat storage model by assuming all heat generated by the MeOH reactor will be stored and then consumed by the reboiler in the carbon capture subsystem. Thus, it is necessary to verify the validity of this formulation by checking the levelised heating cost (via the heat storage unit), which is found to be 19.7 and 15.8 \$/MWh for Norderney and Kramer Junction, respectively. These costs are sufficiently lower than the electrical heating, and thus the simplification in formulation does not affect the economics. On the other hand, if the levelised heating cost is expensive (e.g. above 100 \$/MWh), the formulation should be revised to allow heat curtailment.

In a case where process flexibility leads to a net economic gain, this gain is not merely shaped by the flexibility available in chemical production, but rather a

consequence of the holistic optimisation of the whole system that includes also electrolysis and H_2-based ESS. In this work, the modelling of electrolysis considered the variation of its efficiency with load (Beerbühl et al., 2015). While a simple assumption of a constant electrolyser efficiency is often adopted in the present literature (e.g. the work of Nayak-Luke et al. (2018)), the overall design of the power-to-MeOH system in this work is shown to be clearly benefited from the optimal trade-off between an improved energy use efficiency (which increases at lower load fractions) and an additional capital cost of electrolysers (arising from capacity over-sizing). This points to the importance of considering a load-dependent efficiency of electrolysers in future work on any system where electrolysis dominates the overall energy consumption. From a modelling point of view, the inclusion of a load-dependent efficiency would increase the complexity of the mathematical model. In this work, a linear efficiency-load function is adopted for electrolysis to reduce the complexity introduced (see Eq. 6.1). This still caused a bilinear term in one of the model equations (arising from the combination of Eqs. 6.10 and 6.15) and required a linearisation technique to retain the linearity of the optimisation model. Note that a more accurate efficiency-load function is more likely to be nonlinear and concave (Beerbühl et al., 2015), which would predict a higher energy efficiency compared with that modelled by a linear function, although the use of such a function will lead to a more complex mathematical model.

The sensitivity study in this work shows that, with a certain range, the level of process flexibility significantly affects the potential economic gain, which calls for rigorous assessment of the attainable load range of any chemical processes to be integrated with renewable energy. A similar study has been performed focusing on ammonia reactors (Cheema and Krewer, 2018); however, the operationality of MeOH reactors is yet to be investigated. Such studies will not only indicate an operation envelop of the flexible processes but also offer detailed analyses of the dynamic behaviour of the chemical production (Matthischke et al., 2018), which has not been considered in this work. Knowledge about the dynamic responses should be used to determine the ramping rate at which the load level of a process unit can vary, which may impose additional constraints that need to be considered in determining

the optimal allocation of "duties" between VRE storage and process flexibility for handling the variability of energy supply. More importantly, the dynamic behaviours help to identify the fluctuation in product specifications at the reactor outlet. Another future direction lies in the development of optimisation techniques for renewable chemical production. In the current work, the optimisation model can only deal with one particular flowsheet. The optimisation of a superstructure composed of different process designs is challenging at present. Such sophisticated optimisation tasks could be handled in the future by making the use of novel methods developed for energy optimisation (Geng et al., 2020) and production planning (Wang et al., 2021) in complex chemical systems.

6.5 Conclusions

Using MeOH production as an example for electrification and the use of renewable energy in the chemical industry, this work reveals the clear potential of incorporating load flexibility in the chemical processes to improve the economics of integrating variable renewable energy. The demonstrated benefits of process flexibility arise from reduced expensive energy (hydrogen) storage (when the renewable generation is expensive) and, in certain cases, improved energy utilisation due to the reduction of curtailment and energy conversion losses (when the renewable generation is cheap). The process flexibility-enabled design has been shown to be particularly beneficial when the renewable energy supply is highly variable and when the desired level of renewable penetration is high. The implementation of a flexible process requires over-sizing of the flexible process units. It also requires storage units for the intermediate products and for energy to be exchanged between different process units, to allow these units to operate at different load levels. In the MeOH case study, these additional "flexibility" costs are outweighed by the economic gains. This cost-benefit analysis needs to be evaluated on a case-by-case basis when applying the flexibility concept elsewhere, bearing in mind that the relatively small cost portion attributed to the flexible process unit (i.e. the synthesis reactor) and the moderate physical conditions for the additional storage units are among the key

factors leading to favourable economics in the MeOH example. Where these factors hold true, this work demonstrates that systematically optimised design that makes the best combination of energy storage and process flexibility may offer a viable route for future sustainable chemical production powered by renewables, which deserves attention from both industrial policymaking and engineering practices.

Chapter 7

Concluding Remarks

DECARBONISATION of the chemical industry heavily relies on renewable energy utilisation; however, challenges and barriers exist in many aspects, such as: how the renewable energies are delivered to the end-use sectors; how to overcome the variability and intermittency of the renewable energy sources; what should be the extent of renewable energy utilisation in the chemical industry; and what are the implications and impacts on future energy demand. This thesis investigated the above challenges in a hierarchical order, taking methanol (MeOH) production with a size of 400,000 tonnes per annum as a case study. First, electrification schemes were proposed for the MeOH production process, aiming to supplant fossil-based energy supply (direct electrification) and feedstock (indirect electrification). The energy analysis shows that the indirect scheme represents deep electrification and requires significant electricity demand, whereas the impact of the direct electrification through heat pump implementation is limited by the total heating requirement and the heat that can be delivered by a heat pump. Profound implications can be drawn from the impacts on future energy demand and structure since the direct electrification aims at the modifications of the existing chemical plants, contrasting to the indirect electrification scheme which requires new process designs. The indirect electrification scheme for MeOH production renders a carbon dioxide (CO_2) hydrogenation

process with CO_2 captured from a point source and hydrogen produced from water electrolysis.

Based on the CO_2 hydrogenation process, which presents a fully electrified MeOH process, renewable energy systems were designed to fulfil its load requirement. Aiming at the economic optimality, the size of electrolysers and hydrogen storage, the ratio of wind and solar source in renewable power generation, and the dispatch of energy and materials were optimised using meteorological data from Norderney (Germany) and Kramer Junction (USA). The two locations were selected due to their world-class wind and solar energy source, respectively. Although the locations only have one favourable renewable source, the other source was also considered in the optimisation throughout the analysis, aiming to evaluate the impact of renewable source complementarity. In addition, the impact of renewable source variability on energy storage needs was investigated, proving that it is more challenging to balance the energy supply and demand when a more variable source is incorporated. The correlation between the energy storage size and the dispatchable energy requirement shows a highly concave trend, meaning that the importance of energy storage decreases with a further extension of storage size. Similarly, the correlation between dispatchable energy price and renewable energy penetration also exhibits a two-regime behaviour. The same optimisation methods and renewable energy systems were adopted to explore curtailed renewable power, which results from the optimal design. The novel analysis provides a basis for the economic evaluation of the voluntary curtailment, which in turn reflects the cost of power intermittency. The results show a significant reduction in levelised energy cost when the curtailed renewable power is used for the second MeOH process. However, only an insignificant portion of the curtailed power can be economically utilised, meaning that the improvement on the current levelised MeOH cost is compromised after taking economies of scale into account.

The final piece of work within this thesis explored the benefits brought about by introducing process flexibility to the same electrified MeOH process. The flexible synthesis subsystem allows the load demand to adjust and coincide with the variability of renewable energy sources, thus bridging the gap between demand-side

management and chemical production. The added complexity requires careful management to align the feedstock supply, which is addressed by using material and energy (heat) storage. The economic evaluation shows that the process flexibility can reduce the levelised MeOH cost by approximately 21 and 34 % for the production located in Norderney and Kramer Junction, respectively. Detailed analysis of the optimal energy and material dispatch reveals the underlying reasons for the beneficial flexible operation, of which the economic improvement is attributed to the savings from hydrogen storage or renewable generation—depending on the cost structure before introducing a flexible process. Although process flexibility is highly desirable to the case study MeOH process, prerequisites were identified for its economic implementation. Moreover, it is found that a flexible process would be a trade-off to process heat integration; thus, its overall benefit has to be evaluated on a case-by-case basis. Considering the continuous advances in technology development and decreasing cost for renewable power generation, both conservative and progressive economic parameters were used. Although the two scenarios generate significantly different economic performance, the cost reduction results from process flexibility is consistent.

The main contributions of the work presented in this thesis are twofold: (1) it demonstrates and compares different electrification schemes, which suggest the future electricity demand; (2) renewable energy systems were designed and optimised for such an electrified chemical process, with insights into the process interplay. The findings in both areas promote each other and facilitate future work on renewable chemical production. The utilisation of curtailed renewable power opens up a new way of thinking to evaluate the cost of intermittency. In the past, it was difficult to incorporate demand-side management into chemical production powered by renewable energy sources due to the rigorous end-use load. The novel concept of process flexibility bridges the gap by enabling the load variation of chemical synthesis, which also addresses many challenges at the subsystem level such as cross-system heat integration, design of mechanical vapour recompression system, and intermediate product storage. These studies provide insights for both policymakers and engineering decision-makers.

The limitations of this project are: (1) the electrification and renewable energy systems were designed only for MeOH processes; (2) only two locations were investigated as a case study; (3) meteorological data for only one year were used; (4) a specific energy integration strategy was adopted for the flexible MeOH process; and (5) the dynamic behaviour of the flexible process was not considered. Although the justifications for focusing on MeOH processes have been provided, there are many equally important chemicals worth detailed analysis of their electrification schemes and the subsequent renewable energy systems. The investigation on the other chemical processes helps to generate a holistic view of the renewable chemical industry. Similarly, the analysis using the meteorological data from Norderney and Kramer Junction should expand to other global sites, taking the local context into account. In future work, the same analysis should be performed focusing on other platform chemicals and taking the global context into account. Regarding the flexible MeOH process, there are many designs available for both single and cross-subsystem energy integration. Although the one chosen here is reasonable, different layouts should be analysed in future work to explore the impact of heat integration on the implementation of process flexibility. More importantly, the dynamic behaviour of the flexible MeOH process should be explored, which may provide important insights into the variation of product specification and its potential impact on the production.

Appendix A

Operation unit design

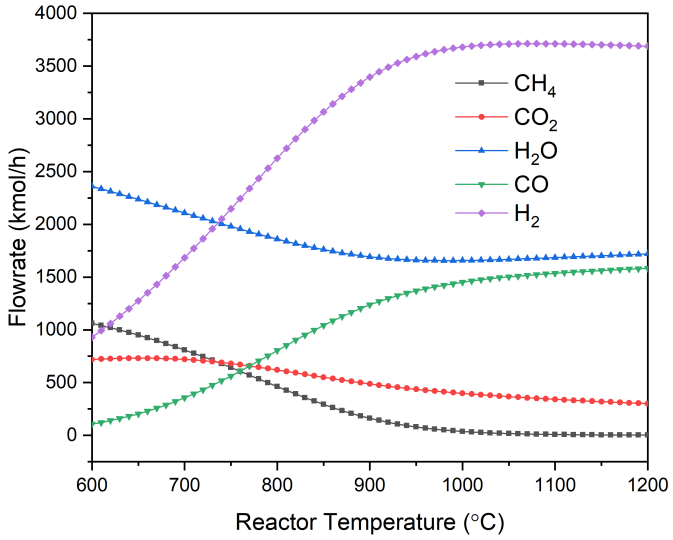


Figure A.1. Flowrate of all species in the produced syngas with respect to reactor temperature (R1 in Figure 3.2).

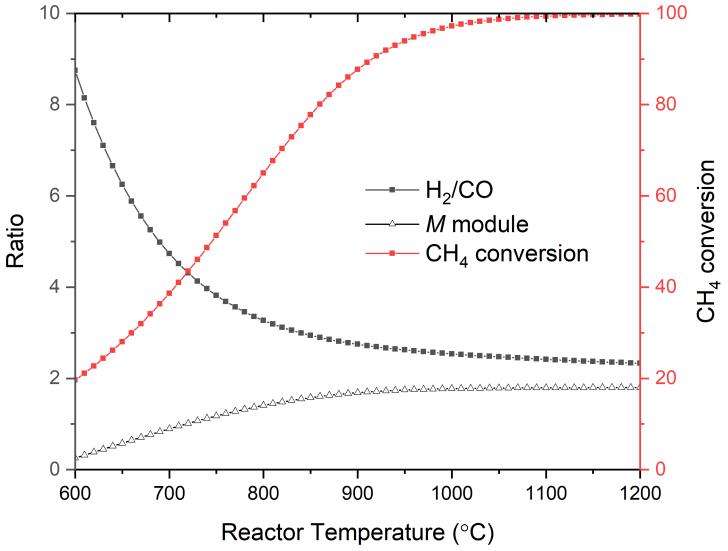


Figure A.2. Profiles of H_2/CO, M module and CH_4 conversion with respect to reactor temperature (R1 in Figure 3.2).

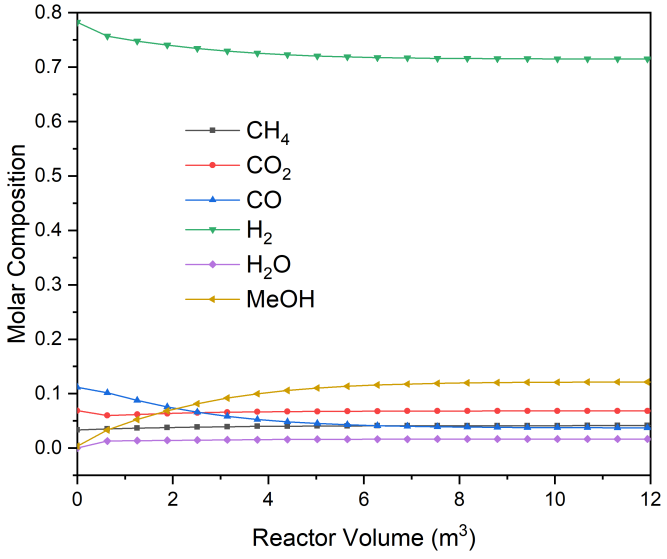


Figure A.3. Molar composition of species in the MeOH reactor (R2 in Figure 3.2).

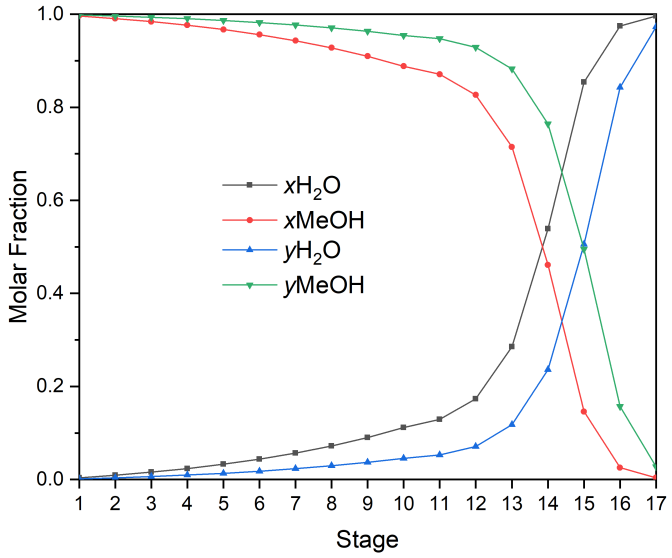


Figure A.4. Fraction distribution of MeOH and water in both liquid (x) and vapour phase (y) at each corresponding distillation stage (DT in Figure 3.2). Sharp liquid-vapour separation upstream is assumed.

Process simulation results

Table A.1. Summary of the utility use in the reference MeOH plant (Figure 3.2) before heat integration.

	Unit name	Inlet stream		Outlet stream		Duty (kW)	Utility
		P (bar)	T (°C)	P (bar)	T (°C)		
R1	Reformer	20.0	949.8	20.0	950.0	79,114.1	Fired heat
R2	MeOH Reactor	71.0	255.0	70.0	255.0	−41,333.4	Cooling water
HX1	Heater	20.0	301.5	20.0	950.0	21,466.4	Fired heat
HX2	Heater	19.5	28.0	20.0	950.0	58,800.4	Fired heat
HX3	Cooler	20.0	950.0	19.5	30.0	−82,072.6	Cooling water
HX4	Heater	71.0	203.3	71.0	255.0	2,443.7	VHP steam
HX5	Cooler	70.0	255.0	70.0	40.0	−46,535.2	Cooling water
HX6	Heater	70.0	40.0	71.0	255.0	19,837.2	VHP steam
HX7	Heater	70.0	40.0	71.0	255.0	1,050.7	VHP steam
HX8	Cooler	1.1	66.7	1.0	40.0	−1,181.1	Cooling water
HX9	Cooler	1.1	101.7	1.0	40.0	−287.3	Cooling water
DT1	Condenser	1.1	66.8	1.1	66.7	−29,571.1	Cooling water
DT1	Reboiler	1.1	98.2	1.1	101.7	31,906.8	LP steam
CP1	Compressor	2.0	40.0	20.0	282.0	3,772.1	Electricity
CP2	Compressor	1.0	30.0	20.0	350.3	2,157.7	Electricity
CP3	Pump	1.0	25.0	20.0	25.2	13.1	Electricity
CP4	Compressor	19.5	30.0	71.0	203.3	8,032.5	Electricity

Table A.2. Summary of the utility use in the CO_2 hydrogenation plant (Figure 3.3) before heat integration.

	Unit name	Inlet stream		Outlet stream		Duty (kW)	Utility
		P (bar)	T (℃)	P (bar)	T (℃)		
R1	MeOH Reactor	71.0	255.0	70.0	255.0	−26,011.9	Cooling water
HX1	Heater	71.0	196.2	71.0	255.0	3,990.1	VHP steam
HX2	Cooler	70.0	255.0	70.0	40.0	−94,737.8	Cooling water
HX3	Heater	70.0	40.0	71.0	255.0	4,349.4	VHP steam
HX4	Heater	70.0	40.0	71.0	255.0	43,824.7	VHP steam
HX5	Cooler	1.1	66.7	1.0	40.0	−1,209.5	Cooling water
HX6	Cooler	1.1	100.0	1.0	40.0	−2,143.2	Cooling water
DT1	Condenser	1.1	66.8	1.1	66.7	−29,110.7	Cooling water
DT1	Reboiler	1.1	93.5	1.1	100.0	33,423.3	LP steam
CP1	Cooler-1	3.1	132.7	3.1	35.0	−2,004.4	Cooling water
CP1	Cooler-2	8.8	138.7	8.8	35.0	−2,134.1	Cooling water
CP1	Cooler-3	25.0	138.7	25.0	35.0	−2,134.1	Cooling water
CP2	Cooler-1	4.1	232.1	4.1	35.0	−7,763.4	Cooling water
CP2	Cooler-2	17.1	248.8	17.1	35.0	−8,422.8	Cooling water
CP1	Multi-compressor	1.1	30.0	71.0	138.7	8,503.5	Electricity
CP2	Multi-compressor	1.0	25.0	71.0	248.8	24,997.8	Electricity
CP3	Compressor	70.0	40.0	71.0	41.7	8.9	Electricity

Table A.3. Summary of the utility use in the carbon capture process (Figure 3.1) with regard to the reference plant.

	Unit name	Inlet stream		Outlet stream		Duty (kW)	Utility
		P (bar)	T (℃)	P (bar)	T (℃)		
HX1	Cooler	2.0	59.1	2.0	40.0	−19,185.8	Cooling water
DES	Condenser	2.0	108.8	2.0	40.0	−15,523.6	Cooling water
DES	Condenser	2.0	40.0	2.0	18.0	171.0	Electricity
DES	Reboiler	2.0	119.3	2.0	119.3	35,825.8	LP steam
CP1	Pump	1.0	48.6	2.0	48.6	1.1	Electricity
CP2	Pump	1.0	53.3	2.9	53.1	177.0	Electricity

Table A.4. Summary of the utility use in the carbon capture process (Figure 3.1) with regard to the CO_2 hydrogenation plant.

	Unit name	Inlet stream		Outlet stream		Duty (kW)	Utility
		P (bar)	T (℃)	P (bar)	T (℃)		
HX1	Cooler	2.0	59.1	2.0	40.0	−62,716.7	Cooling water
DES	Condenser	2.0	108.8	2.0	40.0	−50,745.2	Cooling water
DES	Condenser	2.0	40.0	2.0	18.0	558.9	Electricity
DES	Reboiler	2.0	119.3	2.0	119.3	117,111.3	LP steam
CP1	Pump	1.0	48.6	2.0	48.6	3.5	Electricity
CP2	Pump	1.0	53.3	2.9	53.1	578.5	Electricity

Economic and environmental parameters

Table A.5. CO_2 emission for different utilities. Data obtained from US Energy Information Administration (2016).

Utility	Source	CO_2 emission (kg/kWh)
Heating	Natural gas combustion	0.18
Electricity	Pulverised coal plant	0.86
Electricity	RES	0

Table A.6. Price for utilities and their corresponding supply temperature.

Utility	Cost factor	Cost ($/MWh)	T (°C)	Source
Cooling water	1.0	0.85	25	AEA
LP steam	9.0	7.61	125	AEA
MP steam	10.4	8.79	175	AEA
HP steam	11.8	9.98	250	AEA
VHP steam	16.5	13.95	400	AEA
Fired heat	20.0	16.91	1,000	AEA
Electricity	74.5	63.00	–	Zhang et al. (2017)

Table A.7. Raw material and product price. All costs are converted to US dollar based on 1€ = 1.14 $.

	Price	Unit	Source
Methanol	456	$/tonne	Perez-Fortes et al. (2016)
Monoethanolamine	2.09	$/kg	Ramezan et al. (2007)
Process water	0.02	$/tonne	Cañete et al. (2017)
Natural gas	4.09	$/MMBtu	Cañete et al. (2017)
Flue gas	0	–	Perez-Fortes et al. (2016)

Table A.8. Total fixed capital cost estimation for each plant. Note that the electrolysers cost for the CO_2 hydrogenation plant is listed separately.

Items	Ratio factor	Reference plant (M$)	CO_2 hydrogenation plant (M$)
Purchased equipment cost	1.00	60.65	108.77
Installation cost	0.47	28.50	51.12
Instrumentation and controls	0.36	21.83	39.16
Piping	0.68	41.25	73.96
Electrical systems	0.11	6.67	11.96
Building and services	0.18	10.92	19.57
Yard improvements	0.10	6.06	10.88
Service facilities	0.70	42.45	76.13
Total direct cost		218.33	391.54
Engineering and supervision	0.33	20.02	35.89
Construction expenses	0.41	24.86	44.60
Legal expenses	0.04	2.43	4.35
Contractor's fee	0.22	13.34	23.93
Contingency	0.44	26.69	47.86
Total indirect cost		87.34	156.61
TFCC		305.6	548.1

Appendix B

Energy structure of the fully electrified MeOH plant

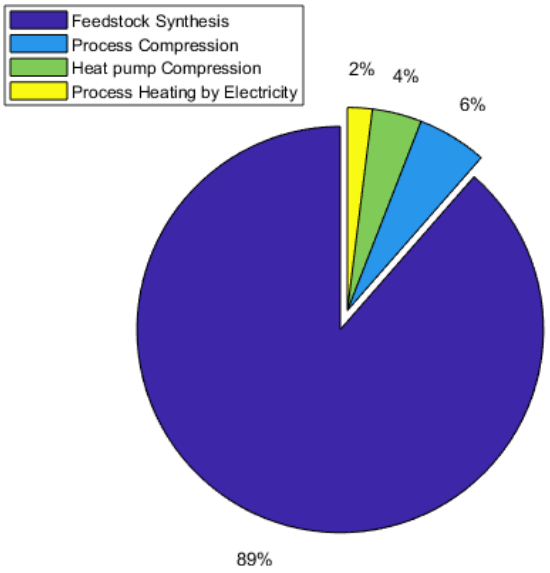


Figure B.1. Energy composition for the fully electrified MeOH production. Data obtained from Chapter 3.

Storage profiles

The profiles of unconstrained $L(t)$ at varied f_{W} and γ are plotted in Figures B.2 and B.3, respectively. The unconstrained $L(t)$ represents the storage of VRE without a cap, and it also indicates the potential amount of VRE available for storage, which is highly dependent on γ. The change in renewable mix has little impact on the unconstrained $L(t)$ profiles.

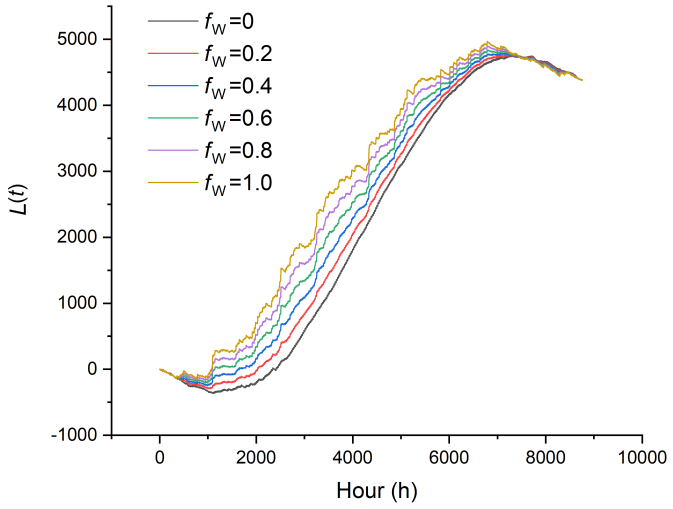


Figure B.2. Time series of unconstrained storage profiles at different fractions of wind energy for $\gamma = 1.5$. The round-trip efficiency of energy storage is assumed to be 100 %.

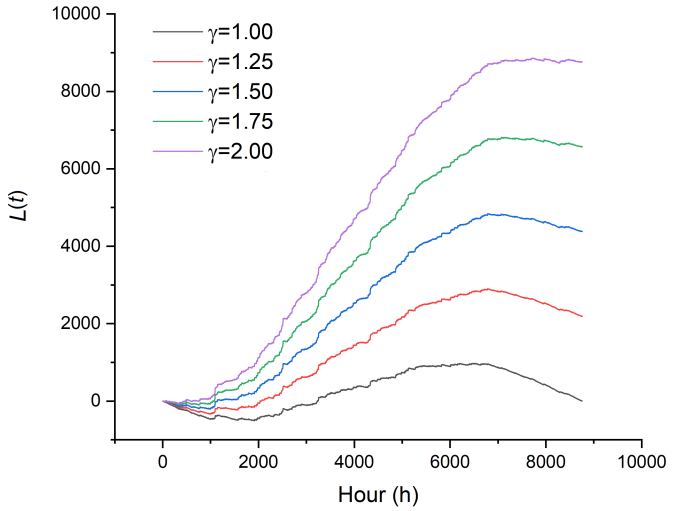


Figure B.3. Time series of unconstrained storage profiles at different γ for $f_{\mathrm{W}} = 0.6$. The round-trip efficiency of energy storage is assumed to be 100 %.

The impact of γ on L^{cap} is significant and its influence has shown strong dependence. In the particular case demonstrated in Figure B.4, when γ is doubled from 1.0 to 2.0, L^{cap} is reduced from approximately 1,400 to 200. It is noticeable that a steady-state operation of VRE storage with decreasing conversion efficiency (η_{ch} and η_{dis}) requires higher values of γ. For instance, when $\gamma = 1.0$ all of the positive $P_\delta(t)$ has to be stored and then used in chemical production. If the conversion efficiency is less than 100 % (i.e. loss of positive P_δ), the storage profile will diverge, thus leading to an infinite L^{cap}. A plot of diverging $L(t)$ over a 4-year operation using repeated VRE data with decreasing conversion efficiencies is shown in Figure B.5.

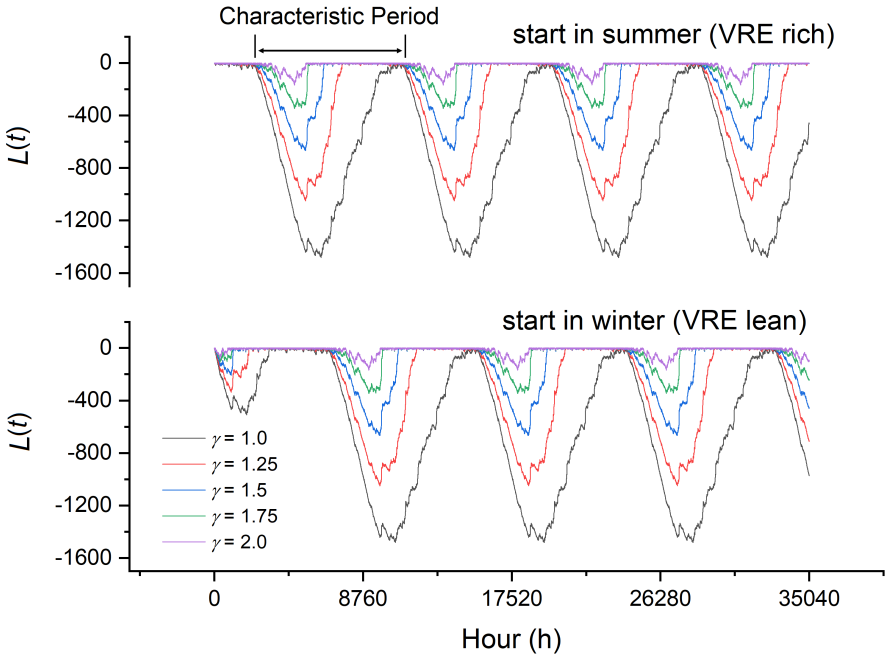


Figure B.4. Representative storage profiles for Kramer Junction for a period of 4 years with varied γ. Wind fraction is fixed at $f_{\text{W}} = 0.6$. (Top) Operation starts in summer when VRE is rich; (Bottom) operation starts in winter when VRE is lean. The unit of $L(t)$ is given in hourly energy consumption normalised by hourly load (MWh). Conversion efficiency is assumed to be 100 % in both charging and discharging mode.

To permit a fully renewable operation, a minimum value of γ is required. The value of $\gamma_{\min}$ is typically a function of storage efficiency and variability of the renewable sources. If the value of γ fails to meet the constraint, a L^{cap} that permits the fully renewable operation would not exist. As an illustration, $L(t)$ profile at a fixed γ with decreasing efficiency is plotted in Figure B.5 over a 4-year period using repeated VRE data. Note that when the efficiency is below 0.8, the operation becomes unsustainable, i.e. the storage profile diverges.

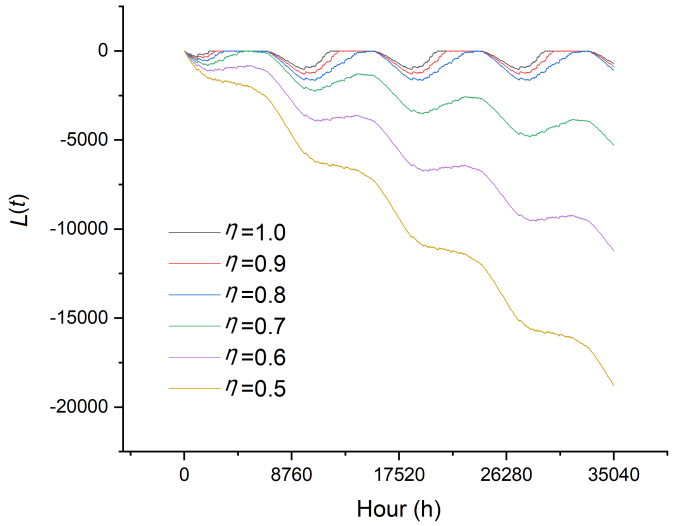


Figure B.5. Storage profiles with decreasing efficiencies. Excess generation is fixed at $\gamma = 1.25$ and the wind fraction is fixed at $f_{\text{W}} = 0.6$. It is assumed that $\eta_{\text{ch}} = \eta_{\text{dis}} = \eta$.

Operation policy and calculation

In the case of a partially renewable operation (due to the use of dispatchable power), $L(t)$ profile is calculated by time series of revised power mismatch, $P_\delta^{\mathrm{re}}(t)$. Due to the fact that the time series of $L(t)$ and $P_\delta^{\mathrm{re}}(t)$ rely on each other, the calculation is shown using an algorithm, as listed below:

Algorithm 1 Calculation for $L(t)$ and $P_\delta^{\mathrm{re}}(t)$ profiles.

for each $L^{\mathrm{dv}} \in [0, L^{\mathrm{cap}}]$ **do**
  for $t \in [1, T]$ **do**
    if $P_\delta(t) \geqslant 0$ **then**
      $P_\delta^{\mathrm{re}}(t) = P_\delta(t)$
    else
      if $P_\delta(t) + L(t) \geqslant 0$ **then**
        $P_\delta^{\mathrm{re}}(t) = 0$
      else
        $P_\delta^{\mathrm{re}}(t) = P_\delta(t) + L(t)$
      end if
    end if
    if $P_\delta^{\mathrm{re}}(t) \geqslant 0$ **then**
      $L(t+1) = \eta_{\mathrm{ch}} P_\delta^{\mathrm{re}}(t) + \{L(t) - [P_\delta^{\mathrm{re}}(t) - P_\delta(t)]\}$
    else if $-f_{\mathrm{ELY}}^{\mathrm{SYN}} \leqslant P_\delta^{\mathrm{re}}(t) < 0$ **then**
      $L(t+1) = P_\delta^{\mathrm{re}}(t) + \{L(t) - [P_\delta^{\mathrm{re}}(t) - P_\delta(t)]\}$
    else
      $L(t+1) = \{L(t) - [P_\delta^{\mathrm{re}}(t) - P_\delta(t)]\} - f_{\mathrm{ELY}}^{\mathrm{SYN}} + \frac{1}{\eta_{\mathrm{dis}}}[P_\delta^{\mathrm{re}}(t) + f_{\mathrm{ELY}}^{\mathrm{SYN}}]$
    end if
    if $L(t+1) \geqslant L^{\mathrm{dv}}$ **then**
      $L(t+1) = L^{\mathrm{dv}}$
    end if
    if $L(t+1) < 0$ **then**
      $L(t+1) = 0$
    end if
  end for
end for

The calculation of $L(t)$ for different operation scenarios is summarised in a flow chart in Figure B.6. The power scheduling is visualised in Figure B.7.

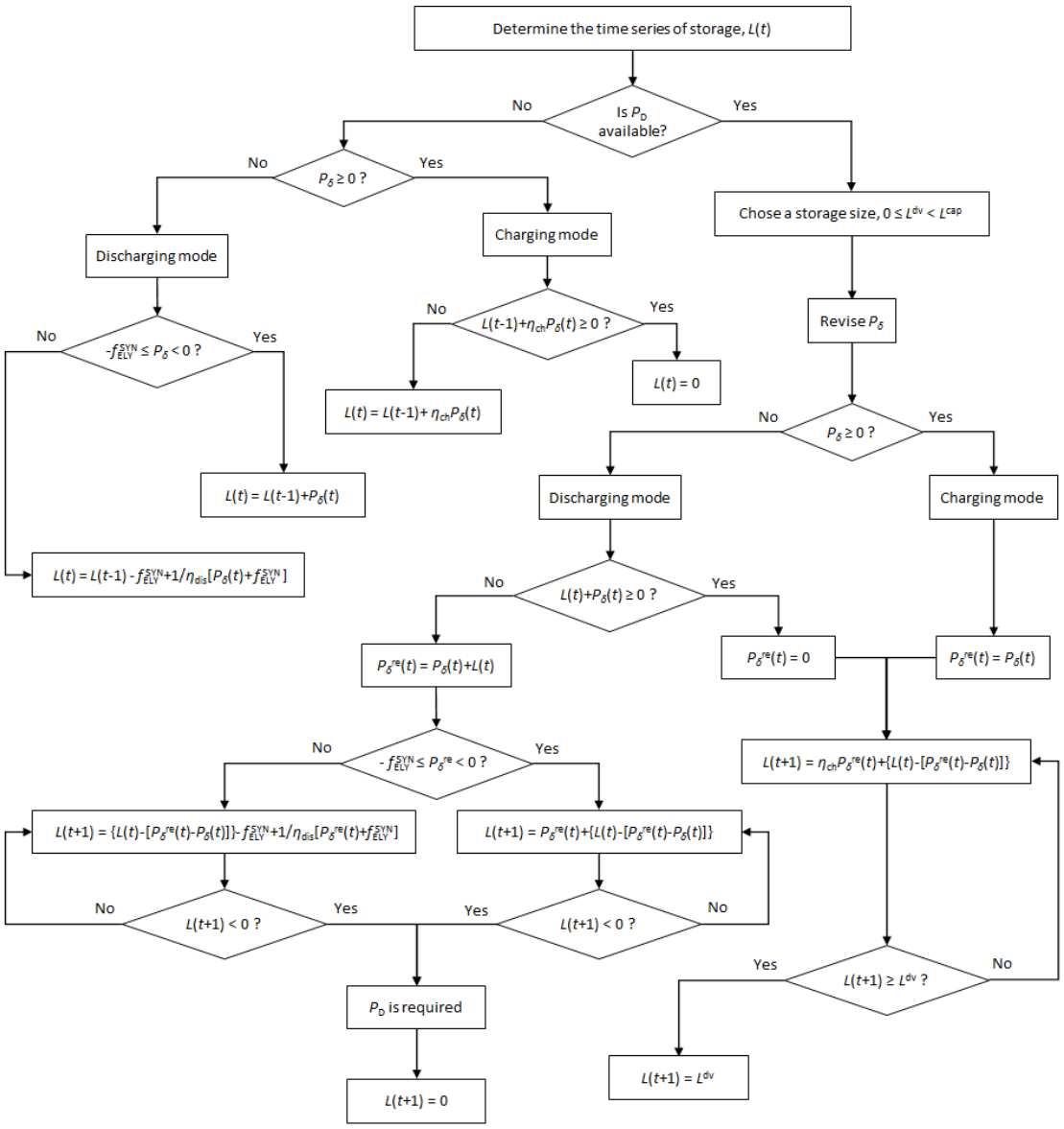


Figure B.6. Flow chart of how to determine $L(t)$.

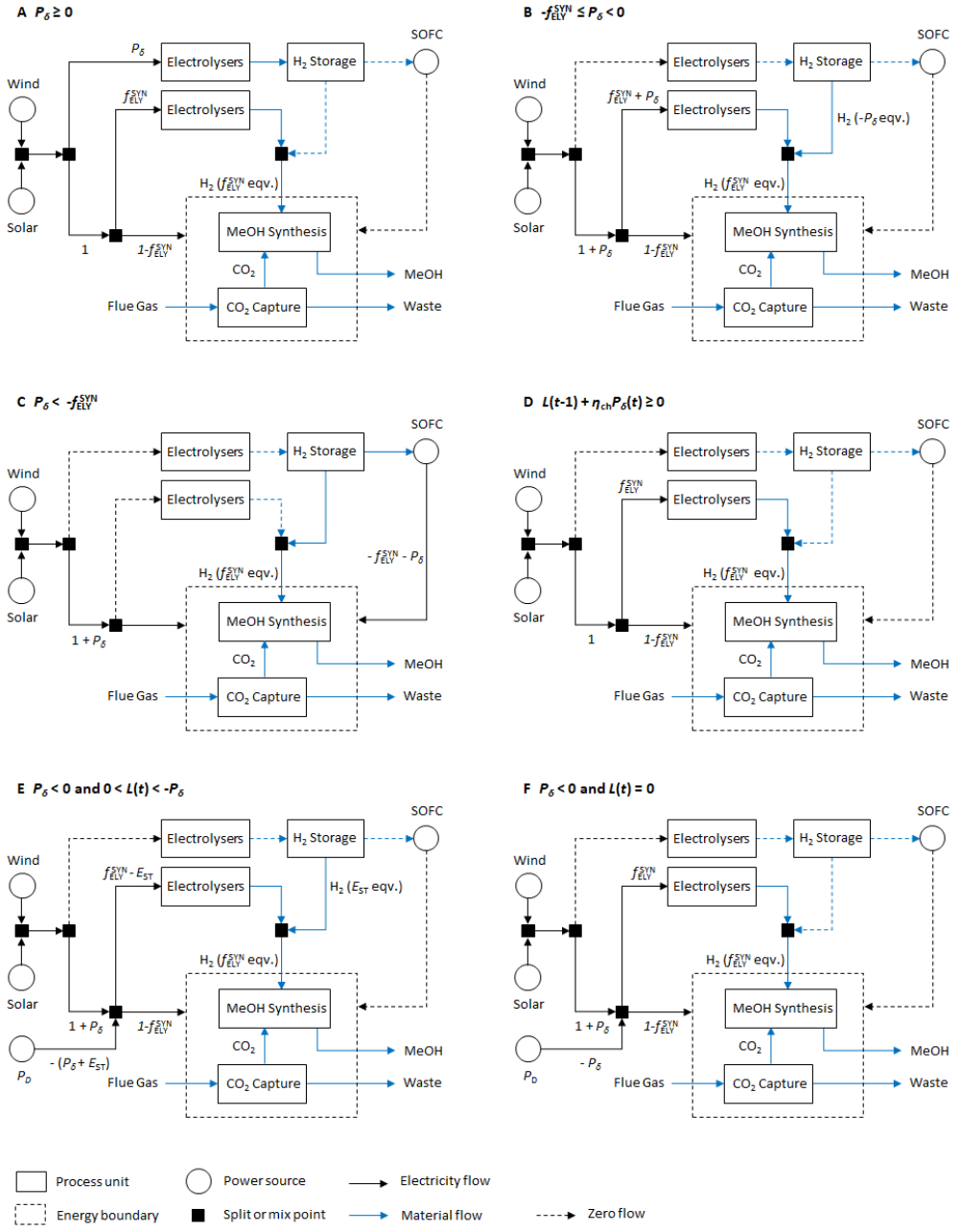


Figure B.7. Scheduling of power for the fully electrified MeOH production with a load of 1 MW. When VRE and ESS combined output is sufficient: (A) charging mode; (B) discharging mode when the deficit is small, i.e. H_2 fuel cells are not in operation; (C) discharging mode when the deficit is large, i.e. H_2 fuel cells are in operation; (D) VRE curtailment due to full storage. When VRE and ESS are insufficient: (E) balancing required from dispatchable power when storage is not empty (but insufficient at the particular time interval); (F) balancing required from dispatchable power when storage is empty. A dashed arrow indicates zero flow. Note that the power flow is converted to energy flow by $P \times 1$ hour.

Parameters for economic analysis

Table B.1. Total fixed captial cost estimation for the MeOH plant. Purchased equipment cost obtained from Chapter 3. Ratio factor obtained from Zhang et al. (2017).

Items	Ratio factor	Cost (M$)
Purchased equipment cost	1.00	108.4
Installation cost	0.47	51.0
Instrumentation and controls	0.36	39.0
Piping	0.68	73.7
Electrical systems	0.11	11.9
Building and services	0.18	19.5
Yard improvements	0.10	10.8
Service facilities	0.70	75.9
Total direct cost		390.3
Engineering and supervision	0.33	35.8
Construction expenses	0.41	44.5
Legal expenses	0.04	4.3
Contractor's fee	0.22	23.9
Contingency	0.44	47.7
Total indirect cost		156.1
TFCC		546.4

Table B.2. Raw material and process utility price for the analysis in Chapter 4. All costs are converted to US $ based on 1€ = 1.14 $.

	Price	Unit	Source
Process water	0.02	$/tonne	Cañete et al. (2017)
Flue gas	0	–	Perez-Fortes et al. (2016)
Cooling water	0.85	$/MWh	AEA
Electricity	LEC	$/MWh	NLP solver

Table B.3. Fixed annualised cost of electrolysers for MeOH synthesis ($C_{\mathrm{ELY}}^{\mathrm{SYN}}$), cooling water ($C_{\mathrm{cw}}$) and process water ($C_{\mathrm{pw}}$).

	Size/quantity	Unit	Annualised cost ($)
Electrolysers for MeOH synthesis	545,702	kW	29,084,000
Cooling water	617,800	MWh	505,400
Process water	513,328	tonne	11,650

Table B.4. Renewable technology costs for the analysis in Chapter 4. The original costs from Delucchi and Jacobson (2011) are available for the year of 2008 and 2030; thus, the costs cited are interpolated to 2019.

	CapEx $/kW	CapEx $/tonne	OpEx $/kW	Life Years	Source
Inland wind	1,533	–	30.3	30	Delucchi and Jacobson (2011)
Solar PV	4,372	–	11.7	30	Delucchi and Jacobson (2011)
H_2 storage	–	751,700[a]	–	30	Steward (2009)
SOFC	170	–	–	30	Scataglini et al. (2015)
Electrolyser	600[b]	–	–	30	Saba et al. (2018)

[a] CapEx of H_2 storage includes steel tanks and compressors.
[b] This is estimated based on alkaline electrolysers at 1 atm.

Table B.5. Parameters for 0 % variance in the sensitivity test for Chapter 4.

Parameter	Value	Unit	Source
c_D (dispatchable energy)	230	$/MWh	Eurostat, 2017a
CF (solar)	21.0	%	Delucchi and Jacobson (2011)
CF (wind)	29.4	%	Calculated
CapEx (solar)	4,372	$/kW	Delucchi and Jacobson (2011)
CapEx (wind)	1,533	$/kW	Delucchi and Jacobson (2011)
OpEx (solar)	11.7	$/kW	Delucchi and Jacobson (2011)
OpEx (wind)	30.3	$/kW	Delucchi and Jacobson (2011)
H_2 storage	751,700	$/tonne	Steward (2009)

Renewable data

To estimate the wind power, the wind velocity is first converted to the hub height using Eq. B.1:

$$U_1 = U_2 \left(\frac{\ln \frac{H_1}{z}}{\ln \frac{H_2}{z}} \right) \tag{B.1}$$

where U_1 and U_2 represent the velocity at a height of $H_1 = 80$ and $H_2 = 10\,\mathrm{m}$, respectively, and z represents the open ground roughness level (taken as $0.03\,\mathrm{m}$). The hub height velocity is then input to a power profile (see Figure B.8) to obtain the wind power. The cut-in and cut-out speeds are set as 4 and $25\,\mathrm{m/s}$, respectively (Vestas Wind Systems, 2004).

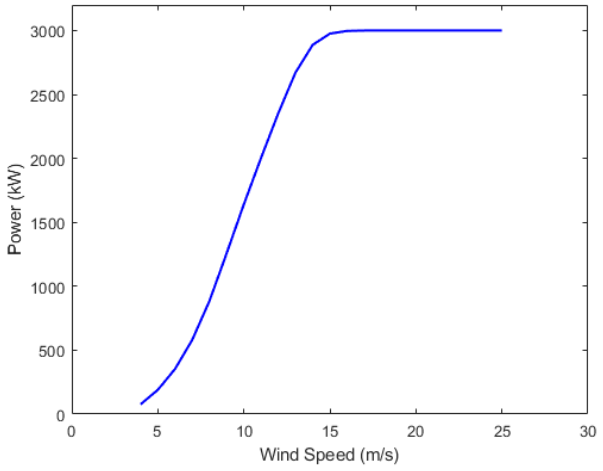


Figure B.8. Power curve for V90 3.0 MW turbine. Air density is assumed to be $1.225\,\mathrm{kg/m^3}$. Data obtained from Vestas Wind Systems (2004).

Table B.6. Standard deviation (σ) of year-round wind and solar power in Kramer Junction and Norderney.

Kramer Junction		Norderney	
Wind	Solar	Wind	Solar
2.09	1.39	1.07	1.59

Auxiliary results for Chapter 4

The intersecting profiles of Figure 4.3A and B at fixed excess generation ($\gamma = 1.5$) is plotted in Figure B.9. Clearly, Kramer Junction requires much more dispatchable energy in nearly full range of wind fraction (except for 0–10 %). This is consistent with the plot of σ for the energy mismatch (Figure B.10).

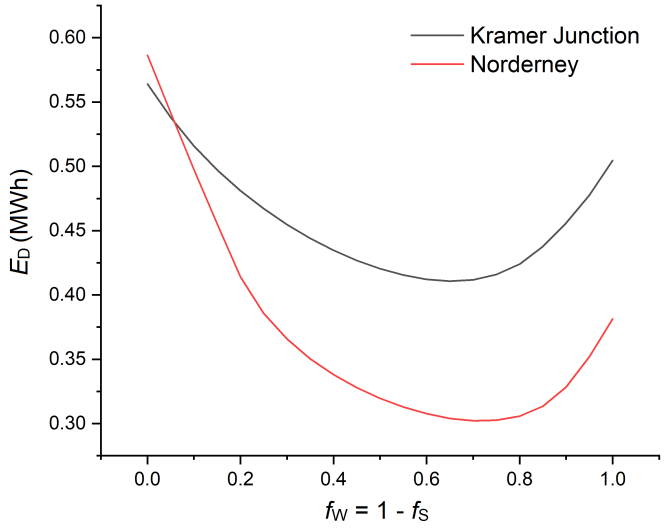


Figure B.9. Total dispatchable energy requirement E_D for both locations at varied wind fraction in power generation. γ is fixed at 1.5. The unit of E_D is given in yearly load requirement (MWh).

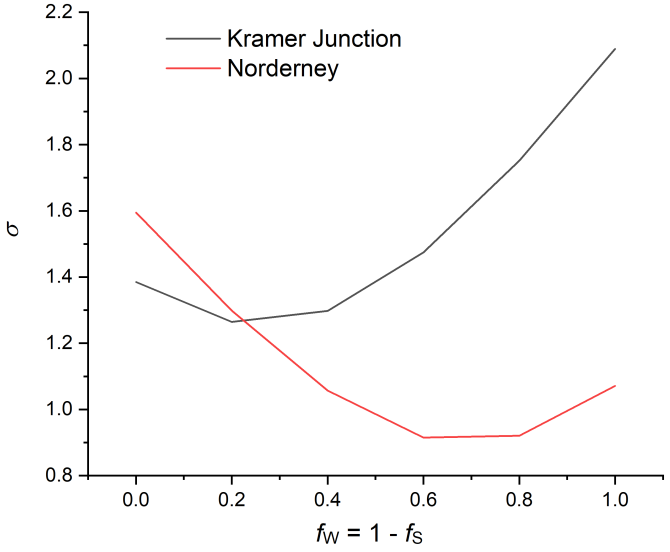


Figure B.10. Standard deviation of year-round energy mismatch as a function of wind fraction in energy generation. Excess generation is fixed at $\gamma = 1.0$.

To prove that the two-regime behaviour of E_{D} is ascribed to the solar power, E_{D} is plotted in Figure B.11 at two extremes of renewable mix, i.e. f_{W} at 99 and 1 %. Clearly, for solar power intraday storage is vital, and thus it exhibits a sharp change at a storage size equivalent to 18 hours of production. Regarding wind power, the two-regime behaviour is not very clear because intraday and seasonal storage become equally important.

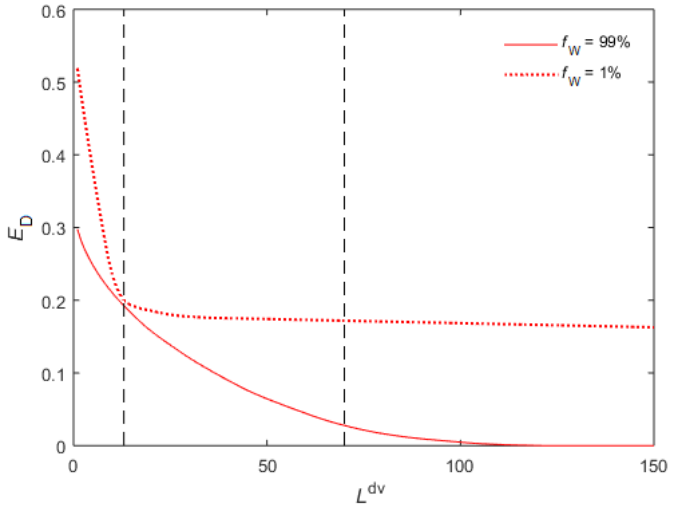


Figure B.11. Dispatchable energy requirement E_{D} as a function of L^{dv} for Norderney at $f_{\mathrm{W}} = 99\,\%$ and $f_{\mathrm{W}} = 1\,\%$. γ is fixed at 2.00. The vertical lines roughly indicate the tipping point of the two-regime behaviour.

A sample of the energy structure of load (for the most economical scenarios) is illustrated in Figure B.12 over a period of 1 week. From Figure B.12A, it can be seen that a large amount of dispatchable energy is required periodically for Kramer Junction. This is ascribed to the diurnal pattern of solar power (in the most economical scenario solar source is the only renewable source in the power generation). In the case of no dispatchable power backup, E_{D} is replaced by E_{ST} and the size of the storage is increased to meet the requirement. Figure B.12C does not show any dispatchable energy in the selected operation period because dispatchable energy is rarely used in Norderney (E_{D} only accounts for 7 % of the total load).

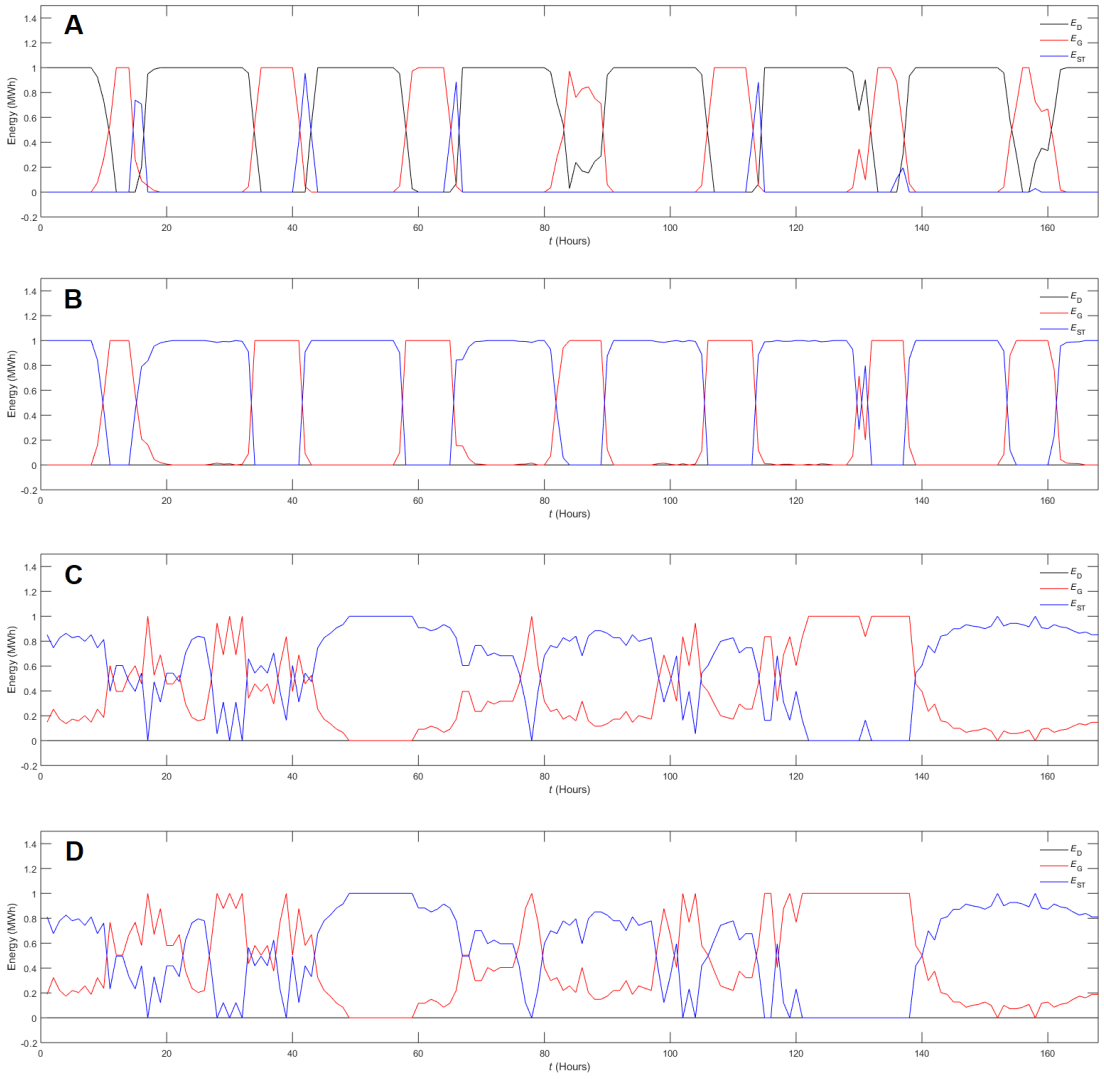


Figure B.12. A sample of load met by E_{D}, E_{G} and E_{ST} plotted in the most economical scenario for a period of 1 week. (A) Operation with dispatchable backup in Kramer Junction; (B) operation without dispatchable backup in Kramer Junction; (C) operation with dispatchable backup in Norderney; (D) operation without dispatchable backup in Norderney. All energy terms are normalised by hourly load.

Appendix C

Carbon capture process

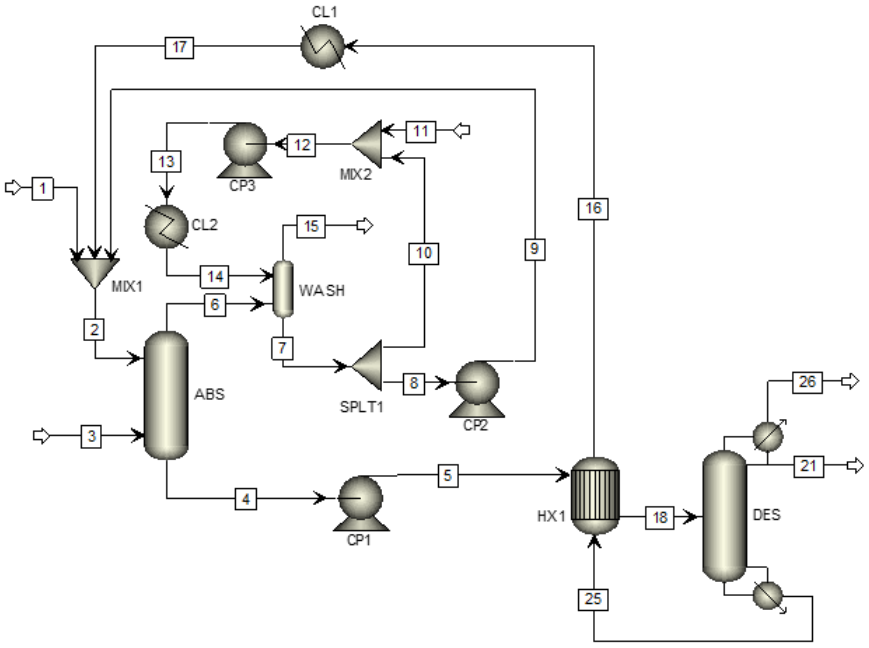


Figure C.1. Process flow diagram of the carbon capture subsystem (for Chapter 6) simulated in Aspen Plus.

Table C.1. Key stream conditions for the carbon capture process (Figure C.1). Note that the trace amounts of other ions such as hydroxide ion and carbonate are not shown in this table.

Stream	1	2	3	4	5	6	8	10	11	15	18	21	25	26
T (°C)	40.0	18.0	48.0	53.3	53.1	48.6	48.6	48.6	20.0	43.9	112.9	18.0	119.3	18.0
P (bar)	2.0	2.0	1.0	1.0	2.9	1.0	1.0	1.0	2.0	1.0	2.9	2.00	2.00	2.0
F (kg/h)	82.1	3.4×10^6	1.2×10^6	3.4×10^6	3.4×10^6	1.1×10^6	3.6×10^4	4.9×10^5	3.3×10^4	1.1×10^6	3.4×10^6	3.3×10^4	3.3×10^6	8.1×10^4
Composition (wt%)														
MEA	100.0	13.0	0.0	6.2	0.1	0.0	0.0	0.0	0.0	0.0	7.9	0.0	13.9	0.0
H_2O	0.0	67.7	0.1	66.1	0.7	0.1	1.0	1.0	1.0	7.6	65.6	99.5	67.2	0.4
CO_2	0.0	0.0	0.1	0.0	0.0	0.0	0.0	0.0	0.0	1.8	0.0	0.3	0.0	99.4
N_2	0.0	0.0	0.7	0.0	0.0	0.8	0.0	0.0	0.0	79.8	0.0	0.0	0.0	0.1
O_2	0.0	0.0	0.1	0.0	0.0	0.1	0.0	0.0	0.0	10.8	0.0	0.0	0.0	0.0
$MEAH^+$	0.0	7.4	0.0	10.5	0.1	0.0	0.0	0.0	0.0	0.0	10.4	0.1	7.3	0.0
$MEACOO^-$	0.0	11.6	0.0	16.9	0.2	0.0	0.0	0.0	0.0	0.0	14.1	0.0	10.7	0.0

Carbon dioxide hydrogenation process

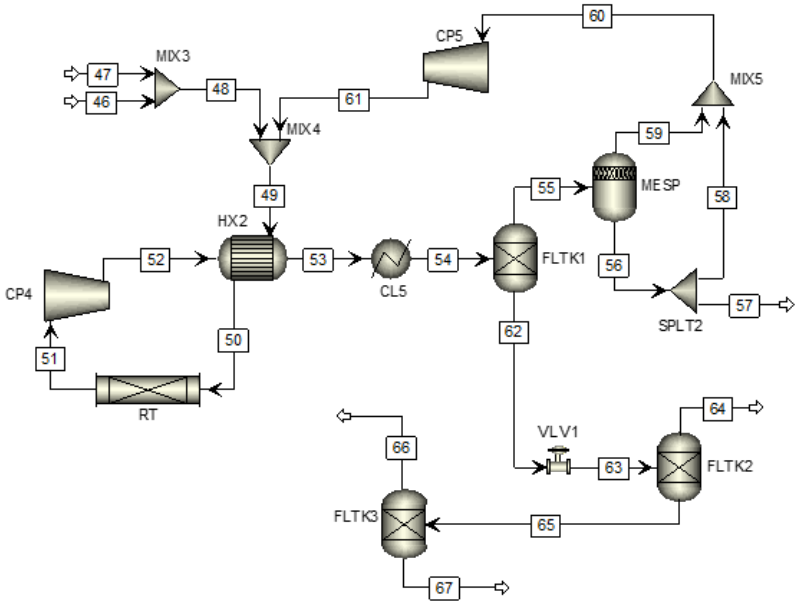


Figure C.2. Process flow diagram of the CO_2 hydrogenation subsystem (for Chapter 6) simulated in Aspen Plus.

Table C.2. Key stream conditions for the CO_2 hydrogenation process (Figure C.2).

Stream	49	50	51	53	55	62	65	67
T (°C)	74.7	255.0	255.0	125.4	40.0	40.0	35.5	35.5
P (bar)	70.0	70.0	70.0	74.0	70.0	70.0	1.1	1.1
F (kg/h)	239,755	239,755	239,755	239,755	151,622	88,141	80,442	79,224
Composition (wt%)								
Methanol	0.9	0.9	22.3	22.3	1.5	58.1	62.5	63.4
H_2O	0.1	0.1	12.3	12.3	0.2	33.0	36.0	36.6
H_2	25.0	25.0	21.0	21.0	33.2	0.1	0.0	0.0
CO_2	69.2	69.2	39.5	39.5	57.4	8.8	1.5	0.0
CO	4.7	4.7	4.9	4.9	7.7	0.1	0.0	0.0

Methanol distillation process

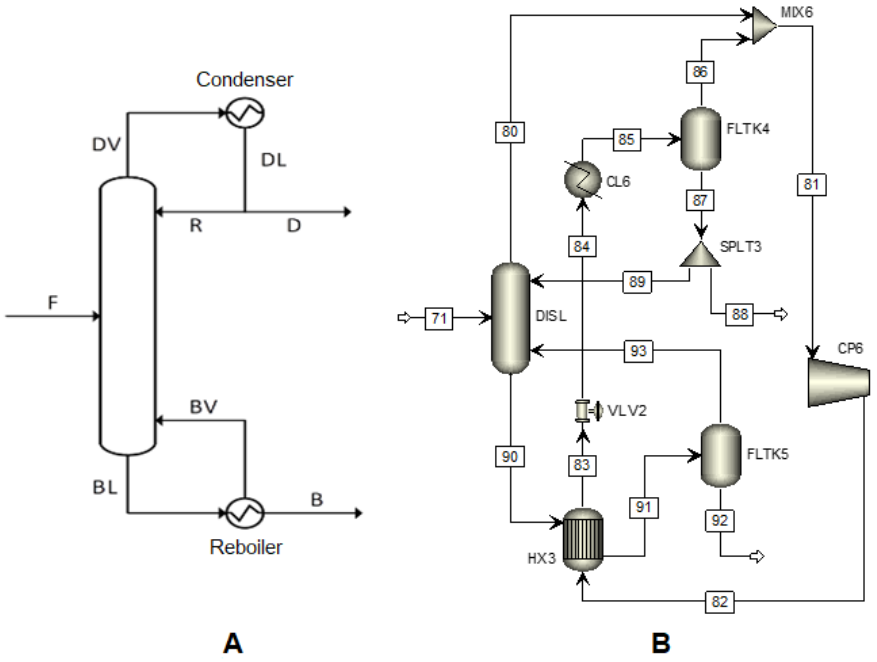


Figure C.3. (A) Schematic diagram of a traditional distillation column. (B) Process flow diagram of the distillation subsystem (for Chapter 6) modified with a design of mechanical vapour recompression.

Table C.3. Physical meaning of the key streams in Figure C.3.

(A)	(B)	Description
F	71	Feed to the distillation column
D	88	Distillate product
B	92	Bottom product
R	89	Reflux to the second stage
DV	80	Second stage vapour
DL	87	First stage liquid
BV	93	Boilup to the penultimate stage
BL	90	Penultimate stage liquid

Table C.4. Stream conditions for the distillation process (Figure C.3B).

Stream	T (°C)	P (bar)	F (kg/h)	Composition (wt%)	
				Methanol	H_2O
80	66.8	1.1	95,326	99.8	0.2
81	66.8	1.1	106,854	99.8	0.2
82	188.2	4.8	106,854	99.8	0.2
83	110.0	4.8	106,854	99.8	0.2
84	66.7	1.1	106,854	99.8	0.2
85	66.7	1.1	106,854	99.8	0.2
86	66.7	1.1	11,528	99.9	0.1
87	66.7	1.1	95,326	99.8	0.2
88	66.7	1.1	49,649	99.8	0.2
89	66.7	1.1	45,677	99.8	0.2
90	93.5	1.1	86,215	10.8	89.2
91	100.0	1.1	86,215	10.8	89.2
92	100.0	1.1	29,574	2.3	97.7
93	100.0	1.1	56,641	15.1	84.9

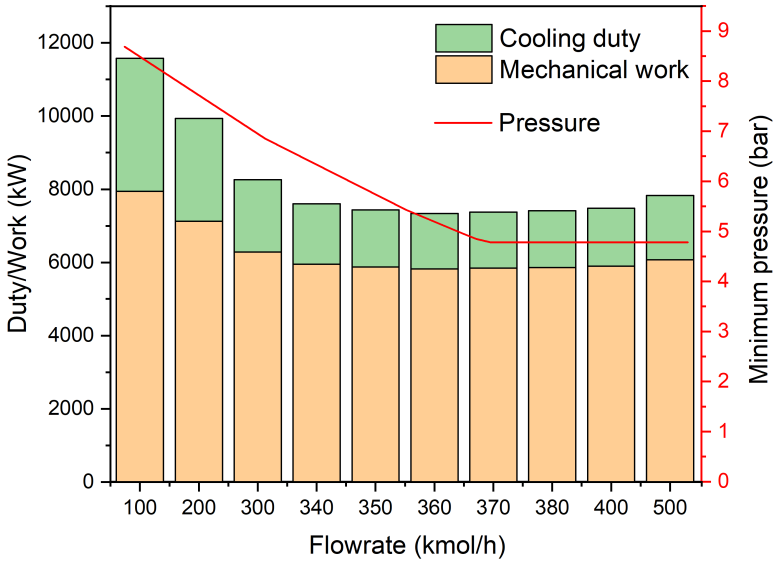


Figure C.4. Requirement of mechanical work, cooling duty and minimum target pressure with respect to the flowrate of the working fluid.

Table C.5. Utilities and cost for the main equipments shown in Figure 6.1. Note that the electrical power consumed by DES comprises electrical heating by the reboiler and mechanical work by the refrigerator (refg.) of the condenser. All of the equipment costs (except the catalytic reactor) are obtained from Aspen Process Economic Analyser directly after process simulations. The cost of the catalytic reactor (RT) is estimated via the six-tenths factor rule based on the work of Zhang et al. (2015).

	Mechanical work (kW)	Electrical heating (kW)	Cooling water duty (kW)	Equipment cost ($)
CC subsystem				
CL1	0.0	0.0	−62,717.4	541,400
CL2	0.0	0.0	−1,762.8	28,000
CP1	578.5	0.0	0.0	116,400
CP2	3.5	0.0	0.0	5,700
CP3	50.2	0.0	0.0	15,500
HX1	0.0	0.0	0.0	5,982,200
ABS	0.0	0.0	0.0	33,384,600
DES	0.0	117,111.4	−50,745.2	12,502,180
DES (refg.)	558.9	0.0	0.0	–
DT subsystem				
DISL	0.0	0.0	0.0	510,300
HX3	0.0	0.0	0.0	479,400
FLTK4	0.0	0.0	0.0	31,700
FLTK5	0.0	0.0	0.0	34,400
CL6	0.0	0.0	−1,515.6	18,900
CP6	5,828.3	0.0	0.0	13,899,400
SYN subsystem				
MCP1	7,099.6	0.0	−4,974.8	5,004,100
MCP2	24,997.8	0.0	−16,186.1	36,512,500
CL5	0.0	0.0	−45,045.5	371,100
HX2	0.0	0.0	0.0	2,970,800
RT	0.0	0.0	−26,017.6	15,441,003
MSEP	0.0	0.0	0.0	112,800
FLTK1	0.0	0.0	0.0	102,300
FLTK2	0.0	0.0	0.0	29,000
FLTK3	0.0	0.0	0.0	29,000
CP4	2,807.4	0.0	0.0	1,375,400
CP5	8.9	0.0	0.0	702,700

Variables and constant parameters

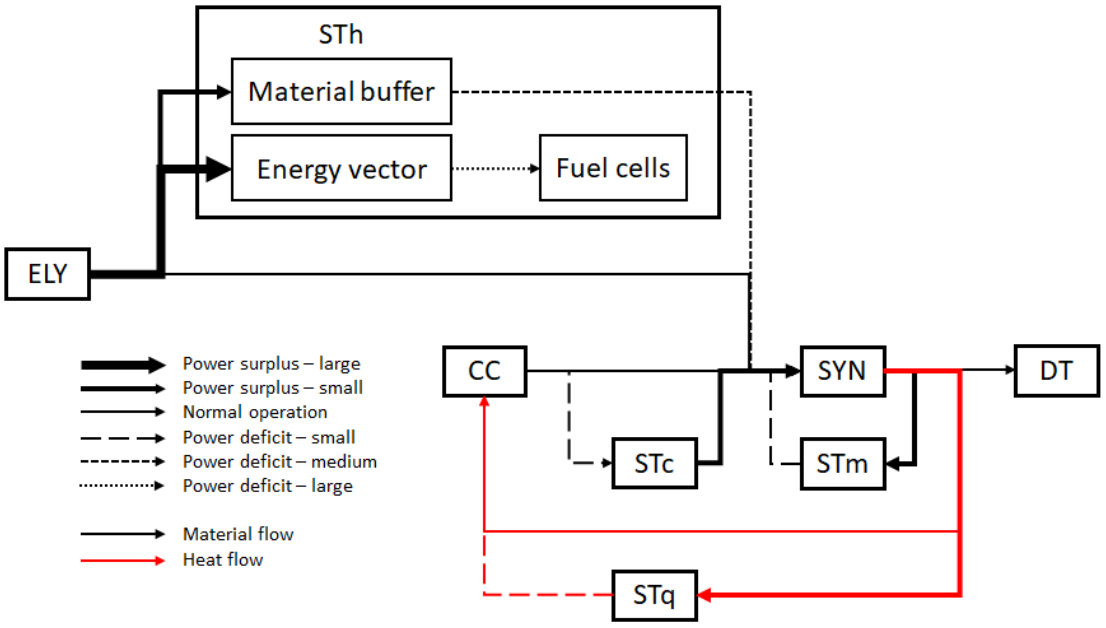


Figure C.5. Schematic illustration of a simplified operation policy on material and heat flow.

Table C.6. Key decision variables and their descriptions.

	Unit	Domain	Description
F_{32}	kg/h	Time	H_2 storage charging schedule
F_{35}	kg/h	Time	H_2 fuel cells output schedule
F_{41}	kg/h	Time	CO_2 storage charging schedule
F_{68}	kg/h	Time	Raw methanol storage charging schedule
$\dot{Q}_3$	kW	Time	heat storage charging schedule
$\dot{Q}_4$	kW	Time	heat storage discharging schedule
P_{D}	kW	Time	dispatchable power use
ϕ	–	Time	load fraction of an operation unit
f_{W}	–	singular	wind fraction in renewable power generation
γ	–	singular	excess generation of the renewable power
$x_{\mathrm{el,max}}^{\mathrm{ELY}}$	kW	singular	maximum size of the electrolysers
$\dot{\xi}_{\mathrm{max}}$	kmol/h	singular	maximum size of the methanol reactor

Table C.7. Summary of constant parameters.

	Value	Unit	Description
Process coefficient			
a_1^{STh}	3.03	kWh/kg	specific electricity consumption of MCP3
a_2^{STh}	1.07	kWh/kg	specific electricity consumption of HT2
a_3^{STh}	22.28	kWh/kg	specific electricity output of FC
a_4^{STh}	0.21	kWh/kg	specific electricity output of TUB
a_5^{STh}	2.99	kWh/kg	specific cooling duty of MCP3
a_1^{SYN}	7,099.64	kW	electricity consumption of MCP1
a_2^{SYN}	2.55	kWh/kg	specific electricity consumption of MCP2
a_3^{SYN}	1.76	kWh/kmol	electricity coefficient for SYN recycle loop
a_4^{SYN}	4,974.81	kW	cooling duty of MCP1
a_5^{SYN}	1.65	kWh/kg	specific cooling duty of MCP2
a_6^{SYN}	28.16	kW/kmol	cooling duty coefficient for SYN recycle loop
a_1^{STc}	0.05	kWh/kg	specific electricity consumption of HT3
a_2^{STc}	0.05	kWh/kg	specific cooling duty of CL4
b_{h}	6.12	kg/kmol	coefficient for hydrogen flowrate to SYN
b_{m}	8.09	–	coefficient for raw methanol flowrate to DT
b_{c}	8.31	–	coefficient for carbon dioxide flowrate to SYN
b_{q}	16.26	kWh/kmol	specific heat output of RT
Process stream			
F_{26}	81,426.93	kg/h	flowrate of carbon dioxide generated from CC
F_{71}	79,222.96	kg/h	flowrate of raw methanol feed to DT
F_{88}	49,648.94	kg/h	flowrate of methanol product from DT
F_{92}	29,574.02	kg/h	flowrate of waste water from DT
ρ_{42}	647.56	kg/m^3	density of stored carbon dioxide stream in STc
ρ_{67}	838.09	kg/m^3	density of stored raw methanol stream in STm
Utility parameter			
$x_{\mathrm{el},0}^{\mathrm{CC}}$	92,290.68	kW	electricity required by CC excluding heat
$x_{\mathrm{el}}^{\mathrm{DT}}$	5,828.30	kW	electricity required by DT
$x_{\mathrm{cw}}^{\mathrm{CC}}$	115,225.43	kW	cooling duty in CC
$x_{\mathrm{cw}}^{\mathrm{DT}}$	1,515.63	kW	cooling duty in DT
$\dot{Q}_5$	26,011.88	kW	process heat fed to CC
Operation parameter			
$\dot{\xi}_0$	1,599.68	kmol/h	hourly baseline extent of hydrogenation reaction
ϕ_{min}	0.1	–	minimum load of SYN
$e_{\mathrm{max}}^{\mathrm{ELY}}$	55.7 [a]	kWh/kg	maximum specific energy requirement for eletrolyser
$e_{\mathrm{min}}^{\mathrm{ELY}}$	39.4 [b]	kWh/kg	minimum specific energy requirement for eletrolyser

[a] This value is obtained from Zeng and Zhang (2010).
[b] This value is obtained from Wang (2006).

Economic parameters

Note 1: Pressure vessel cost

The cost approximation for pressure vessels is adopted from Douglas' method (Douglas, 1988), which is based on empirical correlations. The cost function is rearranged into Eq. C.1:

$$\textit{Pressure Vessel Cost} = \Big(\frac{\text{M\&S}}{280}\Big)101.9D^{1.07}H^{0.82}(2.18 + 2f_{\text{m}}f_{\text{p}}) \tag{C.1}$$

where D and H denote the diameter and height of the vessel, respectively, f_{m} and f_{p} denote the correction factor for material and pressure, respectively, and M&S denotes the Marshall and Swift Cost Index, taken as 1,638. Material selection and values of the correction factors are tabulated in Table C.8. Assuming an aspect ratio of 3:1, the annualised cost for STc and STm are rearranged and given by

$$C^{\text{STc}} = 111.27f^{\text{CR}}\Big(\frac{\text{M\&S}}{280}\Big)\Big(\frac{L^{\text{STc}}_{\text{max}}}{\rho_{42}}\Big)^{0.63} \tag{C.2}$$

$$C^{\text{STm}} = 64.78f^{\text{CR}}\Big(\frac{\text{M\&S}}{280}\Big)\Big(\frac{L^{\text{STm}}_{\text{max}}}{\rho_{67}}\Big)^{0.63} \tag{C.3}$$

where ρ_{42} and ρ_{67} denote the density of the pressurised CO_2 (Stream 42 in Figure 6.1) and the raw methanol (Stream 67), respectively. Since the maximum capacity of a pressure vessel is constrained, a linear cost function is derived from Eqs. C.2 and C.3 based on a maximum capacity of 200 tonnes. This is justified by the fact that $L^{\text{STc}}_{\text{max}}$ and $L^{\text{STm}}_{\text{max}}$ are much larger than the capacity of a single vessel.

Table C.8. Correction factors for pressure vessels.

	Material	T (℃)	P (bar)	f_{m}	f_{p}
STc	carbon steel, solid	29.3	71.0	1.00	2.50
STm	stainless steel, clad	30.0	1.0	2.25	1.00

Total fixed capital cost for production processes

Table C.9. Total fixed capital cost estimation for the methanol plant including the subsystems of CC, DT and SYN (with MCP1 listed separately) at the baseline size. The ratio factors are selected for fluid processing plant and obtained from Peter and Timmerhaus (1991).

Items	Ratio factor	Subsystem cost (M$)			
		CC	DT	MCP1	SYN
Purchased equipment cost	1.00	52.58	14.97	5.31	57.34
Installation cost	0.47	24.71	7.04	2.50	26.95
Instrumentation and controls	0.36	18.93	5.39	1.91	20.64
Piping	0.68	35.75	10.18	3.61	38.99
Electrical systems	0.11	5.78	1.65	0.58	6.30
Building and services	0.18	9.46	2.70	0.96	10.32
Yard improvements	0.10	5.26	1.50	0.53	5.73
Service facilities	0.70	36.80	10.48	3.72	40.14
Total direct cost		189.27	53.91	19.11	206.43
Engineering and supervision	0.33	17.35	4.94	1.75	18.92
Construction expenses	0.41	21.56	6.14	2.18	23.51
Legal expenses	0.04	2.10	0.60	0.21	2.29
Contractor's fee	0.22	11.56	3.29	1.17	12.62
Contingency	0.44	23.13	6.59	2.33	25.23
Total indirect cost		75.71	21.56	7.65	82.57
TFCC		264.98	71.47	26.76	288.99

Technology costs

Table C.10. Technology costs used for the base case scenario. All costs are converted to US dollar based on 1 € = 1.14 $.

	CapEx $/kW	CapEx $/tonne	CapEx $/MWh	OpEx $/kW	Source
Inland wind	1,473[a]	–	–	–	Gielen et al. (2020)
Solar PV	995[a]	–	–	–	Gielen et al. (2020)
Electrolyser	600[b]	–	–	–	Saba et al. (2018)
SOFC	194[c]	–	–	–	Scataglini et al. (2015)
H_2 storage	-	751,700[d]	–	–	Steward (2009)
Heat storage[e]	-	–	25	40	Hauer (2013)
Gas turbine	240[f]	–	–	–	Pauschert (2009)

[a] This indicates the weighted averages of total installed cost.
[b] This is estimated based on alkaline electrolysers at 1 atm.
[c] This indicates the stack cost estimated based on 100 kW and 1,000 systems per year.
[d] CapEx of H_2 storage includes steel tanks and compressors.
[e] A lower bound is adopted from the source due to its moderate operating conditions.
[f] This is adopted based on large simple cycle case.

Table C.11. Conservative technology costs. All costs are converted to US dollar based on 1 € = 1.14 $.

	CapEx	Unit	Year	Source
Inland wind	2,450[a]	$/kW	2019	Gielen et al. (2020)
Solar PV	2,400[a]	$/kW	2019	Gielen et al. (2020)
Electrolyser	1,064	$/kW	2020	Buttler and Spliethoff (2018)
SOFC	1,039[b]	$/kW	2015	Scataglini et al. (2015)

[a] This indicates the 95$^{\text{th}}$ percentile of the source.
[b] This indicates the stack cost estimated based on 10 kW and 100 systems per year.

Table C.12. Progressive technology costs. All costs are converted to US dollar based on 1 € = 1.14 $.

	CapEx	Unit	Year	Source
Inland wind	1,100[a]	$/kW	2019	Gielen et al. (2020)
Solar PV	750[a]	$/kW	2019	Gielen et al. (2020)
Electrolyser	414	$/kW	2019	Gonzalez-Garay et al. (2019)
SOFC	166[b]	$/kW	2015	Scataglini et al. (2015)

[a] This indicates the 5$^{\text{th}}$ percentile of the source.
[b] This indicates the stack cost estimated based on 250 kW and 50,000 systems per year.

Auxiliary results

Table C.13. Size of individual units for the 100 % renewable operations in the two locations.

		Norderney		Kramer Junction	
		Flexible	Non-flexible	Flexible	Non-flexible
Power generation					
Wind power	MW	1,330.9	1,432.1	0	0
Solar power	MW	151.1	350.9	1,987.2	3,693.5
Production units					
Electrolysers	kW	1,254.6	1,236.9	1,746.9	2,094.7
Synthesis	kmol/h	4,232.5	1,599.7	2,511.4	1,599.7
Storage units					
H_2 storage	tonne	200.7	1,866.9	247.6	883.4
CO_2 storage	tonne	54,020.9	0	123,887.7	0
raw MeOH storage	tonne	52,559.8	0	120,536.8	0
Heat storage	MWh	39,585.8	93,406.5	152,677.2	109,883.3
Fuel cells	MW	17.1	111.0	149.9	121.9

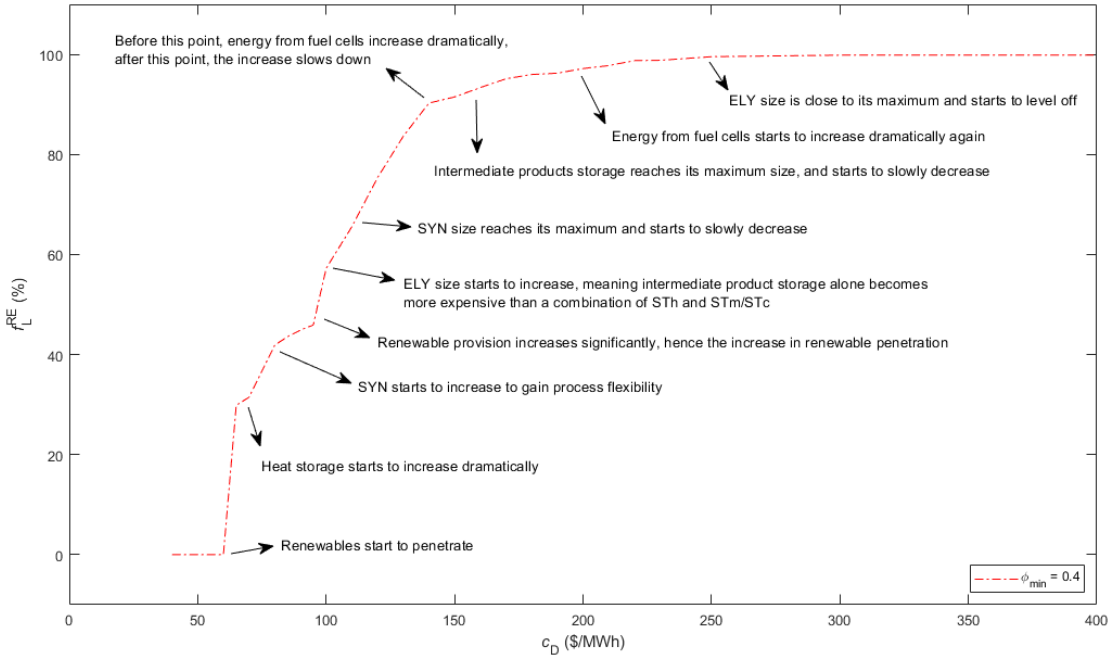


Figure C.6. Analysis of the renewable penetration behaviour from a mechanistic viewpoint using the case of $\phi_{\min} = 0.4$ in Norderney as an example.

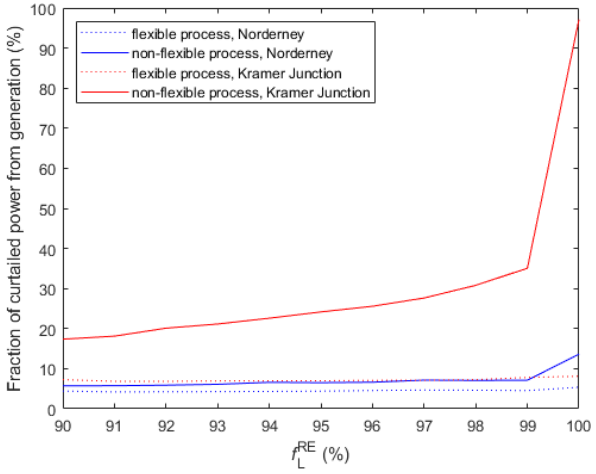


Figure C.7. Fraction of the curtailed renewable power P_{out} plotted against f_{L}^{RE}.

Table C.14. Key variables for Norderney at selected ramp limits (for both ramp-up and -down). Ramp limit is measured in terms of fraction of rated capacity.

Ramp limit %	LCOMeOH $/tonne	$\dot{\xi}$ kmol/h	$L_{\text{max}}^{\text{STh}}$ tonne	$L_{\text{max}}^{\text{STm}}$ tonne	f_{W} %
0.01	1,201.9	1,884	1,248	28,041	80.6
0.1	1,136.1	2,527	986	37,859	82.1
1	1,017.3	4,303	354	50,476	93.7
5	984.6	4,249	200	52,934	95.1
10	983.2	4,234	200	52,596	95.4
20	982.4	4,229	201	52,520	95.5
Unlimited	982.2	4,233	201	52,560	95.5

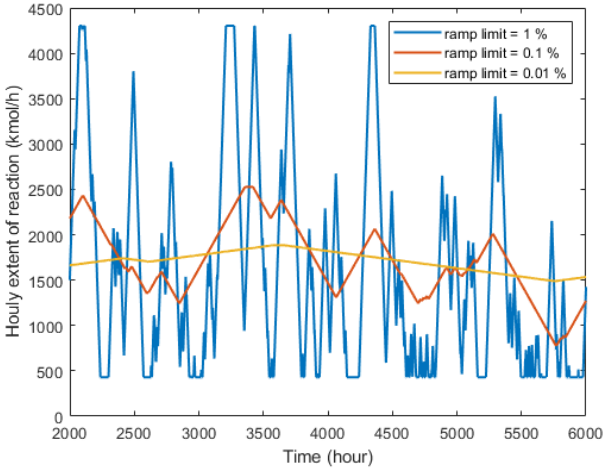


Figure C.8. Example of reactor operation for selected ramp limits. Ramp limit is measured in terms of fraction of rated capacity.

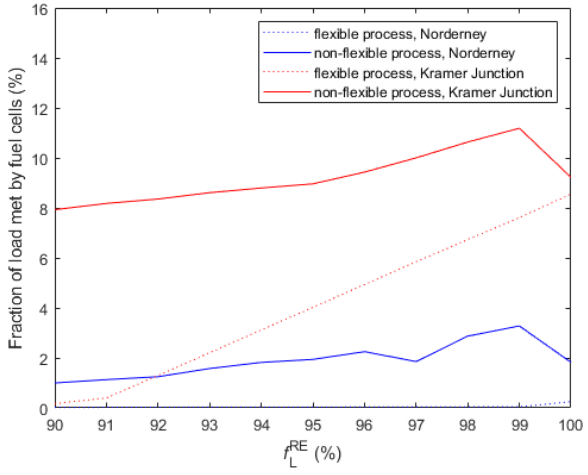


Figure C.9. Fraction of the load met by E_{ST} plotted against f_L^{RE}.

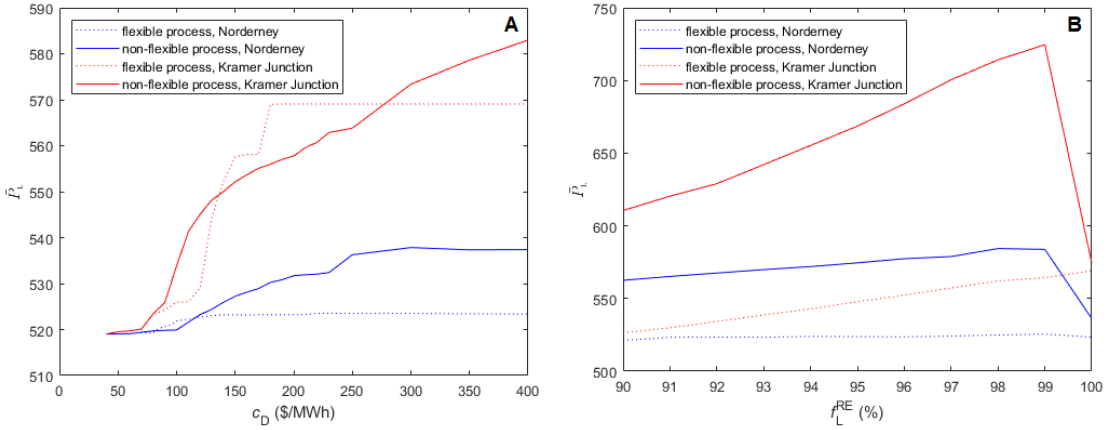


Figure C.10. Average load of the methanol production process ($\overline{P_L}$) plotted against (A) c_D and (B) f_L^{RE} for the optimal operations.

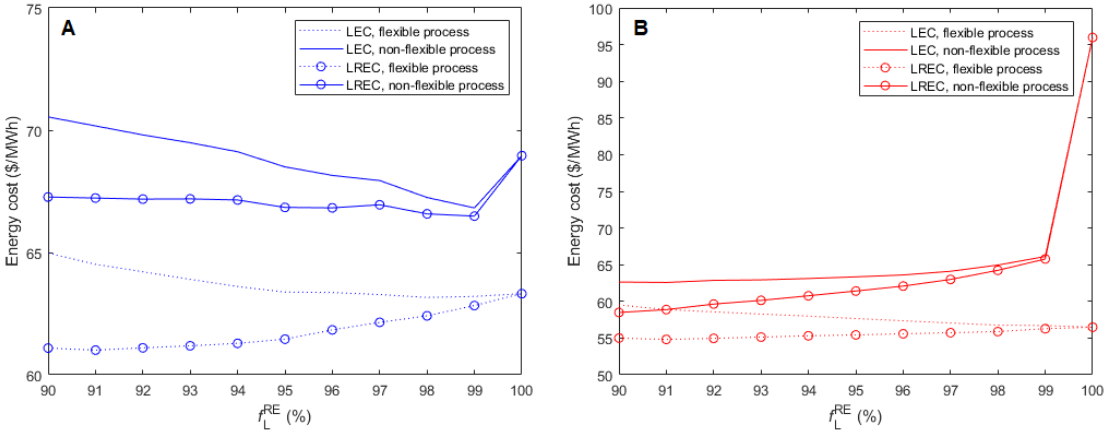


Figure C.11. Levelised energy cost (LEC) and levelised renewable energy cost (LREC) plotted against f_L^{RE} for the optimal operations in (A) Norderney and (B) Kramer Junction.

References

Abdulrahman, A. O., Huisingh, D., and Hafkamp, W. Sustainability improvements in Egypt's oil & gas industry by implementation of flare gas recovery. *Journal of Cleaner Production*, 98:116–122, 2015.

Ahman, M., Nilsson, L. J., and Johansson, B. Global climate policy and deep decarbonization of energy-intensive industries. *Climate Policy*, 17(5):634–649, 2017.

Akikusa, J. and Khan, S. U. M. Photoelectrolysis of water to hydrogen in p-SiC/Pt and p-SiC/n-TiO_2 cells. *International Journal of Hydrogen Energy*, 27:52–58, 2002.

Allman, A. and Daoutidis, P. Optimal scheduling for wind-powered ammonia generation: Effects of key design parameters. *Chemical Engineering Research and Design*, 131:5–15, 2018.

Alsayegh, S., Johnson, J., Ohs, B., and Wessling, M. Methanol production via direct carbon dioxide hydrogenation using hydrogen from photocatalytic water splitting: Process development and techno-economic analysis. *Journal of Cleaner Production*, 208:1446–1458, 2019.

Amin, N. A. S. and Yaw, T. C. Thermodynamic equilibrium analysis of combined carbon dioxide reforming with partial oxidation of methane to syngas. *International Journal of Hydrogen Energy*, 32(12):1789–1798, 2007.

Ampelli, C., Passalacqua, R., Genovese, C., Perathoner, S., and Centi, G. A novel photo-electrochemical approach for the chemical recycling of carbon dioxide to

fuels. *Chemical Engineering Transactions*, 25:683–688, 2011.

Appl, M. *Ullmann's Encyclopedia of Industrial Chemistry*, chapter Ammonia. American Cancer Society, 2006.

Arakawa, H. Research and development on new synthetic routes for basic chemicals by catalytic hydrogenation of CO_2. *Studies in Surface Science and Catalysis*, 114:19–30, 1998.

Archer, C. L. and Jacobson, M. Z. Supplying baseload power and reducing transmission requirements by interconnecting wind farms. *Journal of Applied Meteorology and Climatology*, 46(11):1701–1717, 2007.

Aresta, M. and Dibenedetto, A. Utilisation of CO_2 as a chemical feedstock: Opportunities and challenges. *Dalton Transactions*, pages 2975–2992, 2007.

Armijo, J. and Philibert, C. Flexible production of green hydrogen and ammonia from variable solar and wind energy: Case study of Chile and Argentina. *International Journal of Hydrogen Energy*, 45(3):1541–1558, 2020.

Aspen Technology, Inc. Rate-based model of the CO_2 capture process by MEA using Aspen Plus. Dataset, 2012.

Bañares-Alcántara, R., Dericks III, G., Fiaschetti, M., Grünewald, P., Lopez, J. M., Tsang, E., Yang, A., Ye, L., and Zhao, S. Analysis of islanded ammonia-based energy storage systems. Report, University of Oxford, 2015.

Bagajewicz, M. J. and Barbaro, A. F. On the use of heat pumps in total site heat integration. *Computers & Chemical Engineering*, 27(11):1707–1719, 2003.

Baronia, R., Goel, J., Gautam, G., Singh, D., and Singhal, S. K. Synthesis and characterization of nitrogen doped reduced graphene oxide (N-rGO) supported PtCu anode catalysts for direct methanol fuel cell. *Journal of Nanoscience and Nanotechnology*, 19(7):3832–3843, 2019a.

Baronia, R., Goel, J., and Singhal, S. K. High methanol electro-oxidation using PtCo/reduced graphene oxide (rGO) anode nanocatalysts in direct methanol fuel cell. *Journal of Nanoscience and Nanotechnology*, 19(7):4315–4322, 2019b.

Barton, J. L. Electrification of the chemical industry. *Science*, 368(6496):1181–1182, 2020.

Beaudin, M., Zareipour, H., Schellenberglabe, A., and Rosehart, W. Energy storage for mitigating the variability of renewable electricity sources: An updated review. *Energy for Sustainable Development*, 14(4):302–314, 2010.

Beerbühl, S. S., Fröhling, M., and Schultmann, F. Combined scheduling and capacity planning of electricity-based ammonia production to integrate renewable energies. *European Journal of Operational Research*, 241(3):851–862, 2015.

Bühler, F., Zühlsdorf, B., Nguyen, T.-V., and Elmegaard, B. A comparative assessment of electrification strategies for industrial sites: Case of milk powder production. *Applied Energy*, 250:1383–1401, 2019.

Bird, L., Cochran, J., and Wang, X. Wind and solar energy curtailment: Experience and practices in the United States. Report, National Renewable Energy Laboratory, 2014.

Bos, M., Kersten, S., and Brilman, D. Wind power to methanol: Renewable methanol production using electricity, electrolysis of water and CO_2 air capture. *Applied Energy*, 264:114672, 2020.

Boyle, G. *Renewable Energy: Power for a sustainable future*, chapter Solar Thermal Energy, pages 55–56. Oxford University Press, 2004.

Brown, T. Renewable hydrogen for sustainable ammonia production. *Chemical Engineering Progress*, 115(8):47–53, 2019.

Budischak, C., Sewell, D., Thomson, H., Mach, L., Veron, D. E., and Kempton, W. Cost-minimized combinations of wind power, solar power and electrochemical storage, powering the grid up to 99.9% of the time. *Journal of Power Sources*, 225:60–74, 2013.

Bukhtiyarova, M., Lunkenbein, T., Kähler, K., and Schlögl, R. Methanol synthesis from industrial CO_2 sources: A contribution to chemical energy conversion. *Catalysis Letters*, 147(2):416–427, 2017.

Buttler, A. and Spliethoff, H. Current status of water electrolysis for energy storage, grid balancing and sector coupling via power-to-gas and power-to-liquids: A review. *Renewable and Sustainable Energy Reviews*, 82:2440–2454, 2018.

Cañete, B., Brignole, N. B., and Gigola, C. E. Methanol production from high CO_2 content natural gas. *Computer Aided Chemical Engineering*, 44:151–156, 2018.

Cañete, B., Gigola, C. E., and Brignole, N. B. Synthesis gas processes for methanol production via CH_4 reforming with CO_2, H_2O, and O_2. *Industrial & Engineering Chemistry Research*, 53(17):7103–7112, 2014.

Cañete, B., Gigola, C. E., and Brignole, N. B. Enhancing the potential of methane combined reforming for methanol production via partial CO_2 hydrogenation. *Industrial & Engineering Chemistry Research*, 56(22):6480–6492, 2017.

Carlson, E. Don't gamble with physical properties for simulations. *Chemical Engineering Progress*, 92(10):35–46, 1996.

Celik, A. N. Techno-economic analysis of autonomous PV-wind hybrid energy systems using different sizing methods. *Energy Conversion and Management*, 44(12):1951–1968, 2003.

Chatterjee, S. and Huang, K.-W. Unrealistic energy and materials requirement for direct air capture in deep mitigation pathways. *Nature Communications*, 11(1), 2020.

Cheema, I. I. and Krewer, U. Operating envelope of Haber–Bosch process design for power-to-ammonia. *RSC Advances*, 8:34926–34936, 2018.

Chen, C. Using dispatchable energy price as a tool to predict and influence the renewable penetration in chemical production. In *Proceedings of the 23rd Conference on Process Integration, Modelling and Optimisation for Energy Saving and Pollution Reduction*. 2020.

Colmenares, T. R. and Seider, W. D. Heat and power integration of chemical processes. *AIChE Journal*, 33(6):898–915, 1987.

Delucchi, M. A. and Jacobson, M. Z. Providing all global energy with wind, water, and solar power, Part II: Reliability, system and transmission costs, and policies. *Energy Policy*, 39(3):1170–1190, 2011.

Demirbas, M. F. Producing hydrogen from biomass via non-conventional processes. *Energy Exploration & Exploitation*, 22(4):231–239, 2004.

Demiroren, A. and Yilmaz, U. Analysis of change in electric energy cost with using renewable energy sources in Gökceada, Turkey: An island example. *Renewable and Sustainable Energy Reviews*, 14(1):323–333, 2010.

Deng, L. and Adams, T. A. Methanol production from coke oven gas and blast furnace gas. *Computer Aided Chemical Engineering*, 44:163–168, 2018.

Denholm, P., Kulcinski, G. L., and Holloway, T. Emissions and energy efficiency assessment of baseload wind energy systems. *Environmental Science & Technology*, 39(6):1903–1911, 2005.

Dennis, K., Colburn, K., and Lazar, J. Environmentally beneficial electrification: The dawn of 'emissions efficiency'. *The Electricity Journal*, 29(6):52–58, 2016.

Díez, E., Langston, P., Ovejero, G., and Romero, M. D. Economic feasibility of heat pumps in distillation to reduce energy use. *Applied Thermal Engineering*, 29(5):1216–1223, 2009.

Douglas, J. M. *Conceptual design of chemical processes*. McGraw-Hill Book Company, 1988.

Dupuy, M. Making China's electricity markets work for clean energy. `https://www.raponline.org/blog/making-chinas-electricity-markets-work-clean-energy/`, 2018. Accessed on: August 2, 2020.

Ebrahimi, S., Kinnon, M. M., and Brouwer, J. California end-use electrification impacts on carbon neutrality and clean air. *Applied Energy*, 213:435–449, 2018.

Ekren, O. and Ekren, B. Y. Size optimization of a PV/wind hybrid energy conversion system with battery storage using response surface methodology. *Applied Energy*, 85(11):1086–1101, 2008.

Ekren, O. and Ekren, B. Y. Size optimization of a PV/wind hybrid energy conversion system with battery storage using simulated annealing. *Applied Energy*, 87(2):592–598, 2010.

Ekren, O., Ekren, B. Y., and Ozerdem, B. Break-even analysis and size optimization of a PV/wind hybrid energy conversion system with battery storage – A case study. *Applied Energy*, 86(7):1043–1054, 2009.

EL-Halwagi, M. M. *Sustainable Design Through Process Integration*, chapter Integration of Combined Heat and Power Systems, pages 178–180. Elsevier Inc., 2012.

Energy Transitions Commission. Reaching net-zero carbon emissions from harder-to-abate sectors by mid-century. Report, 2018.

Engelien, H. K. and Skogestad, S. Selecting appropriate control variables for a heat-integrated distillation system with prefractionator. *Computers & Chemical Engineering*, 28(5):683–691, 2004.

Esposito, D. V. Membraneless electrolyzers for low-cost hydrogen production in a renewable energy future. *Joule*, 1(4):651–658, 2017.

European Commission. The roadmap for transforming the EU into a competitive, low-carbon economy by 2050. Report, 2011.

Eurostat. Statistics on the production of manufactured goods. Report, 2016.

Eurostat. Electricity price statistics. Report, 2017a.

Eurostat. Energy balance sheets 2015 data. Dataset, 2017b.

Evans, A., Strezov, V., and Evans, T. J. Assessment of sustainability indicators for renewable energy technologies. *Renewable and Sustainable Energy Reviews*, 13(5):1082–1088, 2009.

Feng, X. and Berntsson, T. Critical COP for an economically feasible industrial heat-pump application. *Applied Thermal Engineering*, 17(1):93–101, 1997.

Fiaschi, D., Manfrida, G., Secchi, R., and Tempesti, D. A versatile system for offshore energy conversion including diversified storage. *Energy*, 48(1):566–576, 2012.

Fúnez Guerra, C., Reyes-Bozo, L., Vyhmeister, E., Jaén Caparrós, M., Salazar, J. L., and Clemente-Jul, C. Technical-economic analysis for a green ammonia production plant in Chile and its subsequent transport to Japan. *Renewable Energy*, 157:404–414, 2020.

Frattini, D., Cinti, G., Bidini, G., Desideri, U., Cioffi, R., and Jannelli, E. A system approach in energy evaluation of different renewable energies sources integration in ammonia production plants. *Renewable Energy*, 99:472–482, 2016.

Freguia, S. and Rochelle, G. T. Modeling of CO_2 capture by aqueous monoethanolamine. *AIChE Journal*, 49(7):1676–1686, 2003.

Funk, J. E. Thermochemical hydrogen production: Past and present. *International Journal of Hydrogen Energy*, 26(3):185–190, 2001.

Ganesh, I. Conversion of carbon dioxide into methanol - a potential liquid fuel: Fundamental challenges and opportunities (a review). *Renewable and Sustainable Energy Reviews*, 31:221–257, 2014.

Gao, X., Ma, Z., Yang, L., and Ma, J. Simulation and optimization of distillation processes for separating the methanol–chlorobenzene mixture with separate heat-pump distillation. *Industrial & Engineering Chemistry Research*, 52(33):11695–11701, 2013.

Gattrell, M., Gupta, N., and Co, A. A review of the aqueous electrochemical reduction of CO_2 to hydrocarbons at copper. *Journal of Electroanalytical Chemistry*, 594(1):1–19, 2006.

Gellings, C. and Blatt, M. Program on technology innovation: Industrial electrotechnology development opportunities. Report, Electric Power Research Institute, 2009.

Geng, Z., Zhang, Y., Li, C., Han, Y., Cui, Y., and Yu, B. Energy optimization and prediction modeling of petrochemical industries: An improved convolutional neural network based on cross-feature. *Energy*, 194:116851, 2020.

Giddey, S., Badwal, S. P. S., Munnings, C., and Dolan, M. Ammonia as a renewable energy transportation media. *ACS Sustainable Chemistry & Engineering*, 5(11):10231–10239, 2017.

Gielen, D., Boshell, F., Gorini, R., Kiruja, J., Komor, P., Masuyama, T., and Parthan, B. Renewable power generation costs in 2019. Report, International Renewable Energy Agency, 2020.

Gonzalez-Garay, A., Frei, M. S., Al-Qahtani, A., Mondelli, C., Guillen-Gosalbez, G., and Perez-Ramirez, J. Plant-to-planet analysis of CO_2-based methanol processes. *Energy & Environmental Science*, 12(12):3425–3436, 2019.

Grigoriev, S. A., Porembsky, V. I., and Fateev, V. N. Pure hydrogen production by PEM electrolysis for hydrogen energy. *International Journal of Hydrogen Energy*, 31(2):171–175, 2006.

Gutiérrez-Martín, F. and Guerrero-Hernández, I. Balancing the grid loads by large scale integration of hydrogen technologies: The case of the Spanish power system. *International Journal of Hydrogen Energy*, 37(2):1151–1161, 2012.

Hank, C., Gelpke, S., Schnabl, A., White, R. J., Full, J., Wiebe, N., Smolinka, T., Schaadt, A., Henning, H.-M., and Hebling, C. Economics & carbon dioxide avoidance cost of methanol production based on renewable hydrogen and recycled carbon dioxide – power-to-methanol. *Sustainable Energy Fuels*, 2:1244–1261, 2018.

Harnisch, F., Rosa, L. F. M., Kracke, F., Virdis, B., and Krömer, J. O. Electrifying white biotechnology: Engineering and economic potential of electricity-driven

bio-production. *ChemSusChem*, 8(5):758–766, 2015.

Hart, E. K. and Jacobson, M. Z. A Monte Carlo approach to generator portfolio planning and carbon emissions assessments of systems with large penetrations of variable renewables. *Renewable Energy*, 36(8):2278–2286, 2011.

Hauer, A. Thermal energy storage. Report, International Renewable Energy Agency, 2013.

Heide, D., Greiner, M., von Bremen, L., and Hoffmann, C. Reduced storage and balancing needs in a fully renewable European power system with excess wind and solar power generation. *Renewable Energy*, 36(9):2515–2523, 2011.

Heide, D., von Bremen, L., Greiner, M., Hoffmann, C., Speckmann, M., and Bofinger, S. Seasonal optimal mix of wind and solar power in a future, highly renewable Europe. *Renewable Energy*, 35(11):2483–2489, 2010.

Holladay, J. D., Hu, J., King, D. L., and Wang, Y. An overview of hydrogen production technologies. *Catalysis Today*, 139(4):244–260, 2009.

Holttinen, H., Milligan, M., Kirby, B., Acker, T., Neimane, V., and Molinski, T. Using standard deviation as a measure of increased operational reserve requirement for wind power. *Wind Engineering*, 32(4):355–377, 2008.

Hu, G., Chen, C., Lu, H. T., Wu, Y., Liu, C., Tao, L., Men, Y., He, G., and Li, K. G. A review of technical advances, barriers and solutions in the power to hydrogen (P2H) roadmap. *Engineering*, 6(12):1364–1380, 2020.

Hwangbo, S., Nam, K., Heo, S., and Yoo, C. Hydrogen-based self-sustaining integrated renewable electricity network (HySIREN) using a supply-demand forecasting model and deep-learning algorithms. *Energy Conversion and Management*, 185:353–367, 2019.

IHS Markit. Methanol, Chemical Economics Handbook. Report, 2017.

Ismail, M., Moghavvemi, M., Mahlia, T., Muttaqi, K., and Moghavvemi, S. Effective utilization of excess energy in standalone hybrid renewable energy systems for

improving comfort ability and reducing cost of energy: A review and analysis. *Renewable and Sustainable Energy Reviews*, 42:726–734, 2015.

Ivy, J. Summary of electrolytic hydrogen production. Report, National Renewable Energy Laboratory, 2004.

Jacobsen, H. K. and Schröder, S. T. Curtailment of renewable generation: Economic optimality and incentives. *Energy Policy*, 49:663–675, 2012.

Jørgensen, C. and Ropenus, S. Production price of hydrogen from grid connected electrolysis in a power market with high wind penetration. *International Journal of Hydrogen Energy*, 33(20):5335–5344, 2008.

Kafandaris, S. Buying greenhouse insurance: The economic costs of CO_2 emission limits. *Journal of the Operational Research Society*, 45(4):479–480, 1994.

Kajaste-Rudnitskaja, R., Hurme, M., and Oinas, P. Methanol-managing greenhouse gas emissions in the production chain by optimizing the resource base. *AIMS Energy*, 6:1074–1102, 2018.

Karuturi, S. K., Shen, H., Duong, T., Narangari, P. R., Yew, R., Wong-Leung, J., Catchpole, K., Tan, H. H., and Jagadish, C. Perovskite photovoltaic integrated CdS/TiO_2 photoanode for unbiased photoelectrochemical hydrogen generation. *ACS Applied Materials & Interfaces*, 10(28):23766–23773, 2018.

Kempton, W., Pimenta, F. M., Veron, D. E., and Colle, B. A. Electric power from offshore wind via synoptic-scale interconnection. *Proceedings of the National Academy of Sciences*, 107(16):7240–7245, 2010.

Khatib, T., Mohamed, A., Sopian, K., and Mahmoud, M. Optimal sizing of building integrated hybrid PV/diesel generator system for zero load rejection for Malaysia. *Energy and Buildings*, 43(12):3430–3435, 2011.

Kim, J., Henao, C. A., Johnson, T. A., Dedrick, D. E., Miller, J. E., Stechel, E. B., and Maravelias, C. T. Methanol production from CO_2 using solar-thermal energy: process development and techno-economic analysis. *Energy & Environmental Science*, 4:3122–3132, 2011.

Kim, J., Johnson, T. A., Miller, J. E., Stechel, E. B., and Maravelias, C. T. Fuel production from CO_2 using solar-thermal energy: system level analysis. *Energy & Environmental Science*, 5:8417–8429, 2012.

Kohn, M. P., Castaldi, M. J., and Farrauto, R. J. Auto-thermal and dry reforming of landfill gas over a $Rh/\gamma Al_2O_3$ monolith catalyst. *Applied Catalysis B: Environmental*, 94(1):125–133, 2010.

Kondratenko, E. V., Mul, G., Baltrusaitis, J., Larrazábal, G. O., and Pérez-Ramírez, J. Status and perspectives of CO_2 conversion into fuels and chemicals by catalytic, photocatalytic and electrocatalytic processes. *Energy & Environmental Science*, 6:3112–3135, 2013.

Koohi-Fayegh, S. and Rosen, M. A review of energy storage types, applications and recent developments. *Journal of Energy Storage*, 27:101047, 2020.

Kopp, M., Coleman, D., Stiller, C., Scheffer, K., Aichinger, J., and Scheppat, B. Energiepark Mainz: Technical and economic analysis of the worldwide largest Power-to-Gas plant with PEM electrolysis. *International Journal of Hydrogen Energy*, 42(19):13311–13320, 2017.

Lechtenböhmer, S., Nilsson, L. J., Åhman, M., and Schneider, C. Decarbonising the energy intensive basic materials industry through electrification – implications for future EU electricity demand. *Energy*, 115:1623–1631, 2016.

Lee, S. G., Sawant, A., Rodrigues, K., and Kulik, C. J. Effects of carbon dioxide and water on the methanol synthesis catalyst. *Energy & Fuels*, 3(1):2–7, 1989.

Leroy, R. L., Bowen, C. T., and Leroy, D. J. The thermodynamics of aqueous water electrolysis. *Journal of the Electrochemical Society*, 127(9):1954–1962, 1980.

Levene, J. I., Mann, M. K., Margolis, R. M., and Milbrandt, A. An analysis of hydrogen production from renewable electricity sources. *Solar Energy*, 81(6):773–780, 2007.

Lewis, N. S. and Nocera, D. G. Powering the planet: Chemical challenges in solar energy utilization. *Proceedings of the National Academy of Sciences*, 103(43):15729–15735, 2006.

Li, B. H., Zhang, N., and Smith, R. Simulation and analysis of CO_2 capture process with aqueous monoethanolamine solution. *Applied Energy*, 161:707–717, 2016.

Li, C., Shi, H., Cao, Y., Wang, J., Kuang, Y., Tan, Y., and Wei, J. Comprehensive review of renewable energy curtailment and avoidance: A specific example in China. *Renewable and Sustainable Energy Reviews*, 41:1067–1079, 2015.

Li, P.-H. and Pye, S. Assessing the benefits of demand-side flexibility in residential and transport sectors from an integrated energy systems perspective. *Applied Energy*, 228:965–979, 2018.

Licht, S. Solar water splitting to generate hydrogen fuel: Photothermal electrochemical analysis. *Journal of Physical Chemistry B*, 107(18):4253–4260, 2003.

Logan, B. E. and Rabaey, K. Conversion of wastes into bioelectricity and chemicals by using microbial electrochemical technologies. *Science*, 337(6095):686–690, 2012.

Lux, B. and Pfluger, B. A supply curve of electricity-based hydrogen in a decarbonized European energy system in 2050. *Applied Energy*, 269:115011, 2020.

Manenti, F., Leon-Garzon, A. R., and Bozzano, G. Energy-process integration of the gas-cooled/water-cooled fixed-bed reactor network for methanol synthesis. *Chemical Engineering Transactions*, 35:1243–1248, 2013.

Mansilla, C., Dautremont, S., Shoai Tehrani, B., Cotin, G., Avril, S., and Burkhalter, E. Reducing the hydrogen production cost by operating alkaline electrolysis as a discontinuous process in the French market context. *International Journal of Hydrogen Energy*, 36(11):6407–6413, 2011.

Markvart, T., Fragaki, A., and Ross, J. PV system sizing using observed time series of solar radiation. *Solar Energy*, 80(1):46–50, 2006.

Matthischke, S., Roensch, S., and Güttel, R. Start-up time and load range for the methanation of carbon dioxide in a fixed-bed recycle reactor. *Industrial & Engineering Chemistry Research*, 57(18):6391–6400, 2018.

Matzen, M., Alhajji, M., and Demirel, Y. Chemical storage of wind energy by renewable methanol production: Feasibility analysis using a multi-criteria decision matrix. *Energy*, 93:343–353, 2015.

Methanol Market Services Asia. Methanol supply and demand balance 2008-2013. Dataset, 2013.

Miah, J., Griffiths, A., McNeill, R., Poonaji, I., Martin, R., Yang, A., and Morse, S. Heat integration in processes with diverse production lines: A comprehensive framework and an application in food industry. *Applied Energy*, 132:452–464, 2014.

Mignard, D. and Pritchard, C. On the use of electrolytic hydrogen from variable renewable energies for the enhanced conversion of biomass to fuels. *Chemical Engineering Research and Design*, 86(5A):473–487, 2008.

Milligan, M. R. and Factor, T. Optimizing the geographic distribution of wind plants in Iowa for maximum economic benefit and reliability. *Wind Engineering*, 24(4):271–290, 2000.

Mor, G. K., Varghese, O. K., Paulose, M., Shankar, K., and Grimes, C. A. A review on highly ordered, vertically oriented TiO_2 nanotube arrays: Fabrication, material properties, and solar energy applications. *Solar Energy Materials and Solar Cells*, 90(14):2011–2075, 2006.

Mores, P., Scenna, N., and Mussati, S. CO_2 capture using monoethanolamine (MEA) aqueous solution: Modeling and optimization of the solvent regeneration and CO_2 desorption process. *Energy*, 45(1):1042–1058, 2012.

Morgan, E. R. *Techno-Economic Feasibility Study of Ammonia Plants Powered by Offshore Wind*. Thesis, University of Massachusetts Amherst, 2013.

Moro, A. and Lonza, L. Electricity carbon intensity in European member states: Impacts on GHG emissions of electric vehicles. *Transportation Research Part D: Transport and Environment*, 64:5–14, 2018.

Naterer, G., Fowler, M., Cotton, J., and Gabriel, K. Synergistic roles of off-peak electrolysis and thermochemical production of hydrogen from nuclear energy in Canada. *International Journal of Hydrogen Energy*, 33(23):6849–6857, 2008.

National Renewable Energy Laboratory. Technology brief: Analysis of current-day commercial electrolyzers. Report, 2004.

Nayak-Luke, R., Bañares-Alcántara, R., and Wilkinson, I. "Green" ammonia: Impact of renewable energy intermittency on plant sizing and levelized cost of ammonia. *Industrial & Engineering Chemistry Research*, 57(43):14607–14616, 2018.

Nayak-Luke, R. M. and Bañares-Alcántara, R. Long-term energy storage: What is the need and is ammonia a solution? *Computer Aided Chemical Engineering*, 44:1843–1848, 2018.

Nayak-Luke, R. M. and Bañares-Alcántara, R. Techno-economic viability of islanded green ammonia as a carbon-free energy vector and as a substitute for conventional production. *Energy & Environmental Science*, 13:2957–2966, 2020.

Nguyen, T. B. and Zondervan, E. Methanol production from captured CO_2 using hydrogenation and reforming technologies - environmental and economic evaluation. *Journal of CO_2 Utilization*, 34:1–11, 2019.

Nielsen, M., Alberico, E., Baumann, W., Drexler, H.-J., Junge, H., Gladiali, S., and Beller, M. Low-temperature aqueous-phase methanol dehydrogenation to hydrogen and carbon dioxide. *Nature*, 495:85–89, 2013.

Ocsachoque, M., Pompeo, F., and Gonzalez, G. Rh-Ni/CeO_2-Al_2O_3 catalysts for methane dry reforming. *Catalysis Today*, 172(1):226–231, 2011.

Olah, G. A. The methanol economy. *Chemical & Engineering News Archive*, 81(38):5–5, 2003.

Olah, G. A. Beyond oil and gas: The methanol economy. *Angewandte Chemie International Edition*, 44(18):2636–2639, 2005.

Olah, G. A., Goeppert, A., Czaun, M., and Prakash, G. K. S. Bi-reforming of methane from any source with steam and carbon dioxide exclusively to metgas ($CO–2H_2$) for methanol and hydrocarbon synthesis. *Journal of the American Chemical Society*, 135(2):648–650, 2013.

Palys, M. J. and Daoutidis, P. Using hydrogen and ammonia for renewable energy storage: A geographically comprehensive techno-economic study. *Computers & Chemical Engineering*, 136(106785), 2020.

Pauschert, D. Study of equipment prices in the power sector. Report, Energy Sector Management Assistance Program, 2009.

Peng, S.-Y., Jin, G.-P., Cui, J.-S., Lv, X.-Y., Yu, Y.-X., and Tang, H.-W. Preparation of nickel hexacyanoferrate/heterogeneous carbon composites for CO_2 continuous electrocatalytic reduction to formic acid. *Journal of Environmental Chemical Engineering*, 6(6):6931–6938, 2018.

Perez-Fortes, M., Schoneberger, J. C., Boulamanti, A., and Tzimas, E. Methanol synthesis using captured CO_2 as raw material: Techno-economic and environmental assessment. *Applied Energy*, 161:718–732, 2016.

Peter, M. S. and Timmerhaus, K. D. *Plant design and economics for chemical engineers*. McGraw Hill, 1991.

Peterson, A. A., Abild-Pedersen, F., Studt, F., Rossmeisl, J., and Nørskov, J. K. How copper catalyzes the electroreduction of carbon dioxide into hydrocarbon fuels. *Energy & Environmental Science*, 3(9):1311–1315, 2010.

Pettersson, J., Ramsey, B., and Harrison, D. A review of the latest developments in electrodes for unitised regenerative polymer electrolyte fuel cells. *Journal of Power Sources*, 157(1):28–34, 2006.

Phair, J. W. and Badwal, S. P. S. Materials for separation membranes in hydrogen and oxygen production and future power generation. *Science and Technology of Advanced Materials*, 7(8):792–805, 2006.

Philibert, C. Renewable energy for industry: From green energy to green materials and fuels. Report, International Energy Agency, 2017.

Ramezan, M., Skone, T. J., ya Nsakala, N., and Liljedahl, G. N. Carbon dioxide capture from existing coal-fired power plants. Report, National Energy Technology Laboratory, 2007.

Rasmussen, M. G., Andresen, G. B., and Greiner, M. Storage and balancing synergies in a fully or highly renewable pan-European power system. *Energy Policy*, 51:642–651, 2012.

Renewable Fuels Association. Industry statistics: World fuel ethanol production. Dataset, 2017.

Roberts, D. The key to tackling climate change: electrify everything. `https://www.vox.com/2016/9/19/12938086/electrify-everything`, 2017. Accessed on: Auguet 2, 2018.

Rodera, H. and Bagajewicz, M. J. Targeting procedures for energy savings by heat integration across plants. *AIChE Journal*, 45(8):1721–1742, 1999.

Ross, J. R. H. Natural gas reforming and CO_2 mitigation. *Catalysis Today*, 100(1-2):151–158, 2005.

Rudd, A. New direction for UK energy policy. `https://www.gov.uk/government/news/new-direction-for-uk-energy-policy`, 2015. Accessed on: August 4, 2018.

Saba, S. M., Müller, M., Robinius, M., and Stolten, D. The investment costs of electrolysis – a comparison of cost studies from the past 30 years. *International Journal of Hydrogen Energy*, 43(3):1209–1223, 2018.

Samsatli, S. and Samsatli, N. J. The role of renewable hydrogen and inter-seasonal storage in decarbonising heat – comprehensive optimisation of future renewable energy value chains. *Applied Energy*, 233-234:854–893, 2019.

Sarbu, I. and Sebarchievici, C. A comprehensive review of thermal energy storage. *Sustainability*, 10(1):191–223, 2018.

Saygin, D., Patel, M. K., Tam, C., and Gielen, D. J. Chemical and petrochemical sector: Potential of best practice technology and other measures for improving energy efficiency. Report, International Energy Agency, 2009.

Scataglini, R., Mayyas, A., Wei, M., Chan, S. H., Lipman, T., Gosselin, D., D'Alessio, A., Breunig, H., Colella, W. G., and James, B. D. A total cost of ownership model for solid oxide fuel cells in combined heat and power and power-only applications. Report, Ernest Orlando Lawrence Berkeley National Laboratory, 2015.

Schiffer, Z. J. and Manthiram, K. Electrification and decarbonization of the chemical industry. *Joule*, 1(1):10–14, 2017.

Schill, W.-P., Pahle, M., and Gambardella, C. Start-up costs of thermal power plants in markets with increasing shares of variable renewable generation. *Nature Energy*, 2(17050), 2017.

Searchinger, T., Heimlich, R., Houghton, R. A., Dong, F., Elobeid, A., Fabiosa, J., Tokgoz, S., Hayes, D., and Yu, T.-H. Use of U.S. croplands for biofuels increases greenhouse gases through emissions from land-use change. *Science*, 319(5867):1238–1240, 2008.

Shaahid, S., Al-Hadhrami, L., and Rahman, M. Review of economic assessment of hybrid photovoltaic-diesel-battery power systems for residential loads for different provinces of Saudi Arabia. *Renewable and Sustainable Energy Reviews*, 31:174–181, 2014.

Shaner, M. R., Atwater, H. A., Lewis, N. S., and McFarland, E. W. A comparative technoeconomic analysis of renewable hydrogen production using solar energy.

Energy & Environmental Science, 9:2354–2371, 2016.

Shenvi, A. A., Herron, D. M., and Agrawal, R. Energy efficiency limitations of the conventional heat integrated distillation column (HIDiC) configuration for binary distillation. *Industrial & Engineering Chemistry Research*, 50(1):119–130, 2011.

Simonis, B. and Newborough, M. Sizing and operating power-to-gas systems to absorb excess renewable electricity. *International Journal of Hydrogen Energy*, 42(34):21635–21647, 2017.

Sinden, G. Characteristics of the UK wind resource: Long-term patterns and relationship to electricity demand. *Energy Policy*, 35(1):112–127, 2007.

Song, C. and Pan, W. Tri-reforming of methane: a novel concept for catalytic production of industrially useful synthesis gas with desired H_2/CO ratios. *Catalysis Today*, 98(4):463–484, 2004.

Soroush, M. and Chmielewski, D. J. Process systems opportunities in power generation, storage and distribution. *Computers & Chemical Engineering*, 51:86–95, 2013.

Steinfeld, A. Solar thermochemical production of hydrogen - A review. *Solar Energy*, 78(5):603–615, 2005.

Steward, D. Scenario development and analysis of hydrogen as a large-scale energy storage medium. Report, National Renewable Energy Laboratory, 2009.

Strbac, G. Demand side management: Benefits and challenges. *Energy Policy*, 36(12):4419–4426, 2008.

Suhartanto, T., York, A. P. E., Hanif, A., Al-Megren, H., and Green, M. L. H. Potential utilisation of Indonesia's Natuna natural gas field via methane dry reforming to synthesis gas. *Catalysis Letters*, 71(1-2):49–54, 2001.

Tan, L. S., Lau, K. K., Bustam, M. A., and Shariff, A. M. Removal of high concentration CO_2 from natural gas at elevated pressure via absorption process in packed column. *Journal of Natural Gas Chemistry*, 21(1):7–10, 2012.

Taqvi, S. A., Dendana Tufa, L., Zabiri, H., Mahadzir, S., Maulud, A. S., and Uddin, F. Rigorous dynamic modelling and identification of distillation column using Aspen Plus. In *IEEE 8th Control and System Graduate Research Colloquium*, pages 262–267. 2017.

Tountas, A. A., Peng, X., Tavasoli, A. V., Duchesne, P. N., Dingle, T. L., Dong, Y., Hurtado, L., Mohan, A., Sun, W., Ulmer, U., Wang, L., Wood, T. E., Maravelias, C. T., Sain, M. M., and Ozin, G. A. Towards solar methanol: Past, present, and future. *Advanced Science*, 6(8):1801903, 2019.

Townsend, D. W. and Linnhoff, B. Heat and power networks in process design. Part I: Criteria for placement of heat engines and heat pumps in process networks. *AIChE Journal*, 29(5):742–748, 1983a.

Townsend, D. W. and Linnhoff, B. Heat and power networks in process design. Part II: Design procedure for equipment selection and process matching. *AIChE Journal*, 29(5):748–771, 1983b.

Tunå, P., Hulteberg, C., and Ahlgren, S. Techno-economic assessment of nonfossil ammonia production. *Environmental Progress & Sustainable Energy*, 33(4):1290–1297, 2014.

Turner, J., Sverdrup, G., Mann, M. K., Maness, P. C., Kroposki, B., Ghirardi, M., Evans, R. J., and Blake, D. Renewable hydrogen production. *International Journal of Energy Research*, 32(5):379–407, 2008.

US Energy Information Administration. Carbon dioxide emissions coefficients. Dataset, 2016.

US Energy Information Administration. Monthly energy review December 2019. Report, 2019.

US Energy Information Administration. Electric power monthly with data for January 2020. Report, 2020.

Van-Dal, E. S. and Bouallou, C. Design and simulation of a methanol production plant from CO_2 hydrogenation. *Journal of Cleaner Production*, 57:38–45, 2013.

Van Kranenburg, K., Schols, E., Gelevert, H., De Kler, R., Van Delft, Y., and Weeda, M. Enpowering the chemical industry: Opportunities for electrification. Report, Netherlands Organisation for Applied Scientific Research (TNO), 2016.

Vanden Bussche, K. M. and Froment, G. F. A steady-state kinetic model for methanol synthesis and the water gas shift reaction on a commercial $Cu/ZnO/Al_2O_3$ catalyst. *Journal of Catalysis*, 161(1):1–10, 1996.

Varone, A. and Ferrari, M. Power to liquid and power to gas: An option for the German Energiewende. *Renewable and Sustainable Energy Reviews*, 45:207–218, 2015.

Velu, S. and Suzuki, K. Selective production of hydrogen for fuel cells via oxidative steam reforming of methanol over CuZnAl oxide catalysts: Effect of substitution of zirconium and cerium on the catalytic performance. *Topics in Catalysis*, 22(3):235–244, 2003.

Vestas Wind Systems. General specification for V90 – 3.0 MW: 60 Hz variable speed turbine. Report, 2004.

Wang, C. *Modeling and Control of Hybrid Wind/Photovoltaic/Fuel Cell Distributed Generation Systems*. Thesis, Montana State University, 2006.

Wang, G., Mitsos, A., and Marquardt, W. Conceptual design of ammonia-based energy storage system: System design and time-invariant performance. *AIChE Journal*, 63(5):1620–1637, 2017.

Wang, P., Xie, C., Xu, S., and Ge, Y. Study of direct compression heat pump energy-saving technology. *Procedia Environmental Sciences*, 12:394–399, 2012.

Wang, Z., Han, Y., Li, C., Geng, Z., and Fan, J. Input-output networks considering graphlet-based analysis for production optimization: Application in ethylene plants. *Journal of Cleaner Production*, 278:123955, 2021.

Weddle, N. Europe Chemical Profile: butadiene. Database, Independent Commodity Intelligence Services, 2013.

White, S., Allis, R., Moore, J., Chidsey, T., Morgan, C., Gwynn, W., and Adams, M. Natural CO_2 reservoirs on the Colorado Plateau and Southern Rocky Mountains, USA: A numerical model. In *6th International Conference on Greenhouse Gas Control Technologies*, pages 423–428. 2003.

Worrell, E., Phylipsen, D., Einstein, D., and Martin, N. Energy use and energy intensity of the U.S. chemical industry. Report, University of California, Berkeley, 2000.

Yamamoto, T., Tryk, D. A., Fujishima, A., and Ohata, H. Production of syngas plus oxygen from CO_2 in a gas-diffusion electrode-based electrolytic cell. *Electrochimica Acta*, 47(20):3327–3334, 2002.

Yang, C.-J. and Jackson, R. B. China's growing methanol economy and its implications for energy and the environment. *Energy Policy*, 41:878–884, 2012.

Yang, M., Feng, X., and Chu, K. H. Graphical analysis of the integration of heat pumps in chemical process systems. *Industrial & Engineering Chemistry Research*, 52(24):8305–8310, 2013.

Yang, Y., Long, Y., and Gao, W. Analysis on characteristics for energy saving effect of tower top vapor recompressing heat pump distillation. *Journal of Jilin Institute of Chemical Technology*, 27(2), 2010.

Yanine, F. F. and Sauma, E. E. Review of grid-tie micro-generation systems without energy storage: Towards a new approach to sustainable hybrid energy systems linked to energy efficiency. *Renewable and Sustainable Energy Reviews*, 26:60–95, 2013.

Yarulina, I., Chowdhury, A. D., Meirer, F., Weckhuysen, B. M., and Gascon, J. Recent trends and fundamental insights in the methanol-to-hydrocarbons process. *Nature Catalysis*, 1(6):398–411, 2018.

Zeng, K. and Zhang, D. Recent progress in alkaline water electrolysis for hydrogen production and applications. *Progress in Energy and Combustion Science*, 36(3):307–326, 2010.

Zhang, C., Jun, K.-W., Gao, R., Kwak, G., and Kang, S. C. Efficient utilization of associated natural gas in a modular gas-to-liquids process: Technical and economic analysis. *Fuel*, 176:32–39, 2016.

Zhang, C., Jun, K.-W., Gao, R., Kwak, G., and Park, H.-G. Carbon dioxide utilization in a gas-to-methanol process combined with CO_2/steam-mixed reforming: Techno-economic analysis. *Fuel*, 190:303–311, 2017.

Zhang, C., Jun, K.-W., Gao, R., Lee, Y.-J., and Kang, S. C. Efficient utilization of carbon dioxide in gas-to-liquids process: Process simulation and techno-economic analysis. *Fuel*, 157:285–291, 2015.

Zhao, Z., Fan, J., Xie, M., and Wang, Z. Photo-catalytic reduction of carbon dioxide with in-situ synthesized CoPc/TiO_2 under visible light irradiation. *Journal of Cleaner Production*, 17(11):1025–1029, 2009.